SPIRALS AND VORTICES SPIRALS AND
VORTICES SPIRALS AND VORTICES SPI
RALS AND VORTICES SPIRALS AND VO
RTICES SPIRALS AND VORTICES SPIRA
LS AND VORTICES SPIRALS AND VOR
TICES SPIRALS AND VORTICES SPIRALS
AND VORTICES SPIRALS AND VORTICES
SPIRALS AND VORTICES SPIRALS AND
VORTICES SPIRALS AND VORTICES SPI
RALS AND VORTICES SPIRALS AND VO
RTICES SPIRALS AND VORTICES SPIRA
LS AND VORTICES SPIRALS AND VOR
TICES SPIRALS AND VORTICES SPIRALS
AND VORTICES SPIRALS AND VORTICES
SPIRALS AND VORTICES SPIRALS AND
VORTICES SPIRALS AND VORTICES SPI
RALS AND VORTICES SPIRALS AND VO
RTICES SPIRALS AND VORTICES SPIRA

Kinko Tsuji · Stefan C. Müller *Editors*

SPIRALS AND VORTICES

In Culture, Nature, and Science

Springer

THE FRONTIERS COLLECTION

THE FRONTIERS COLLECTION

The books in this collection are devoted to challenging and open problems at the forefront of modern science and scholarship, including related philosophical debates. In contrast to typical research monographs, however, they strive to present their topics in a manner accessible also to scientifically literate non-specialists wishing to gain insight into the deeper implications and fascinating questions involved. Taken as a whole, the series reflects the need for a fundamental and interdisciplinary approach to modern science and research. Furthermore, it is intended to encourage active academics in all fields to ponder over important and perhaps controversial issues beyond their own speciality. Extending from quantum physics and relativity to entropy, consciousness, language and complex systems—the Frontiers Collection will inspire readers to push back the frontiers of their own knowledge.

More information about this series at https://link.springer.com/bookseries/5342

For a full list of published titles, please see back of book or springer.com/series/5342

Kinko Tsuji · Stefan C. Müller
Editors

Spirals and Vortices

In Culture, Nature, and Science

Springer

Editors
Kinko Tsuji
Shimadzu Europa GmbH
Duisburg, Germany

Stefan C. Müller
Institute of Physics
Otto von Guericke University Magdeburg
Magdeburg, Germany

Foreword

According to one of our most famous books, the bible, at the beginning the world was completely disordered. This is also reflected by our present view of the "big bang" initiating the expansion of the universe from an initial state of non-equilibrium. But interactions between the constituents and the general laws of physics led to the formation of astronomic structures, among which the galaxies contain already the element of spirals, as, for example, expressed by the term "spiral nebula."

When life developed on our planet, a large group of animals, the ammonites, with characteristic spiral shapes were widely existing for many millions of years, and this structural element is also found with many other living systems.

On the other hand, the emerging human culture adopted very soon the symbol of a spiral, as can be found as relics in many different places. Apart from its symbolic character, the spiral inspired through its aesthetic appeal many artists until today. Attempts to understand the formation of spirals date back to ancient times where a simple prescription for their construction is attributed to Archimedes, the most famous mathematician of this period.

The physical origin of these structures in nature has to be traced back to their roots from a state far from equilibrium, and theory permits their modeling in many cases. In chemistry, for example, the interplay between reaction and diffusion may cause the formation of various spatiotemporal structures, including spirals. The study of these phenomena is the object of intense current research.

The present book provides an extensive overview of the various aspects of the appearance of these fascinating structures ranging from the arts to natural sciences and even medicine. In particular, it should become clear how these different phenomena are linked together in a general sense.

Berlin, Germany   Gerhard Ertl
November 2018

Preface

The unfolding of ordered and irregular structures and their temporal evolution is an omnipresent phenomenon in our natural environment. Their presence and their formation and decay are fascinating features of the world where we live. There exist a plethora of shapes and dynamics that play an important role not only in the living and inanimate nature and the natural sciences, but also in cultural history and the arts, reaching back many thousand years. As of today, these are still essential both for living organisms and non-living materials.

These structures are not only the phenomena to be observed, but also the objects to be investigated. Already in the 19th century, Friedlieb Ferdinand Runge (1794–1867) carried out many experiments relevant to spatially inhomogeneous reactions. He used special paper for identifying chemical species by their color, thus setting the basis for paper chromatography. When dropping at regular time intervals chemical substances on a paper impregnated with a reactive counterpart, he discovered a large number of solution pairs for which this procedure results, upon spreading of the drops into the surrounding area, in quite spectacular, symmetric, and colorful structures. He called them "Bilder" (paintings). He published them in two self-printed books "Color chemistry. Sample images for friends of beauty and for use by sketchers, painters, decorators, and printers, prepared by chemical interaction"[1] and "The formative tendency of substances illustrated by autonomously developed images"[2] (both originally in German). His work made an impression and constitutes a salient contribution to the research on self-organization.

---

[1] F. F. Runge, *Farbenchemie. Musterbilder für Freunde des Schönen und zum Gebrauch für Zeichner, Maler, Verzierer und Zeugdrucker, dargestellt durch chemische Wechselwirkung (Color chemistry. Sample images for friends of beauty and for use by sketchers, painters, decorators, and printers, prepared by chemical interaction)* (self-published, Berlin, 1850).

[2] F. F. Runge, *Der Bildungstrieb der Stoffe. Veranschaulicht in selbständig gewachsenen Bildern (The formative tendency of substances illustrated by autonomously developed images)* (self-published, Oranienburg, 1855).

Thus, Runge is considered as a pioneer on pattern formation. In fact, in his systems ring-shaped regions of precipitate can be observed (see the right painting in the figure below), for which experimental evidence was presented by Deiss.[3] The work of the Chemist Liesegang gave ample proof of this phenomenon by his systematic studies in 1896 and in later years.
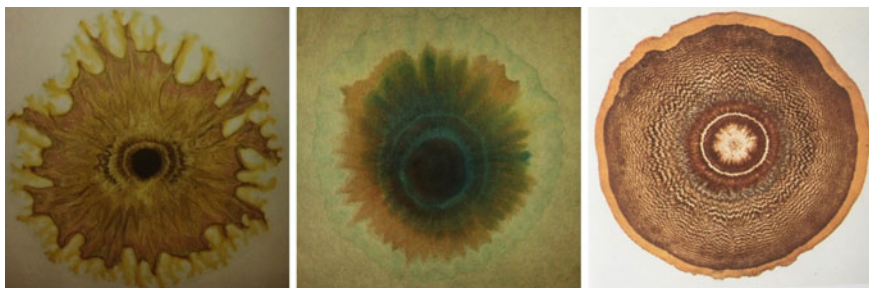
The left and middle images show two examples which SCM managed to produce by himself. If you like to make such "Runge's paintings" by yourself, we recommend to look at the recipes given in the book of Harsch and Bussemas.[4]

Among the multitude of structures, spirals and vortices possess a special fascination, being part of the eternal theme of interaction between science and art. Many spirals and vortices appear in our universe: in stone carvings, architecture, sculpture, decoration, performing arts, and literature on the one hand and, on the other hand, in many natural appearances/phenomena like spiral galaxies, hurricanes, snails, helices of proteins, and many others.

Our idea to edit a book about spirals and vortices goes back for more than 30 years. SCM presented on the occasion of inaugurating his new laboratory some experiments: pattern formation in some chemical reactions in liquids, in gels, as well as on filter papers. There appeared concentric circles, hexagonal patterns, spirals, helices, and some more complicated forms. For KT such phenomena were completely new, although she worked as a scientist in the same institute. As a specialist of pattern formation, SCM explained how and why such interesting shapes occur. Since this presentation, KT has started to look for suitable motives in the surrounding world. Amazingly there are so many regular and irregular forms: pattern on the sand at seashores, the shape of airplane turbines, short-term patterns during rice cooking, various motives in textiles, photographs of tornadoes etc.

---

[3] E. Deiss, Über Runge-Bilder und Liesegangringe auf Filtrierpapier. Kolloid Z. **89**, 146–161 (1939).

[4] G. Harsch and H. H. Bussemas, *Bilder, die sich selber malen. Der Chemiker Runge und seine Musterbilder für Freunde des Schönen* (DuMont Buchverlag, Köln, 1985).

The team

Here, in this book, we write about spirals and vortices: demonstrating their beauty, their amazing and impressive aesthetic nature, their important role in mathematics and natural sciences, and their impact on artistic masterpieces. Everybody who has a sense of curiosity—not only scientists or would-be scientists—is welcome to read this volume. But, in order to avoid unnecessary misunderstanding, we emphasize that we will concentrate our discussion mainly on scientific points of view. We will not touch ethereal or religious meanings of spirals or vortices. On this basis, readers are certainly encouraged to talk to each other and exchange their views with historians, artists, musicians, writers, mathematicians, physicists, chemists, biologists, medical scholars as well as with all people who work in interdisciplinary fields.

In Part I, readers are taken on an aesthetic and scientific journey through the world of spiral forms, introducing various spirals and vortices as they appear in the following chapters: *Cultural History*, *Appearance in Nature*, and *The Arts and Beyond*. As an inset in the second chapter, we talk about the theme "Science meets the Arts," focusing on work by Johann Wolfgang von Goethe who is not only the famous writer of novels, poetry, and dramas, but also author of Works on Natural Science (Naturwissenschaftiche Schriften). There he formulates his thoughts and ideas about spirals in the metamorphosis of plants and animals.

As the next, in Part II spirals and vortices of various shapes and in various modalities are introduced. Andrey Polezhaev provides relevant mathematical data on spirals in two- and three-dimensional polar coordinate systems with mathematical equations. In an inset of his chapter, pioneering works of the painter and mathematician Albrecht Dürer are shown: how he draws the Archimedean spiral

and a helix-like spiral with compass and ruler. *Acoustic Spirals* written by KT is a piece on tonal equivalents of spirals discovered by her in the musical work of Johann Sebastian Bach.

After mathematics, there follows chemistry in turn (Part III). As mentioned above, the patterns of Runge and of Liesegang are both caused by the chemical reaction of two substances, distributed inhomogeneously in space. The essential differences between their systems are the chemicals used and the matrix in which the reactants move (filter paper or aqueous gel). Both have in common that they represent some of the earliest manifestations of chemical self-organization displaying color and beauty. Sabine Dietrich writes about Liesegang structures, which belong to mainly quiescent spirals. On the other hand, there are different kinds of spirals: rigidly rotating spirals and irregularly moving spirals. SCM explains how spirals start rotating and shows instructive examples. Subsequently, Patricia Pfeiffer presents works on *Chemical Oscillations and Spiral Waves*. She shows some historical experiments of the Belousov–Zhabotinsky reaction, as well as her own new experiments of pattern formation in microemulsions. Harm H. Rotermund describes the CO oxidation on platinum observed by the photoemission electron microscope and analyzes the surface reactions.

Spirals and vortices appear also in biology, physiology, and medical fields (Part IV). Cornelius J. Weijer tells a story about social amoebae, which build spiral-formed aggregates. A fatal rhythm of atrial or ventricular fibrillation as induced by rotating spiral waves is presented by Alexander Panfilov. Niklas Manz shows some diseases causing spiral patterns to evolve on tongue or skin. In the last chapter of this part, we offer some more spirals and vortices in biology and biomedicine: glycolytic oscillations, calcium waves, spreading depression, and epilepsy.

In the last part (Part V), three theoretically oriented articles are presented for better understanding the creation of spirals and vortices. Markus Bär explains, by using several reaction–diffusion models, how spiral patterns are built in nature, in chemical reactions, and in biological systems. Next, Simon Syga and co-authors stand at a different angle, which means not for continuous systems but for discrete ones, and construct spirals by means of a cellular automaton model. Vladimir Zykov concludes this volume with his treatise on the *Kinematics of Spiral Waves in Excitable Media*, investigating what is essential to determine their shape and rotation frequency, in order to prevent dangerous activity of self-organizing rotating vortices (e.g., hurricanes, tornadoes, and fibrillations in the heart).

We, as the editors, hope that all readers will enjoy to see many spirals and vortices from various scientific points of view. And we hope to write about further developments of these fields in the near future.

Acknowledgements

Covarrubias is acknowledged heartily for his illustration of "The team". Finally, we thank Sho Tsuji for her professional assistance.

Duisburg, Germany   Kinko Tsuji
Magdeburg, Germany   Stefan C. Müller
November 2018

Contents

Contributors

Markus Bär Physikalisch-Technische Bundesanstalt, Berlin, Germany

Lutz Brusch Centre for Information Services and High Performance Computing, Technische Universität Dresden, Dresden, Germany

Markus A. Dahlem Medical Affairs, Newsenselab GmbH, Berlin, Germany

Andreas Deutsch Centre for Information Services and High Performance Computing, Technische Universität Dresden, Dresden, Germany

Sabine Dietrich Department of Earth Sciences, Technical University Berlin, Berlin, Germany

Flavio H. Fenton School of Physics, Georgia Institute of Technology, Atlanta, GA, USA

Thomas Mair (Deceased author)

Niklas Manz Department of Physics, The College of Wooster, Wooster, OH, USA

Stefan C. Müller Institute of Physics, Otto von Guericke University Magdeburg, Magdeburg, Germany

Josué M. Nava-Sedeño Centre for Information Services and High Performance Computing, Technische Universität Dresden, Dresden, Germany

Alexander V. Panfilov Department of Physics and Astronomy, Ghent University, Ghent, Belgium;
Laboratory of Experimental Cardiology, Department of Cardiology, Heart Lung Center, Leiden University Medical Center, ZA, Leiden, The Netherlands

Patricia Pfeiffer Institute of Physics, Otto von Guericke University Magdeburg, Magdeburg, Germany

Andrey Polezhaev P.N. Lebedev Physical Institute, Russian Academy of Sciences, Moscow, Russia

Harm H. Rotermund Department of Physics and Atmospheric Science, Dalhousie University, Halifax, Canada

Simon Syga Centre for Information Services and High Performance Computing, Technische Universität Dresden, Dresden, Germany

Kinko Tsuji Shimadzu Europa GmbH, Duisburg, Germany

Cornelis J. Weijer Division of Cell and Developmental Biology, School of Life Sciences, University of Dundee, Dundee, UK

Vladimir S. Zykov Max Planck Institute for Dynamics and Self-Organization, Göttingen, Germany

Part I
Spirals and Vortices in Our Universe

Natur und Kunst, sie scheinen sich zu fliehen
Und haben sich, eh' man es denkt, gefunden.

Nature and art, they seem to flee from each other
And have, before one may reflect, found their common ways.

— Johann W. von Goethe

Cultural History

Kinko Tsuji and Stefan C. Müller

Abstract We introduce various spirals which were made during the time from 11,000 BC (Neolithic Period) to 1500 AD (early Renaissance). Concentric circles were created much earlier (40,000–20,000 BC). For the period between 5000 and 2000 BC spirals in Megalithic arts, Scythian treasures and Japanese clay figures are presented as examples. From 2000 to 1 BC spirals are found worldwide: in Europe, Egypt, Thailand, India, or South America. From 1 to 1500 AD a large number of spirals in Christian, Moslem and Buddhistic cultures were created. At the end spirals and vortices in the Nordic, Medieval and Renaissance arts are exhibited.

1 Introduction

Concentric circles in rock art found in Columbia or Australia are among the oldest geometric shapes created by homo sapiens. These date back to 40,000 until 20,000 BC. Much later, in the new stone age (Neolithic Period) from 8000 BC on, spiral patterns (mathematically more complicated than circles) were carved on stones and temple walls in many places all over the world, for example, in Newgrange (Ireland), Gobekli Tepe in Turkey and on Malta. At the same time spiral patterns also appeared on Greek potteries, Scythian ornaments, Japanese clay figures, and other objects.

A simple question, although difficult to answer, is why spiral patterns or other symbols (swastikas, meanders, serpents,...), as well, appeared in the ancient cultures

K. Tsuji (✉)
Shimadzu Europa GmbH, Albert-Hahn-Straße 6-10, 47269 Duisburg, Germany
e-mail: kts@shimadzu.eu

S. C. Müller
Institute of Physics, Otto von Guericke University Magdeburg,
Universitätsplatz 2, 39106 Magdeburg, Germany
e-mail: tsuji-mueller@t-online.de

independently in various places. There was no obvious way to communicate with each other. How did these symbols come to be universally shared?

Since they are frequently found in places of worship, it is often believed that spirals at that time probably had some religious or mythological meaning. The spiral might indicate an eternal life outward and death inward, or renewal, rebirth and growth. The old dies away and is replaced with the new. On the other hand, geometrically spiral forms have just developed from simple lines or curved line segments. Therefore, any intelligent ancient people could create/draw spirals. However, we will not discuss the possibility of a deeper meaning of spirals here but show some typical examples of spirals in our human history from the pre-historic period on to the middle ages and the Renaissance period, leaving it to the readers to think about the particular properties of spirals.

The sections of this chapter are divided according to the arrow of time: Sect. 2 "Older than 5000 BC", Sect. 3 "From 5000 to 2000 BC", Sect. 4 "From 2000 to 1 BC", and Sect. 5 "From 1 to 1600 AD". Spirals/vortices in various cultures are shown chronologically with some exceptions where there is a temporal overlap of two cultures.

For further introductory reading some general books are suggested [1–3].

2   Older than 5000 BC

Rock Arts in Chiribiquete National Park and Nitmiluk National Park

Symbolic paintings have been created by mankind ten thousands of years ago. Prehistoric paintings on vertical rock faces in the Amazonian wilderness in Columbia were recently photographed and filmed. The once populous Karijona Tribe most likely painted these masterpieces. The tribe continues to live uncontacted in the vast rainforest. Anthropologists and explorers have studied the region for hundreds of years [4, 5].

Images of rock art of this age have been discovered, for instance, in Chiribiquete, Columbia (Fig.1). A remarkable symbol here is the set of concentric circles close to a boat, as if the boat people are close to a dangerous eddy.

Concentric circles ("target patterns") belong to the earliest elements of symbolic art, as documented also in the Nitmiluk National Park in the Northern Territory of Australia. In this park some of Australia's oldest Aboriginal art can be seen. On the sandstone of a gorge system paintings appear in many styles, believed to date back 40,000 years. "Targets" are frequently used, but some of them seem to exhibit breaks at their centers, perhaps a first step to create spiral-shaped symbols [6].

Drawing spirals instead of circles may not appear to require much imagination. Both symbols ask the painter to draw circular or almost circular traces. But there is a basic topological difference: a spiral drawn this way starts at some point and ends at another, whereas the circle rotates without beginning or ending. Naively this looks like a simple difference, but conceptually it is a very big one. From the historical point of view the symbolic use of spirals may have evolved much later than that of circular patterns. (Details on the difference between circles and spirals are described in the introduction of chapter **Appearance in Nature**.)

Fig. 1 Rock art in Chiribiquete, Columbia. Photograph: F.F. Bonell/Ecoplanet

3   From 5000 to 2000 BC

3.1   *Megalithic Art in the Neolithic*

Some of the most ancient spirals, painted on a wall or carved into stone, have been discovered in Ireland. The first farmers who settled in Ireland, sometime before 3000 BC, arrived here from the Mediterranean, bringing with them the skills of crop-growing, domestication of animals and pottery. They came by the Atlantic sea-route and made their way northwards and westwards. Their most characteristic monuments are the great megalithic tombs for collective burials, the earliest works of architecture which survive in France, Britain and Ireland.

The most elaborate of these tombs are the passage-graves - large round mounds of stone covering a burial chamber. There is a magnificent tomb we can admire at Newgrange, built around 3200 BC, placing it prior to other mainstream guesses at the ages of Stonehenge and the Egyptian pyramids (Fig. 2). Newgrange is located west of Drogheda on the north side of the river Boyne [7].

This art in Ireland is purely abstract - spirals, zig-zags, meanders, and many other forms - and the designs have been placed onto the tombs by carving with a stone point, quartz or flint, because this was before the knowledge of metal. This abstract art obviously had a deeply felt religious significance, a meaning now lost to us.

Other outstanding examples can be found on Gavrinis island, which is a small island situated in the Gulf of Morbihan in Brittany, France. It contains the Gavrinis tomb, a megalithic monument notable for its abundance of artistic carvings. Among

Fig. 2 Megalithic art: the entrance passage to Newgrange and the carved kerb entrance stone

them a Neolithic dolmen stone, a decorated slab with an anthropomorphic "shield" motif on top is famous.

At the time of its construction, around 3500 BC, the island was still connected with the mainland. The rich internal decorations make Gavrinis one of the major treasuries of European megalithic art.

3.2 Malta Temples

The most famous and ancient of all these spirals are undeniably the ones found in Malta. The megalithic temples of Tarxien in Malta (built 3600–2500 BC) present another example of the arts in Neolithic times, now far away from Ireland (Fig. 3). This temple site is a complex of four megalithic structures built by the mysterious

Fig. 3 Spiral pattern in a Tarxien Temple, Malta

creed known as the "Temple Builders". The four temples are rich in megalithic art, constructed as they are from stone blocks adorned with relief-work in spiral patterns, as well as the carving of goats, bulls, pigs, and a ram. The significance of the spirals remains 'occult' in the strictest sense, though archaeologists believe that the animals depicted may have been sacrificial offerings. The Ġgantija-Temples on the island Gozo in the archipelago of Malta belong to the oldest man-made structures in the world (comparable with architectural marvels like Stonehenge or the pyramids). The spirals which were etched at Ġgantija may well be the oldest ever recorded. They are at present too faint to be clearly recognizable with one's naked eye, however tracings taken in 1829, when the temple was first excavated, are still pertinent [8].

Legend says that a giantess erected this structure within a single night, while holding her baby on her arms.

3.3 Scythian Gold

During many centuries the east of the ancient continent Europe has been attacked and invaded by horseback warriors and nomadic hordes: the Huns, Avars, Magyars, and Mongoles. Very long before (between the 9th until the 1st century BC) the Scyths inhabited the areas north of the Black Sea and dominated the western and central Eurasian steppes. Not much has been written about them, the best-known account is in the Histories of Herodot. And this people is mentioned also in the Bible.

The Scyths, probably related to Iranian people, were among the earliest nomads to master mounted warfare. They fought with bows and arrows on horseback. They developed a rich culture characterized by opulent tombs, fine metalwork and brilliant

Fig. 4 Golden Scythian pectoral or neckpiece, from a royal kurgan (burial mound) in Tosta Mohyla, Pokrov, Ukraine, dated to the second half of the 4th century BC. The pectoral is made of solid 24 carat gold and weighs about 1150 g

art style. At their peak, they came to dominate the entire steppe zone, stretching from the Carpathian Mountains to China and South Siberia [9].

The golden pectoral in Fig. 4 gives ample proof for the high level of goldsmithing of this people. The style is quite certainly Greek, although the imagery reflects Scythian interests. It consists of three sections: top section reflecting Scythian daily life; middle section representing Scythian connection to nature with numerous ornamental spirals of opposite chirality; and lowest section thought to represent Scythian belief in the cosmos and their myth.

As they had appeared from practically nowhere, they suddenly disappeared, but not without leaving permanent traces. At places now covered by thin grass, one has to dig deep. With some luck one will discover precious treasures, many of them made of gold and also mummies who tell about life at distant times.

3.4 Doguu, Japan

There are two kinds of old clay figures in Japan, doguu and haniwa. Both are figures of human beings or animals. Doguus were made during the prehistoric Jomon period (14000–400 BC), while haniwas were produced much later (3rd–6th centuries). Different from haniwa, which were found together with a dead body in mounded

Fig. 5 Doguu with various spiral patterns found in Muroran, Hokkaido, Japan (Tokyo National Museum)

tombs, it is not clear for which purpose doguus were created. About 15000 doguus have been found across Japan. Interestingly, there are no whole figures among them. They might have been intentionally broken. Figure 5 shows one of the doguus found in Hokkaido, Japan. The estimated time of creation is 1000–400 BC [10]. The clothes of this doguu exhibit spirals of different shapes, some of them composed in an intricate way.

4 From 2000 to 1 BC

4.1 Celtic Art

The Celts were an ancient people occupying the regions north of the Alps from 800 BC on. Later (450–60 BC) they settled from the Atlantic to the Black Sea and even as mercenaries in the region around today's Ankara in Turkey. There are no written records about them and their history and rituals have been transmitted by say [11].

Spirals are very common in Celtic symbolism. The Celts developed different spiral shapes which are presented in the following table, including short characterizations of their possible symbolism and meaning.

Celtic spirals

(a) spiral	(b) spiral	(c) double spiral	(d) cradle
(e) double spiral	(f) doubly centered spiral	(g) triskele	(h) spiral of life

a Basic structure of a left-winding spiral, found on many dolmen and burying places in Ireland and France. Its real meaning has still not been deciphered. One assumes that it signifies travels from the inside life to the outer soul, carrying along the notion of growth and cosmic energy

b Starting clock-wise from the center this spiral is strongly connected with water, power, independent motions and migration of tribes

c Two connected spirals are a variation of the basic spiral. Their chirality is opposite. It serves as a symbol for Becoming and Passing. The path of the spiral starts from a point, then approaches the end of the way, a point again

d This is a variant of the double spiral

e A further variant of the double spiral: more difficult to draw

f This spiral system denotes the duality of nature and equilibrium. There is a correspondence to the Yin Yang symbol. It symbolizes the number 2, which is also the symbol for the Moon

g This threefold spiral, also called triskele, is an ancient symbol of the druides. It symbolizes the becoming and the ending of life in our world. Aspects flowing outward come back to the point where everything began

h This example without beginning and without end symbolizes the threefold goddess. It is connected with the number 3 and is a symbol for the Sun

After Caesar's occupation of Gallia (a Celtic territory), the Celtic culture is severely damaged and mixed with Roman culture In the height of their existence

Fig. 6 The Celtic knot in "The Book of Kells". Reprint permitted by the Trinity College Library Dublin

the Celts suddenly disappear east of the Rhine river. But on the long run there remain areas where they can continue their life and their artistic achievements. On the British islands, after the breakdown of Roman rule (around 400 AD), Celtic traditions remain alive but under difficult conditions against the newly invading Angels and Saxons. This people has been slowly pushed towards the western boundaries of the continent, thereby preserving their ancient languages such as Irish, Scottish Gaelic, Welsh, Cornish, and Manx.

Celtic art, as popular as it is in our days, has an old history starting with Neolithic origins. Many symbols and ornaments are popular now, and they have been communicated to us through the centuries by a number of documents, for instance the richly illustrated "Book of Kells" [12] (8th or 9th century AD).

Also important is the abstract art that characterizes Celtic manuscripts. The main motif is the Celtic knot or Eternal knot. (See Celtic knot [13].) However, the Book of Kells features representational art, especially fantasized animals (Fig. 6).

4.2 Egyptian Spirals

Ancient Egyptian culture flourished between about 5500 BC with the rise of technology (as evidenced, for instance, in the glass-work of faience) and 30 BC with the death of Cleopatra VII, the last Ptolemaic ruler. This culture is famous today for

the magnificent monuments which celebrated the triumphs of the rulers and honored the gods of the land. The ancient Egyptian dynasties have been the source of amazing works of architecture and art.

When searching for the early use of spiral symbols, however, one is surprised how little they have been used during the centuries. But there are exceptions, although some of them may be found far away from the Egyptian heartland. We refer here to the ruins of Naqa, located in Nubia (today mostly in Sudan), the southern close neighbor of Egypt, which had a sometimes rather turbulent and often hostile relationship with the North. (The Kingdom of "Kush" even conquered Egypt around 700 BC and black pharaohs reigned the country for a while.)

Naqa Amun Temple

Naqa was only a camel or donkey's journey from the Nile, and could serve as a trading station on the way to the east; thus it had strategic importance, since rulers had to travel through the steppes when using a bridge between the Mediterranean world and Africa.

The site has two notable temples, one of them dedicated to the Egyptian deity Amun-Ra. The first European travelers reached Naqa in 1822 and since 1995 Naqa has been excavated. Archaeologists have cited Naqa as one of the most important centers of this first civilization coming from the deep south of Black Africa [14].

Amun was a deity in Egyptian mythology who in the form of Amun-Ra became the focus of the most complex system of theology in Ancient Egypt. Amun was often worshiped as a ram, God of their flocks and their fertility. Amun represented the essential and hidden, whilst in Ra he revealed divinity. The sculptures in Naqa temple, built around 50 AD, show the diversity of styles - there are clear influences from the hellenistic-roman and also from the Egyptian culture, thereby emphasizing in the figures the African ideal of beauty. The colossal twelve ram statues in front of the Amun temple show a classic-Egyptian posture of rams, where the stylistic spirals on one of them is without equal in Egypt (Fig. 7).
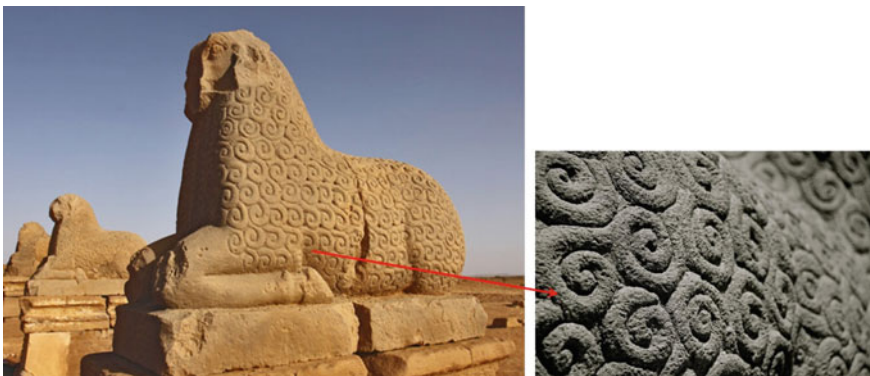
Fig. 7 Left: Rams as guards in front of the Amun temple of Naqa; right: close-up of spirals on the skin of a ram may represent fluffy curls of wool. Reprint permitted by D. Wildung/Naga Project

The inhabitants of Naqa left their city suddenly about 1800 years ago. Nobody knows why. The buildings were preserved by the sand similar to Pompeji under the lava streams. Thus it offers genuine information to archeology.

4.3   Thai Pottery

Ban Chiang denotes an archeological site located in Nong Han district, north-east Thailand. Discovered in 1957, the Ban Chiang Archaeological site attracted enormous publicity due to its distinctive red painted pottery.

Villagers in the Nong Han District in North East Thailand had uncovered some pottery without insight into its age or historical importance. In 1966 scientists familiar

Fig. 8   Bowl with base. Lopburi Thailand, Bang Chiang culture. 210–200 BC. Reprint permission by Museum für asiatische Kunst, Berlin

with possible ancient origins of civilization in Southeast Asia stumbled by chance into a place with exposed tops of pottery jars of small and medium sizes made by very rudimentary techniques.

According to the radiocarbon method the earliest grave dates from about 2100 BC, the latest about 200 AD. Bronze objects include bracelets, rings, anklets, wires and rods, spearheads, axes and adzes, hooks, blades, and little bells. Finally however, further analysis suggests that the initial settlement of Ban Chiang took place by about 1500 BC, with the transition to the Bronze Age about 1000 BC. Still the ceramics belong to the oldest on earth.

Many bowls are painted with red ornaments including imaginative patterns, bands or compact spirals. These are not so different from paintings on Egyptian pre-dynastic pottery of about 5000 years ago. Figure 8 shows a beautiful example of an elegant, filigran spiral that could be the product of a modern artist.

The importance of the Ban Chiang site to discovering the roots of the people of Thailand is a firm statement. UNESCO's designation of the Ban Chiang Archaeological Site as a World Heritage Site in 1992 highlights this importance [15].

4.4 Phaistos Disc

The ancient city of Phaistos on the south coast of Crete was part of the growing Minoan empire. While the city dates perhaps as far back as 6000 BC, the first Minoan palace was erected around 2000 BC.

It was destroyed by a strong earthquake in 1700 BC caused by a volcano erupting on the nearby island of Thera (now Santorini) and rebuilt on top of the old one. The palace was again destroyed a few centuries later, and again rebuilt. Around 1400 BC, Crete was invaded by the Achaeans of Greece and both cities of Phaistos and Knossos were destroyed.

The Phaistos Disc made of fired clay was discovered in 1908 in the Phaistos palace-site (see Fig. 9). It possibly dates back to the second millennium BC. The disk is about 15 cm in diameter and covered on both sides with stamped symbols. The inscription was apparently made by pressing hieroglyphic "seals" into the soft clay creating a body of text with reusable characters: an early document of movable type printing. It features 45 distinct signs in a clockwise sequence spiraling toward the center of the disk. Its purpose and meaning, and even its original geographical place of manufacture, remain disputed, making it one of the most famous mysteries of archeology.

Many attempts have been made to decipher the code behind the disk's signs. They have been compared with different writing systems: e.g., hieroglyphs, Linear A (undeciphered systems used in Minoan Crete), Linear B (Mycenian Greek, developed later than Linear A) and others. These attempts are generally thought to be unlikely to succeed unless reasonable comparison to other inscriptions can be made [16, 17].

Fig. 9 The Phaistos Disc, Creta, ≈ 2000 BC. Archaeological Museum of Heraklion

4.5   Maya Temple

Chichen Itza on Yucatan peninsula in Mexico was once a center of the Maya culture. It was a regional capital from the 10th century (the end of the late classic period) to the 13th century (the beginning of the terminal classic period). El Castillo is a step pyramid at Chichen Itza and it served the god Kukulkan, a feathered serpent. Therefore, it is also called the Temple of Kukulkan. The sculpture of the Kukulkan head at the foot of this pyramid has spirals on its right and left cheeks (see Fig. 10). Spirals are not common in Maya glyphs, but there are quite a few stelas, pottery bowls and columns with spiral patterns [18].

Fig. 10 A feathered serpent sculpture, Kukulkan, at the base of one of the stairways of El Castillo

4.6   Nazca Lines and Cantalloc Aqueducts

The Nazca lines are huge geoglyphs in the desert close to Nazca and Palpa in Peru. The area of the Nazca plain is about 500 km^2. There are lines, geometric shapes (triangles, trapezoids, circles, spirals, or combination of them) as well as figures of human beings, animals ("The Monkey" with a spiral tail, as shown in Fig. 11, left), and plants. These remarkable figures were created between 500 BC and 500 AD. The area of the largest figure is about 370 m^2. Why did they make such huge figures? How did they make them? There are various theories and speculations: religious reasons, astronomical aspects, or some useful applications [19, 20]. But till now there is no clear explanation yet.

Beyond their mysterious drawings in the sand Nazca people developed a practical sense for using spiral structures. They built ingenious aqueducts (more than 40) in the shape of spirals leading into depth, which were used all year round (see in Fig. 11, right). The aqueducts ensured the supply of water to the city of Nazca and the surrounding fields, allowing the cultivation of cotton, beans, potatoes, and other crops in an arid region [21].

Fig. 11 Left: "The Monkey" of the Nazca lines; right: Cantalloc aqueducts

4.7 Stupa at Sanchi, Bhopal, India

Sanchi is a town in central India and is famous for its Buddhist structures. The Great Stupa is one of the most famous Buddhist building complexes (Fig. 12, left), constructed 175–125 BC [22]. It has four gateways (south, north, west, and east). Each of them consists of three intricatedly carved architraves (crossbeams) supported by figures of elephants or other creatures. As shown in Fig. 12, (upper right, the northern gateway), both ends of each architrave are spirals, one being the mirror image of the other, which may be footprints of Buddha, or a Bodhi tree under which, as is widely alleged, Gautama became the Buddha, or a part of a snake (lower right of Fig. 12).

Fig. 12 Left: the Great Stupa at Sanchi viewed through the southern gateway; upper right: right and left ends of the crossbeams of the northern gate showing spirals; lower right: a Naga coil (serpent) with a small figure attached to it

5 From 1 to 1600 AD

5.1 Trajan's Column and Bernward's Column

Towering monumental columns have been frequently built to honor the glorious life of influential people. There are many of them in different cultures. Here we show in Fig. 13 (left) as an early and famous example the Columna Traiana erected for the Roman Emperor Trajan (53–117 AD) on the Forum Romanum. It was constructed from marble blocks and weighs 1100 tons. Placed there in the name of the Roman senate it has been a prototype for later honor or victory columns [23].

The stonemasons chose a ribbon climbing upward for about 27 m and winding 23 times as a helical band around the cylindrical column surface, thus creating a continuous band (length, 200 m) for the sculptors to present scenes from the life of the honored person (Fig. 13, middle). Scenes about successful wars are depicted and about 2500 persons appear.

This piece of architecture with a remarkable stability has remained at the same place until today. It is hollow and a spiral staircase with a whole turn every 14 steps leads upwards. Its steps have remained even and well-proportioned through all these centuries. The column shows an elegant way to tell an interesting story in space and time.

In the Romanesque cathedral of Hildesheim in Germany's north one can admire Bernward's Column, also called the Christ column (see Fig. 13, right). It is a
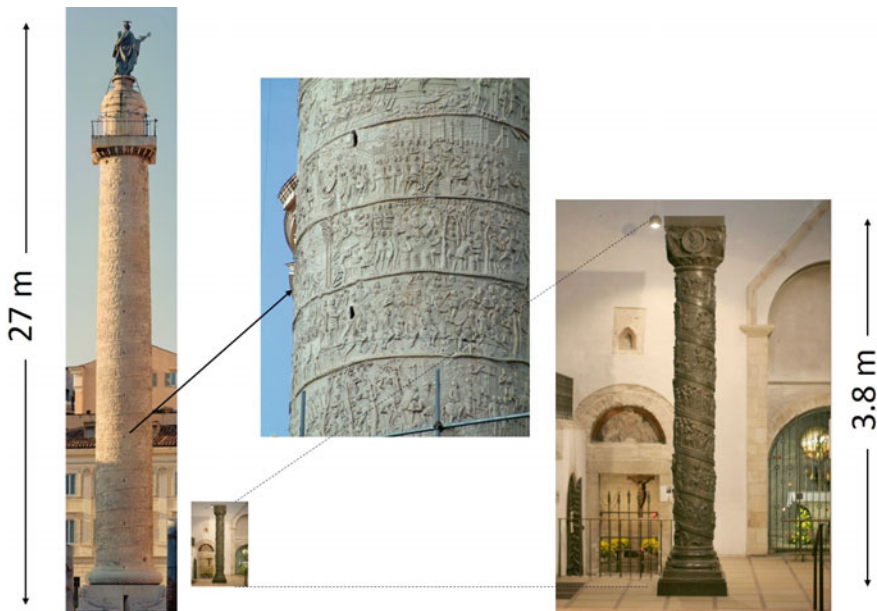

Fig. 13 Trajan's Column, Rome (left) and Bernward's Column, Hildesheim (right)

masterpiece of Ottonian art from the time of Bishop Bernward (993–1022), which had enormous significance together with some other artistic highlights of the time: e.g., the bronze Bernward Doors and the painted wooden ceiling of the Romanesque St. Michael's Church showing the genealogical tree of Jesus Christ and also located in Hildesheim (as a UNESCO World Heritage Site).

This is an honor column in conscious imitation of Trajan's marble column in Rome. It uses the same principle as Trajan's Column in that it depicts a sequence of events along a spiraling ribbon winding around the cylindrical surface of the column. The column had been cast in bronze (height 3.8 m, diameter 58 cm). Just as stone columns in Rome present the military deeds of the Emperor in an upward spiraling frieze, so Bernward's Column depicts the peaceful deeds of Christ, beginning with his baptism at the Jordan and ending with his triumphal entry into Jerusalem. The column was originally crowned with a triumphal cross [24].

Apart from the remarkable technical achievement, the scenes on this column express a liveliness and dynamic motion which was very unusual for the time. It reflects Bernward's efforts to create a Nordic Rome for the renewed Christian Imperium Romanum.

5.2 Nordic Symbols

A picture stone, or figure stone, is an ornate slab of stone, usually limestone, which was raised in Germanic Iron Age and Viking Age in Scandinavia. More than four hundred picture stones are known today [25]. The greatest number of well conserved stones is found on the island of Gotland (see Fig. 14, left) [26]. Cultural achievements in the northern parts of Europe may have been lost, because wood as a working material has decayed during the centuries. Stones have survived though, and thus we can admire ornamental patterns like many-fold spirals on picture stones often found on a pagan graveyard close to some church (provenance 5–14th century). Spirals may symbolize the Sun and may be related to the life cycle - birth and death. These spirals are reminiscent of Celtic symbols like the triskele (see Sect. 4.1), but usually have more than three spirals.

A characteristic symbol of Nordic art alluding to a rotating spiral is the vortex wheel (a modification of the swastika), dated to the 5th and 6th centuries AD (Germanic Iron Age) and mostly found in Sweden. This ornament is also engraved into slabs of stone. For understanding its suggestive appeal one should see the colors which have not been conserved up to our days. Probably red was combined with black and white. Many other motives have been used for decorating this type of stones such as fighting warriors, dragons, serpents, and others.

The half-moon shaped segments of the vortex wheel appear 6-, 12-, 16-, or 24-fold. Sometimes small triangles between these segments emphasize the impression of a rotating structure. The decorative edge is likely to represent the radiation of the Sun.

Fig. 14 Left: Vortex wheel on a picture stone found in Havor, Gotland, Sweden [26]; right: the stones or steles with spiral patterns discovered in the ruined city Citânia de Briteiros, Northern Portugal

A comparable tradition is found on the Isle of Man where high funeral crosses of stone were richly ornamented with the same teeming world of warriors and Norse deities as the image stones of Gotland.

Quite amazingly, wheels like the ones in Scandinavia were also known from the Iberian Peninsula. The stones or steles discovered in the ruined city Citânia de Briteiros, Northern Portugal, in Oppidum Santa Terga, Galicia, or in Cantabria, Northern Spain, are all about 1000 years older than the Nordic discoveries (Fig. 14, right) [27].

5.3 Buddha, Nara

The Rushanabutsu (Fig. 15, left) of the Todaiji Temple in Nara, the old capital of Japan, is familiar under its conventional name "Daibutsu" (the big Buddha). The construction began in 745 AD and took 7 years till the ceremony for "opening eyes". It was burned down twice in 1180 and 1567, and each time reconstructed. The height of the statue is 14.7 m. His head consists of hair forming a univalve shell. Buddha statues of Gandhara (an ancient Indian kingdom, now in Pakistan) has wavy
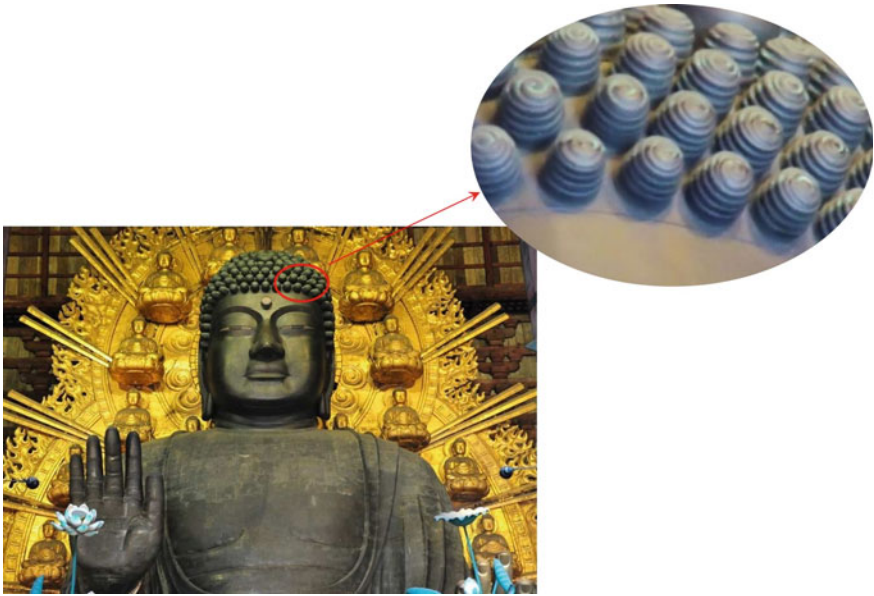
Fig. 15 Rushanabutus (big Buddha) in Todaiji, Nara, Japan 750 AD and the helix-shaped hairs

hairs, affected by Greek culture, while in Mathura (an Indian city, believed to be the birthplace of Krishna) the hairs form a helix shape, as shown in Fig. 15 (right). This shape was kept on its way through China and Korea to Japan. The diameter of the hair helix is 22 cm, the length 21 cm and its weight 1.2 kg [28].

5.4 Book of Gospels (Evangeliar), Quedlinburg

This luxurious Carolingian manuscript was written about 840 AD and richly decorated with numerous magnificent pictures. It was passed to the monastery of Quedlinburg, Germany (founded around 936 AD). As part of the treasure of the monastery's church it was robbed in 1945, but could be retrieved in 1989 under dramatic circumstances. Today it is exhibited in the Pierpont Morgan Library, New York [29].

Our picture shows the beginning of the Gospel according to John (in German, Johannes-Evangelium) with blue background and a text written in golden capital letters:
IN CHRISTI NOMINE INICIUM SANCTI EVANGELII SECUNDUM IOHANNEM [30] (Fig. 16).

An ornament is woven into the blue background: a vortex with a golden/blue abyss at its center, resembling the eye of a hurricane (see Fig. 2 in chapter **Appearance in Nature**). There is no explicit comment about its meaning, but it may relate to the first verses of the Genesis.

Fig. 16 Gospel Book Germany, Westphalia, mid 10th century. MS M.755 fol. 157r. Morgan Library and Museum

In the first book Moses, Chapter 1,1-2 the just created earth was without form and void, and darkness was about the deep and the Spirit of God moved upon the waters. Following some exegists the notion of a chaotic state without any shape was introduced (the Tohuwabohu), which is invaded by a primal flood, the abyss, symbolizing the abysm of the cosmos. And over all this the Spirit of God was moving.

What a scenario! Is it caught by the picture we have presented here?

5.5 *Samarra*

The minaret with a twisted spiral form in Samarra (the Great Mosque) was built in the middle of the 9th century by Abbasid Caliph Al-Mutawakkil (see Fig. 17, right).
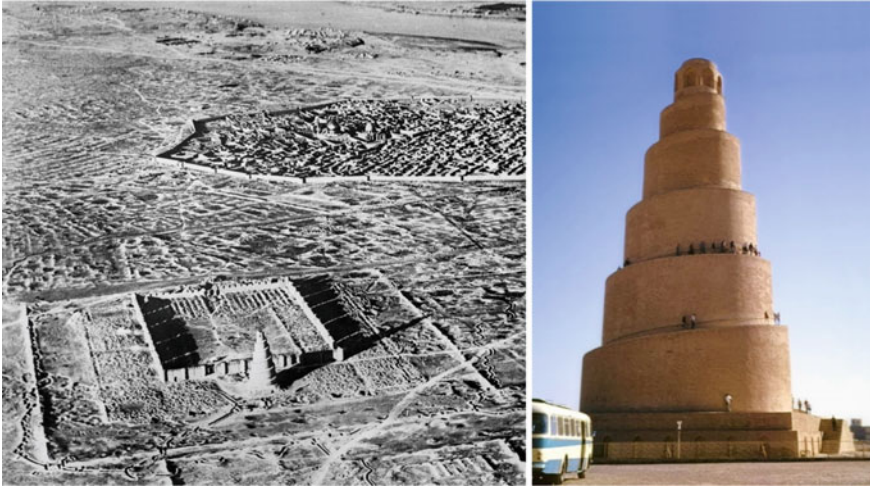
Fig. 17 Left: Samarra during the early 20th century, the mosque and its enclosure at the foreground and the city at the background; right: the great mosque of Samarra

Samarra is located in central Iraq and was the capital of the Abbasid Caliphate from 836 to 892: the capital before and after was Bagdad. Since the occupation was only short, the ruins of Samarra are well preserved as shown in the left photograph of Fig. 17 taken during the early 20th century. The tower stood at an outer enclosure of $444{\times}376$ m^2. Minarets with a spiral form were constructed during the 9th century in Egypt, too. Later the form of a minaret was changed to a column, dome or pencil form. But there often is a spiral staircase or slope inside [31].

5.6 Spiral Motives in the Medieval and the Renaissance Arts

Middle Ages

In the period between the Classical Age and the Renaissance, spirals continued to appear in Western Art, but in **Romanesque** (1000 ≈ 1200 AD) and **Gothic** style (≈1150–1500 AD) one does not encounter so many any more. Many surviving examples are rudimentary and simple, although some are more complex. The spiral pattern seems to have flourished mainly as an element of decoration, and - instead - labyrinths, plated bands or plant motives became dominating ornaments [32, 33].

Let us show a few examples in Fig. 18.

About 17 km west of Jerewan, Armenia, one finds the ruins of Swartnoz and the remains of the Armenian "Celestial Angels Cathedral" erected here in the middle of the 7th century and dedicated to the Holy Gregor. At the time of its construction this area had been overrun by Muslim Arabs and intensifying wars between the Byzantine and Arab armies influenced this building endeavor. The exterior church

Fig. 18 Top-left: "Armenian Ionic" capital on top of a column in the ruins of Swartnoz; bottom-left: capital in the Église Saint-Étienne de Franchesse; top-right: front of the inner portal bow of the church of the village San Pedro de Gaíllos (Province Segovia, Spain) displaying - also small spirals (1200 AD); middle-right: in the tympanon of the church of Bembrive (in the province Pontevedra, Northwest Spain) one detects 3 spirals (12th century); bottom-right: Prats-de-Mollo-la-Preste, the wooden church entrance door shows original iron-mounts with spiral motives (13th century)

design, featuring basket capitals with Ionic volute mounts, reveals the influence of Syrian and northern Mesopotamian architecture (see Fig. 18, top-left).

Another capital with spiral design is found in the church of the village Franchesse, located in central France between the cities Moulins and Nevers (Fig. 18, bottom-left). Frequently arches or tympani are chosen for the display of sculptures and symbols including spirals, as shown in the upper two pictures on the right side of Fig. 18. Finally spirals have been used for decorating wooden doors, as in the village Prats-de-Mollo-la-Preste ("Meadows of Mollo") located in the canton Le Canigou

in the Pyrénées near the Spanish border (Fig. 18, bottom-right). Similar decorations are found in Navata, province Girona, Spain, for the Prieuré de Marcevol in the Roussillon and for other Romanesque doors in the Pyrénées.

But we do not recall any important treatise from medieval times that focuses on the meaning and significance of the spiral in a religious, spiritual, scientific or artistic sense. There are exceptions, of course: the name of Hildegard von Bingen (1098–1179) has to be mentioned as the outstanding woman of the time. She was, as a Benedictine, an abbess, poet, composer and a well-known universal scholar concerned with mysticism, medicine, ethics, and cosmology. She was worshiped for her personality as a holy person. Although she did not explicitly include spirals into her teaching, she is frequently quoted with the sentence:
Angles fly in spirals, the devil only straight ahead (what experts think she never said).

The Gothic workmen of the 13th century welcomed the spiral as a decorative motive almost more warmly than their Greek predecessors had admired it before them. But factually, in the decorations of the facades or the spacious interior of Gothic cathedrals one does not find so many spirals. Instead, one used ornaments like flamboyant patterns, plants as templates, especially oak leaves or the gable (Wimperg in German). The window painting was preferred to frescos.

Renaissance

The advent of the Renaissance epoch (15/16th century) signifies the European cultural changes in the times of a rebuilding phase leading the Middle Ages to Modern Times. Efforts were made to revive the cultural achievements of the Greek and Roman antique. Starting from Italy, artists and scientists influenced other countries, in particular those north of the Alps, by their innovative painting, architecture, sculpture, literature, and philosophy [34].

A significant influx of Islamic civilization, culture and science contributed to these new and modern ways, such that revival in the Renaissance of central Europe implemented Arabic elements from Spain or from Asiatic countries: for example, from Samarkand in Uzbekistan which was an important station on the silk road. This local capital preserves until today magnificent buildings of Islamic Renaissance art.

The overwhelmingly rich artistic and architectural resources used in the Renaissance period do not assign a particular importance to spirals or vortices. Nevertheless, these symbols found acceptance in decoration and architecture when spirals were introduced, for instance, in arabesques or in the form of volutes.

The arabeske (from Italian arabesc) developed from ornaments exhibiting Hellenistic examples. It mainly consists of entwined lines of stylized plant tendrils. Originally there is a connection to Arabic graphic characters (see Fig. 19). It made its way to Europe through Moorish art in Spain. Some of the most impressive arabesques can be admired in the halls of the Alhambra in Grenada, Spain.

In Renaissance art we often find volutes (French expression for "rolled up"), also derived from Hellenistic art. In the design of capitals of Greek columns one had developed different types. Besides the Doric and the Corinthian column the Ionic one with a pair of volutes was very popular (Fig. 20, left). Volute may be found at consoles, gables or capitals.

Fig. 19 Part of a 15th century ceramic panel from East Islamic Samarkand with white calligraphy on a blue arabesque background

In the construction of basilica-type churches there are angles to be considered which form between the broad lower façade and the upper narrower parts (Fig. 20, right). An S-shaped form together with small volutes at the lower end is then incorporated to conceal the abrupt transition between lower and upper portion of the façade. Later on, these spirals in form of volutes will be highlights in the Baroque era and the Art Nouveau (e.g., in the work of Gustav Klimt, see chapter **The Arts and Beyond**).

In Renaissance sculpture the Figura Serpentinata (serpent-like) denotes a tortuously designed figure. From the ornamental point of view this belongs to the spiral motives. It is a characteristic feature of the mannerism, a style developed in the late stages of Renaissance art. As an antique masterpiece of this style we show the famous Laocoön group, created probably around 200 BC by Greek sculptors from Rhodos. A copy of the lost original was excavated in Rome in 1506 and then displayed in the Vatican (Fig. 21). Early representations of such "screwed" figures were created by da Vinci, Raffael and Michelangelo.
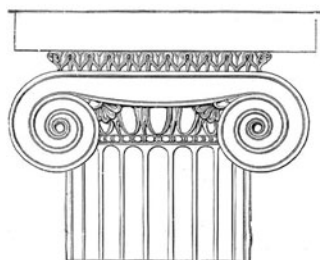
Fig. 20 Left: Ionic Capital from the Temple of Minerva Polias at Priene in West Turkey, north of Milet (≈ 700 BC); right: Basilica Cattedrale di Santa Maria Assunta in Carpi, Italy

Fig. 21 The Laocoön group in the Vatican museum

With this compact overview of Medieval and Renaissance art we close the chapter on Cultural History. For all the aspects that have flown into the developments of modern history, some relevant information can be found in a subsequent chapter **The Arts**

and Beyond. There is a number of personalities and artists to be introduced. Cultural achievements of interest in modern times will be highlighted and acknowledged.

Picture credits

Fig. 1 Permitted by Francisco Forero Bonell/Ecoplanet, Fig. 2 CC BY-SA 2.0, Fig. 3 CC SA 3.0. Fig. 4 FAL 1.3, Photograph: D. Kolosov, Fig. 5 Photograph: Saigen Jiro, Public domain, Fig. 6 Trinity College Library Dublin, Fig. 7 Photograph: Naga Project Staatliches Museum Ägyptischer Kunst München, permitted by Prof. Dr. Dietrich Wildung, Head of the Naga Project, Fig. 8 Publication permission from Abt. Süd-, Südost- und Zentralasien Museum für asiatische Kunst Staatliche Museen zu Berlin - Stiftung Preußischer Kulturbesitz, Fig. 9 Publication permission from Ministry of culture and sports, Hellenic Republic, Fig. 10 Photograph: Kinko Tsuji, Fig. 11 Left photograph Maria Reiche, Public domain, right Photograph: Diego Delso, CC-BY-SA, Fig. 12 Left photograph: Suyash Dwivedi, CC BY-SA 3.0, top right CC BY 3.0, bottom right photograph: Anandajoti Bhikkhu, CC BY 2.0, Fig. 13 CC BY-SA 3.0, Fig. 14 CC BY-SA 4.0, Fig. 15 Publication permission from the Todaiji Museum, Fig. 16 Publication permission from the Morgan Library and Museum, Fig. 17 Left: Created and released by the Imperial War Museum on the IWM Non Commercial Licence. Public domain, right: photograph, IgorF - vlastni, CC BY-SA 3.0, Fig. 18 CC BY-SA 3.0, Fig. 19 By Marie-Lan Nguyen (User:Jastrow), 2009-02-28, CC BY 2.5, https://commons.wikimedia.org/w/index.php?curid=6097314, Fig. 20 CC BY-SA 3.0, Fig. 21 CC BY-SA 4.0

References

1. *dtv-Atlas Weltgeschichte - Von den Anfängen bis zur Gegenwart*, 3rd edn. (Deutscher Taschenbuch Verlag, München, 2010)
2. J. Diamond, *Guns, Germs, and Steel: The Fates of Human Societies* (W.W. Norton and Company, New York, London, 1999)
3. H. Hartmann, H. Mislin (eds.), *Die Spirale: im menschlichen Leben und in der Natur, eine interdisziplinäre Schau* (Birkhäuser AG, Basel und Reinach, 1985)
4. https://www.iucn.org/content/colombia-makes-history-huge-expansion-largest-national-park
5. D. Alberge (20 June 2015). World's most inaccessible art found in the heart of the Colombian jungle. The Guardian. 20 June 2015. https://www.theguardian.com/world/2015/jun/20/colombia-wilderness-film-maker-prehistoric-rock-art
6. https://www.smithsonianmag.com/sponsored/australia-northern-territory-ancient-aboriginal-rock-art-sites-cultural-outdoor-travel-180962576/
7. M.J. O'Kelly, *Newgrange: Archaeology, Art and Legend* (Thames and Hudson, London, 1982)
8. K. Mayrhofer, *The Prehistoric Temples of Malta and Gozo: A Description by Prof. Sir Themistocles Zammit*, 2nd edn. (S. Masterson, Cincinnati, 1997)
9. C.I. Beckwith, *Empires of the Silk Road: A History of Central Eurasia from the Bronze Age to the Present* (Princeton University Press, Princeton, 2009)
10. Bulletin of the National Museum of Japanese History, vol. 68 (National Museum of Japanese History, Sakura-city, Japan, 1996)
11. N. Chadwick, *The Celts* (Penguin books, London, 1998)
12. P. Brown, *The Book of Kells (48 pages and details in colour from the manuscript in Trinity College Dublin)* (Thames and Hudson, London, 1980), p. 24
13. I. Bain, *Celtic Knotwork* (Constable, London, 1990)
14. *A Brief Guide to Naqa, Musawwarat-Es-Sofra, Meroe* (Archaeological Research, Sudan, 1994)
15. A.J. Labbé, *Prehistoric Thai Ceramics: Ban Chiang, Lopburi, and Khok Phanom Di and Related Sites in Regional Cultural Perspective* (White Lotus Press, Chonburi, Thailand, 2002)
16. J. Chadwick, *The Decipherment of Linear B* (Cambridge University Press, Cambridge, 1958)

17. M. Paulus, *Der Diskos von Phaistos/The Phaistos Disk* (Verlag Dr. Kovač, Hamburg, 2014)
18. M.D. Coe, *The Maya*, Revised edn. (Thames and Hudson, London, 1980)
19. J. Golomb, Nasca Lines - The Sacred Landscape. National Geographic 23 August 2016. https://www.nationalgeographic.com/archaeology-and-history/archaeology/nasca-lines/
20. C. Rohrbach, *Botschaften im Sand: Reise zu den rätselhaften Nazca-Linien in Peru*, 2nd edn. (National Geographic und Frederking and Thaler, München, 2006)
21. https://en.wikipedia.org/wiki/Cantalloc_Aqueducts
22. J. Shaw, *Buddhist Landscapes in Central India: Sanchi Hill and Archaeologies of Religions and Social Change, C (Thrid Century BC to Fifth Century AD* (Routledge, New York, 2016)
23. F. Leppard, S. Frere, *Trajan's Column* (Fonthill Media, Stroud, 2016)
24. B. Gallistl, *Der Dom zu Hildesheim und sein Weltkulturerbe: Bernwardstür und Christussäule* (Bernward, Hildesheim, 2000)
25. K. Düwel, *Runeninschriften als Quellen interdisziplinärer Forschung* (Walter de Gruyter, Berlin, 1998)
26. https://www.eixdelmon.com/engraved-stone-found-in-havor-gotland/
27. P.L. MacKendrick, *The Iberian Stones Speak: Archaeology in Spain and Portugal* (Funk and Wagnalls, New York, 1969)
28. http://www.todaiji.or.jp/contents/qa/qa.html#q5, http://www.todaiji.or.jp/contents/qa/qa.html#q6
29. E. Sano, D. Kusin (eds.), *The Quedlinburg Treasury* (Dallas Museum of Art, Dallas, 1991)
30. F. Mütherich, K. Bierbrauer, B. Fischer (eds.), *Das Quedlinburger Evangeliar* (Prestel, München, 1991)
31. A. Northedge, *The Historical Topography of Samarra* (British School of Archaeology, Iraq, 2005)
32. A. Hartmann-Virnich, *Was ist Romanik? Geschichte, Formen und Technik des romanischen Kirchenbaus* (Wissenschaftliche-Buchgesellschaft, Darmstadt, 2004)
33. G. Binding, *Was ist Gothik? Eine Analyse der gotischen Kirchen in Frankreich, England und Deutschland 1140–1350* (Wissenschaftliche-Buchgesellschaft, Darmstadt, 2000)
34. H. Günther, *Was ist Renaissance? Ein Charakteristik der Architektur zu Beginn der Neuzeit* (Wissenschaftliche-Buchgesellschaft, Darmstadt, 2009)

Appearance in Nature

Stefan C. Müller and Kinko Tsuji

Abstract Many spirals and vortices appear in nature both in the inanimate and the living world. As examples of the non-living nature some spirals and vortices of various sizes are selected: spiral galaxies, hurricanes and tornadoes, aerodynamic turbulence, crystal growth on surfaces and carbon nanotubes. In the realm of living structures, we consider rigid spiral forms (for example, seashells and snails), as well as flexible ones like the tail of a chameleon or a sea horse. Beyond fauna we find in flora many flowers and leaves that are arranged in spiral form. A general spiral tendency in vegetation is discussed, following ideas proposed by J.W. Goethe. The Fibonacci numbers, which are closely related to the positioning of leaves, are introduced. Other interesting topics are Leonardo's flying spiral, insect eyes and fish vortices.

1 Introduction

A homework for school children: "Find spiral forms in nature".

The next day some children brought snails or some kind of fiddlehead ferns, some children showed their fingerprint and hair whirl, and others had made a photograph of water flow at the suction opening in the bathtub or showed a photograph of a tornado which had appeared in a newspaper.

S. C. Müller (✉)
Institute of Physics, Otto von Guericke University Magdeburg,
Universitätsplatz 2, 39106 Magdeburg, Germany
e-mail: tsuji-mueller@t-online.de

K. Tsuji
Shimadzu Europa GmbH, Albert-Hahn-Straße 6-10, 47269 Duisburg, Germany
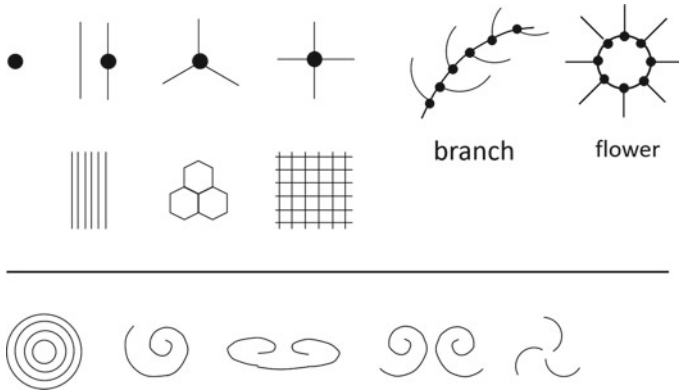e-mail: kts@shimadzu.eu

Fig. 1 Nodal points of crossing lines and curved forms

There are in fact many spirals and vortices in our environment: in fauna and flora, as well as in the non-living world. But why are spirals formed? Would it be a problem for snails to have a circular cone? Why does water not flow straight away from the bathtub? Why or how are tornadoes created? Why have some proteins helical form? Here we encounter many, many questions. And to each question there is for many cases an appropriate answer.

Before we try to answer such questions, we will identify some of the structural elements, which play an important role in the processes of pattern formation in nature. Many of these elements are found by a reduction to basic aspects of the mathematical field of topology (see Fig. 1).

Let us start from a simple point which in mathematics has zero dimension, i.e., it can, in principle, not be seen, but it exists at the designed location. Points will play a role for pointed patterns like the arrangement of leaves in a sunflower. As a next step we introduce a line having dimension 1 and extending indefinitely. Many such lines in parallel produce well known patterns, as they appear in cloud streets, stripes on animal skins, in desert sand, and elsewhere. These occupy the plane, i.e., a two-dimensional domain.

As illustrated in Fig. 1 a line may be divided by a nodal point from which lines or line segments extend into two opposite (or different) directions. More interestingly, three arms may emanate from the point into three different directions. This is the elementary pattern as a basic step to form, for instance, a hexagonal structure, as we know it from honey combs, hydrodynamic convection, insect eyes and many more cases. Again these expand into two dimensions. Considering a nodal point of the order of 4 (starting point for 4 directions), we find the element of quadratic patterns covering the plane.

Successively arranged nodal points can form patterns which closely resemble biological ones, such as branches or flowers as shown in the upper right of Fig. 1. Certainly higher orders also exist.

The lower part of Fig. 1 shows further developed forms. Around a point a circle or concentric circles can form. A line can form a spiral. In the framework of mathematical descriptions a simple circle requires three parameters to be defined: the location

of its center in the plane (two coordinates) and the radius determining the trace of the angular motion along the circular curve. A simple and regular spiral (like an Archimedean one) requires at least four parameters: the two center coordinates, the initial angle of motion and the growing distance from the center, yielding the spiral pitch (see chapter **Spirals, Their Types and Peculiarities**). Not to speak about the location of beginning and ending points. Thus, a spiral is a more intricate symbol than the circle.

A spiral can be left-wound, right-wound, both curled up or curled down or, in a pair, one curled up and the other curled down. When a line is divided into two directions, two spirals would develop from it. For a nodal point of the order 3, a triskele can emanate and further on, for higher order, multi-armed spirals can form, for instance, in the leaf arrangement.

In this chapter we proceed for the inanimate world from very large spirals of the order of 10^{20} m (galaxies) to very small helices of the order of 10^{-8} m (carbon nanotubes). We include the aurora, spiral forms on Mars, various air flows/turbulences and the surface of minerals. There are various mechanisms for their origin, most of them certainly relating to nonlinear phenomena. For plants such nonlinearities appear often in the leaf arrangement (phyllotaxis), for example patterns seen in a pine cone. The Fibonacci numbers and the golden angle, which are strongly related to the leaf arrangement, are explained in detail in the Appendix and Sect. 3.4. Interestingly, J.W. Goethe has already thought about spiral formation in the metamorphosis of plants and animals. Other spiral examples are: lichen, some corals and algae, or insect eyes. We also show a "collective spiral": different from spirals of individual objects, some creatures (for example, amoebae and fish) behave as a collective and actively form spirals or vortices.

We will explore various mechanisms of spiral creation. Some of these have already been established on solid scientific arguments. In other cases, if based on speculative evidence, we restrict ourselves to qualitative reasoning.

2 From Big to Small in the Inanimate World

2.1 Spiral Galaxy [1]

In our long journey through space we follow a complex path. We may not be astronauts in a small capsule, but just living on the surface of our planet Earth is sufficient to experience a compound pathway: we rotate around the axis of our planet once a day (with a maximum speed of 0.465 km/s). Since the Earth circles around the Sun once every year, we have to include a speed of 29.8 km/s. In addition to these circular motions the location and dynamics of the solar system in our galaxy (the "Milky Way") has to be considered. In this huge assembly of stars or our Sun is located about 28,380 light years (721×10^{12} km) away from its center and moves with a speed of 250 km/s. One revolution around the galaxis center would last 220×10^6 years.

Fig. 2 Barred spiral galaxy NGC 1300, viewed nearly face-on. Hubble space telescope image, ESA, NASA

Thus, our Milky Way rotates, and this rotation is connected with its spiral shape. Beyond our own Milky Way, other rotating galaxies which we cannot see with the naked eye (except for our neighbor, the Andromeda galaxy, and the Maghellan clouds) are abundant in our universe.

Shape and Dynamics

A galaxy is a gravitationally bound system of stars, interstellar gas, dust, and dark matter. Galaxies range in size from dwarfs with just a few hundred million stars to giants (10^{14} stars), each orbiting the center of mass of the galaxy.

Galaxies have elliptical, spiral or irregular shapes. Among the spiral galaxies one has a subdivision for barred spiral galaxies including our own Milky Way, which is a large disk-shaped barred spiral galaxy about 30 kpc[1] in diameter and a kiloparsec thick. It contains about 200 billion stars and has a total mass of about 600 billion times the mass of the Sun.

Figure 2 shows the barred spiral galaxy NGC 1300. There are linear, bar-shaped bands of stars that extend outward to either side of the core, then merge into the spiral arm structure.

Galactic spiral arms have the shape of an approximate logarithmic spiral, a pattern that can be theoretically shown to result from a disturbance in a uniformly rotating mass of stars. In earlier years astronomers had discussed the "winding problem" thinking that the spiral arms were material. But then the arms would become more and more tightly wound, since the matter nearer to the galaxy center rotates faster

---

[1] 1 pc $\approx$ 3.26 light years $\approx 30.9 \times 10^{15}$ m.

than the matter at its edge. The arms would become indistinguishable after only a few spiral orbits.

Lin and Shu proposed in 1964 [2] that the arms were made up of areas of varying density, similar to a traffic jam on a highway. The cars move through the traffic jam: the density of cars increases in the middle of it. The traffic jam itself, however, does not move much. In the galaxy, stars, gas, and dust move through the density waves, are compressed, and then move out of them. More specifically, this density wave theory argues that the gravitational attraction between stars at different radii prevents the so-called winding problem, and actually maintains the spiral pattern [3]. In fact, like the stars, spiral arms rotate around the center and they do so with constant angular velocity.

As an implication, when clouds of gas and dust enter into a density wave and are compressed, the rate of star formation increases as some clouds collapse to form new stars. Since star formation does not happen immediately, the stars are slightly behind the density waves. The compression wave triggers star formation preferentially on the leading edge of the arm, where young massive (blue) stars exist, whereas one has an abundance of old, red stars in the remainder of the galactic disk.

Bars are thought to be temporary structures that can occur as a result of a density wave radiating outward from the core, or else due to a tidal interaction with another galaxy. Many barred spiral galaxies are active, possibly as a result of gas being channeled into the core along the arms.

Recent estimates of the number of galaxies in the observable universe range from 200 to 2000 billion or more, containing more stars than all the grains of sand on the planet Earth. The space between galaxies is filled with a tenuous gas having an average density of less than one atom per cubic meter.

2.2 Aurora [4]

Those of us who had the chance to watch polar lights will often say that this was the most impressive and breathtaking experience of a natural phenomenon they ever had. The phenomenon can be observed in northern latitudes as Aurora Borealis or equally well and almost symmetrically in the south as Aurora Australis.

In greenish dim light the Aurora appears above the horizon and displays magically moving patterns, often like fluttering "curtains" or, in rare cases, as a large radiating spiral as shown in Fig. 3.

Imagine an isolated proton or electron traveling into deep space. It just has been ejected from the upper atmosphere of the Sun, the corona, and travels with the solar wind and the embedded interplanetary magnetic field. Maybe it will approach the surface of the Earth. Its radiation would do severe damage to any life that might exist, but the magnetic field of the Earth serves as a shield, redirecting the charged material around the planet so that it streams beyond it. Due to a process called "reconnection", charged particles flow back to the magnetic poles of the planet, guided through the geomagnetic field by curling around the field lines. This causes the display of the aurora.

Auroras can be amazingly rich in color. It depends on intensity of the solar wind and altitude where the aurora occurs. Red auroras appear at the highest altitudes emitted from excited atomic oxygen, but are visible only under very intense solar activity. At lower altitudes a green emission dominates. In fact, green auroras are the most common ones. The excited molecular nitrogen plays a role here, as it can transfer energy by collision to an oxygen atom. The radiated wavelengths correspond to forbidden transitions of atomic oxygen. Blue and purple auroras are seen at yet lower altitudes, where atomic oxygen is uncommon. There, molecular nitrogen and ionized molecular nitrogen are responsible for these colors. Purple emissions show up at the highest levels of solar activity.

The connection between the aurora and sunspot activity has been suspected since about 1880. We know now that during sunspot periods a much increased amount of electrons and protons from the Sun are blown towards the Earth in the 'solar wind' and are deflected by the magnetosphere of the Earth.

Polar lights frequently appear as a diffuse glow in form of a quiet arc or, at higher intensity, as active "curtains" which evolve and change rapidly, with an impressive motion recalling the wind blowing through the curtains' lower edge. Rippling of the curtains consist of many parallel rays, each lined up with the local magnetic field of the magnetosphere. The light emission generally extends from 80 km, where the density of atmospheric oxygen strongly decreases, to as high as 640 km above the surface of the Earth. Behind this amazing phenomena there are in part the complex laws of magnetohydrodynamics - the study of electrically conducting fluids - interacting with the impinging charged particles. If the fluid is moving, magnetic fields induce currents, which in turn polarize the fluid and change the magnetic field itself.

Fig. 3 Aurora vortex above Sandvika in Norway. Licenced from PA picture alliance

In polar areas all around the globe the aurora has given rise to myths and stories. The Saami in Norther Scandinavia associate polar light with dancing women or with their deceased ancestors who want to communicate with them. Indians of North America believe that medicine men meet to get into contact with them.

2.3 Spiral Formations on Mars

Before returning to our own planet Earth, we notice a spiral formation on our neighbor Mars. Observations have been made of spiral troughs of the polar ice caps with deep canyons spiraling out from the north and south poles, covering a distance of hundreds of miles (Fig. 4). These may be the product of changing seasons on Mars, scientists say. They show that summer sunlight has melted small cracks to build troughs in the ice, each half of the size of the Great Canyon at 8 km wide and 800 m deep.

In a model calculation based on equations for excitable media (see chapter **Kinematics of Spiral Waves in Excitable Media**) propagating waves are reproduced over thousands of years very similar to those in the north polar ice cap. The canyons deepened and aligned over time into the curious spirals seen only on Mars. Forming such spirals requires a large ice cap, a thin atmosphere and temperatures around the freezing point during the summer [5].
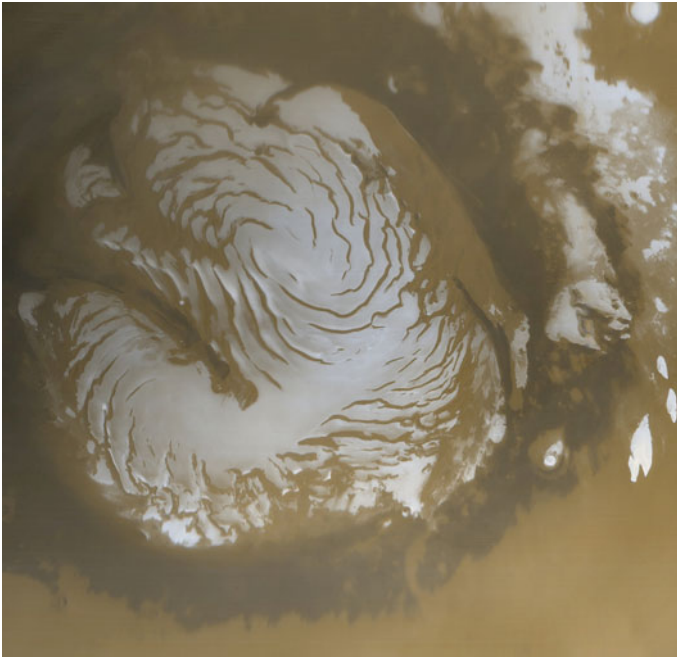

Fig. 4 Martian north polar cup. NASA/JPL/Malin space science system

2.4 Hurricanes and Tornadoes

Hurricanes belong to the strongest storms on the Earth. They are tropical cyclones that mainly appear in the equatorial region of the Atlantic and in the northeastern Pacific Ocean. Similar vortex-like motion of atmosphere and water appear in the northwestern Pacific Ocean under the name typhoon. These can move towards the coastlines of countries in East and South-East Asia [6].

Wind speeds may reach 300 km/h causing immense damage when they hit a coast with mostly unprotected settlements. This is much higher than the wind speed of violent storms of 118 km/h. For hurricanes and typhoons special categories from 1 to 5 have been introduced. Each higher category involves a higher wind speed.

Hurricanes (an example shown in Fig. 5) form in the zone of trade winds at a water temperature above 26.5 °C. Water evaporates in large quantities and rises due to convection. Condensation leads to the formation of large clouds. This condensation of large water volumes releases enormous energies which contribute to heating the clouds. A high air pressure above the clouds then causes a counter-directed vortex. Subsequently, spiral-shaped rainy bands form. The air masses directed towards the bottom are subjected to the Coriolis force and start to rotate with their winds
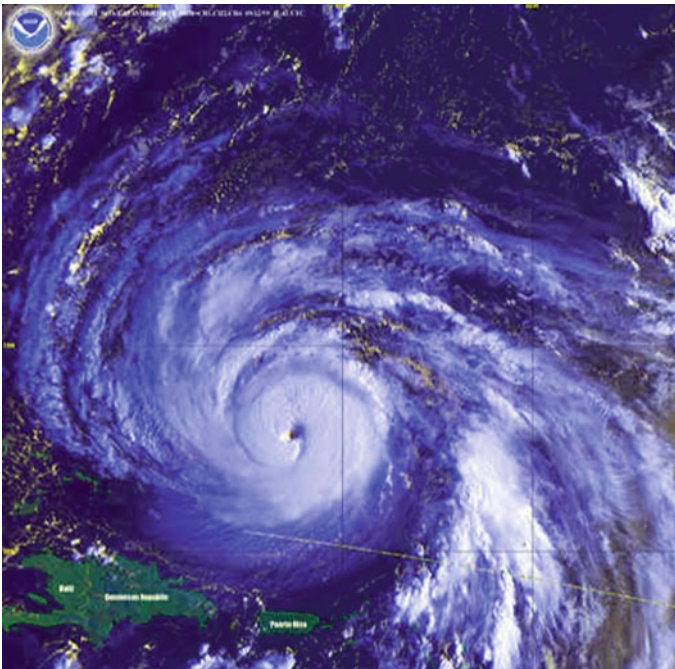

Fig. 5 Category 4-hurricane Floyd (1999) seen from a weather satellite. Highest wind speed: 250 km/h. Affected areas: Florida, Bahamas, North Carolina, Maryland. Photographed by NOAA (National oceanic and atmospheric administration), NASA

blowing counterclockwise in the northern hemisphere and blowing clockwise in the southern hemisphere. Tropical cyclones are typically between 100 and 2,000 km in diameter. The upper circulation of strong hurricanes extends into the tropopause of the atmosphere, which is at 15,000–18,000 m altitude.

Although their effects on human populations are often devastating, tropical cyclones can relieve drought conditions. They also carry heat energy away from the tropics and transport it toward temperate latitudes. This may play an important role in modulating regional and global climate.

Hurricane Eye and Center

At the center of a mature tropical cyclone, air sinks rather than rises. For a sufficiently strong storm, air may sink over a layer deep enough to suppress cloud formation, thereby creating a clear "eye". Weather in the eye is calm and free of clouds, although the sea may be extremely violent. The eye has normally a circular shape, and is about 30–65 km in diameter, though eyes as small as 3 km and as large as 370 km have been observed (see Fig. 5).

The cloudy outer edge of the eye is called the "eyewall". The eyewall typically expands outward with height, resembling an arena football stadium; this phenomenon is sometimes referred to as the stadium effect. The eyewall is located where the greatest wind speeds are found: air rises most rapidly, clouds reach to their highest altitude, and precipitation is the heaviest.

Similar but not the Same: Tornadoes [7]

One could call the tornado the small brother of the hurricane, because it is an air vortex in the atmosphere of the Earth on a much smaller spatial scale than a hurricane. But its destructive potential is comparatively large, as we know from so many incidents.

A tornado is a vortex with almost vertical rotation axis extending from the bottom to the lower boundary of the clouds (Fig. 6, left). The fierce storms can happen at any time of year but are very common in May and June in North America, when atmospheric conditions tend to be just right for their formation. The most notoriously affected region in the United States, called "Tornado Alley," includes the Great Plains states of Kansas, Nebraska, and the Dakotas, as well as parts of Texas with about 1200 strikes per year. In Europe the yearly number is 330. Tornadoes remain deadly and relatively unpredictable, despite recent advancements in weather science.

Most tornadoes last for less than ten minutes, but large tornadoes usually last longer - around 30 min. Powerful tornadoes have wind speeds of up to 470 km/h. Actually, the highest ever recorded wind speed is 496 km/h (Oklahoma, 1999). They can be more than 3 km wide and spin across the ground for dozens of miles. However, the more common tornadoes have wind speeds of less than 180 km/h, are about 80 m across, and travel only a few miles before they dissipate.

The generation of tornadoes is a very complex phenomenon and until today investigated by many scientists. The most intense tornadoes (called "twisters") emerge from what are called supercell thunderstorms. These require certain ingredients including warm moisture near the surface and relatively cold, dry air above. The warm air will be buoyant, and like a hot-air balloon it will rise. A supercell requires

Fig. 6 Left: Tornado in the Canadian province Manitoba, 2007. ©Justin1569 at English Wikipedia; right: spiral-shaped waves of excitation that also rotate around a quasi-quiescent center. ©Hess, Markus, Müller, Plesser, 1987, Dortmund

also winds that increase in strength and change direction with height. Then the updraft tends to rotate, and that makes a supercell. It churns high in the air and frequently leads to the formation of a tornado below it. This happens when air descending from the supercell causes rotation near the ground. Interestingly, one does not yet understand how tornadoes die.

Cyclones and tornadoes live from a driving energy available by local meteorological conditions. Both form vortices of rotating water and air that move around a relatively calm center. The center itself is usually subjected to a significant motion itself. Remarkably, in chemistry a quite analogous behavior is observed in reactive media in which an excitable state is formed [8]. This type of systems (see chapter **Chemical Oscillations and Spiral Waves**) is apt to form spiral-shaped waves of excitation that also rotate around a quasi-quiescent center (the core) and display a reaction distribution that resembles the typical shape of a tornado (the "chemical" tornado, see Fig. 6, right).

2.5   Air Flow and Turbulence Caused by Obstacles

Kármán Vortex Street

In our age of satellite observation, phenomena on the surface of the Earth become visible that we have never seen before. In meteorology one focuses this technology to detect cloud formations for predicting the weather. In this context, sometimes unusual cloud patterns are observed as shown in Fig. 7 (top): a street of successive vortices hundreds of kilometers long and developing behind an island, which can be barely identified in the upper left corner. Fact is that the flow of atmospheric air over obstacles such as islands or isolated mountains sometimes gives birth to Kármán vortex streets. When a cloud layer is present at the relevant altitude, the streets become visible.
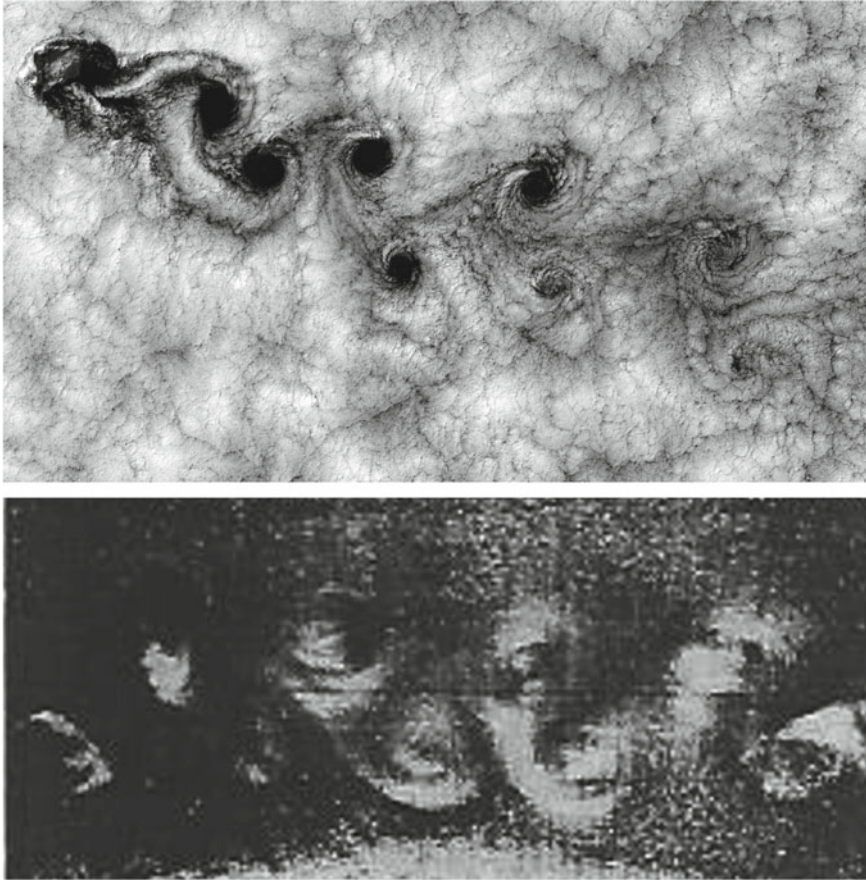
Fig. 7 Top: Kármán vortex street generated by the mountain tops of the island Alejandro Selkirk in Chile. Photograph taken by NASA GSFC; bottom: downstream wake development behind a flat plate, Re = 8150, visualized by aluminium dust, illuminated by a sheet of light [9]. Reprint permission from JPS Japan

An analogous phenomenon had been found much earlier in the laboratory and theoretically analyzed by von Kármán in 1911 [10]. This vortex street is a phenomenon of fluid dynamics, where behind an obstacle in a flow repeating pattern of swirling vortices form, caused by a process known as vortex shedding, which is responsible for the unsteady separation of flow of a fluid around blunt bodies. (Henri Bénard had done corresponding experiments already in 1908.) Taneda observed the flow at a great distance downstream from the body and visualized such a Kármán vortex street successfully by using aluminium dust suspended uniformly in water [9] (Fig. 7, bottom). This pattern is very similar to that of Fig. 7 (top).

A vortex street will only form in a certain range of flow velocities, specified by a range of Reynolds numbers (Re),[2] typically above a critical value (Re_c) of about 90. If Re is smaller than Re_c, the flow is laminar. If Re is larger than Re_c, the flow becomes turbulent.

Kármán vortices may appear in the wake of obstacles in a flowing medium. Periodic crosswind forces set up by vortices along the sides of objects can be highly undesirable, and hence it is important for engineers to account for the possible effects of vortex shedding when designing a wide range of structures, from submarine periscopes to industrial chimneys and skyscrapers.

Even more serious instability can be created, for example, in concrete cooling towers, especially when built together in clusters. Furthermore, Kármán vortices are responsible for such phenomena as the "singing" of suspended telephone or power lines and the vibration of a car antenna at certain speeds.

Wake Turbulence of Large Aircraft

We may notice air flow by the wind that touches our face. But rarely do we really know where this flow comes from. We know, of course, that a lot of air is moved when an airplane starts or lands. But how does it move?

Figure 8 shows the large aerodynamic turbulent motion caused by landing airplane, visualized by using colored smoke rising from the ground. Such turbulence is dangerous for destructive action in the neighborhood, especially in the flow field

Fig. 8 Wake turbulence of large aircraft. The air flow from the wing of the plane was made visible by using colored smoke rising from the ground. Photographed by NASA langley research center (NASA-LaRC)

---

[2]The (global) Reynolds number for a flow is a measure of the ratio of inertial to viscous forces in the flow of a fluid around a body or in a channel, and may be defined as a nondimensional parameter of the global speed of the whole fluid flow:

$$Re = \frac{\rho \cdot v \cdot d}{\eta}$$

where ρ denotes density, v, velocity, d, characteristic length and η, dynamic viscosity.
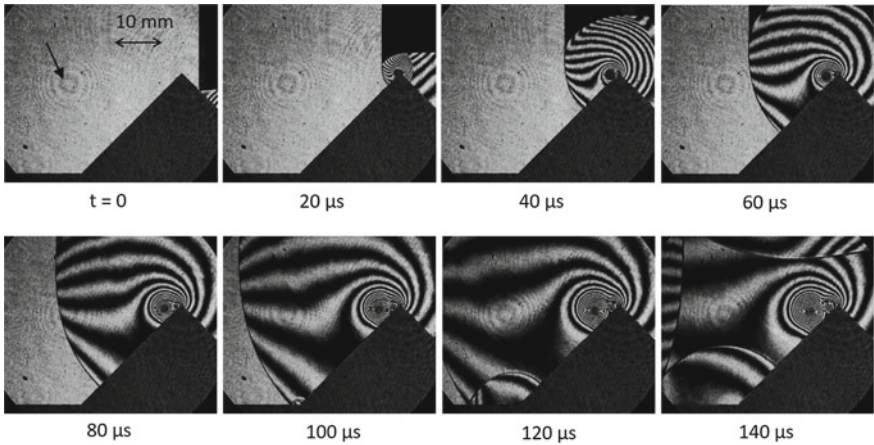
Fig. 9 Development of a compressible vortex after a shock (coming from the right) interacting with a half-diamond cylinder. Observation with a Mach–Zehnder interferometer, Mach number = 1.19. The weak concentric circles marked by an arrow are caused by a tiny particle sticking on the surface of the inner glass window

behind the plane. Interestingly, experienced pilots worry less about wake vortices in rough weather, because the vortex is dissipated by wind more rapidly.

Many such air vortices may form (and remain invisible), when rotating appliances are used, in production processes or even in the household.

Vortex Formation by Interaction of a Shock Wave with an Obstacle

Shock waves in transparent media are invisible. To visualize them we use the fact that a shock wave substantially changes the density of the medium that it traverses. Such density changes in the medium can be observed by Schlieren optics, shadow graph methods or an interferometer [11].

Figure 9 illustrates the interaction of a shock wave with a half-diamond cylinder observed by a Mach–Zehnder interferometer. After the front of the shock wave (the top right straight line at t = 0) reaches the diamond tip, the front is curved and a vortex is formed (t = 20 and 40 μs). One can see that the vortex is growing and that its center is sliding down the opposite slope of the triangular profile (t from 60 to 140 μs). Quite interestingly, vortices of a chemical reaction are also created, when excitation fronts are guided along a wall with a sharp, rectangular edge [12].

2.6 Crystal Growth on Surfaces

Many of us have made crystals in school or at home, and wonder about their regular structures. Just dissolve common salt in water as much as you can at an elevated temperature (reaching saturation), and wait till the solution cools down to room temperature (becoming supersaturated). After a while many small, cubic-shaped crystals will appear with a certain distribution of sizes. To obtain larger crystals one

may put some of the smaller ones (nuclei) into another hot saturated solution, wait for a few days, and see what happens.

Not surprisingly, different dissolved substances will give rise to differently shaped crystals. We can see various crystals in different forms. However, it is not simple to observe how crystals grow. Development of atomic-force microscopy (AFM) and scanning tunneling microscopy (STM) provide the opportunity to study at the nanometer level the surface topology during crystal growth and how it is affected by impurities, defects, and solution conditions.

With AFM we can see during crystal growth molecules bonding and dissolving, attaching to some surface - and occasionally forming a spiral structure. Spiraling steps tend to develop on "screw" dislocations, often located at actual breaks in the structure of the crystal. Such dislocations create spiraling or multilayered mounds called vicinal hillocks (Fig. 10, left) [13].

About 10 years before this image was published, Wada investigated in 1985 spiral growth of nacre (the mother of pearl) *in vivo*, produced in some molluscs as an inner shell layer (see Fig. 10, right) [14]. He assumed that the spiral growth originated from screw dislocation on the host crystal face under the particular environment of a nacre mineralization front.

Not only nacre but a wide variety of organisms from bacteria to humans produce such biominerals, synthesizing inorganic complexes like bones, shells, teeth, and even magnetic material.[3] This is intricately related to processes of self-organization and the generation of patterns, which may lead to synthesis of new functional materials (frequently on the nanometer scale) [15].
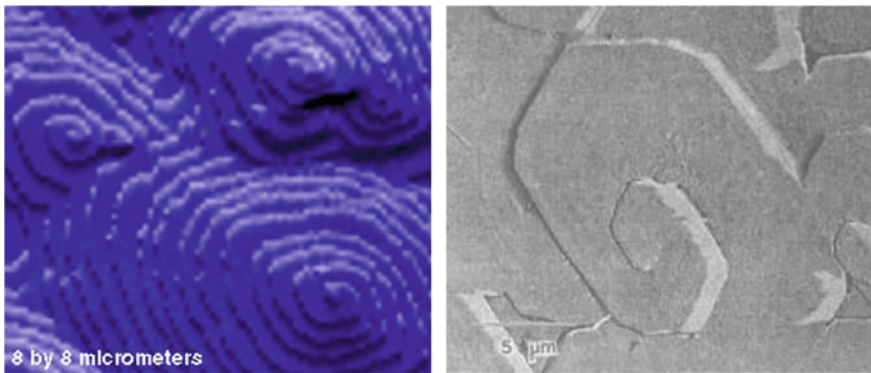

Fig. 10 Left: many crystals grow at low supersaturation on dislocations that produce spiraling mounds. A crystal of potassium dihydrogen phosphate is shown. Permitted for reuse from [13]; right: electron micrograph of a growing spiral of nacre. Reprint permission from Japan association of crystal growth [14]

---

[3]For example, magnetotactic bacteria orienting themselves along the field lines of the magnet field of the Earth.

AFM and STM will help to answer many questions on biomineralization of nanostructures, for example, questions about the mechanisms or the kinetic factors to control growing crystals. Supersaturation levels, impurities and defects may affect growth (compare chapter **Liesegang Rings, Spirals and Helices**).

2.7   Nanostructures

Spirals or helices as fundamental structures can be found on virtually all length scales that we have seen in our explorations of outer space or the nano-world. We started this chapter with a short presentation about galaxies, many of them with a pitch of spiral arms being of the order of 10^{20} m. Structuration processes on the planets, like the canyon on Mars or a hurricane may occupy an area of diameter of 10^5 m, the air flow from the wing of an airplane 10^2 m, crystal hillocks 5×10^{-6} m. Further, we will demonstrate here that in the world of nanostructures there are nanotubes developing with a helical pitch of only 10^{-8} m [16]. A clear indication that patterns due to evolutionary processes and self-organization of matter act at the basis of the physical laws that determine our world.

As an example for spiraling effects in a cylindrical nanotube we show three possible molecular structures: armchair, zigzag and chiral. The left sketch of Fig. 11 is the armchair configuration building on a regular binding structure between adjacent carbon atoms, forming vertical lines of hexagons. The zigzag structure sees a phase shift of the hexagons in vertical direction (Fig. 11, middle). The right sketch

Fig. 11 Three types of cylindrical carbon nanotubes. Left: the armchair configuration; middle: the zigzag structure; right: a chiral pattern. Reprint permitted by M. de Crescenzi
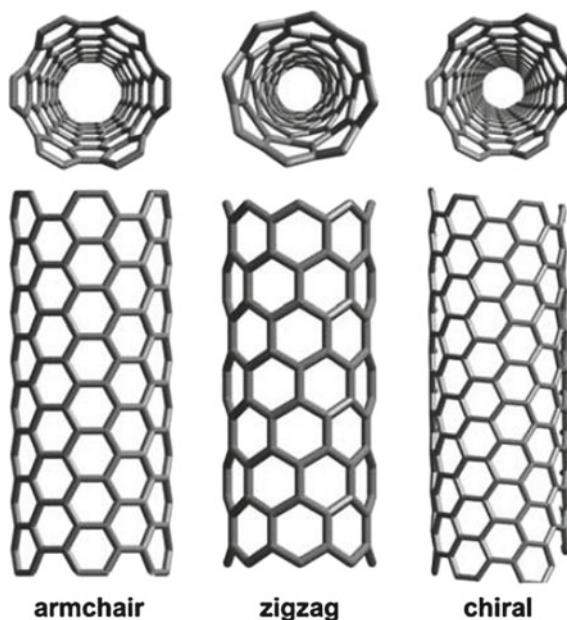
of Fig. 11 shows the interconnected hexagonal units following a torque along the
vertical direction, which forms a chiral pattern, leading to a helix with a certain
pitch.

3 Living Nature

So far we have considered pattern-forming systems in the inanimate world, be it in
distant, large star assemblies or in much smaller objects as crystals or nanotubes.
Now we proceed to look at the living nature and search for spirals and vortices
there. We will find ample proof for how "popular" their structures have become
during biological evolution. Scales, sizes, ages may be quite different, but many
fundamental mechanistic aspects are comparable or even analogous. We start with
an historical treatise by J.W. Goethe on metamorphosis of plants and animals.

Science Meets the Arts

Johann Wolfgang von Goethe (1749–1832)
Spirals in the Metamorphosis of Plants and Animals

He believed in a general spiral tendency in vegetation, through which, in con-
junction with vertical striving, all plant formation would be achieved following
the laws of metamorphosis. There is no necessity to introduce Johann Wolfgang
von Goethe, the prominent German writer and statesman with his enormous
creative work known worldwide. Somewhat less known are his many trea-
tises and essays on issues of natural science, assembled in his compendium
"Naturwissenschaftliche Schriften" [17]. Beyond his famous contributions to
geology, mineralogy, meteorology, optics and his well known theory of col-
ors one finds a large number of articles on biological themes, in particular on
nature, morphology and the metamorphosis of plants and animals.

Around 1790 his poems "Die Metamorphose der Pflanze (The metamorpho-
sis of the plant)" and "Metamorphose der Tiere (Metamorphosis of animals)"
[18] appeared together with a treatise "Attempt to explain the metamorphosis
of plants". At that time Goethe was concerned about a contradiction in his
arguments which were connected with Newton's law of gravitation [19]. Two
basic driving forces would be implemented in the plant, one for expansion
and development (vis centrifuga) and the other for conservation of form (vis
centripetal). Following a suggestion from the young botanist Ernst H.F. Meyer
(1791–1858) a symbolic plant science was introduced by an ellipse: the first
force would be assigned to one of the foci (F_1), the other to the second focus
(F_2). This is a static picture. To consider also dynamic processes one should
replace the elliptic foci by spirals and thus create a symbolism, where the
foci remain unchanged, but their radii are steadily augmented (see illustration
below).
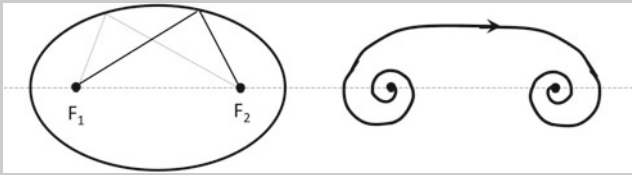
Left: Ellipse, the full and the pointed straight lines connecting F_1 and F_2 have the same length; right: a spiral pair consisting of two counter-rotating spirals

Without alluding to details of the arguments, Goethe finally comes up with a principle still based on Newton's laws, hereby partially following Ritter von Martius (1794–1868) [20]. We have a literally visual result of the conversations between Goethe and Martius. They exchanged two schematic sketches on the front and back of a sheet of paper; these show the arrangement of the leaves of a plant around its stem: as seen, they are arranged in a spiral pattern as shown below.

The arrangement of leaves of a plant around its stem according to a sketch in [20, 21]. This is an early design quite relevant for the field of phyllotaxis (see Sect. 3.4 Leaf arrangement)

Goethe now assigns the vis centrifuga to a vertically rising growth, the vis centripetal corresponds to a spiral system. In fact, the spiral system, the evolving, multiplying, winds around the vertical stem, the conserved essence, enduring, as seen in many concrete examples from our flora, and described by him in some detail. None of these systems can be considered separately, they always act together in a perfect equilibrium.

These ideas were put down in the article "Über die Spiraltendenz der Vegetation (On the spiral tendency of vegetation)" written in 1831, rather late in Goethe's life. Remarkably he calls the tendency to form spirals the "basic law of life" and further on formulates corresponding laws for the cultural development of mankind [21, 22].

Fibonacci Dream

Today the analysis and the modeling of leaf arrangements has become a field of natural science. The left picture below shows a result based on the assumption that the angular distance between subsequently growing petals should be determined by a specific angle (in particular the golden angle, derived from the Fibonacci numbers, see Appendix for details). At each intersection of the crossing spiral arms a new petal will grow.

This scenario is also shown as an artistic variation in the image to the right. At first glance it appears like a symmetrical picture, but the right and left winding spirals break the mirror symmetry. The pattern is also based on the golden angle, as followed by nature in leaf and flower constellations, when maximal irrationality is useful [23].
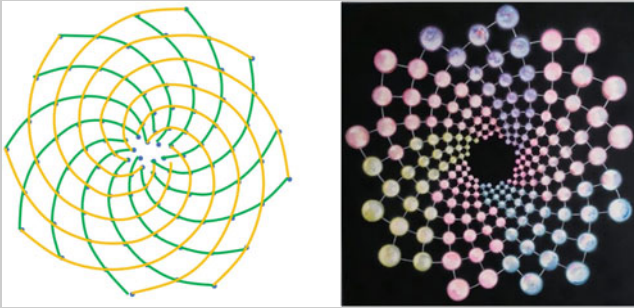
Left: leaf arrangement in a simulation according to [23]; right: "13–21" by Marita Kraus, Acryl auf Leinwand, Aalen

3.1 Seashells and Snails

A seashell is the hard exoskeleton of marine molluscs (the biological class of animals without a backbone) that protects and supports their bodies. It is composed largely of calcium carbonate or chitin secreted by the mantle, a skin-like tissue in the mollusc's body wall. Thereby the calcium salts are extracted from the sea water. Seashells are usually made up of several layers of distinct microstructures. One of the most distinctive microstructures is nacre, or the mother of pearl, which occurs as an inner layer in some special shells of some gastropods. Incremental growth takes place only at the shell margin, described in Sect. 2.6.

In tropical waters many seashells tend to grow to medium or large sizes. In the Caribbean a frequently found shell is the queen conch. The queen conch starts building its shell as soon as it hatches from the egg and even before. When the small conch is 2 or 3 months old, its shell is white; when it is 5 or 6 month old, it starts to show

Fig. 12 Left: Queen conch seashell, Puerto Rico; right: cut through the spiral axis

brown stripes. On its foot, a horny claw called operculum enables it to leap, so it can escape or fight against predators and lock itself up within its shell.

The grown example shown in Fig. 12 (left) may be 3–4 years old. Followed a spiral structure, its growth has most likely of logarithmic shape, as can be detected when cutting the shell into slices perpendicular to its central axis (Fig. 12, right). In a complicated morphogenetic process the shell starts growing at the inner end of the spiral. Then, along the growth edge, it follows a spiraling direction.

Interestingly, these seashells have been used as musical instruments (wind instruments) for many hundreds if not thousands of years. Most often the shells of large sea snails are used, as trumpets, by cutting a hole into the spire of the shell or cutting off the tip of the spire altogether. The characteristic sound is largely determined by the pitch of the internal spiral.

Note that the names "shell" and "snail" are often confounded. Snail is a common name loosely applied to shelled gastropods. However, the common name snail is also used for most of the members of the molluscan class Gastropoda that have a coiled shell large enough for the animal to retract completely into. When the word "snail" is used, it generally includes not only just land snails but also numerous species of sea snails, the shell of which consists of only one piece (univalve shells). The seashells which have two elastically connected valves (bivalve mollusc) are often called "mussels".

Frequently one observes on the surface of shells simple or intricate colored patterns of great beauty (see Fig. 13). These evolve when some pigment is incorporated in an appropriate way at the growing edge. During further growth, the pigment becomes visible as a pattern on the shell surface, like in a time-space plot of the moving growth

Fig. 13 Right: A specimen of Terebridae, commonly referred to as auger shells or auger snails, a family of small to large predatory marine gastropods. They have extremely high spired shells with numerous whorls; middle: sundial shell with circular color variation. Its colored windings and the dashed circumference may evoke the surface of a sundial; left: Oxymeris maculata, a species of marine gastropod mollusc of the family Terebridae

edge. Pattern formation and spiral growth are intimately connected with each other. H. Meinhard has demonstrated in his book "The algorithmic beauty of seashells" [24] that many of these patterns can be explained on the basis of a reaction-diffusion model of the Turing type, involving activator, inhibitor and substrate as dynamic variables (see chapter **Reaction-Diffusion Patterns and Waves**).

3.2 Ammonites

Ammonites are marine animals which lived during the Devonian from about 420 million years ago till the Cretaceous–Palegogene extinction events (66 million years ago).[4] Although ammonites have shells, they do not belong to the order of seashells or snails, but are closely related to soft-bodied creatures (molluscs) like octopuses and squids [25]. There are compartments inside of their shell as seen in Fig. 14 (right), where the shells of seashells and snails have no compartments (Fig. 12, right). The ammonite occupied only the entrance compartment, and others were separated by septa, but connected with a thin tube, extending from the ammonite's body. Liquids and gases were exchanged because of the hyperosmotic transport and these air compartments helped ammonites to float (or swim).

---

[4]Sudden mass extinction of some three-quarters of the plant and animal species on the Earth, approximately 66 million years ago.
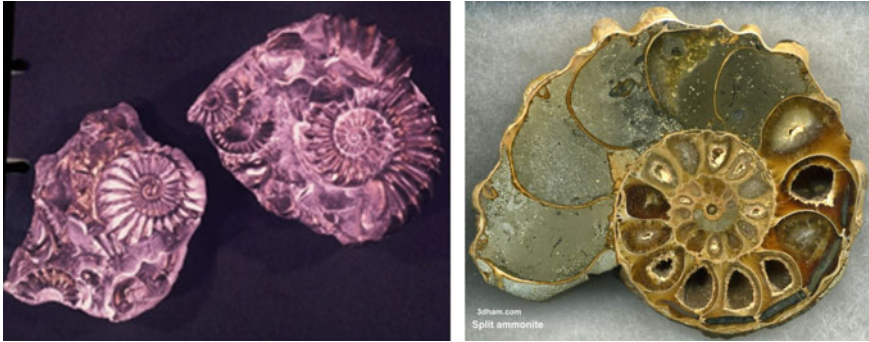
Fig. 14 Left: outside of two ammonites; right: an ammonite shell viewed in section, revealing the internal chambers and septa. Large polished examples are prized for their aesthetic appeal, as well as scientific value. Photograph taken by John Alan Elson

The exterior appearance of ammonites is also different from that of univalve shells or snails, although both spirals are logarithmic. The direction of the spiral elongation is quasi two-dimensional for ammonites, while the spiral of universal shells or snails is really a helix (three-dimensional).

3.3 Spiral Form in Our Fauna

There are various kinds of spirals seen in our fauna in the form of horns, tails, tongues, tentackles, flagella, and others. We can classify them into two groups: rigid and flexible. A typical example of the rigid spirals is shown in Fig. 15 (top left), the horns of a blackbuck (Indian antelope). Such horns are found mainly among the ruminant artiodactyla (hoofed animals), in the families antilocapridae and bovidae (cattle, goats, antelopes etc.). The spiral form may be developed not only for battles but also for attracting females. Many of them are now not so practical for fighting any more.

The second group of spirals are more functional. For example, a proboscis of a large white (also called a cabbage butterfly, pieris brassicae) with its photograph in Fig. 15 (bottom left), is usually wound up, but it is uncoiled very quickly to reach the food. The tail of a chameleon (Fig. 15, top right) is wound in rest, while it is rapidly stretched, when it moves in a rush. A seahorse (Fig. 15, bottom right) fixes its body with the spiral tail.

Fig. 15 Spirals in the animal world. Top left: black buck at Mahavir Harini Vanasthali National Park, Hyderabad; bottom left: a proboscis of a large white (pieris brassicae). Licenced from Hecker; top right: Parsons chameleon (Calumma parsonii) with a spiral tail. Photographed by J. A. Elson; bottom right: seahorse. Photographed by M. Al Momany, NOAA

3.4 Leaf Arrangement (Phyllotaxis)

In this section on the growth of leaves we are more explicit about a modeling approach than in most other chapters, because the systems offer quite successful arguments for the occurrence of the parastichies. We will see that the model may well describe the role of an activator and an inhibitor. But neither the biochemical nature of these two agents is identified, nor their diffusion coefficients are really known. For this a model of the reaction-diffusion type is needed [26].

3.4.1   Parastichies in Nature

If you make a walk through the forest close to your living place you may want to pick a pine cone and notice that its leaves are arranged in a quite regular fashion. In fact, looking at the cone from below the eye generates spiral-shaped patterns by following the lines of contact between neighboring leaves. There are right- and left-handed spirals (parastichies) with different pitch, and one can count their number for each full turn (see Fig. 16). We find for the pine cone: 8 right-handed and 13 left-handed parastichies: $Q = 8/13$.

Just look at the branch of a fir and you will find them.

Comparable leaf arrangements are found in other plants, e.g.,

$$\text{cactus}: Q = 5/8 \text{ to } 13/21$$
$$\text{sunflower}: Q = 21/34 \text{ to } 89/144$$
$$\text{thistles}: Q = 21/89 \text{ to } 34/55$$

Note that the numbers appearing in the above quotients belong to the series of **Fibonacci numbers** [27] (details see Appendix).

Such regular patterns in phyllotaxis are found all over the world [28], for instance in the desert of Baja California, where the endemic plant called Cirio grows and covers the whole landscape (Fig. 17, left). It leaves dried-out chunks from its tree-like growth structure (see Fig. 17, right). While so far, we have considered leaves growing in a discoidal geometry along spiral-shaped lines, we find here a helicoidal arrangement of leaves growing on the cylindrical stem of a cactus (up to 20 m high). Here we can also detect left- and right-handed parastichies tracing lines along the cylindrical surface.
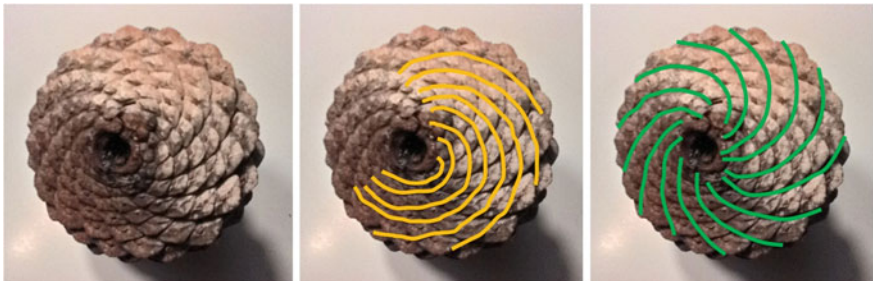

Fig. 16 Left: Pine cone seen from the bottom; middle: 8 right-handed spirals are indicated in orange; right: 13 left-handed spirals are indicated in green

Fig. 17 Left: Cirio in Baja California, Mexico; right: dry cactus stem from Baja California

3.4.2 Analysis of Leaf Arrangement

We analyze the geometrical order of leaves by a phenomenological model based on qualitative assumptions for the interaction between activating and inhibitory processes.

Looking at the leaf arrangement in the pine cone, one should ask the question, how the leaves grow in time and occupy their specific and stable location. One finds that the so-called "divergence angle", i.e., the angle between two leaves successively growing on the tree, is close to the golden angle G, which subdivides the circle as the golden cut g subdivides the line. Using $g' = 1 - g = 0.618\ldots$ (instead of $g = 1.618\ldots$) the golden angle is

$$G = (1 - g') \cdot 360° = 137.5°$$

Note that we follow here the genetic spiral, which connects the leaves in the sequence of their formation (not in the full-grown form of all leaves together). The assertion is: The golden angle of the genetic spiral implies the Fibonacci character of all other spirals (parastichies). If this is correct, then one should be able to explain the universal occurrence of G with a morphogenetic model. In the first case, we consider a discoidal geometry where the genetic spiral develops in radial direction. Plotting points (x, y) according to the rule

$$(x_k, y_k) = (r_0 + k\Delta r)(\cos kG, \sin kG),$$

where Δr is the growth rate and k = 0, 1, 2, …, yields the graphics shown in the third figure of the inset **Science meets the Arts**. One finds: Fast growth $\leftrightarrow$ low F_i; slow growth $\leftrightarrow$ large F_i with denser packing. Nearest neighbors are always connected by Fibonacci lines (parastichies).

In helical geometry the genetic spiral develops only along the central axis of a stem or a branch. In Fig. 16 (right) the Fibonacci patterns are unwrapped from the

cylinder and spread out on the plane. As in Case 1, we have small compactness for high and large compactness for low growth velocity.

Deviations from $G = 137.5°$ (even slight ones of a few %) result in a rupture of the described order and terminate the Fibonacci sequence at a certain stage. Therefore, the occurrence of fairly high numbers (55, 89 or even 144) requires a delicate control of G.

3.4.3   The Golden Angle and Lateral Inhibition

The most commonly accepted view concerning pattern formation is that inhibitory influences emanate from activated centers and thereby play a regulatory role on further activation. Here we treat mainly the role of the golden angle, but of course, there exist in nature other leaf positions, e.g., alternating or oppositely arranged.

For an explanation of the role of G one assumes that there is an interaction between activating and inhibitory substances, which enter in contact by diffusion:

activation A   autocatalytic process with short spatial range
inhibition I   relatively long range process stabilizing the developing structure.

Different ranges are due to mobility, i.e. the diffusion coefficients of the respective substances. The decay of these substances follows a simple kinetics (rates proportional to concentration).

How does the inhibitory effect of already existing leaves influence the position of new ones? We will explain it by using the projection of a cylindrical sprout on a plane perpendicular to its axis, as illustrated in Fig. 18.
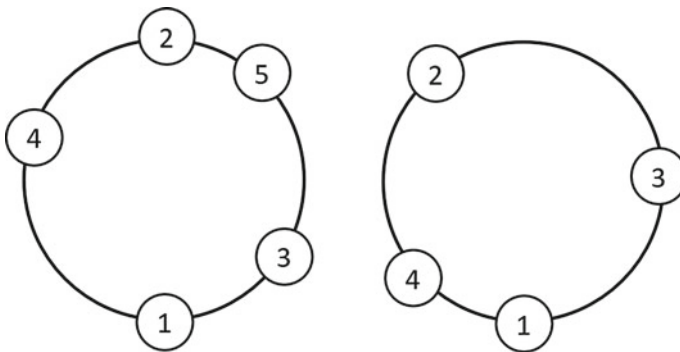

Fig. 18 Projections of a cylindrical sprout on a plane perpendicular to its axis for the explanation of the leaf arrangement, see text below

The sequence of events on the left circle in Fig. 18 is the following: the first leaf grows at arbitrary position 1. Due to **inhibition I** the second leaf forms at position 2 on the opposite side (at 180°). For the third leaf, one has to note that the sources of **I**, on the newly formed leaves, have a somewhat longer lifetime, so that when positioning the leaf 3 is about to be determined, leaf 1 is still actively repelling it, although not as strongly as leaf 2 does. Leaf 3 usually makes now a random (symmetry-breaking) choice as to which way the genetic spiral will be wound, and it will be closer to leaf 1 than to leaf 2. Then, leaf 4 has to find the locus of minimal **I**. Repulsion from 3 will be most effective, but leaves 2 and 1 still have an influence. If we assume exponential decay of the morphogens and constant time intervals between the expression of new leaves, then the inhibitory strengths i_m of the various leaves behave as

$$i_3 : i_2 = i_2 : i_1$$

Since 4 is still not so distant from 1, at least three preceding leaves contribute to the positioning of a new one. On the other hand, since 5 will be located far away from 1, we may neglect precursors earlier than the third.

After a transient period, a stationary situation will be reached where the angles between successive leaves are all equal (the right circle of Fig. 18). Plausibility and a short calculation [23] let us conclude that the angle between successively growing leaves is the golden one, G.

This simplified argument still contains much arbitrariness and more rigor would be desirable. A lot of details are not known (in particular the nature of the inhibitor) which one would need for an approach with a reaction - diffusion system.

However, the model described makes the role of the Fibonacci numbers in this morphogenetic process plausible. Since the number g is considered as the "most irrational" number, its role in the angle G leads to a minimal overlap of leaves, such that photosynthesis is less hindered. The plants try to keep their leaves at a maximal distance. Thus (as already guessed by Leonardo da Vinci), the plant can use sunlight in an optimal fashion.

The irrational number g plays an outstanding role in many respects. It often appears in an aesthetic context, so in the arts, architecture and design, symmetries in nature, and human perception of beauty.

3.5   *Lichen*

When walking through barren mountains or exploring the flora of cold regions under subarctic conditions one may enjoy the fascination of multicolored lichen with a broad spectrum of colors from white through radiating yellow, several shades of brown, orange, rose, olive, blue-green and deep black. There are 25,000 species of lichen worldwide. Lichen has only small need for metabolism and can survive on minerals from dust or nutrients contained in rain water or dissolved in the ground.

Fig. 19 A double spiral of lichen found in the Siberian tundra

Therefore, one can find it under extreme conditions: on bare rock, at altitudes exceeding 5000 m, in the desert or in regions of permafrost. It can exist at temperatures between −47 and +80°C.

In such difficult environments it grows very slowly, about a few millimeters per year or less. It belongs to the organisms with record life times, at least a few hundred years [29]. Lichen assumes regular or irregular shapes depending on the surrounding climate. Under rare conditions it may grow to form a spiral-shaped geometry, as photographed in Fig. 19.

3.6 Deep Sea Corals and Spirogyra

In 1883 Verrill reported on a beautiful, spirally coiled octocoral (genus Iridogorgia), which were found during an expedition of the US coast [30]. Iridogorgiids grow on underwater mountains (known as seamounts), island ridges and rocky continental slopes in both the Atlantic and Pacific Oceans. During three expeditions to New England and Corner Rise Seamounts (2003–2005) some new species of chrysogorgiid octocorals with the spiral Iridogorgiid growth form were found. As shown in Fig. 20, Iridogorgia has a spiral axis, which is further branched [31]. A close-up photograph of genus Iridogorgia reveals further branching, suggesting a characteristic feature of fractals (see Sect. 6 of **Spirals, Their Types and Peculiarities**).
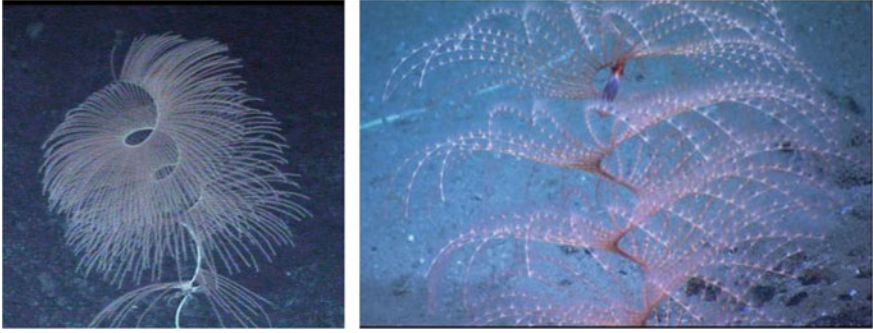
Fig. 20 Left: Iridogorgia, a spiral-shaped coral. From photogallery of Ocean Exploration and Research, taken by WHOI; right: lovely spiraling Iridigorgia coral, with brightly colored commensal shrimp. Image courtesy of the Mountains in the Sea Research Team; the IFE Crew; and NOAA
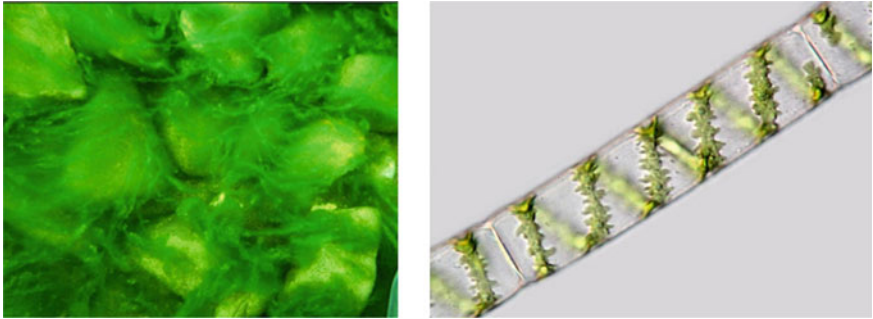

Fig. 21 Left: Spirogyra algae in natural environment [32]; right: single cylindrical algae cell with helicoidal chloroplasts

Spirogyra (mermaid's tresses, pond scum, water-silk) is one of 400 species of free-floating green algae found in freshwater environments all over the world: ponds, lakes, rivers, puddles etc. Named for their beautiful spiral chloroplasts, spirogyras are filamentous algae that can form masses floating near the surface of streams and ponds.

The algae (diameter 10–50 μm) stick together like a chain forming unbranched threads (length up to several cm) that consist of cylindrical cells (see weak boundaries between adjacent cells in Fig. 21, right). The chloroplasts are organelles responsible for photosynthesis and thus the pigment chlorophyll is incorporated in specialized membranes. Their spatial arrangement is indicated by their green color and follows as a band along the path of a cylindrical helix (see Fig. 13 of chapter **Spirals, Their Types and Peculiarities**).

Remarkably, here a quite simple unicellular organism chooses a mathematically well defined route for its purposes. They move with the flow of the water, because the cells have no flagella, and, therefore, cannot move by themselves.

3.7   Snail Clover and Leonardo's Flying Spiral

The snail clover (Medicago orbicularis) is a plant belonging to the family of legume (Fabaceae like beans and peas). The genus Medicago comprises about 110 species worldwide and is mostly home in the Mediterranean area. The best known species, the Luzerne (Medicago sativa), serves as animal food and is one of the oldest cultured plants in the world, once introduced by King Darius from Persia (549–486 BC) to Greece.

The species Medicago orbicularis is a clover-like plant having helicoid or spirally coiled pods. Looking at Fig. 22 (left), this specific structure becomes evident. The leaves grow according to a helix with large diameter and small pitch (see chapter **Spirals, Their Types and Peculiarities**). Almost all species of Medicago grow in Greece. They are usually small and inconspicuous with small yellow blossoms.

In the Paris Manuscripts of Leonardo da Vinci (a collection of 12 booklets with notes and drawings) one finds, among many other topics, a drawing of his invention "Helix Pteron",[5] as shown in Fig. 22 (right) [33]. He communicated this drawing around 1487–1490. He applied the principles later used for constructing the helicopter.

His invention could not be realized, because he lacked sufficiently light material and a "motor" to elevate heavy mass into the air. Only after 450 years was the first real helicopter developed. But some aspects of the principle of uplift had been discovered. Most remarkably we notice a structural similarity between Leonardo's flying spiral and the leaf constellation of the snail clover.
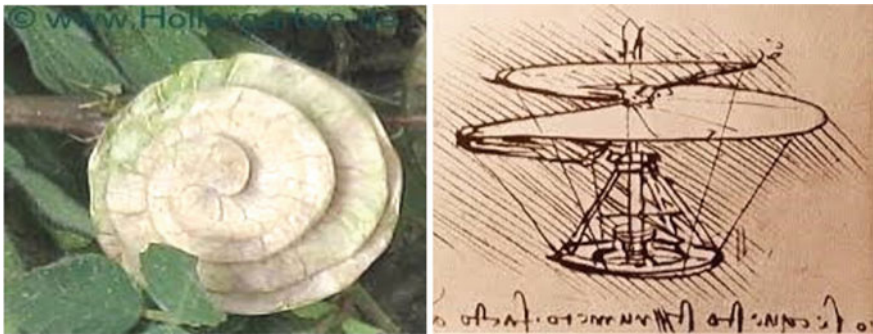

Fig. 22 Left: Snail clover, growing leaves with helicoidal shape. Reprint permitted by S. Wahler, Hollergarten; right: Leonardo's drawing of a flying spiral, "Helix Pteron" [33]

---

[5]"Helix" and "pteron" are Greek words, meaning "coil" and "wing", respectively.

3.8 Optical Sensors in the Eye of the Firefly

Many insects have compound eyes, each of which consists of up to several thousands ommatidia (individual eyes: tiny independent photoreception units of about 10 µm in diameter). The structure of an ommatidium is illustrated in Fig. 23 (right). Among such insects the firefly has unique ommatidia: the corneal lens (A in Fig. 23, right) extends into the region occupied normally, for other insects, by a crystalline cone (B in Fig. 23, right). The elongated corneal cones are laminated in a series of concentric paraboloids [34]. Quite specially, the electron microscopy investigation of the compound eye of the firefly *Photuris pennsylvanica* reveals spiral structures in cross section (see Fig. 23, left) [35].

Interestingly the pattern of the individual hexagonally arranged sensors shown in Fig. 23 (left) are strongly reminiscent of spirals in the Belousov–Zhabotinsky reaction (see chapter **Chemical Oscillations and Spiral Waves**), suggesting a self-organizing reaction to occur here [36]. The spiral pattern of the firefly eyes can be explained by chiral orientation of rod-like molecules which are the main composition of the lens of firefly eyes: they orient slightly differently at different levels, thus creating spiraling ribbons. Note that with a polarizing microscope a study has been performed of microlens arrays made of nematic liquid crystals containing chiral dopants, which leads to the observation of concentric ring structures due to interference [37].
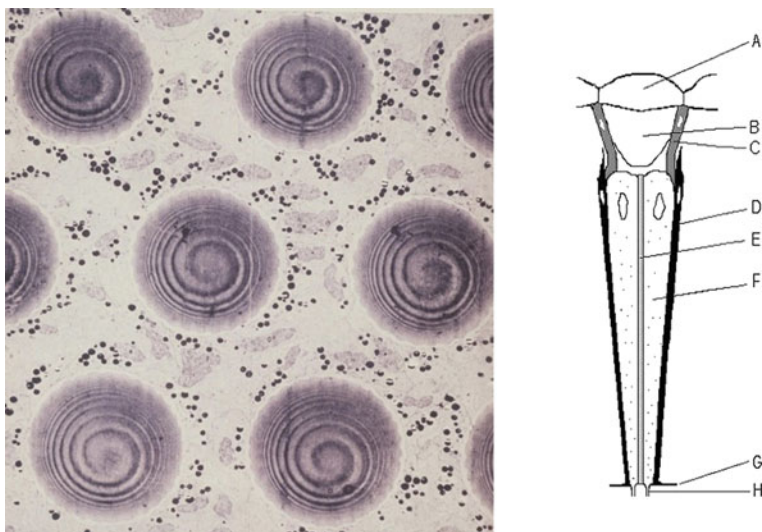

Fig. 23 Left: optical sensors in the eye of a firefly (Photuris pennsylvanica) taken by an electron microscope [35]; right: structure of an ommatidium, A - cornea, B - crystalline cone, C and D - pigment cells, E - rhabdom (light transmitting axial rod), F - photoreceptor cells, G - membrana fenestrata, H - optic nerve

Fireflies communicate among each other with optical signals of bioluminescence.[6] The light is emitted as a glowing or flashing signal from the lower part of their abdomen. The receptors have high light sensitivity, because they should detect bioluminescence during twilight to attract mates or prey.

3.9   Fish Vortex

We finally turn to the example of a school of fish that forms a vortex. It illustrates the phenomenon of swarm intelligence, which is the collective behavior of decentralized, self-organized systems, in nature or under artificial conditions.

In Fig. 24 we notice typical features of a vortex as found in wind and cloud patterns (see hurricane, Fig. 5). There is the characteristic central core where one finds only little movement (the "eye" of the hurricane), whereas a swirling motion evolves around this core. Only that here we are not dealing with water or air molecules under certain thermodynamic conditions, but with a large number of living individuals caught in a superposed coordinated motion [38].

Such swarms consist of a population of simple agents interacting locally with one another and with their environment. The inspiration of swarm dynamics often comes from nature, especially biological systems. The agents follow simple rules. Although there is no centralized control structure dictating how individual agents should behave, interactions between them lead to the emergence of "intelligent" global behavior unknown to the individual agents. Examples in natural intelligent swarms include ant or termite colonies, bird flocking, animal herding, bacterial growth, amoebae, fish schools, microbial intelligence, and humans (see chapter **Patterns and Humans**).

Obviously, a fish swarm is a good candidate for swimming in vortices, because it can move in three dimension. This way it establishes protection against predators. Animal herds may form spiral-like defensive groups on the ground, whereas bird flocks will find quite individual structures in the air. But look at the microsystems such as the social amoebae, aggregating in regular spirals (see chapter **Spiral Waves of the Chemo-attractant cAMP Organise Multicellular Development in the Social Amoebae**).

Concepts elaborated for the description and explanation of the complex motion of swarms are employed in works on artificial life. In programs on artificial life simulating the flocking behavior of birds. Some rules for emergent behavior has been developed, where the complexity arises from the interaction of individual agents. The main rules applied are: *separation*: steer to avoid crowding local flockmates; *alignment*: steer towards the average heading of local flockmates; and *cohesion*: steer to move toward the average position (center of mass) of local flockmates [39].

---

[6]In the presence of magnesium ions, ATP and oxygen the enzyme luciferase acts on the luciferin and produces light. The color is yellow, green or pale red.

Fig. 24 A large school of
sardines forming a vortex

In this and other models for swarm behavior the members of the swarm are usually treated as objects without individual features. Some of them may be successful for reproducing swarm geometry and dynamics like for the fish vortices, but a consideration of the biological features of the participating entities is missing. The relevant behavioral parameters may not yet have been captured.

We have shown, how creative nature is in inventing beautiful and intelligent forms and patterns. Spirals and vortices belong to structures that are readily selected. Nature does not always need to emphasize certain goals that may be claimed to assign a specific function or distinctive meaning to these forms, as humans tend to do, when they leave spiral carvings in stone or meditate about spiral-shaped courses in the sand.

In this sense nature is most sincere and has its own ways to use shapes for growth and survival. Contemplating the artful natural forms makes it easy to let one's mind float to man-made art or related work, as we will do in the following chapter.

Appendix: Fibonacci Numbers

The famous mathematician Leonardo da Pisa, also called Fibonacci (1170–1240) introduced around the year 1200 AD the Indian-Arabic number system 0, 1, 2, 3,…to Italy. He also made a few significant calculations, one of which led to the series of "Fibonacci numbers" [27]. These play an important role until today, in such diverse disciplines like the arts, architecture or biology.

The Fibonacci numbers are
$F_n = 0, 1, 1, 2, 3, 5, 8, 13, 21, 24, 55, 85, 144, 233, \ldots$ ($n = 0, 1, 2, \ldots$)

There is a simple rule, how a follow-up number is formed by 2 precursors:

$$F_{n+1} = F_n + F_{n-1}.$$

You can check this easily:
$1 + 0 = 1, 1 + 1 = 2, 2 + 1 = 3, 3 + 2 = 5, 5 + 3 = 8, \ldots$

These numbers have amazing properties. They describe the arrangement of petals of a pine cone, or in a sunflower. They are closely related to the "golden cut (or golden ratio) g", because the following quotient converges towards g:

$$F_{n+1}/F_n = 1, 0, 2, 0, 1.5, 1.666\ldots, 1.6, \ldots, 1.61803\ldots \to g \ (for \ n \to \infty).$$

The golden cut g is originally defined as a certain division of a straight line of length l. The line would then be

$$0\underline{\hspace{4cm}}|\underline{\hspace{2cm}}l$$
$$b \qquad\qquad\qquad a$$
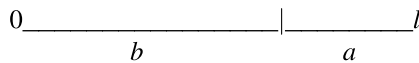
For defining g: The line should be divided into two parts a and b, such that the quotient b/a is equal to the quotient l/b, i.e.

$$l/b = b/a = g.$$

Small calculation: with $l = a + b$

$$(a + b)/b = b/a$$

$$g = b/a \ \to \ (a + b)/b = g \ \to \ 1/g + 1 = g$$

$$1 + g = g^2 \ \to \ g^2 - g - 1 = 0$$

$$g_{+,-} = \frac{1}{2} \pm \sqrt{\frac{1}{4} + 1} = \frac{1}{2} \pm \frac{1}{2}\sqrt{5}$$

Only positive numbers make sense as a solution:

$$\rightarrow g = \frac{1}{2}(1 + \sqrt{5}) = 1.61803\ldots$$

How did Fibonacci find his famous number sequence?

He considered a problem of population dynamics: How does the number of rabbits in a population grow from generation to generation (generation length, say, 1 month)? The generations are numbered consecutively 0, 1, 2, 3,..., n, ...

At the beginning (time 0): one couple of rabbits is born.

Then, for each month, another couple is born to this first one. Simultaneously, each newly born couple matures in the corresponding month for an additional birth. (This way the population is immortal!)

After n months we count

J_n young couples, and
A_n adult couples.

Now let's count:
For
$n = 0$: $J_0 = 1$, $A_0 = 0$ one couple is born
$n = 1$: $J_1 = 0$, $A_1 = 1$ the young couple is now adult
$n = 2$: $J_2 = 1$, $A_2 = 1$ the adult couple gives birth to a young couple
$n = 3$: $J_3 = 1$, $A_3 = 2$ this young couple gets adult, adult couple gives birth to
                                                                another couple
$n = 4$: $J_4 = 2$, $A_4 = 3$ and further on

Generally written we have:
$J_{n+1} = A_n$
$A_{n+1} = A_n + J_n$
with $J_n = A_{n-1} \rightarrow A_{n+1} = A_n + A_{n-1}$, where $A_0 = 0$ and $A_1 = 1$.

Now we replace "A" by "F" (symbol for the Fibonacci numbers) and find for the number of rabbit pairs in subsequent generations n:
$A_n = F_n = 0, 1, 1, 2, 3, 5, 8, 13, 21, \ldots$.

This is the number sequence we already know.
Furthermore one finds for the golden cut the continued fraction:

$$g = 1 + \cfrac{1}{1 + \cfrac{1}{1 + \cfrac{1}{1 + \frac{1}{\ldots}}}}$$

Interestingly, there is a very simple relationship for the inverse golden cut:

$$g^{-1} = \cfrac{1}{1 + \cfrac{1}{1 + \cfrac{1}{1 + \cfrac{1}{\cdots}}}} = g - 1$$

Picture credits

Fig. 2 Hubble Heritage Team, ESA, NASA, Fig. 3 Licenced from PA Picture Alliance, Fig. 4 NASA/JPL/Malin Space Science Systems, Fig. 5 NOAA (National Oceanic and Atmospheric Administration), NASA, Fig. 6 Left: Justin1569 at English Wikipedia, right: ©Hess, Markus, Müller, Plesser, 1987. Dortmund, Fig. 7 Top: NASA GSFC, bottom: permitted by JPS Japan, Fig. 8 NASA Langley Research Center (NASA-LaRC), Fig. 10 right: permitted by Japan Association of Crystal Growth, Fig. 11 Permitted from Maurizio De Crescenzi, Dipartimento di Fisica Università di Roma "Tor Vergata", Fig. 14 Left: photograph taken by Stefan Müller, right: photograph taken by John Alan Elson, CC BY-SA 4.0, Fig. 15 Top right: CC BY 2.0, top right: photograph taken by John Alan Elson CC BY 2.0, bottom left: Licenced from Hecker, bottom right: Photographed by Mr. Mohammed Al Momany, NOAA, Fig. 20 Left: NOAA (National Oceanic and Atmospheric Administration), NASA, right: Landcare Research CC BY 4.0 Iridogorgia, a spiral shaped coral, as seen on Alvin dive 3901. Photo WHOI. Lovely spiraling Iridigorgia coral, with brightly colored commensal shrimp. Image courtesy of the Mountains in the Sea Research Team; the IFE Crew; and NOAA. A close-up of Iridogorgia showing the coral polyps. Photo WHOI, Fig. 21 Left: reprint permission from J. Great Lakes Res., right: public domain, Fig. 22 Left: permitted by Stefanie Wahler, http://www.Hollergarten.de, right: public domain, life plus 100, Fig. 23 Reprint permission by Springer, Fig. 24 Free to use.

References

1. E. Hubble, *The Realm of the Nebulae* (Dover Publications, Mineola, 1958)
2. C.C. Lin, F.H. Shu, On the spiral structure of disk galaxies. Astrophys. J. **140**, 646–655 (1964)
3. S. Phillipps, *The Structure & Evolution of Galaxies* (Wiley, Hoboken, 2005), pp. 132–133
4. R.H. Eather, *Majestic Lights: The Aurora in Science, History, and the Arts* (American Geophysical Union, Washington, 1980)
5. M.H. Carr, J.W. Head, Oceans on mars: an assessment of the observational evidence and possible fate. J. Geophys. Res. **108**, 8-1–8-28 (2003)
6. https://web.archive.org/web/20090827030639/, http://www.aoml.noaa.gov/hrd/tcfaq/A15.html
7. http://www.hurricanescience.org/society/impacts/tornadoes/
8. J. Ross, S.C. Müller, C. Vidal, Chemical waves. Science **240**, 460–465 (1988)
9. S. Taneda, Downstream development of the wakes behind cylinders. J. Phys. Soc. Jpn. **14**, 843–848 (1959)
10. T. von Kármán, *Aerodynamics* (McGraw-Hill, New York, 1963)
11. H. Kleine, High-speed imaging of shock waves and their flow fields, in *The Micro-World Observed by Ultra High-Speed Cameras—We See What You Don't See*, ed. by K. Tsuji (Springer Nature, Heidelberg, 2017), pp. 127–155
12. K. Agladze, J. Keener, S.C. Müller, A. Panfilov, Rotating spiral waves created by geometry. Science **264**, 1746–1748 (1994)
13. J. de Yoreo, T. Land, The secrets of crystal growth. Sci. Technol. Rev. (1995) https://str.llnl.gov/str/DeYoreo.html
14. K. Wada, Growth of $CaCO_3$ crystals in bivalve shell mineralization. J. Jpn. Assoc. Cryst. Growth **12**, 57–70 (1985)
15. S. Mann, Die Chemie der Form. Angew. Chem. **112**, 3532–3548 (2000)

16. C. Pintossi, G. Salvinelli, G. Drera, S. Pagliara, L. Sangaletti, S. Del Gobbo, M. Morbidoni, M. Scarselli, M. De Crescenzi, P. Castrucci, Direct evidence of chemically inhomogeneous, nanostructured, Si-O buried interfaces and their effect on the efficiency of carbon nanotube/Si photovoltaic heterojunctions. J. Phys. Chem. C **117**, 18688–18696 (2013)
17. J.W. von Goethe, *Naturwissenschaftliche Schriften* (Rudolf Steiner, Dornach, 1982)
18. J.W. von Goethe, Gedichte, in *Werke*, vol. 1 (Artemis & Winker, München, 1972), pp. 242–244
19. R. Ulshöfer, Johann Wolfgang von Goethe, Polarität und Steigerung - das Universalgesetz der Natur, der Geschichte und des künstlerischen Schaffens, in *Literatur des 18. Jahrhunderts und der Romantik, in neuer Sicht* (Königshausen and Neumann, Würzburg, 2010), pp. 106–109
20. R. von Martius, *Goethe und Martius* (Nemayer, Mittenwald, 1932)
21. S. Mainberger, "In the Vortex of the Spiral Tendency"—Questions of Aesthetics, Literature and Natural Sciences in the work of Goethe (engl. Version from "No remoinho da tendêencia-espiral" -Questões de estética, literatura e ciências naturais naobra de Goethe). Estud. Av. **24**, 203–217 (2010). http://www.scielo.br/pdf/ea/v24n69/en_v24n69a13.pdf
22. J.W. von Goethe, *Über die Spiraltendenz der Vegetation, in Naturwissenschaftliche Schriften* (Rudolf Steiner, Dornach, 1982), pp. 217–238
23. P.H. Richter, R. Schranner, Leaf arrangement. Naturwissenschaften **65**, 319–327 (1978)
24. H. Meinhard, *The Algorithmic Beauty of Seashells*, 4th edn. (Springer, Heidelberg, 2009)
25. D. Staaf, *Squid Empire: The Rise and Fall of the Cephalopods* (University Press of New England, Lebanon, 2017)
26. A. Gierer, H. Meinhardt, A theory of biological pattern formation. Kybernetik **12**, 30–39 (1972)
27. L. Sigler, *Fibonacci's Liber Abaci a Translation into Modern English of Leonardo Pisano's Book of Calculation* (Springer, New York, 2002)
28. F.M.J. van der Linden, Creating phyllotaxis from seed to flower, in *Symmetry in Plants*, ed. by R.V. Jeam, D. Barabé (World Scientific Publishing, Singapore, 1998)
29. T. Makry, Lichens from Baikal region (Siberia) new to Russia. Cryptogam. Mycol. **20**, 329–334 (1999)
30. A.E. Verrill, Report on the Anthozoa, and on some additional species dredged by the "Blake" in 1877–79, and by the U.S. fish commission steamer "Fish Hawk" in 1880–82. Bull. Mus. Comp. Zool. Harv. Coll. **11**, 1–72 (1883)
31. L. Watling, A review of the genus Iridogorgia (Octocorallia: Chrysogorgiidae) and its relatives, chiefly from the North Atlantic Ocean. J. Mar. Biol. Assoc. U. K. **87**, 393–402 (2007)
32. O.A. Timoshkin et al., Rapid ecological change in the coastal zone of Lake Baikal (East Siberia): is the site of the world's greatest freshwater biodiversity in danger? J. Gt. Lakes Res. (2016). https://doi.org/10.1016/j.jglr.2016.02.011
33. L. da Vinci, *Paris Manuscript B* (Collection of Institut de France, Paris), Folio 83v
34. G.A. Horridge, The eyes of the firefly Photuris. Proc. R. Soc. B **171**, 445–463 (1969)
35. J.J. Wolken, *Invertebrate Photoreceptors, A Comparative Analysis* (Academic, New York, 1971), pp. 57–61
36. A. Bewersdorff, P. Borckmans, S.C. Müller, Chemical pattern formation, in *Fluid Science and Materials Science in Space*, ed. by H.U. Walter (Springer, Berlin, 1987), p. 281
37. P. Popov, L.W. Honaker, M. Mirheydari, E.K. Mann, A. Jákli, Chiral nematic liquid crystal microlenses. Sci. Rep. **7**, 1603 (2017)
38. E.E. Russell, S. Yuhui, *Swarm Intelligence* (Morgan Kaufmann, Burlington, 2001)
39. A. Vicsek, E. Ben-Jacob, I. Cohen, O. Shochet, Novel type of phase transition in a system of self-driven particles. Phys. Rev. Lett. **75**, 1226 (1995)

The Arts and Beyond

Kinko Tsuji and Stefan C. Müller

Abstract Spirals play a very favorite role as motives for modern European paintings. Here we assemble some examples for quiescent spirals (Klimt), spirals starting to move (Itten and Klee) and storming spirals (da Vinci, van Gogh, and Turner). There are also circles or curved lines which look like spirals, but are not. In parallel to the European culture, a lot of spiral patterns appear in Japan, as well: for example the famous Ukiyo-e of the Naruto whirlpools, patterns for Kimonos and toys. In our daily life spiral forms are used for practical and/or ornamental reasons: musical instruments, staircases, data storage devices like CD and DVD, and others.

1 Introduction

In the literature one finds many stories about hurricanes and tornadoes and their destructive force. For example, in 1834 there appeared an article by Archibald Duncan in The Mariner's Chronicle under the title "A Report on the Maelstrom of Drontheim" describing in detail the dangerous whirlpool of the Maelstrom (Moskenstraumen) close to the Lofoten Islands in northern Norway [1]. This became in 1841 the template for Edgar Allan Poe's story "A Descent into the Maelström" with statements like "it raged with such noise and impetuosity that the very stones of the houses on the coast fell to the ground..." [2]. The Irish stained-glass artist and book illustrator Harry Clarke made a drawing of the lethal vortex for this story in 1919. This picture will be shown later together with a Japanese whirlpool (Fig. 11).

K. Tsuji (✉)
Shimadzu Europa GmbH, Albert-Hahn-Straße 6-10, 47269 Duisburg, Germany
e-mail: kts@shimadzu.eu

S. C. Müller
Institute of Physics, Otto von Guericke University Magdeburg,
Universitätsplatz 2, 39106 Magdeburg, Germany
e-mail: tsuji-mueller@t-online.de

In poetry we can admire the ballad of Friedrich von Schiller "Der Taucher (The Diver)" (1797) [3].
German original:

> .....
> .....
> Wohl manches Fahrzeug, vom Strudel gefasst,
> Schoss jäh in die Tiefe hinab,
> Doch zerschmettert nur rangen sich Kiel und Mast,
> Hervor aus dem alles verschlingenden Grab.
> Und heller und heller, wie Sturmes Sausen,
> Hört man's näher und immer näher brausen.
>
> Und es wallet und siedet und brauset und zischt,
> Wie wenn Wasser mit Feuer sich mengt,
> Bis zum Himmel spritzet der dampfende Gischt,
> Und Well auf Well sich ohn Ende drängt,
> Und wie mit des fernen Donners Getose
> Entstürzt es brüllend dem finstern Schosse.
> ......
> ......

In English [4]:

> .....
> .....
> Full many a ship, by the whirlpool held fast,
> Shoots straightway beneath the mad wave,
> And, dashed to pieces, the hull and the mast
> Emerge from the all-devouring grave.
> And the roaring approaches still nearer and nearer,
> Like the howl of the tempest, still clearer and clearer.
>
> And it boils and it roars, and it hisses and seethes,
> As when water and fire first blend;
> To the sky spurts the foam in steam-laden wreaths,
> And wave passes hard upon wave without end.
> And, with the distant thunder's dull sound,
> From the ocean-womb they all-bellowing bound.
> ...
> ...

After reading this ballad, one can virtually see a turbulent flow under the cliff.

In music there are also some kinds of spirals. One can imagine spirals moving when listening to some music pieces. Such "acoustic spirals" are introduced in chapter **Acoustic Spirals: Analysis of Bach's Prelude in C Major**. In this chapter, however, we show spirals and vortices more by visual perception.

Our eyes in connection with neurophysiological processing of optical signals in the visual cortex of our brain are extremely well prepared and sensible to recognize spatial patterns and their dynamical changes. The patterns that we observe, be it in nature or in our usual cultural environment where we work and live, may be simple

or complex, but they shape to a large extent the impressions and feelings that we develop in our daily life, be it in "normal" or exceptional situations.

Should anyone try to analyze some of the more complex patterns noticed during the day, he or she may come to the conclusion that despite all the complexity there are a few structural elements which, in one way or another, are dominating the ways to create spatial arrangements of an impressive variability, beauty, and usefulness.

Wassily Kandinsky, in his book "Point and Line to Plane", has provided an artistic view of this succession of elementary steps in art works [5]. In his writings, Kandinsky analyzed the geometrical elements which make up every painting - the point and the line. He called the physical support and the material surface on which the artist draws or paints the basic plane. He did not analyze them stringently, but from the point of view of their inner effect on the observer.

The painter to consider the curved line of a spiral in an artistic context was Paul Klee [6]. In fact, circular and spiral shapes extend the realm of elementary patterns. Circles will be described by their radius and can be arranged in a concentric way. Spirals, on the other hand, need more parameters to be characterized. They may be left or right-handed. They may have one or more arms. Their center may be a stable point or no stable center exists, i.e. the spiral may turn inward indefinitely (see graphics in the inset "Spiral dynamics in the work of Paul Klee").

Thus, spirals have some properties that other line structures lack. They are a most interesting multi-facetted pattern and thus constitute the central topic of this chapter, with their dynamics to form vortices included. We start with paintings of quiescent spirals, continue with moving spirals and storming spirals. There are false spirals: they look like spirals, but they are either circles or lines. In Japanese culture motives of spirals or vortices are often used. One more aspect of spirals and vortices, which we should not forget, is its usefulness in the form of practical spirals. We will show some examples.

2 Painting

2.1 Quiescent Spirals

2.1.1 Gustav Klimt (1862–1918)

Among the most popular and appreciated painters of his time the work of the Austrian artist Gustav Klimt reached a worldwide distribution, through the cultural channels but also in the mass media, exceeding that of artists like Dali, Picasso or Warhol. He was said to have shown the world in a female form ("Gestalt"). Among his rich Œuvre we refer here to his Stoclet-Frieze, a mosaic frieze in the Palais Stoclet, Brussels, of the years 1905–1909 [7].

On this frieze the branches of the "Tree of Life" extend from the tree trunk in the center (see Fig. 1) far to the left and to the right. The surfaces are covered with ornaments, most of them with regular and similar spirals which apparently symbolize the leaves of the tree. This frieze does not communicate any action, no time-determined

Fig. 1 Gustav Klimt, Tree
of Life, Stoclet Frieze
(1909). Photo:
©MAK/Georg Mayer
Ownership credit: MAK -
Austrian Museum of Applied
Arts/Contemporary Art

goal. Any aspect of communication lies in the priority of the decorative and orna-
mental elements of a mosaic created with luxurious materials.

Without noticeable events, rather static, and clues from contemporary art missing,
there is no way for a clear interpretation. Klimt himself has not provided many
comments on that. Some human figures are part of the frieze, a dancer, for instance
(not shown in Fig. 1). They are purely two-dimensional and almost disappear in
the ornaments. A figure becomes itself an abstract mosaic, which could be an early
symptom of a crisis in the portrayal of figures in modern art.

2.2 Starting to Move

2.2.1 Johannes Itten (1888–1967)

The Swiss expressionist painter, designer and theorist Johannes Itten was closely associated with the School of Art, Design and Architecture "Bauhaus", founded by the German architect Walter Gropius in 1919 in Weimar. The conception of the Bauhaus presented something completely new in that it brought together art and craftsmanship [8]. Among Itten's colleagues we find eminent names like Lyonel Feininger, Josef Albers, Paul Klee, and Wassily Kandinsky. They contributed to the movement of Concrete Art with a strong emphasis on geometrical abstraction which had worldwide influence.

The abstract painting "The Meeting" (Fig. 2) was created three years before the foundation of the Bauhaus. It anticipated some characteristic features of the Bauhaus art with its abstract elements: the design of geometrical forms like circle, square and spiral, as well as bright/dark contrasts and varying colors. Following the many graded color sequences within the spiral, one can imagine that it starts moving.

Itten's work on colors is said to be an inspiration for analyzing color types which correlate the skin tone, eye and hair color with clothing and make-up, and is also useful for interior design. The goal is an optimal harmony between an individual with

Fig. 2 Johannes Itten, The Meeting (1916). ©VG Bild-Kunst, Bonn 2018
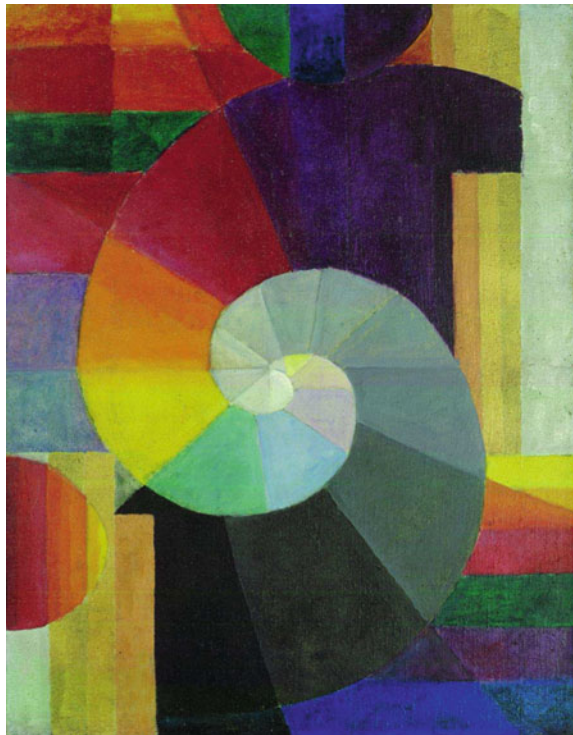
his living environment (color consultation). His studies of color palettes and color interaction directly influenced the Optical Art movement and other color abstraction movements. Cosmetologists today continue to use his color analysis, a tribute to the early work by Itten [9].

2.2.2 Paul Klee (1879–1940)

Paul Klee is considered as one of the most imaginative masters of modern art, producing work that spanned an amazing stylistic range. Klee's delicate works are filled with wit and references to dreams, music (he masterfully played the violin) and poetry. It blended primitive art, surrealism, cubism and children's art. Initially creating surreal, satirical pen-and-ink drawings, Klee's life and art were forever altered when he visited Tunisia and was overwhelmed by its intense light and color. Klee also used a complex array of signs and symbols drawn from the unconscious, that were meant to fuse abstraction with reality. Klee's work impacted all 20th century surrealist and nonobjective artists, and the abstract expressionist movement.

He developed a special "sympathy" for the spiral shape, which is well documented in his writings and paintings. The "Spiral blossoms" (Fig. 3, created in 1926 are an aesthetically appealing display of flowers with spiral-shaped blossoms displayed on a kind of theater stage. In his painting "Crucifers and spiral flowers" (Fig. 4) spirals may be less frequent, but the crucifer reminds us of the vortex wheel in Nordic art (chapter **Cultural History**).

His lectures and "Writings on Form and Design Theory" (Schriften zur Form und Gestaltungslehre [6]), published in English as the Paul Klee Notebooks, are held to be as important for modern art as Leonardo da Vinci's "A Treatise on Painting" [10] for the Renaissance. Klee and Kandinsky both taught in the 1920s at the Bauhaus school of art, design and architecture. His works reflect his dry humor and his sometimes childlike perspective, his personal moods and beliefs, and his musicality. During his 10 Bauhaus years several pioneering scripts were published, among them, the Creative Credo (Schöpferische Konfession (1920) [11]), where the famous statement *"Art does not reproduce the visible; rather, it makes visible"* appeared, and many others [12].

Fig. 3 Paul Klee, Spiral blossoms (1926). Private property in Japan

Fig. 4 Paul Klee, Crucifers and spiral flowers (1925). Private property

Spiral dynamics in the work of Paul Klee

The spiral was considered by Paul Klee as the *purest form of motion*. Klee writes in his *Pedagogical Sketch Book* [14]:

> ...We have to know the direction of motion, because the question depending on increase or retraction of the radius has psychological relevance. The question is: Do I get released from the center in more and more liberated motion? Or do my motions get increasingly bound by a center, until it finally devours me completely? - This question means nothing less than life or death. And the decision about this is made by the small arrow (see the drawing below).
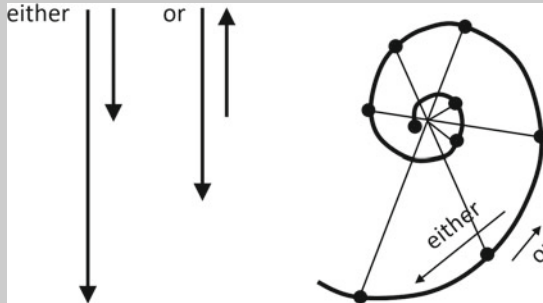
The spiral (drawing after Klee in [14]): in this figure, Paul Klee has extended the ratio between the rotations and their size, so that one sees the spiral actually opening and closing in a dynamic motion toward expansion or toward contraction. Directions shown by arrows either follow a clockwise motion toward expansion, symbolically life - or an anti-clockwise motion toward contraction, symbolically death.

In his analysis of curves and also the spiral Klee declares views that have not been uncommon in much earlier interpretations of the course that spirals may take. Think of the megalithic graves (chapter **Cultural History**) where one assumes that primordial artists have already well distinguished between outward or inward motion along a spiral. ...

In this context Paul Klee formulates: Gut ist Formung. Schlecht ist Form. Form ist Ende, ist Tod. Formung ist Bewegung, ist Tat. Formung ist Leben. (Good is formation. Bad is form. Form is the end, death. Formation is motion, is action. Formation is life.)

There is a clear correspondence to the dynamical aspects of the spiral, as pointed out at the beginning of this paragraph. (His lecture on the spiral was held on March 20, 1922.) Here one finds a remarkable foresightedness for central issues of modern physics and mathematics: in the field of nonlinear dynamics (see **Generation of Spirals in Excitable Media**) the importance of stability of states is being discussed. A system evolving towards a stable end point lacks the possibility of further dynamic evolution (e.g., the center of the spiral), whereas unstable behavior may evoke further evolution in the future (outgoing spiral arm). The interplay between stability/instability usually determines the future sort of a system and may well decide on life or death, as presented in biological living organisms.

In some of his paintings (see Fig. 5) Paul Klee designed "spirals with corners". The painting (Fig. 5, left) depicts three abstract red roses on a green and blue background. The surrounding shapes could be analyzed for hours and many scholars have found their own meanings and subjects in them; the more you look at the picture, the more possibilities you find.

Although the colors are muted compared to other famous works of the expressionism period they are bright for Paul Klee who had always struggled with color composition and was not so familiar in this area. His mystical-abstract paintings of the late 1910s where much less vibrant than these works [13].

Fig. 5 Left: Paul Klee, Heroic roses (1938). Kunstsammlung Nordrhein-Westfalen, Düsseldorf, Germany; right: Paul Klee, Timid brute (1938), this person has been perhaps designed in a humorous moment, but it has some personality, hasn't it? Private property in New York

2.3 Stormy Spirals

2.3.1 Leonardo da Vinci (1452–1519)

Leonardo da Vinci was a true genius who graced this world with his presence from April 15, 1452 to May 2, 1519. He is among the most influential artists in history, having left a significant legacy not only in the realm of art but in science as well, each discipline demonstrating his mastery of the other. Da Vinci lived in a golden age of creativity and contributed his unique genius to virtually everything he touched. Today, no name better seems to symbolize the Renaissance age than Leonardo da Vinci.

Figure 6 shows detailed drawings of irregular flows forming eddies of varying sizes. It is a realistic and dynamic picture of turbulent behavior, a major topic of modern hydro- and aerodynamics, as already described in chapter **Appearance in**

Fig. 6 Leonardo da Vinci, Deluges and apocalypses: A deluge (1517/18); drawing of a flood. Royal Collection Trust/©Her Majesty Queen Elizabeth II 2018

Nature (refer to Figs. 5, 7, and 8). Our example of a flood shows his mastership of precise observation and representation of a very complex phenomenon.

In his late years Leonardo, disillusioned with the failure of Renaissance in Italy to support either his art or his science, and fascinated by the power of water as a natural force to be exploited and feared, concentrated all his pessimistic forebodings in a series of drawings of "deluges" [15]. In them, armies, cities, horses, trees and even mountains are helpless before the unleashed fury of storm and flood. A major achievement of Leonardo here is his great capability to extract a time instant from a continuous dynamic evolution of a system.

2.3.2 Vincent van Gogh (1853–1890)

Who would not be enthusiastic and deeply impressed by the paintings and drawings of Vincent van Gogh, who sold just one or a few more of his works during his life, whereas nowadays a masterpiece from his legacy may be worth 80 million dollars. In the short period of 10 years he created 864 paintings and about 1000 drawings.

Fig. 7 Vincent van Gogh, The Starry Night (1889). ©2018. Digital image, The Museum of Modern Art, New York/Scala, Florence

One of the outstanding and widely recognized marvels in this collection is the painting "The Starry Night" [16]. It was painted, after van Gogh voluntarily admitted himself to the Saint-Paul-de-Mausole lunatic asylum in Saint-Rémy-de-Provence on 8 May 1889.

The painting depicts the view from the east-facing window of his asylum room at Saint-Rémy-de-Provence, just before sunrise, with the addition of an idealized village. While the cypresses and the colorfulness of the nocturnal sky reflect the landscape of southern France, the village recalls van Gogh's Dutch homeland.

In a clear night we can watch the fixed stars of our galaxis, blinking in many colors due to the fluctuations of our atmosphere and slowly making their way in the sky along trajectories determined by the rotation of the Earth. Van Gogh created instead a fantastic form of a large, winding spiral nebula, eleven giant stars and an unreal, orange moon that radiates even between its horns. Following the pronounced brushstrokes, each object and each image area has its own direction and its own rhythm contributing to the impressive dynamics of the whole. The flaming cypresses are the earthly dark counterpart of the dragon in the sky. So are the rectangular lights emanating from the windows of the village (Fig. 7).

It could well be that Vincent wished to express his yearning for infinity in nature. The ingenious painting would then contain a trace of an apocalyptic fantasy in his stormy brain.

This wonderful and most expressive work of art radiates emotions in topic, wild brush stroke and color. It has inspired poets and composers to contribute their own variations of the theme. We mention the hommage by the American singer Don McLean with his song "Vincent (Starry, Starry Night)" [17]. In some passage of his words we hear:

> ...for they could not love you, but still your love was true
> and when no hope was left in sight on that starry starry night
> you took your life as lovers often do
> but I could have told you Vincent
> this world was never meant for one as beautiful as you....

2.3.3 Joseph M. W. Turner (1775–1851)

During the Romantic period in England, Joseph M. W. Turner was one of the most highly esteemed painters, also renowned for his aquarelles and drawings [18]. His favorite themes were imaginative landscapes and turbulent, often violent marine scenes, all of them in expressive colorization of light and atmosphere. His way of representation leads to a dematerialization of concrete objects, and the color of sunlight, fire and water become the basic elements of his creations. He was an artist who could most stirringly and truthfully measure the moods of nature. This way he strongly influenced the work of the impressionists.

Many of his paintings radiate the spectral colors of sunlight. The strong increase of coloration may have been an effect due to factual changes of the color of the sky because of the globally distributed dust particles after the 1815 eruption of the pacific volcano Tambora.

There are other paintings kept in dark shades with pronounced black and white contrasts. In Fig. 8, we detect the turbulent effects of the snowstorm and a tornado-like structure hitting a steamboat. An inscription on this painting relates that *The Author was in this Storm on the Night the "Ariel" left Harwich*. Turner later recounted a story:

"I did not paint it to be understood, but I wished to show what such a scene was like; I got the sailors to lash me to the mast to observe it; I was lashed for four hours, and I did not expect to escape, but I felt bound to record it if I did."

He was 67 years old at the time. A critic wrote: "This inscription allows us to better understand the scene represented and the confusion of elements."

Other critical responses to the painting were largely negative, with one critic calling it "soapsuds and whitewash". John Ruskin, the leading English art critic of the Victorian era, though, wrote that the painting was "one of the very grandest statements of sea-motion, mist and light, that has ever been put on canvas."; "It is thus, too often, that ignorance sits in judgment on the works of the genius" [19].

Fig. 8 Joseph M. W. Turner, Snow storm: Steam boat off a Harbour's Mouth (1842). Tate Gallery, Britain

2.4 False Spirals

At the first glance on Fig. 9 (left) most of the people "see" a spiral. But if you follow the "spiral" with your finger, your finger circles around, and it shifts neither toward the outside nor toward the inside. The "spiral" is not a spiral but consists of concentric circles. This is an optical illusion, which Fraser described in 1908 [20]. If you look at these circles carefully, you notice that the circular lines look like a rope stranded with black and white threads. Let us try to draw a rope stranded with black threads only, as shown in Fig. 9 (right). Then, it becomes evident that they are circles. Here, the black and white stranded curves on a spiral-formed background induce the optical illusion: circles are "alchemized" to a spiral!

One more example of false spirals is found in ring books. The form of the metal or plastic wiring which binds the book looks like a helix (three-dimensional spiral). However, the wire does not pass through the holes one after the next. The insert of Fig. 10 shows the real shape of the wire. The structure of the wire is a sequence of arcs. Each arc passes through only one hole. In this way book-making becomes easy and fast.
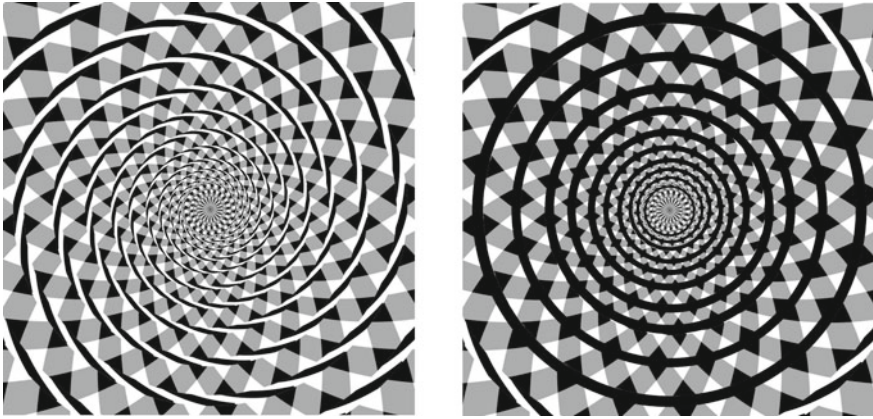
Fig. 9 Left: Fraser's false spiral; right: a modified false spiral

Fig. 10 A ring book and its wiring, insert: wire removed from the ring book. A long wire is folded as shown in the right drawing

3　Spirals in Japanese Culture

A lot of spirals are seen in Japanese culture. Similar to other cultures, the origin of spirals can be water, wind and plants. When water rushes through a narrow straight, water vortices are observed. Naruto whirlpools (lower left in Fig. 11) are formed between Naruto and Awaji island, and the diameter reaches a maximum of 30 m. Hiroshige Ando produced a famous ukiyo-e[1] of the Naruto whirlpool in 1855 (right in Fig. 11) [21]. Interestingly the illustration for the Maelström by Harry Clarke in the short story of Edgar Allan Poe "A descent into the Maelström" [2] shows a similar motif (upper left in Fig. 11). Such motives of whirlpools are also found in Japanese sand/rock gardens, where rocks and sand can be islands and sea [22].

---

[1]Ukiyo-e is one of the Japanese arts - woodblock prints produced form the 17th to the 19th century.
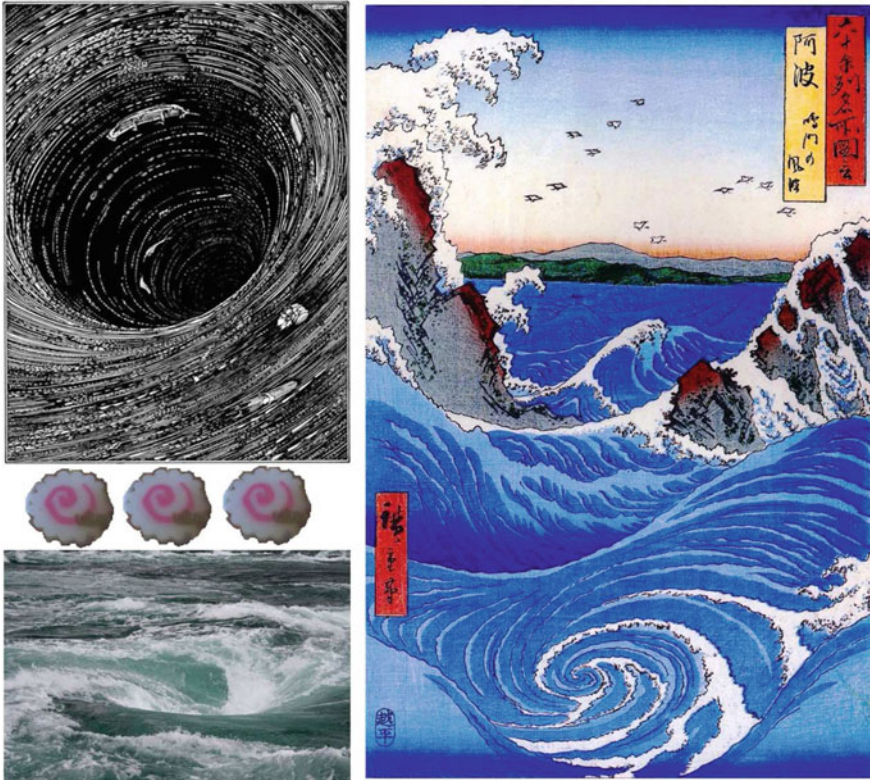
Fig. 11 Top left: Maelström illustrated by Clarke [23]; middle left: sliced fish banger, Naruto-maki; bottom left: Naruto whirlpools; right: Hiroshige's Ukiyo-e of the Naruto whirlpools

Hiroshige's work influences Western painting as a part of the trend in Japonism. Western artists (for example, van Gogh) studied his compositions and painted copies.

There is also food originating from the Naruto whirlpool: fish banger "Naruto-maki". When it is sliced, a spiral pattern appears on the surface (see Fig. 11, middle left). The sliced Naruto-maki is one of the most important toppings for Udon (Japanese noodle soup).

Vortices caused by wind are a kind of symbol of the gods for wind, storm and thunder. Often they carry a ring with spiral elements on their shoulder. Figure 12 (left) is a sculpture of a thunder god in the Sanjūsangen-dō Temple[2] in Kyoto. A toy, pellet drum, the sound of which imitates the roar of thunder has often three comma-shaped figures arranged in a circle (Fig. 12, right).

---

[2]Sanjūsangen-dō (thirty-three ken (unit of length) hall) is a Buddhist temple in Higashiyama District of Kyoto, Japan. It was built in 1164 by Taira no Kiyomori under the order of Emperor Go-Shirakawa. The temple complex was burned out in 1249 and only the main hall was rebuilt in 1266.

Another aspect of Japanese culture are Japanese traditional clothes "Kimono". There are plenty of kimono materials patterned with small vortices in water streams, clouds, winds, and plants, as shown on the left of Fig. 13. One special pattern for

Fig. 12 Left: a thunder god in the Sanjūsangen-dō Temple, Kyoto. Photograph taken by Ogawa [24]; right: a pellet drum with three comma-shaped figures in a circle

Fig. 13 Left: kimono materials with spiral patterns; right: wrapping cloth with "karakusa" pattern and its client, a thief???

textile, different from such elegant patterns as for the Kimono, is the "karakusa pattern" (ornamental arabesque design, upper right of Fig. 13). This pattern is used especially for large, strong and cheap wrapping cloth. Many merchants in the Edo period (17th century to the middle of 19th century) carried their goods in wrapping cloth with the Karakusa pattern. If you have to collect many things quickly for carrying away, this kind of wrapping cloth is very practical. Even today most of Japanese families keep such wrapping cloth at home for emergency cases. It is also convenient for thieves: before stealing things they carry only a folded wrapping cloth in their pocket, and afterwards they can carry away many things altogether with this cloth.

4 Functional Spirals

4.1 Musical Instruments

String instruments belonging to the violin family (violin, viola, cello, and double bass) are valuable pieces of art when made by a skillful luthier. While the main goal is to make their music sound beautiful over the whole range of accessible notes, there is also a pronounced effort to build wonderful pieces of art by observing long established rules and individual features.

A majority of string instruments have a scroll as the decoratively carved beginning of the neck as shown in Fig. 14. The scroll has typically the shape of a rolled-up spiral, although some violins are adorned with carved heads, human and animal, preferentially found with older instruments as a Baroque ornament.

The quality of a scroll is one of the things used to judge the luthier's skills. Scrolls usually approximate a logarithmic spiral (see chapter **Spirals, Their Types and Peculiarities**). They have almost no influence on the sound, but have become a fixed characteristic part in the instrument's design. Below the scroll is a hollowed-out compartment (the pegbox) through which the tuning pegs pass. The instrument's strings are wound around these pegs. The scroll and pegbox are almost always carved out of one piece of wood.

Fig. 14 Scroll of a violin
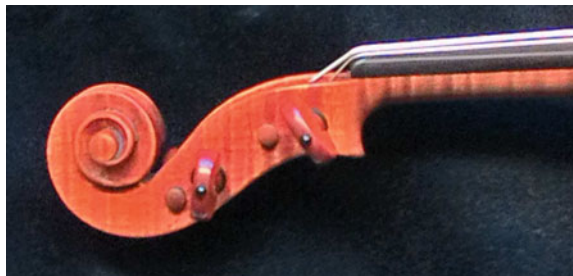
Fig. 15 Brass instruments. Left: saxophone; upper right: trumpet; lower right: an old post horn exhibited in the Spandau citadel, Spandau, Germany

Many brass instruments have a tube of spiral form between the mouthpiece and the bell. Saxophones have only one simple turn (Fig. 15, left), trumpets have one and a half turns (Fig. 15, upper right), post horns (Fig. 15, lower right) have two turns, and others have more complicated shapes. Different from the spiral of violin families, the shape and size of tubes are essential for the tone.

4.2 Staircases, Springs and Screws

Spiral staircases are one of the most favorite objects for photographers. Many of such pictures have an aesthetic touch. However, different from the scroll of the violin, the primary function of spiral staircases is not decoration, but the shape itself. A smooth spiral form helps smooth movement, when one goes up or down the staircase. The staircase shown in Fig. 16 does not have a uniform shape of spiral - partially round and partially square. And therefore, the movement of the person who goes up (or down) this staircase is not constant - going up, changing the angle, walking at the same level. But it is as beautiful as staircases with a smooth helix shape. Architects should find the optimum design for its available space, human movement and aesthetic aspect.

Fig. 16 A spiral staircase consisting of a round part and a square part

In our normal life we use many things which have a spiral form. Springs and screws are inevitable for constructing machines, furnitures or buildings. Due to the spiral form screws convert rotational motion to linear motion. And springs can store mechanical energy.

4.3 Spirals in Data Storage

Applications of the Archimedean spiral can be found today on any data carrier. On a compact disc (CD) data in digital form (with values 1 and 0) start on the innermost track and are written in outward direction in spiral form. Precisely, this is the involute of the circle which defines the innermost radius of data writing and around which the track is wound up. This trace is very close to an Archimedean spiral (see chapter **Spirals, Their Types and Peculiarities**).

Standard parameters of commercial CDs are: diameter $D = 12$ cm, average revolution speed $V = 300$ min^{-1}, duration $T = 80$ min. The recorded tracks are located in a band between 22.5 and 59 mm (with 36.5 mm width) from the disk center, i.e. their average radius is $R \approx 41$ mm. One calculates for the total length L of the track for a recorded piece:

$$L = (2\pi R)VT \approx 6.2 \text{ km}.$$

The width of the track is about 1.2 μm. Then, within the recording interval on the CD away from the center one would expect 3×10^4 tracks passing a certain direction [25].

The DVD functions in a way similar to the CD, but with much higher storage capacity. Also for the older vinyl records a similar storage principle holds, but here data are read from the outside to the inside [26].

For the previously produced audio cassettes information is stored on magnetic tape, which is released from a supply reel and wound up on another tape spool. Here again an involute of a circle is formed. But the magnetic tape assumes practically the shape of an Archimedean spiral. A standard cassette with 60 min playing time has a length of 88 m.

The illustrations in the first part of this chapter present just a small selection of eminent paintings around the theme of this book, and the comments on these can barely touch the meaning and impression they had for the artists and for the people admiring them. We like to contemplate these masterpieces in the frame of culture and nature, the themes of the previous two chapters. We see in such a comparison a potentially strong link between culture, nature and art to be further analyzed by scientific methods. Furthermore one finds many practical application where spirals play a basic role, and this has an great importance in itself.

The subsequent course of this volume's path will emphasize a cross-interdisciplinary approach, in that topics from numerous relevant fields shall be discussed in some detail. Either you want to pick certain topics that meet your specific interest. Or you prefer to read through the book at full length. Have a nice time!

Picture credits

Fig. 1 Photo: ©MAK/Georg Mayer Ownership credit: MAK - Austrian Museum of Applied Arts/Contemporary Art, Fig. 2 ©VG Bild-Kunst, Bonn 2018, Fig. 3 Watercolor on primed gauze on wooden panel; original frame 3.1×28.3/28.1 cm, privatbesitz Japan, Fig. 4 Watercolor on primed paper on cardboard 23.2×30.7 cm Privatbesitz, Fig. 5 Left: Oil on burlap 68×52 cm, Kunstsammlung Nordrhein-Westfalen, Düsseldorf, right: oil and colored paste on paper on burlap; original frame 74×56 cm Privatbesitz New York City. Fig. 6 Royal Collection Trust/©Her Majesty Queen Elizabeth II 2018, Fig. 7 ©2018. Digital image, The Museum of Modern Art, New York/Scala, Florence, Fig. 8 Current location: Tate Britain, Fig. 11 Top left: Harry Clarke-Printed in Edgar Allan Poe's Tales of Mystery and Imagination, 1919, bottom left: public domain, photograph taken by Hellbuny on 4-21-2008, right: public domain, Fig. 12 Left: Public domain, photograph taken by K. Ogawa, published by Shimbi Shoin, right: public domain, Fig. 15 Left: CC BY-SA 4.0, Yamaha Corp., top right: CC BY-SA 3.0, bottom right: CC BY 3.0.

References

1. A. Duncan, A report on the maelstrom of drontheim, in *The Mariner's Chronicle: containing narratives of the most remarkable disasters at sea, such as shipwrecks, storms, fires, and famines* (G. W. Gorton, New Haven, 1834)
2. E.A. Poe, *A Descent into the Maelström* (BookSurge Classics, 2004). Original publication in the May 1841 edition of Graham's Magazine
3. F. Schiller, *Der Taucher* (Carlsen, Hamburg, 2009). Original in 1798
4. https://germanstories.vcu.edu/schiller/taucher_dual.html
5. W. Kandinsky, *Point and Line to Plane* (Courier Corporation, North Chelmsford, 2012). Original publication 1926 in German *Punkt und Linie zu Fläche*
6. P. Klee, *Das bildnerische Denken - Schriften zur Form- und Gestaltungslehre* (Schwabe, Stuttgart, 1956)
7. J. Rogoyska, P. Bade, *Gustav Klimt* (Parkstone International, New York, 2012)

8. M. Droste, in *Bauhaus*, ed. by P. Gossel (Taschen America LLC, 2005)
9. J. Itten, *Design and Form: the Basic Course at the Bauhaus* (Van Nostrand Reinhold, New York, 1975)
10. L. da Vinci, *A Treatise on Painting* (J.B. Nichols and Son, London, 1835)
11. P. Klee, Schöpferische Konfession: Paul Klee, in *Tribüne der Kunst und der Zeit. Eine Schriftensammlung, Band VIII*, ed. by K. Edschmid (Erich ReißVerlag, Berlin, 1920), pp. 28–40
12. P. Klee, *Die unendliche Naturgeschichte* (Schwabe, Stuttgart, 1970); translated in English by H. Norden, *The Nature of Nature* (G. Wittenborn, New York, 1970)
13. H. Hartmann, Die Spirale im bildnerischen Denken von Paul Klee, in *Die Spirale*, ed. by H. Hartmann, H. Mislin (Birkhäuser, Basel, 1985), pp. 94–98
14. P. Klee, *Pedagogical Sketchbook: Introduction by Sibyl Moholy-Nagy* (Farber and Farber, London, 1968)
15. https://www.royalcollection.org.uk/collection/912380/a-deluge
16. A. Boime, Van Gogh's Starry Night: A History of matter and a matter of history. Arts Magazine (1984). http://www.albertboime.com/Articles/Dec1984.pdf
17. https://don-mclean.com/2007/04/11/vincent-starry-starry-night/
18. M. Bockemühl, *J.M.W. Turner: The World of Light and Colour* (Taschen, Köln, 2015)
19. E.T. Cook, A. Wedderburn (eds.), *The Works of John Ruskin* (George Allen, Newarc-on-Trend, 1903)
20. J. Fraser, A new visual illusion of direction. Br. J. Psychol. **2**, 307–320 (1908)
21. I. Oka, *Hiroshige: Japan's Great Landscape Artist* (Kodansha, Tokyo, 1992)
22. K. Seike, M. Kudo, W. Schmidt, *Japanische Gärten und Gartenteile* (Ulmer, Stuttgart, 1980)
23. H. Clarke, printed in Edgar Allan Poe's Tales of Mystery and Imagination (1919)
24. K. Ogawa, in *Selected Relics of Japanese Art*, ed. by S. Tajima, vol 20 (Shinbi Shoin, Kyoto, 1899–1908)
25. https://en.wikipedia.org/wiki/Compact_disc
26. J. Taylor, *DVD Demystified* (McGraw Hill, New York, 1998)

Part II
Spirals and Vortices in Mathematics

Posers make whirls,
But no flow

— Icelandic proverb

Spirals, Their Types and Peculiarities

Andrey Polezhaev

Abstract In this chapter, we provide mathematical data concerning the description of spirals. Before starting with mathematical equations, Albrecht Dürer's pioneering works are briefly introduced. Subsequently, we discuss some properties of different spirals in a plane which make them important in nature and for technical applications. Smooth spirals are usually described by equations which are formulated either in terms of the polar coordinates radius and angle, such spirals being called algebraic, or in terms of curvature and arc length; then they are referred to as pseudo-spirals. We consider in detail a number of spirals of both classes emphasizing their most essential features. Besides 2D spirals we also discuss examples of 3D spirals, usually referred to as helices. To conclude the chapter we mention non-smooth spirals and fractal spirals.

1 Introduction

According to the Encyclopedia of Mathematics [1] 2D spirals are plane curves which usually go around one point (or around several points), moving either towards or away from it (them). This interpretation of the term is not a strict definition. One of the variants of the strict definition, assuming the monotonicity of the polar equation of the curve, is not universal: choosing another pole, we can break the existing monotony, and only because of this the curve "ceases to be a spiral," even though it itself has not changed.

One distinguishes two types of spirals: algebraic and pseudo-spirals [2] Algebraic spirals are spirals whose equations in polar coordinates are algebraic with respect

A. Polezhaev (✉)
P.N. Lebedev Physical Institute, Russian Academy of Sciences,
Leninskiy prosp. 53, 119991 Moscow, Russia
e-mail: apol@lpi.ru

to radius ρ and polar angle φ. These include the hyperbolic spiral, the Archimedean spiral, the Galilean spiral, the Fermat spiral, the parabolic spiral and the lituus.

Pseudo-spirals are spirals whose natural equations can be written in the form $r = as^m$, where r is the radius of curvature and s is the arc length. When $m = 1$ it is the logarithmic spiral, when $m = -1$ - the Cornu spiral, and when $m = 1/2$ it is the involute of a circle [3].

A spiral in three-dimensional space (a helix) is a curve that turns around an axis at a constant or continuously varying distance while moving parallel to the axis.

After a short essay on the eminent mathematician and artist Albrecht Düer we will discuss in detailed properties of all the above mentioned spirals.

Albrecht Dürer (1471–1528)

The German Renaissance artist Albrecht Dürer is acknowledged worldwide for his paintings, drawings, and copper engravings. He established his reputation across Europe at an early age due to his high-quality woodcut prints. His watercolors also mark him as one of the first European landscape artists.

Less known are his achievements as an eminent mathematician. In a well founded and systematic knowledge of geometry he saw the prerequisite for successful artistic creativity. Early enough he studied the Latin translation of the "Elements of Euklid", which had appeared in 1505. He also participated in drawing a map of the northern hemisphere of the Earth together with Johannes Stabius [4].

Historically most important is the first German book on Geometry under the title Four Books on Measurement (*Underweysung der messung mit dem zirckel und richtscheyt in Linien ebnen unnd gantzen corporen, or Instructions for Measuring with Compass and Ruler*), which appeared in 1525. In this work Dürer defines many special curves like the Pascal snail or the shell line, introduces a new construction of an ellipse, and recognizes that ellipse, parabola and hyperbola are specific conic sections. He even develops approximate solutions for the three problems of classical antiquity: divide an angle into 3 parts, transform a circle to a square, and double the volume of a cube. His methods are always deductive and systematic under the recognition of the basic difference between exact and approximate solutions of a problem (not yet always so clear for contemporary colleagues).

The first book of this Œuvre focuses on linear geometry. Dürer's geometric constructions include helices, conchoids (resembling conch shells; see chapter **Appearance in Nature**) and epicycloids. He presents guidelines for the construction for different "Schneckenlinien", i.e. spirals. A few types of spirals are analyzed and suggestions for applications in the arts are discussed.

The second book moves onto two-dimensional geometry, i.e. the construction of regular polygons. Here Dürer favours the methods of Ptolemy over

Euclid. The third book applies these principles of geometry to architecture, engineering and typography. The fourth book completes the progression of the first and second by moving to three-dimensional forms and the construction of polyhedra. Here Dürer discusses the five Platonic solids, as well as seven Archimedean semi-regular solids.

We present now two examples from the first book. The "first construction" in this book deals with the Archimedean spiral (cf. Sect. 2.1). An approximate procedure is based on half-circles with different radii and centers, starting from the black dot in the upper figure as the initial center. Dürer indicates how he performs this construction with compass and ruler.
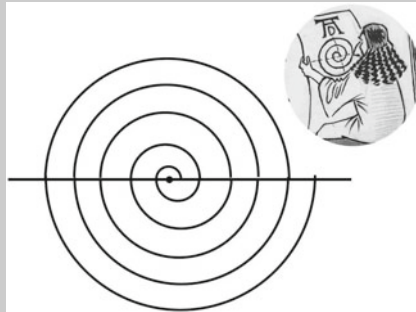
Dürer's "Archimedean" spiral reproduced according to his original drawing in [5]
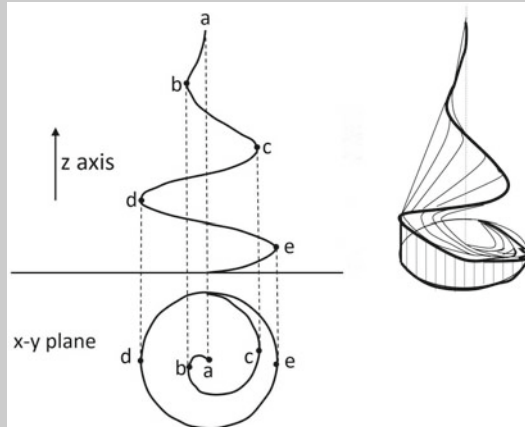
Left: drawing of a 3D spiral, a simplified version from the original construction in [5]; right: the reconstructed object from Dürer's drawing in a perspective view

In another construction he studies a conical helix (cf. Sect. 4.3) on the basis of an Archimedean spiral. He starts with a circle having 12 radial marks, inside which an Archimedean spiral is drawn with points labeled 13–23. Subsequently, the radius starting at point **a** in the lower figure is subdivided

into 24 equal sections. Then this structure is pulled up into a third dimension, where points are moving along the arc and the spiral line and the length of their cosine is projected along an axis of motion.

In this drawing (left) we have illustrated a simplified picture of this construction. The outer circle has only 2 radial marks (d, e) instead of 12, and the inner spiral 3 (a, b, c) instead of 12. The spiral is equally well pulled up in direction of the z-axis on which the cosine is projected. The reconstructed object is shown on the right side.

Since 1508 Dürer had worked on a Teaching Book on Painting, which was finished only in the year of his death. Furthermore, he published four books on human proportions, where he describes the shape of heads and different motion studies under various perspectives, including differences in male and female bodies. As ever, he proved to be a master of descriptive geometry.

2   Algebraic Spirals

2.1   *Archimedean Spiral*

The **Archimedean spiral** (also known as the **arithmetic spiral**) is a spiral named after the 3rd century BC Greek mathematician Archimedes. It is a flat curve, the trajectory of point M (see Fig. 1), which moves uniformly along the ray OV with the origin at O, while the OV ray itself rotates uniformly around O. In other words, the distance $\rho = OM$ is proportional to the angle rotation φ of the beam OV. The rotation of the OV beam into the same angle corresponds to the same increment ρ. The equation of the Archimedean spiral in the polar coordinate system is written as follows:

$$\rho = k\varphi, \tag{1}$$

where k is the displacement of the point M along the ray r, with a rotation by an angle equal to one radian.

The rotation of the straight line by 2π corresponds to the displacement $a = |BM| = |MA| = 2k\pi$. The number a is called the spiral pitch. The equation of the Archimedean spiral can be rewritten as follows:

$$\rho = a\varphi/2\pi.$$

When the ray is rotated counterclockwise, the right-handed spiral is obtained, while rotating clockwise - the left-handed spiral. Both branches of the spiral (right and left) are described by the same Eq. 1 (here and further we will treat negative value of ρ as a centrally symmetric reflection with respect to the origin, i.e. $(-\rho, \varphi) \equiv (\rho, \varphi + \pi)$). Positive values of φ correspond to the right-handed spiral, negative - to the left-

Fig. 1 Archimedean spiral
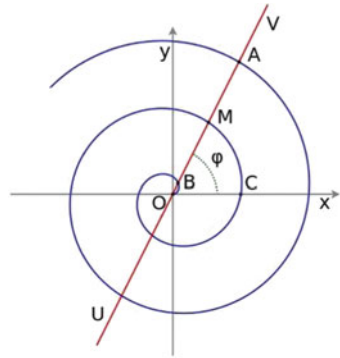
handed spiral. In Fig. 1 only the right-handed spiral is shown. Taking the mirror image of this curve across the y-axis will yield the left-handed spiral.

When the spiral is untwisted, the distance from the point O to the point M tends to infinity, while the spiral pitch remains constant (that is, the farther from the center, the closer the coils of the spiral in shape approach the circle).

Sometimes the Archimedean spiral is described as a spiral with a "constant separation distance" between successive turns. This is somewhat misleading [6]. The constant distances in the Archimedean spiral are measured along rays from the origin, which do not cross the curve at right angles, whereas a distance between parallel curves is measured orthogonally to both curves. There is a curve slightly different from the Archimedean spiral, the involute of a circle (which is discussed in more detail further), whose turns have constant separation distance in the latter sense of parallel curves.

The arc length L of the Archimedean spiral is equal to the integral of dl in the range from 0 to φ:

$$L = \int_0^\varphi k\sqrt{1 + \varphi^2}d\varphi,$$

$$L = \frac{k}{2}\left[\varphi\sqrt{1 + \varphi^2} + \ln(\varphi + \sqrt{1 + \varphi^2})\right].$$

Other examples of algebraic spirals are described by equations of the same form:

$$\rho = a + k\varphi^{(1/c)} \tag{2}$$

and thus are sometimes referred to as general Archimedean spirals while the normal Archimedean spiral occurs when $c = 1$.

2.2 *Hyperbolic Spiral*

The hyperbolic spiral is a plane transcendental curve, whose equation in polar coordinates has the form:

$$\rho = a/\varphi. \tag{3}$$

In Cartesian coordinates $(x = \rho \cdot cos\varphi;\ y = \rho \cdot sin\varphi)$ the representation for the hyperbolic spiral has the form:

$$x = a(cos\varphi)/\varphi, \quad y = a(sin\varphi)/\varphi.$$

The spiral has a horizontal asymptote at $y = a$: for φ approaching zero the ordinate approaches a, while the abscissa grows to infinity:

$$\lim_{\varphi \to 0} x = a \lim_{\varphi \to 0} \frac{cos\varphi}{\varphi} = \infty, \quad \lim_{\varphi \to 0} y = a \lim_{\varphi \to 0} \frac{sin\varphi}{\varphi} = a.$$

The arc length of a hyperbolic spiral between the points $M_1(\rho_1, \varphi_1)$ and $M_2(\rho_1, \varphi_1)$ (see Fig. 2) is calculated as follows:

$$L = a \int_{\varphi_2}^{\varphi_1} \frac{1}{\varphi} \sqrt{1 + \frac{1}{\varphi^2}} d\varphi = a\left[-\frac{1}{\varphi}\sqrt{1 + \varphi^2} + ln\left(\varphi + \sqrt{1 + \varphi^2}\right) \right]_{\varphi_2}^{\varphi_1}.$$

In addition, we can calculate the area of the sector bounded by this arc and two radius vectors ρ_1 and ρ_2 corresponding to the angles φ_1 and φ_2:

$$S = \frac{a^2}{2} \int_{\varphi_2}^{\varphi_1} \frac{1}{\varphi^2} d\varphi = \frac{a^2}{2}\left(\frac{1}{\varphi_2} - \frac{1}{\varphi_1}\right) = \frac{a(\rho_2 - \rho_1)}{2}.$$
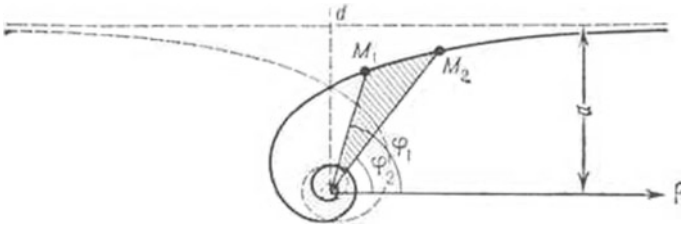
Fig. 2 Hyperbolic spiral

2.3 Parabolic Spiral

The **parabolic spiral** is a plane transcendental curve whose equation in polar coordinates has the form:

$$\rho = a\sqrt{\varphi} + l, \quad l > 0. \tag{4}$$

To each value of φ there correspond two values of $\sqrt{\varphi}$ - positive and negative. The curve has infinitely many double (intersection) points and one inflection point (see Fig. 3).

Fig. 3 Parabolic spiral
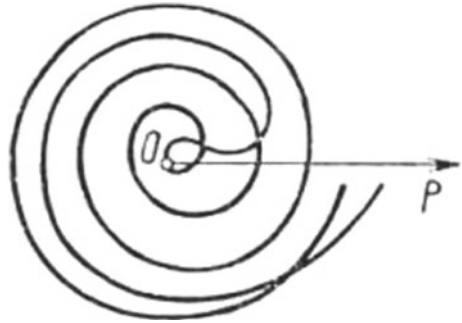
2.4 Fermat's Spiral

When in Eq. 5 we take $l = 0$ we arrive at Fermat's spiral, which may be treated as a special case of the parabolic spiral. The curve has also two branches corresponding to both signs of $\sqrt{\varphi}$ but contrary to the case of the true parabolic spiral it has no double points (see Fig. 4).

2.5 Galilean Spiral

Another example of algebraic spirals is the **Galilean spiral**, which is a plane curve with equation in polar coordinates

$$\rho = a\varphi^2 - l, \quad l \geq 0. \tag{5}$$

The curve is symmetric with respect to the axis x (see Fig. 5) and has a double point at the pole with tangents forming angles equal to $\pm\sqrt{l/a}$ with this axis. On the x-axis there are infinitely many double points at distances $\rho = ak^2\pi^2 - l$ (where $k = 1, 2, 3, \ldots$) from the center.

Fig. 4 Fermat's spiral
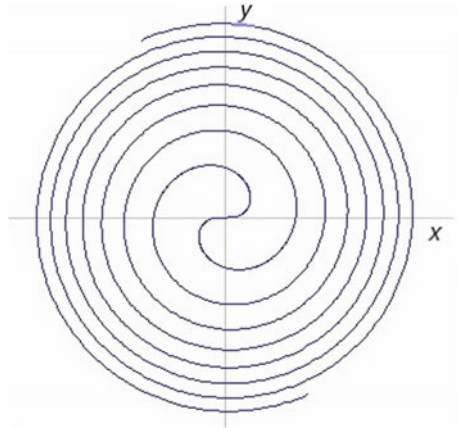
Fig. 5 Galilean spiral
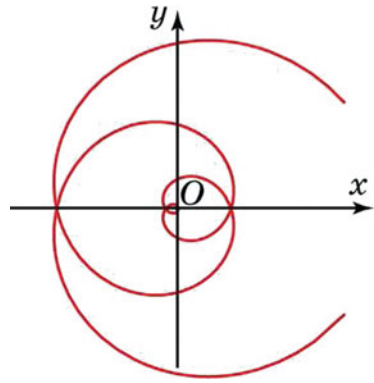
The Galilean spiral can be viewed as a trajectory of a point that is uniformly accelerated along a straight line, and this straight line rotates uniformly around one of its points. It is named after G. Galilei (1683) in connection with his studies on the free fall of solids. Indeed, if we take into account the rotation of the Earth, then the trajectory of the stone falling from a tower is a portion of the Galilean spiral.

2.6 The Lituus

We conclude the review of algebraic spirals by the **lituus**, which is determined in polar coordinates by the equation

$$\rho = a/\sqrt{\varphi}. \tag{6}$$
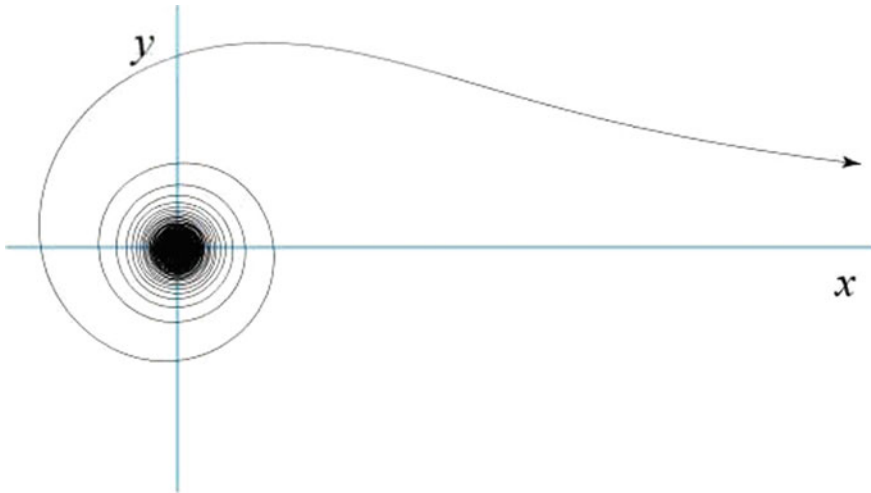
Fig. 6 Lituus (one branch)

This spiral has two branches depending on the sign of $\sqrt{\varphi}$. One of them tends from infinity (where it asymptotically approaches the horizontal axis) to the point the origin at $(0, 0)$, twisting around it in a counterclockwise spiral (see Fig. 6). The other branch is centrally symmetric to the first one with respect to the origin. The size of the spiral is determined by the coefficient a. Each of the branches has one inflection point, correspondingly $(\varphi, \rho) = (\frac{1}{2}, \sqrt{2a})$ and $(-\frac{1}{2}, \sqrt{2a})$. The lituus spiral was studied by Roger Cotes in 1722. It is named after an ancient Roman trumpet called lituus.

3 Pseudo-Spirals

While equations for algebraic spirals in polar coordinates are algebraic with respect to angle and radius, the corresponding equations in the case of pseudo-spirals are algebraic with respect to curvature and length along the curve. They have the form $r = as^m$, where r is the radius of curvature and s is the arc length. Such equations are called natural.

3.1 Logarithmic Spiral

The most well-known and important example of pseudo-spirals is the **logarithmic spiral**. It is a plane transcendental curve with equation in polar coordinates in the form

$$\rho = ae^{b\varphi}, \quad a > 0. \tag{7}$$

Fig. 7 Logarithmic spiral
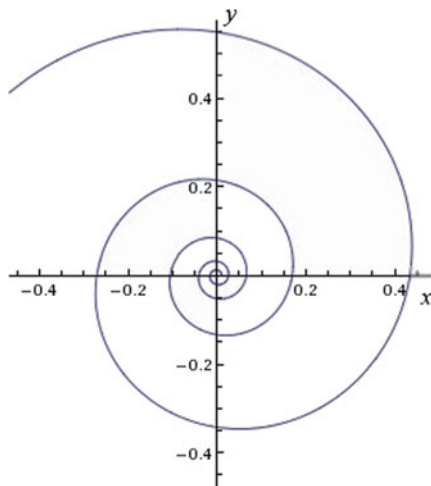
If $b > 0$, as $\varphi \to +\infty$ the logarithmic spiral evolves anti-clockwise, and as $\varphi \to -\infty$ the spiral twists clockwise, tending to its asymptotic point 0 (see Fig. 7). If $b < 0$, the twisting behavior is opposite. Equation 7 of the logarithmic spiral can be presented in the following equivalent form:

$$\rho = ad^\varphi = ak^{\varphi/2\pi}, \tag{8}$$

where $d = e^b$ and $k = e^{2\pi b}$. The parameter k is called growth coefficient. This growth coefficient shows how many times the polar radius of the helix has changed as it rotates through the full angle of 2π (or 360°).

The arc length of a logarithmic spiral between the points $M_1(\rho_1, \varphi_1)$ and $M_2(\rho_2, \varphi_2)$, where $\varphi_1 < \varphi_2$, is calculated as follows:

$$L = \int_{\varphi_1}^{\varphi_2} ae^{b\varphi}\sqrt{1+b^2}d\varphi = a\frac{\sqrt{1+b^2}}{b}(e^{b\varphi_2} - e^{b\varphi_1}) = \frac{\sqrt{1+b^2}}{b}(\rho_2 - \rho_1).$$

Thus, we can see that when φ_1 tends to $-\infty$ the length of the arc remains finite although the spiral circles the origin an unbounded number of times without reaching it. If the arc length is measured from the origin then the natural equation of the logarithmic spiral has the form: $r = bs$.

We can calculate the angle θ between the tangent to the curve and radial line at any point of the spiral: $tan\theta = \frac{\rho}{\rho'_\varphi} = 1/b$. We see that this angle is constant and does not depend on the point. In view of this property, the logarithmic spiral is also called **equiangular**. In fact, the parameter b controls how "tightly" and in which direction the curve spirals. In the extreme case that $b = 0$ ($\theta = \pi/2$) the spiral becomes a circle of radius a. Conversely, in the limit that b is infinity ($\theta \to 0$) the spiral tends toward a straight half-line.

The logarithmic spiral was first described by Descartes and later extensively investigated by Jacob Bernoulli, who called it *Spira mirabilis*, "the marvelous spiral". In fact, the logarithmic spiral has a lot of remarkable properties. Besides the already mentioned property that the logarithmic spiral crosses any radius at a fixed angle, it has another unique property self-similarity. It means that while the size of the spiral increases, its shape is unaltered with each successive curve. Self-similarity of the logarithmic spiral manifests itself in different ways. One of its consequences is the fact that the distances between the turnings of a logarithmic spiral increase in geometric progression. Therefore, the third name of this curve is **geometric** spiral. Scaling of the spiral by a factor $e^{2\pi b}$ gives the same spiral, without rotation. The logarithmic spiral is the only curve, for which involute (a curve traced out by a point in a straight line segment which rolls over the original curve), evolute (the original curve of an involute) and caustic (a curve to which the ray of light, reflected or refracted by the original curve, are tangents) are also, in turn, logarithmic spirals.

The logarithmic spiral is undoubtedly a spiral, which is most often found in nature. The animal kingdom provides us with examples of spirals of shells of snails and shellfish. All these forms indicate a natural phenomenon: the process of winding is associated with the process of growth. In fact, the shell of a snail is no more, no less than a cone wound on itself. The horns of ruminant animals, too, but they are also twisted. Moreover, although the physical laws of growth in different species are different, the mathematical laws that govern them are the same: they all have a geometric spiral, a self-similar curve. If we carefully look at the growth of shells and horns, we will notice another curious property: growth occurs only at one end. And this property keeps the form completely unique among the curves in mathematics, the shape of a logarithmic, or conformal spiral (examples, see chapter **Appearance in Nature**).

Galaxies, storms and hurricanes give impressive examples of logarithmic spirals. And finally, in any place where there is a natural phenomenon, in which expansion or contraction with rotation is combined, a logarithmic spiral appears inevitably. In the plant world, examples are even more striking, because the plant can have an infinite number of spirals, and not just one spiral in each. The location of sunflower seeds in any sunflower, scales in any pineapple, and other various kinds of plants, simple chamomiles give us a real parade of interwoven spirals. If we look from above on any pine cone, we will see that its seeds are arranged in the form of a large number of spirals. And it is not accidental. It is not a coincidence. The seeds are optimally located, i.e., maximizing the use of space, and this optimization of space is achieved by spiraling [7–9] (examples, see chapter **Appearance in Nature**).

3.2 Golden Spiral

A specific case of the logarithmic spiral is the **golden spiral** with a growth coefficient $k = \Phi^4$, where Φ is the golden ratio, equal to $(\sqrt{5} + 1)/2$, which is also known as the number of Phidias [10]. This spiral received its name because of the connection

Fig. 8 Golden spiral
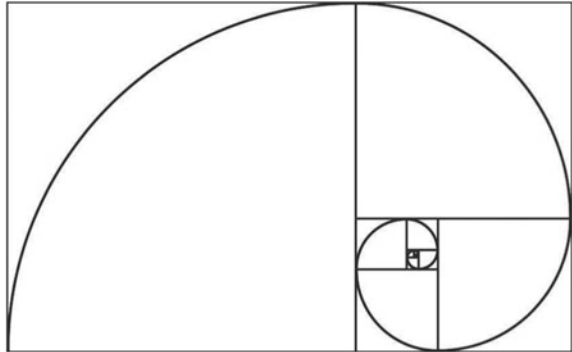
with the sequence of nested rectangles with the ratio of sides equal to Φ, which are usually called golden. A golden spiral can be inscribed into the set of such rectangles and circumscribed around it (Fig. 8).

Its proximity to the **Dürer spiral** made it very famous. Dürer was the first to inscribe into such a sequence of rectangles a spiral formed by circular arcs, an impressively simple method for spiral construction [4, 5].

There are several similar spirals that are close, but do not coincide exactly with the golden spiral, with which they are often confused.

As already written above, when a golden spiral is inscribed into a sequence of golden rectangles (with the golden ratio of the side lengths) embedded in each other, it is approximated by a spiral constructed according to the Dürer method. Albrecht Dürer worked on the geometrical construction of Archimedean and logarithmic spirals (see Inset). He suggested the following procedure: a golden rectangle is divided into a square and a rectangle similar to it, which, in turn, is split in the same way. After continuing this process for an arbitrary number of steps, the result will be an almost complete partitioning of the rectangle into squares. If we connect the corners of these squares by quarter-circles we obtain a curve, which, though not being a true logarithmic spiral, approximates a golden spiral quite well (In fact, Fig. 8 equally describes both golden and Dürer spirals).

3.3 Fibonacci Spiral

Another approximation is the **Fibonacci spiral**, which is constructed like the above-described Durer spiral, except that we start with a rectangle of two squares and then add a square of the same length to the larger side of the rectangle (Fig. 9). The Fibonacci spiral, unlike the golden spiral, has a starting point. Taking its origin in a point, such a figure can unfold indefinitely. The Fibonacci sequence is characterized by the fact that every number after the first two is the sum of the two preceding ones: 1, 1, 2, 3, 5, 8, 13, 21,... It has an interesting property: the ratio between the

Fig. 9 Fibonacci spiral
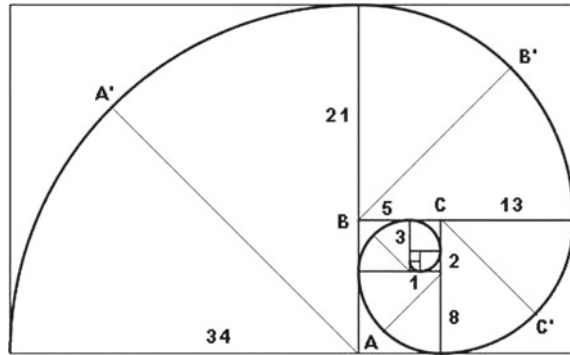
neighboring Fibonacci numbers tends to a golden ratio [11]. Thus the more squares are added the more the spiral approaches the golden spiral (more detail, see chapter **Appearance in Nature**, Appendix).

3.4 Cornu Spiral

The **Cornu spiral** is a curve with its curvature changing linearly with the curve length (the curvature of a circular curve is equal to the reciprocal of the radius). Thus its natural equation is:

$$r = b/s. \tag{9}$$

Its curvature begins with zero at the straight section in the origin and increases linearly with the curve length (see Fig. 10). The curve has infinite length and two asymptotic points.

The Cornu spiral is also commonly referred to as **clothoid**, **Euler spiral** or **Fresnel spiral**. It was studied by Jacques Bernoulli in 1705, Euler in 1743, Fresnel in 1818, Cornu in 1874, Cesaro in 1886 (who gave it the name clothoid).

The clothoid was proposed by Cornu to facilitate the calculation of diffraction in problems of applied optics. It makes a perfect transition spiral as its curvature increases linearly with the distance along the spiral. This spiral is used as a transitional arc in road construction [12]. When the road section in the plan has the shape of a part of the clothoid, the steering wheel of the car turns without jerking. This bend of the road allows you to go through a turn without significantly reducing the speed. For the same reason the spiral is used in ship design, specifying the curvature distribution of an arc of a plane curve while drawing a ship.

Fig. 10 Cornu spiral
(clothoid)
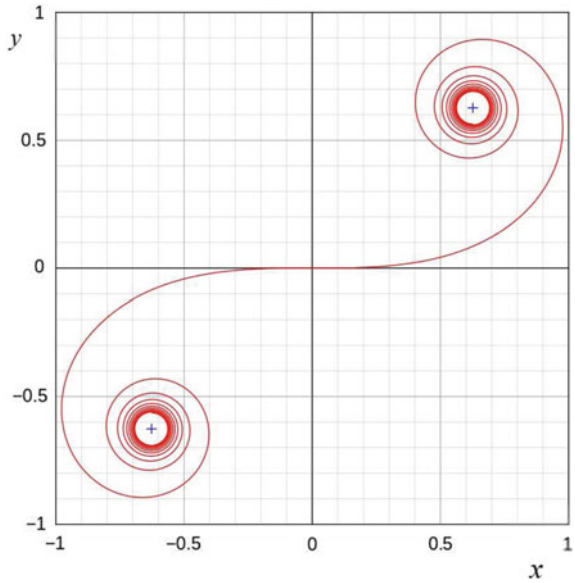
3.5 Involute of a Circle

Another example of a pseudo-spiral is the **involute (evolvent) of a circle**. It is the curve for which all the normals are tangent to a fixed circle of the radius a (see Fig. 11). More practically, it is the curve traced by a hand unwinding a wire reel held in the other hand. Its natural equation (r is the radius of curvature and s is the arc length):

Fig. 11 Involute of a circle
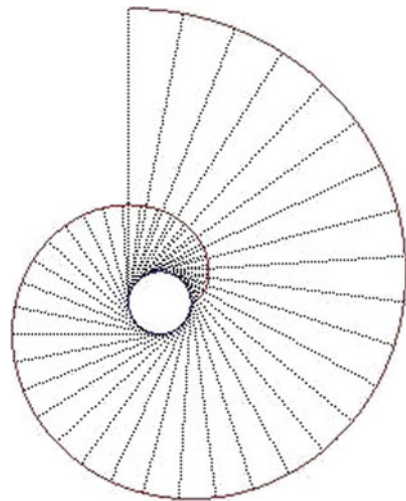
Fig. 12 Involute of a circle
(red) and Archimedean spiral
(blue)
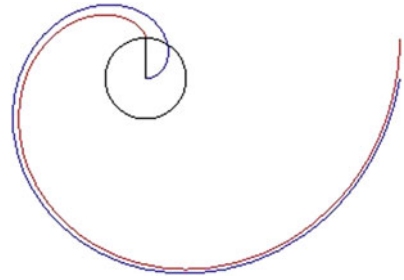
$$r^2 = 2as. \tag{10}$$

The involute of a circle is a special case of an involute of a curve, which may be viewed as the curve traced by the end of a wire tightened along the generating curve and winding itself along the latter. Like any family of involutes of the same curve, the involutes of a circle are parallel to one another. More precisely, the image by a rotation by an angle α of the involute gives a parallel curve at distance αa. In the special case $\alpha = 2\pi$, we get the same curve; the involute of a circle is therefore an auto-parallel curve; its coils are at distance $2\pi a$ from one another. Thus the successive turns of the involute of a circle are parallel curves with constant separation distance, a property which is often (inaccurately) ascribed to the Archimedean spiral. However, for large values of turns, the Archimedean spiral with the equation $\rho = a(\varphi + \pi/2)$ is the asymptotic curve to the involute of a circle (Fig. 12).

The involute of a circle is the curve for which, when it is travelled along with linearly growing speed (with acceleration a), the rotation speed of the tangent to the trajectory is constant. Hence, it has another name - **anti-clothoid**, because the clothoid is the curve for which, when it is travelled along with a uniform movement, the rotation speed of the tangent is linearly changing.

The involute has some properties that makes it extremely important for the gear industry: If two intermeshed gears have teeth with the profile-shape of involutes (rather than, for example, a traditional triangular shape), they form an involute gear system [13]. It allows to transmit motion with a constant ratio. For this, it is necessary that the teeth of the gears be drawn along a curve in which the common normal drawn through the point of contact of the tooth profiles always passes through the same point on the line connecting the centers of the gears, called the gearing pole. Their relative rates of rotation are constant while the teeth are engaged, and also, the gears always make contact along a single steady line of force. With teeth of other shapes, the relative speeds and forces rise and fall as successive teeth engage, resulting in vibration, noise, and excessive wear. For this reason, nearly all modern gear teeth bear the involute shape.

The involute of a circle is also an important shape in gas compressing, as a scroll compressor can be built based on this shape. Scroll compressors make less sound than conventional compressors, and have proven to be quite efficient.

4   Three-Dimensional Spirals

As mentioned above, a spiral in three-dimensional space is a curve that turns around
an axis at a constant or continuously varying distance while moving parallel to the
axis. As in the case of two-dimensional spirals the third variable, h (height), as well
as the radius ρ, is a continuous monotonic function of the angle φ.

   An important type of 3D spirals is a helix, which is determined by the property
that the tangent line at any point of this curve makes a constant angle with a fixed
line called the axis. Helices can be either right-handed or left-handed. With the line
of sight along the helix's axis, if a clockwise screwing motion moves the helix away
from the observer, then it is called a right-handed helix; if towards the observer, then
it is a left-handed helix. Handedness (or chirality) is a property of the helix, not of
the perspective: a right-handed helix cannot be turned to look like a left-handed one
unless it is viewed in a mirror, and vice versa.

4.1   Circular Helix

There are several types of helices. A **circular (cylindrical) helix** is a curve on
the cylinder surface, which is described in Cartesian coordinates by the following
equations:
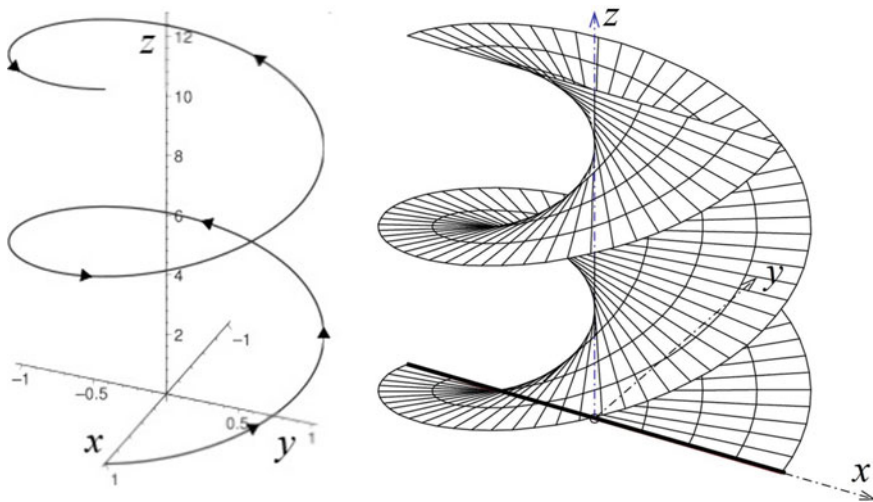
Fig. 13 Left: right-handed cylindrical helix with $a = b = 1$, right: helicoid

$$x = a \cdot cos\varphi,$$
$$y = a \cdot sin\varphi,$$
$$z = b\varphi, \tag{11}$$

where a and b are nonzero constants. The projection of a cylindrical helix on the x, y-plane is a circle (see Fig. 13 left).

The length of one coil of the circular helix ($\varphi \in [0, 2\pi]$): $L = 2\pi\sqrt{a^2 + b^2}$. The pitch of a helix, equal to $2\pi b$, is the height of one complete helix turn, measured parallel to the axis of the helix. Its curvature is $|a|/(a^2 + b^2)$ and its torsion is $b/(a^2 + b^2)$. Thus, a circular helix has constant band curvature and constant torsion.

4.2 Helicoid

The **helicoid** is shaped like an Archimedean screw, but extends infinitely in all directions. Correspondingly, it can be also described by a parametric equations in Cartesian coordinates:

$$x = \rho cos\varphi,$$
$$y = \rho sin\varphi,$$
$$z = \varphi, \tag{12}$$

where ρ and φ range from negative infinity to positive infinity (Fig. 13 right).

The helicoid plays a role as a surface in differential geometry. Besides the plane it is the only simply connected minimal surface in 3D Euklidian space.

4.3 Conical Helix

Another example of 3D spirals is a **conical helix**, which may be viewed as a spiral line on a conical surface. If in Eq. 11 we take the parameter a not as a constant but proportional to the angle φ, then we obtain a conical helix which in projection on the x, y-plane gives an Archimedean spiral (see Fig. 14).

If both the height h and the radius ρ of the 3D spiral depend exponentially on the angle φ: $h, \rho \propto e^{k\varphi}$, we have the case of a conical helix which, while projected on the x, y-plane, produces a logarithmic spiral.

Fig. 14 Conical helix
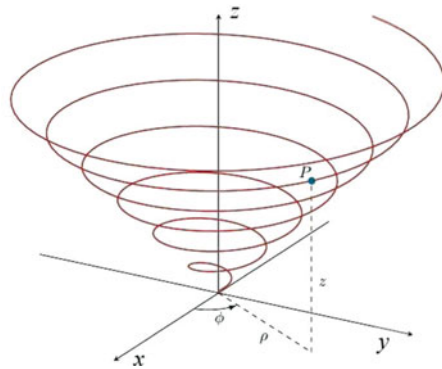
4.4 Loxodrome

Speaking about three-dimensional spirals, we cannot but mention spirals on the surface of a sphere. The first example is the **loxodrome** (also known as a **rhumb line** or **spherical spiral**), which is a curve on the sphere, crossing all meridians at fixed angle (not the right angle). A loxodrome spirals from one pole to the other (see Fig. 15). This curve has an infinite number of turns but reaches the pole in a finite distance. The pole-to-pole length of a loxodrome is (assuming a perfect sphere) the length of the meridian divided by the cosine of the bearing away from true north. Asymptotically near the poles, it behaves like the logarithmic spiral on a plane.

The name is derived from old French or Spanish, respectively: "rumb" or "rumbo", a line on the chart, which intersects all meridians at the same angle. On a plane surface this would be the shortest distance between two points. Over the Earth's surface at low latitudes or over short distances, it can be used for plotting the course of a vehicle, aircraft or ship [14]. Over longer distances and/or at higher latitudes the great circle route is significantly shorter than the rhumb line between the same two points. However, the inconvenience of having to continuously change bearings

Fig. 15 Loxodrome (rhumb line)
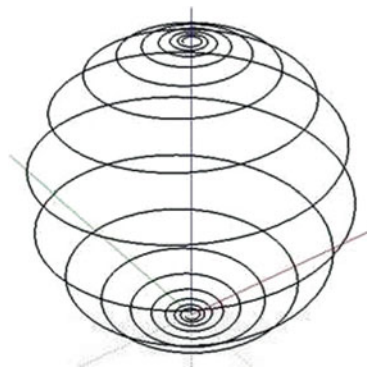
while travelling a great circle route makes rhumb line navigation appealing in certain instances.

4.5 Archimedean Spiral on a Sphere

Another example of a spiral on a sphere is an **Archimedean spiral**, which maintains uniform line-spacing as the curve progresses across the surface of the sphere. Therefore, this line has also finite length, though this is not the same thing as the rhumb line described earlier.

It should be mentioned that Maurits Cornelis Escher (1898–1972) a Dutch graphic artist who made mathematically inspired woodcuts, lithographs, and mezzotints, used spirals patterns, especially the loxodrome, for some of his graphics [15].

5 Non-smooth Spirals

Until now, we discussed spirals both in 2D and in 3D, which were smooth curves. However, there are examples of non-smooth spirals, which usually consist of line segments. One of the most popular among them is the **spiral of Theodorus** (also called square root spiral, Einstein spiral or Pythagorean spiral), which is composed of contiguous right-angled triangles (see Fig. 16). It was first constructed by Theodorus of Cyrene. The spiral is formed by a chain of right-angled triangles, which have a common side. The hypotenuse of one triangle becomes the catheter of the next. The free legs form the spiral. The spiral is started with an isosceles right triangle, with each leg having unit length. Another right triangle is formed, with one leg being the hypotenuse of the prior triangle (with length $\sqrt{2}$) and the other leg having length of 1; the length of the hypotenuse of this second triangle is $\sqrt{3}$. The process then

Fig. 16 Spiral of Theodorus
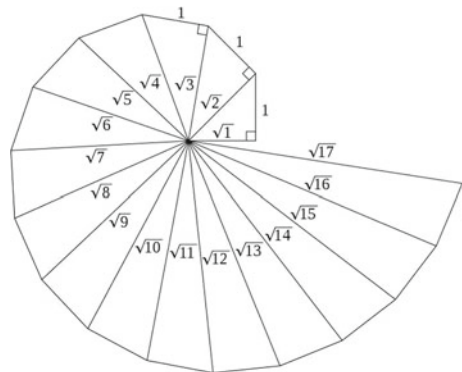
repeats; the ith triangle in the sequence is a right triangle with side lengths $\sqrt{i}$ and 1, and with hypotenuse $\sqrt{i+1}$.

Theodorus stopped his spiral at the triangle with a hypotenuse of $\sqrt{17}$. If the spiral is continued to infinity many triangles and other interesting characteristics are found.

If φ_n is the angle of the nth triangle (or spiral segment), then: $\varphi_n = arctan(\frac{1}{\sqrt{n}})$. The growth of the radius of the spiral at this triangle is $\Delta\rho_n = \sqrt{n+1} - \sqrt{n}$. For large n, $\varphi_n \cong 1/\sqrt{n}$ and $\Delta\rho_n \cong 0.5/\sqrt{n}$. Thus $\Delta\rho_n/\varphi_n \cong 0.5$ and the spiral of Theodorus approximates the Archimedean spiral with a pitch equal to π.

If we construct a spiral according to the same procedure as in the case of the Theodorus spiral but using similar right-angled triangles (they have the same ratio of the corresponding legs), then we obtain a non-smooth analog of the logarithmic spiral. Furthermore, we can generalize this procedure and apply it to arbitrary similar polygons each having at least a pair of non-equal non-parallel sides that will result in the formation of a logarithmic polygon spiral.

6   Fractal Spirals

The analysis of fractality in mathematical and natural objects has been a major field of research in recent years. "Fractals" assume a large variety of shapes and forms, and they require for their characterization a fractal dimension, which generally is not an integer.

For the understanding of fractality the properties of the "Mandelbrot set M" prove to be a most useful source of knowledge. M is the set of all complex numbers c, for which the recursive complex series z_i with

$z_0 = 0$
$z_{n+1} = z_n{}^2 + $ c, (n = 1, 2, 3,...)

is restricted (i.e., limited) to finite values [16].

One also writes:
$z_{n+1} = z_n{}^2 + $ c, c $\in$ M $\leftrightarrow$ $\lim\limits_{n \to \infty} \sup z_{n+1} \leq 2$.

This prescription looks, at first sight, quite simple, but when studying numerically the outcome for different choices of c, an amazing richness of patterns unfolds [17]. The Mandelbrot set M is then drawn in the plane of complex numbers. In a simplistic description, it consists of a main body with a head. It is called "Apfelmännchen" (apple man), because of its shape. Note that the border of the Apfelmännchen is not a simple line. At the border a lot of smaller Apfelmännchen appear, from there still smaller Apfelmännchen grow, and further on. However, the region of M in the complex plane is limited to $-2.4 <$ x < 0.8 and $-1.2 <$ y < 1.2, where x and y are the coordinates of the real and imaginary part of c, respectively.

If one focuses on a narrow region between the main body and the head of the primary Apfelmännchen, one can find spirals evolving at the outer boundary of M, as depicted in Fig. 17. These spirals are fractal structures in that small spiral copies
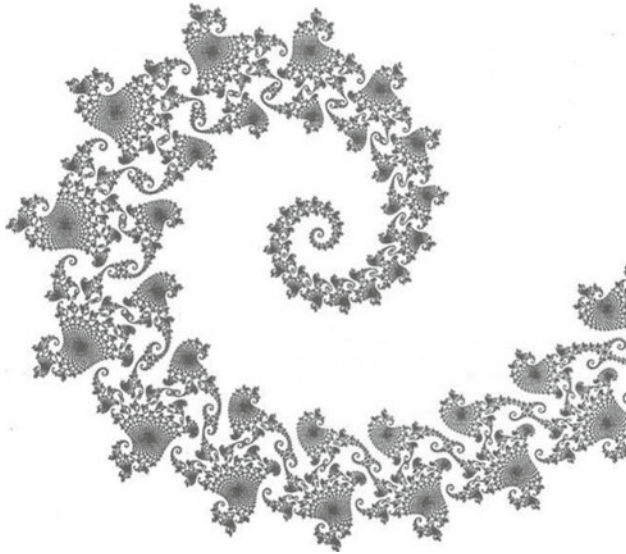
Fig. 17 "In the seahorse valley" - small section at the outer boundary of M

grow in a rather intricate way from the main arm of the "mother" spiral. These are small self-similar replicas of the large spiral.

Fractal structures are seen not only in mathematics but also in nature, for example, the fjord coast in Norway, water sheds, cauliflowers, trees, corals (see Fig. 18) and others.
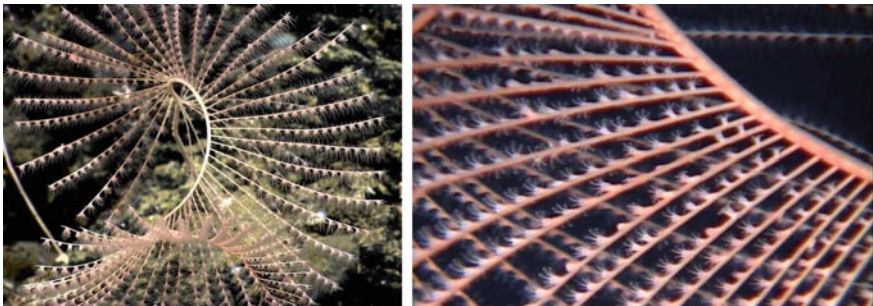
Fig. 18 Left: spiral shape of coral Iridogorgia; right: close-up photograph. Refer to chapter **Appearance in Nature**

References

1. M. Hazewinkel (ed.), *Encyclopaedia of Mathematics* (Kluwer, Alphen aan den Rijn, 1994), http://www.encyclopediaofmath.org
2. A.A. Savelov, *Planar Curves* (Moscow, 1960) (In Russian)
3. J.D. Lawrence, *A Catalog of Special Plane Curves*. Dover Books on Mathematics (Courier Dover, Mineola, 2013), p. 186
4. A. Schioner, *Albrecht Dürer: Genie zwischen Mittelalter und Neuzeit* (Pustet, Regensburg, 2011)
5. A. Dürer, *Instructions for Measuring with Compass and Ruler* (Nuremberg, 1525)
6. J. Havil, *Nonplussed! Mathematical Proof of Implausible Ideas* (Princeton University, Princeton, 2007), p. 109
7. G.J. Chin, Flying along a logarithmic spiral. Science **290**, 1857 (2000)
8. M. Cortie, The form, function, and synthesis of the molluscan shell, in *Spiral Symmetry*, ed. by I. Hargittai, C.A. Pickover (World Scientific, Singapore, 1992), p. 370
9. G. Bertin, C.C. Lin, *Spiral Structure in Galaxies: A Density Wave Theory* (MIT, Cambridge, 1996), p. 78
10. M. Livio, *The Golden Ratio: The Story of Phi, The World's Most Astonishing Number* (Broadway Books, New York, 2002)
11. R.A. Dunlap, *The Golden Ratio and Fibonacci Numbers* (World Scientific Publishing, Singapore, 1997)
12. N.B. Kellogg, *The Transition Curve or Curve of Adjustment as Applied to the Alignment of Railroads*, 3rd edn. (BiblioBazaar, Charleston, 2008)
13. V.G.A. Goss, Application of analytical geometry to the form of gear teeth. Resonance **18**, 817–831 (2013)
14. A. James, Loxodromes: a rhumb way to go. Math. Mag. **77**, 349–356 (2004)
15. B. Ernst, *The Magic Mirror of M. C. Escher* (Random House, New York, 1976)
16. B.B. Mandelbrot, *The Fractal Geometry of Nature* (W. H. Freemann, New York, 1982)
17. H.-O. Peitgen, P. Richter, *The Beauty of Fractals* (Springer, Berlin, 1986)

Acoustic Spirals: Analysis of Bach's Prelude in C Major

Kinko Tsuji

Abstract Bach's prelude in C major of "The Well-Tempered Clavier, Book I" is analyzed with a dynamical approach, by using phase portraits and their two and three-dimensional expressions. Different from the traditional analysis based on the theory of harmony, our method can elucidate how the music develops in the course of time. The numerical calculation leads us to an image of this musical piece, as if one walks down a staircase with several half turns, while spinning around one's own axis.

1 Introduction

I am walking down a spiral staircase, with myself spinning. This is the feeling which I always get when playing the prelude in C major of Bach's "The Well-Tempered Clavier, Book I". For me this piece of music is an acoustic spiral.

Johann Sebastian Bach composed the well-tempered clavier (Bach's original title: "Das Wohltemperierte Clavier") in 1772, a collection of 24 preludes and fugues. The first piece, the prelude in C major, is the most famous one, and many people who can play piano play this piece at least several times in their lives. Some notes at the beginning of this prelude are shown in Fig. 1.

Generally, it is not so easy to express which kind of feeling you have during playing or during listening to music. This was also true for me. When I said that "this is an acoustic spiral!", the only reaction was "What?". "Yes, I am walking down a spiral staircase, with myself spinning." However, this very intuitive explanation alone does not prove that my thought is right: whether ever acoustic spirals do exist?

K. Tsuji (✉)

Shimadzu Europa GmbH, Albert-Hahn-Straße 6-10, 47269 Duisburg, Germany
e-mail: kts@shimadzu.eu

Fig. 1 The beginning part of the prelude in C major of "The Well-Tempered Clavier: Book I", copied from [1]

This prelude has been analyzed by several people: examples are given in [2, 3]. Their analysis is mainly based on the theory of harmony, probably because the prelude consists of sequences of harmonies played as broken cords as seen in Fig. 1. This kind of analysis is static and misses musical flow. In fact, there are three essential elements in music: melody, harmony and rhythm. Here we need a dynamic analysis including melody and rhythm: the dynamic development in the course of time. For this purpose, to make a phase portrait can be an appropriate method, since it presents a geometrical trajectory of dynamical evolution. In other words, in a phase plot dynamic developments are represented in a compact way. It could reveal information about whether this musical system is a limit cycle or another attractor or some other spiral [4].

We will present our strategy for analysis, in which musical notes and physical parameters are combined (Sect. 2) and results of numerical calculations (Sect. 3). Finally, we will discuss how the feeling (of an acoustic spiral) can be expressed by a rather qualitative mathematical analysis.

2 Strategy for Analysis

2.1 Phase Plot for Musical Notes

A phase plot (see chapter **Generation of Spirals in Excitable Media**) may represent the dynamics of location (x) and momentum (proportional to $y = dx/dt$) of harmonic oscillations. Instead of showing directly the time evolution of x and y (by sine and cosine functions) it presents the motion on a xy-plane by a closed curve (circle or ellipse), thus providing a compact image of the system's dynamics. If realistically a damping of the motion is allowed (by friction → dissipation), the closed curve turns into an inward curling spiral, which asymptotically ends in the origin acting here as a point attractor.

This dynamical approach is now used for our analysis. For the music we can attribute x to the frequency and y to the change of the frequency per unit time. The frequency corresponds to the pitch of each note. Different from an oscillator like a physical pendulum, however, x and y are not continuous, but assume discrete values. Therefore, we define:

$$x_n = (f_n + f_{n+1})/2,$$
$$y_n = (f_{n+1} - f_n)/m_n = \Delta f_n / \Delta \tau_n \qquad (1)$$

where f_n is the corresponding frequency of the nth note, $\Delta f_n = (f_{n+1} - f_n)$, and $m_n(= \Delta \tau_n)$ is the time interval between the nth and $(n+1)$th note (arbitrary unit). Here we set m as shown in Fig. 2.

$$m = 8 \quad 4 \quad 2 \quad 1$$

Fig. 2 $m_n = 8$ for a half note, $m_n = 4$ for a quarter note, $m_n = 2$ for an eighth (quiver) note, $m_n = 1$ for a sixteenth (semi quiver) note, and further on

Since we have only discrete points, we have to connect them. After some trial we decided to use a polynomial approximation. There is no physical or mathematical reason for our decision, though. Just sharp edges are avoided, because they do not fit to this music. In fact, Bach's notes create a continuous curve of musical sound, where subsequent notes are intimately connected. Phase plots on this basis will be shown Sect. 3.

2.2 Characteristics of This Musical Piece and Corresponding Treatments

The C major prelude consists of 35 bars. Except for the last three bars the rhythmic structure of the notes is identical throughout: there are two repetitive groups in each bar; in each group there is one half note ($m = 8$) which has the lowest pitch, one double dotted quarter note ($m = 7$) for the second lowest pitch, and six semi quiver notes ($m = 1$) for the upper three pitches (see Fig. 1). We will use, therefore, these 32 bars (from the first bar to the 32th bar) for analysis.

The main difficulty here is how to integrate three different kinds of notes (half note, double dotted quarter note and semi quiver note) into this analysis. (The traditional analysis based on harmony does not take these differences into consideration.)
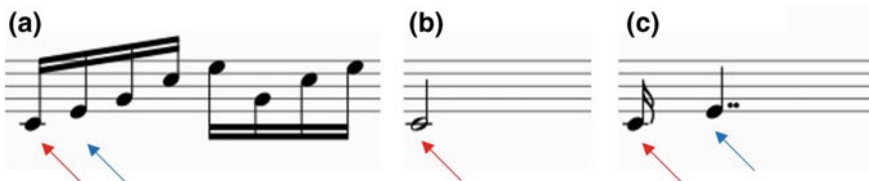
Fig. 3 Examples of categories **a**, **b** and **c**. Red arrows indicate three roles of the lowest tone and blue arrows two roles of the second lowest tone

In order to distinguish these three kinds in our analysis explicitly, we separate each group of notes into three categories (see Fig. 3):

(a) 8 sixteenth notes (the first two longer notes are considered as sixteenth notes, as well),
(b) 1 half note (the lowest pitch),
(c) 1 double dotted quarter note (the second lowest pitch) in combination with the lowest note.

The lowest note has three roles for each half bar: (1) the lowest tone as a half note (red arrow in Fig. 3b), (2) a part of the lowest 2 tones (red arrow in Fig. 3c), and (3) the starting tone of the broken cord of 8 semi quiver notes (red arrow in Fig. 3a). In a similar way the second lowest note has two roles: (1) the rather long double dotted quarter note (blue arrow in Fig. 3c) combined with the lowest tone and (2) the second tone of the sequence of 8 semi quiver notes (blue arrow in Fig. 3a).

At first, we will analyze these three categories independently by using the phase plot (see Sect. 3.1), and later on we will try to combine these results.

2.3 Three-Dimensional Expression

Since the phase plot gives no explicit information for the time evolution, we will introduce an additional axis (z-axis) vertical to the xy-plane, and pull the trajectory along the z-axis (i.e. by introducing a growing scaling factor). This way we can see how the trajectory develops over the course of time.

Example: If you look at a helix-shaped spring from its head (or tail) along its axis, you see only a circle. You have neither information of the length nor the pitch of the spring. This corresponds to a phase portrait in the plane. If you change the angle of view, let us say by 30° with respect to the axis, then you can get an idea for the real shape of this spring (a three-dimensional image).

In order "to change the angle of view" mathematically, we rotate the yz-plane around the x-axis and the xz-plane around the y-axis, and plot the projection on a new xy-plane. We use the following equations to plot the projection (x_p, y_p), when at first the object is rotated α radian around the x-axis and then β radian around the y-axis:

$$x_p = x \cdot \cos \beta - (-y \cdot \sin \alpha + z \cdot \cos \alpha) \cdot \sin \beta,$$
$$y_p = y \cdot \cos \alpha + z \cdot \sin \alpha \tag{2}$$

3 Numerical Calculations

For the analysis of category (a) notes, all notes are numbered from 1 (the first note of the first bar) to 512 (the last note of the 32th bar). The beginning part of the number sequence is shown in Fig. 4.

Fig. 4 Numbering of each note

The running index for the notes is i ($i = 1, 2, 3,\ldots, 512$). According to Eq. 1 x_i is defined as the mean value of the frequency of the ith note and $(i + 1)$th note. It means that the index i of x_i is actually $(i + (i + 1))/2$. In order to avoid unnecessarily complicated notation, we write i for the tone between i and $(i + 1)$ notes.

For the analysis of category (b) as well as (c) notes, it is more practical to number the bars; all bars are numbered from 1 to 35 ($N = 1, 2,\ldots, 35$). The half integer $(N/2)$ means the second part of the corresponding bar. Here also N means $(N + (N + 1))/2$.

3.1 Analysis of Category (a) Notes: Sequence of 8 Semi Quiver Notes

Figure 5 shows examples of the phase plot of the 1st, 5th, 23th and 30th bar. Since the first half sequence is repeated in the second half of each bar, only the plot of the first half of the sequence (consisting of 8 notes) is shown.

Each loop includes a smaller loop. The form of each curve is characteristic for melody and harmony of the bar, since the rhythm is constant all the time. Some consecutive bars possess loops of similar shape: for example, bars 2–4 have loops similar to that shown in Fig. 5a. Grouping of bars according to the shape of the loop agrees with the grouping according to the harmony [2], suggesting that for the analysis of harmony this kind of phase portrait can be used.

The phase plot for all bars can then be expected to express the primary aspect of the C major prelude. However, such a plot cannot give any clear information, because there are too many points (8 points for each bar × 32 bars) to recognize details. We can omit the sub-loop (the smaller loop inside the large loop) for simplification, because the shape of the main loop is independent of the sub-loop. It means that we reduce the number of points in each bar to be 5: the 6th, 7th and 8th notes are omitted so that the next neighboring note of the 5th note is the first note of the next bar. The remaining 5 points in each bar are considered as basic tonal sequence and present the characteristic loop.

The result of such a simplified phase plot through bars 1–32 is shown in Fig. 6. The black loop is the one for the 1st bar. The two red loops indicate the 5th and the 30th bar: the 5th bar is the first bar after the introductory 4 bars and shows the
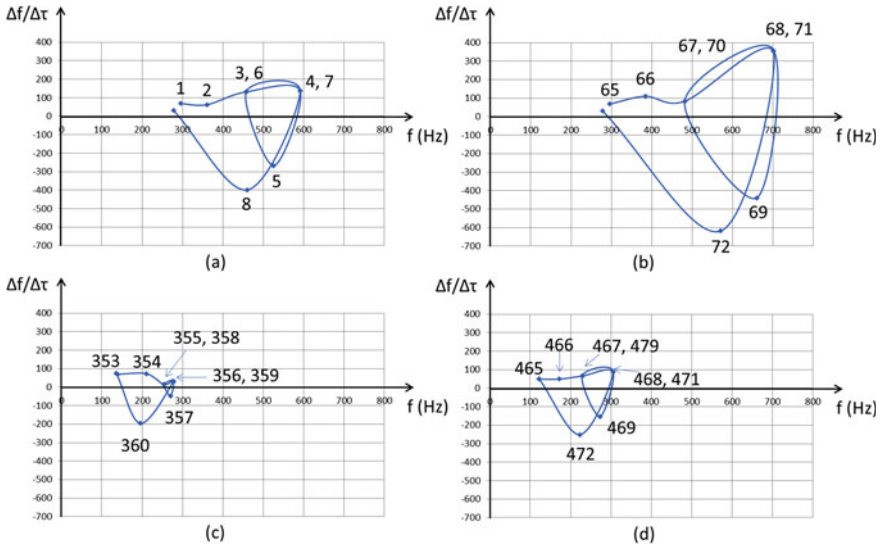
Fig. 5 Examples of the phase plots: **a** 1st bar, **b** 5th bar, **c** 23rd bar, **d** 30th bar. The unit of the ordinate $\Delta f/\Delta \tau$ is arbitrary. The numbers indicated in this figure are the mean value of the corresponding number and the next number (see the text above)
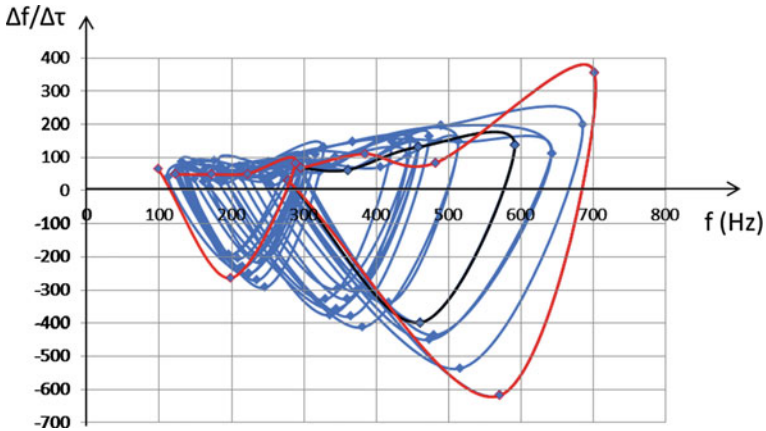
Fig. 6 Simplified phase plot of the category (a) notes for the C major prelude of "das wohltemperierte Klavier: Part I". The black loop indicates the loop of the 1st bar. The right and left red curves correspond to the 5th and 30th bar, respectively. The unit of the ordinate $\Delta f/\Delta \tau$ is arbitrary

largest loop. The 30th bar belongs to the last part before the coda. All other loops are indicated with blue color.

As can be seen in Fig. 6, from the 5th bar on, the loops of each bar shift from higher to lower frequencies over the course of time, which agrees with my feeling of "walking down the staircase".
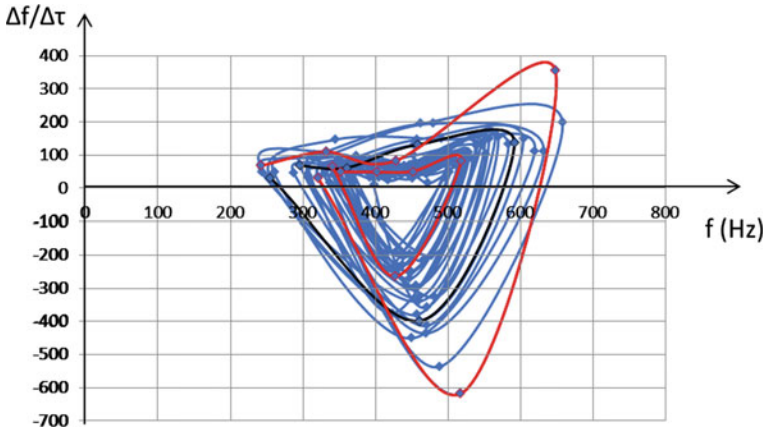
Fig. 7 Phase plot after mean-frequency normalization. The black loop is the first loop, the large and small red loops are for the 5th and 30th bar, respectively

Now we calculate the average frequency of the 5 points in each cycle, and each cycle is laterally shifted, so that the centers of all loops nearly coincide (see Fig. 7). Interestingly, this form reminds us of a kind of "attractor". In fact, if we extend the prelude from the original bars 1–35 to bars $(1–31) + (1'–35')$ (where bars $1'–35'$ mean that the melody is the same as the bars 1–35 but one octave lower), the loops continue with decreasing size in a self-similar manner. Theoretically, we can repeat this procedure: $(1–31) + (1'–31') + (1''–31'')$ (two octaves lower) $+ (1'''–31''')$ (three octaves lower)… Then the loops get smaller and smaller to approach their central region. Whether this is a point attractor (see Sect. 2.1) or not, we will not discuss here. Of course, Bach did not compose such an extension, certainly for musical reasons, but also because pianos at that time were smaller. (The lowest tone of the Christofori's pianoforte which has the 54 keys is C2 (low C) and exactly the lowest tone of this prelude is C2 [5].) For the naming of musical notes, refer to [6].

3.2 Analysis of Category (b) Notes: Half Notes

The category (b) notes are the lowest and longest tone in each bar, suggesting that they build a basic structure of this musical piece. The phase plot from the 1st to 32th bar is shown in Fig. 8. Since the repetitive part (the second half) in each bar is included in this plot, the total number of the points is 63. However, the points shown in Fig. 8 are much less than 63, because the category (b) notes often remain at the same pitch and therefore, quite many points have a value of $\Delta f/\Delta \tau = 0$. Subsequently at a few values on the x-axis some points gather. At the coordinates indicated by orange circles three successive points are overlapping. At the green circle three successive points plus five successive points are overlapping and at the red circle 15 points.
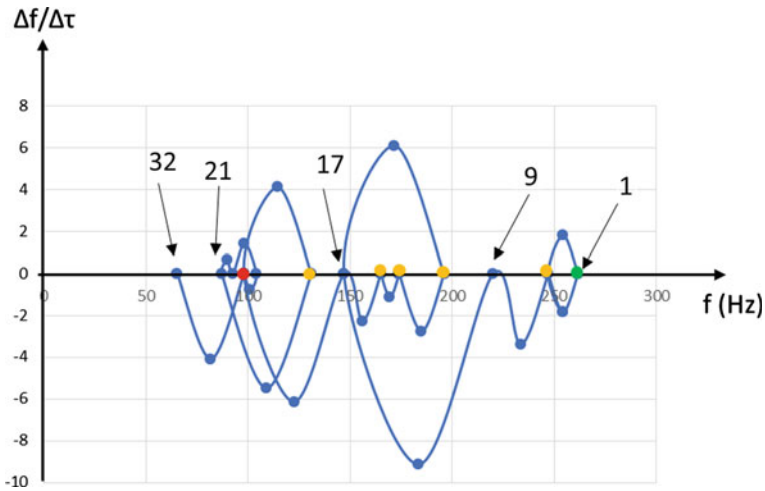
Fig. 8 Phase plot of the category (b) notes from 1st to 32nd bar. At the coordinates indicated by a green circle for three and (once more) five successive points, orange circles for three successive points and red circle for 15 points are overlapping. The numbers indicate the mean value of the corresponding half bar and the next half bar. The unit of the ordinate $\Delta f/\Delta \tau$ is arbitrary

Fig. 9 Phase plot, laterally shifted group-wise. Red: first group (bars 1–9), black: second group (bars 9–17), yellow: third group (bars 17–21), green: fourth group (bars 21–32)

Interestingly, some kind of vague repeated similarity is seen in the curve. In order to verify whether such a similarity exists, the curve is separated into 4 parts (bar 1–9, bar 9–17, bar 17–21 and bar 21–32) and each part is shifted along the frequency axis so that they have a common center. The result is shown in Fig. 9.

In this figure the curves of all four groups are turning around the center in a similar manner, suggesting that there are four discrete turning elements. Their common center is located at the frequency of the note "G2", where both neighbors before and after are also G2, suggesting that the tone "G2" is the conceptional tone. This can be interpreted as a structure of the staircase: the staircase itself is piece-wise turning and it converges towards "G2".

3.3 Analysis of Category (c) Notes: Combination of the Two Lowest Notes

For the category (c) notes, the phase plot looks more complicated (see Fig. 10). The curve displays irregular oscillations between large positive values and small negative values of $\Delta f / \Delta \tau$. Moreover, the shift of the frequency changes its direction several times. The frequency decreases at first (from the 1st bar to the 3rd bar), and then it increases (bar 3–5), decreasing again (bar 5–10) and further on.

Figure 11 summarizes the grouping for categories (b) and (c). There is no clear coincidence between the groups of these categories. We will come back to this point further below after the three-dimensional analysis.
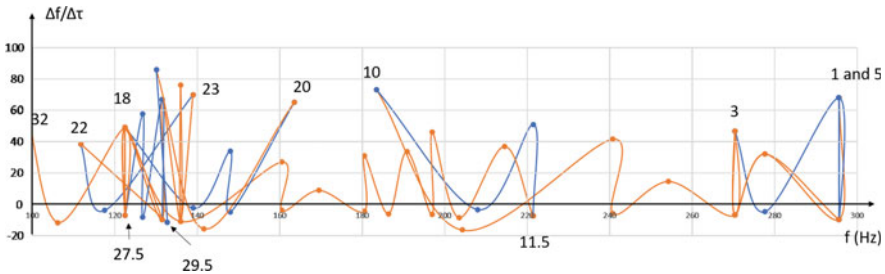
Fig. 10 Phase plot of the category (c) notes. The orange color indicates the direction of decreasing frequency and the blue color of increasing frequency. The numbers indicate the mean value of the corresponding half bar and the next half bar. The unit of the ordinate $\Delta f / \Delta \tau$ is arbitrary

3.4 Three-Dimensional Expression

As mentioned in Sect. 2 the z-axis is introduced as a third coordinate. Then the trajectory shown in Fig. 6 does not stay on the same plane: every point has a different z component (time course). In order to change the angle of view the yz-plane is rotated around the x-axis by 10° ($\pi/18$ rad) and the xz-plane around the y-axis by 330° ($33\pi/18$ rad). According to Eq. 2 the projection of each point is calculated. Figure 12 shows the results: a three-dimensional expression of the category (a) notes.
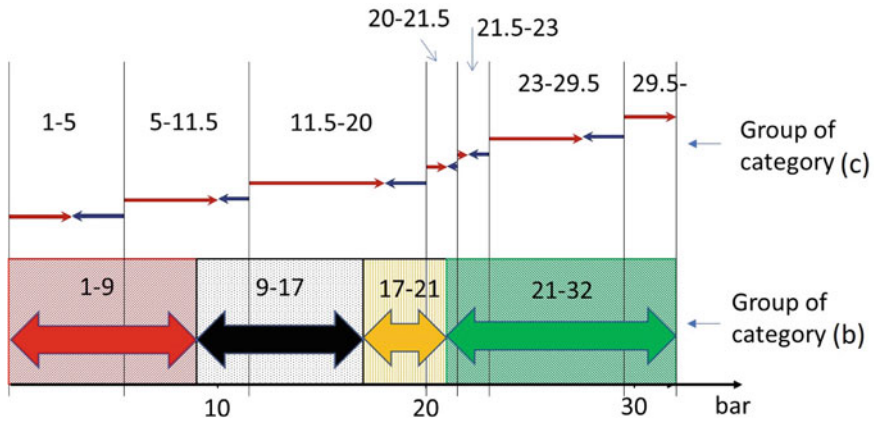
Fig. 11 Comparison of the groups for category (b) and category (c). The numbers indicate the bars: the integers and half-integers are the first half and the second half of the corresponding bars

Here all notes (the first and the second half of each bar, as well as the sub-loop) are included. With this expression we can follow the dynamics of the category (a) notes: over the course of time each tone walks along a helix, the shape of which is illustrated in Fig. 12.
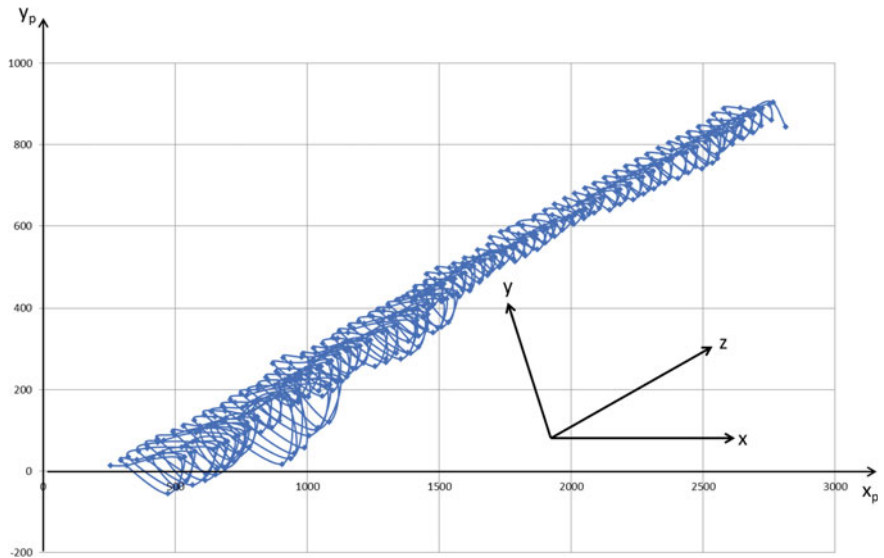
Fig. 12 Three-dimensional presentation of the category (a) notes for bar 1–32. x_p and y_p are the projection axis shown in Eq. 1. x: frequency, y: $\Delta x / \Delta \tau$, z: (arbitrary) time
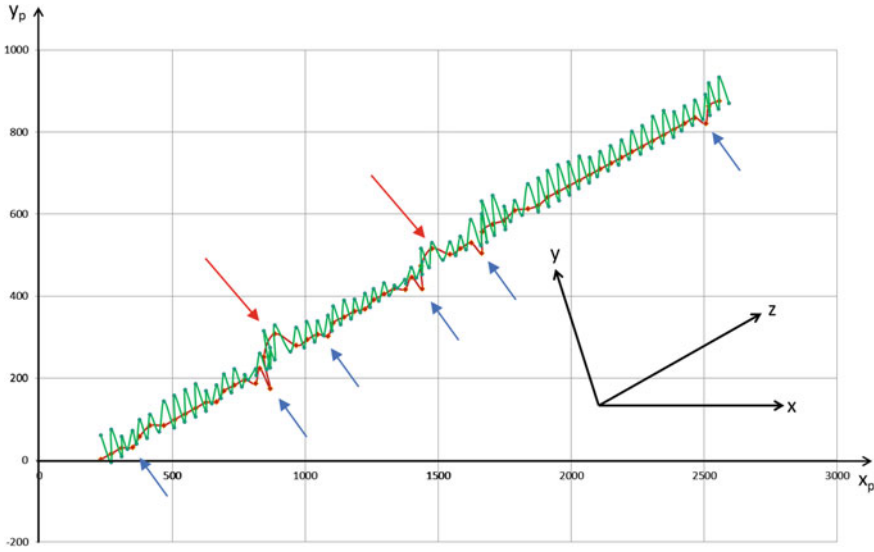
Fig. 13 Three-dimensional expression of the category (b) notes (red curve) and (c) notes (green curve). Red arrow: half turn, blue arrow: bend. x_p and y_p are the projection axis shown in Eq. 1. x: frequency, y: $\Delta x/\Delta \tau$, z: (arbitrary) time

Figure 13 shows the three-dimensional expression of the category (b) and the category (c) notes, in red and green, respectively. The category (b) notes correspond to the "basso continuo" or "Generalbaß". They play the role of a fundament. The three-dimensional expression of this category (see the red curve of Fig. 13) is, therefore, the fundament of this musical piece. It could correspond to the staircase where during playing this piece I am walking down. This staircase goes down straight, in principle, with two significant "half-turns" (marked with red arrows) and some small bends (marked by blue arrows). The green curve (category (c)) oscillates steadily along the (b) notes. Such up and down movements can support and stabilize the rather "unstable" straight line of the (b)-note. The deviation of grouping of category (b) notes from (c) notes (shown in Fig. 11) can also explain that the groups of (c) notes play a role to fix the connection between the individual groups of (b), so that they strengthen the structure of the group of (b) notes.

4 Concluding Remark

The results of the numerical analysis show that there exists spinning within each bar throughout the prelude. The structure of the staircase is not a regularly-formed spiral staircase, but an almost straight one with some half turns and bends. Figure 14 illustrates such a staircase and a dancing person on it. The implications of half-turning and bending depend on how you play this piece. If the lowest tones (category (b)) are emphasized, you feel large turns and bends, subsequently the model is close to

Fig. 14 The final model
which expresses an "acoustic
spiral", where I am walking
down a staircase with myself
spinning

a spiral staircase. If the lowest tones are played only as semi quiver tones, then the staircase is almost straight.

In this chapter we have tried to show an example of an acoustic spiral by using phase plots and their three-dimensional expression. Since the C major prelude of Bach's Well-Tempered Clavier has an exceptionally regular form, it is an ideal case for studying. With these methods we can analyze musical pieces dynamically, and visualize their "acoustic impression". Interestingly, Mussorgski composed his "Pictures at an exhibition" under the influence of his reception of Viktor Hartmann's paintings. Thus, visual and acoustic images often correspond to each other. Our mathematical portrait could contribute to an understanding of musical composition.

For our ideas and methods, there could be certainly a lot of criticism both from music theoreticians and from nonlinear physicists. We admit that there is some prejudice and biased view for developing the strategy of analysis (Sect. 2) and speculations for grouping of bars and explanations by three-dimensional expressions. Nevertheless, we believe that it is worth applying these methods also to other musical pieces.

References

1. O. von Irmer, Original version of J.S. Bach, Das Wohltemperierte Klavier, Teil I (G. Henle Verlag, München, 1974)
2. M. Gorski, Analyse J.S. Bach Praeludium I, BWV 846, C-dur aus "Das Wohltemperierte Klavier, Bd. I", http://www.lehrklaenge.de/PHP/Werkanalyse/AnalysePraeludiumBWV846.php
3. P. Goeth, J.S. Bach's Well-tempered Clavier, http://www.bachwelltemperedclavier.org/index.html
4. H.-G. Schuster, *Deterministic Chaos: An Introduction* (Physik Verlag, Weinheim, 1984)
5. P. Stewart, *The Early Pianoforte* (Cambridge University Press, Cambridge, 1995)
6. http://www.sengpielaudio.com/Rechner-notennamen.htm

Part III
Spirals and Vortices in Chemistry

From the depths of chaos, the path of all striving
Leads upwards to God in thousand spiral rings.

— Christian Morgenstern

Liesegang Rings, Spirals and Helices

Sabine Dietrich

Abstract The periodic precipitation process known as Liesegang ring formation has been investigated during the past 120 years and is one of the most recognized spatial and temporal heterogeneous structures in physical chemistry. If a soluble electrolyte is placed in contact with a second electrolyte in a gelatinous mass and, on interdiffusion, both react to form a poorly soluble salt, rhythmically arranged, separate precipitation develops parallel to the diffusion front. The beauty of this precipitation aside, research into Liesegang rings was mainly stimulated by the obvious parallels to processes in technology, geological structures and patterns in plant and animal life. Structural researchers increasingly consider the Liesegang experiments and their multifaceted manifestations as a basic phenomenon and a model case for a number of structuring processes in inorganic, organic and living nature. A continuous, end-to-end theory that takes the large number of interacting individual factors into account, thus enabling a full description of the complex reaction-diffusion mechanism, is still lacking. This is why attempts to extend the described phenomena of precipitate reactions in gelatinous masses to other structure formation processes are still tentative. This article provides an introduction.

1 Introduction and History of Liesegang Structures

Few areas of experimental physical chemistry, especially colloid chemistry, can match the multifarious manifestations of the Liesegang rings in terms of their intriguing beauty. The periodic precipitations called Liesegang rings are formed by the complex interaction of the diverse processes of the diffusion transport and the chemical reaction of at least two substances in a gelatinous mass, whereby one of the two substances is homogeneously distributed in the gel and the other diffuses into it. Once

S. Dietrich (✉)
Department of Earth Sciences, Technical University Berlin, Berlin, Germany
e-mail: sabine.dietrich@alumni.tu-berlin.de

the substance-specific saturation concentration has been exceeded, a poorly soluble precipitate forms that develops into rhythmically arranged, separate precipitations parallel to the diffusion front.

When the Liesegang experiment is performed in a planar arrangement, for example, in a Petri dish or on a glass plate, shell-shaped concentric rings are formed around the initial point of diffusion. When performed in a cylindrical arrangement, for example, in a test tube or a larger tube, parallel layers develop horizontally from the initial zone of diffusion. In rare cases, spirals or helices form.

In 1855, Runge [1] wrote about chemical reactions performed not by adding substances to a fluid but by dropping them onto blotting paper, thus creating characteristic "Musterbilder/patterned paintings". In 1879, Ord [2] reported on periodic precipitations of calcium oxalate. In 1896, Liesegang discovered periodic precipitations, which he initially refers to as 'A-lines', in the diffusion of silver nitrate in a gel containing chromate [3]. He assumes that the two substances 'can either be mixed for a short period without double decomposition. Or this decomposition occurs immediately, but the insoluble salt remains dissolved: its molecules have not yet combined into molecular complexes.'

To understand the occurrence of Liesegang structures, a number of individual factors in the complex reaction-diffusion process must be considered, such as (1) the chemical reaction and the electrolytic dissociation; (2) the possible complex formation; (3) the influence of the electrolyte on the reaction velocity; (4) the concentration dependence of the diffusion coefficients; (5) the kinetics of nucleation and crystal growth as a function of supersaturation and particle radius; (6) the coagulation of colloidal particles or the accumulation of ions; and (7) the influence of the nature of the gel on the colloidal phase.

The first mention of the Liesegang phenomenon in the 19th century incited the creation of numerous theoretical models at the beginning of the 20th century. Each of the existing models focuses on particular aspects, such as the supersaturation theory according to Wilhelm Ostwald [4], the diffusion wave theory according to Wolfgang Ostwald [5] and the coagulation theory according to Dhar and Chatterji [6]. The supersaturation theory was initially the generally accepted model approach. Wagner [7] was the first to describe the Liesegang experiment as reaction-diffusion system. Other authors such as Keller and Rubinow [8] refined the supersaturation approach. The Prenucleation Model according to Dee [9] and the Competitive Particle Growth Model according to Ortoleva [10] are based mainly on the coagulation model of Dhar and Chatterji and Wilhelm Ostwald's supersaturation theory, and Ostwald ripening. As had become clear in the first Liesegang experiments, the groups around Ortoleva and Ross [10–12], among others, show that the supersaturation approach alone cannot adequately describe the formation of the Liesegang structures and that especially the nucleation and growth of colloidal particles are important for their formation. The simplified model of Chernavskii, Polezhaev and Müller [13] is used to perform a first qualitative synthesis. A first qualitative and quantitative synthesis between the prenucleation and the postnucleation models is successfully performed by Krug and Brandtstädter [14].

A continuous, end-to-end theory that takes the interaction of the numerous individual factors into account and thus fully describes the qualitative and quantitative

complexity of the diffusion-reaction process would be very useful, but is still lacking today.

The announcement of Liesegang's experiments in the late 19th century immediately caught the attention of the international scientific community. The beauty of the periodic deposits aside, researchers were mainly stimulated by the obvious parallels to processes in technology, geological structures and patterns in plant and animal life.

The periodic precipitations do not depend on the specific choice of the diffusion medium but also occur in granular or porous media such as silica sand, sulphur powder, diatomaceous earth and gypsum as well as in gases and even pure water, cf. references in [14, 15], in addition to gelatine and other gelatinous masses. Structural researchers in physical chemistry, therefore, increasingly regard the rhythmic precipitations in gels and their multifaceted manifestations as a basic phenomenon and as a model experiment for numerous structure forming processes in inorganic, organic, and living nature.

2 Spirals and Helices

The fact that spirals or helices sometimes form in Liesegang experiments has been noted from the start. Following the first documentation by Rothmund [16], the discoverer himself, Raphael Eduard Liesegang, reports on spirals in 1914 [17]. Helices are presented soon thereafter, cf. Figs. 1 and 2.

After the initial clustering, experimental investigations and theoretical model considerations on Liesegang rings are again reported from the mid-20th century, including spirals and helices in some cases, cf. Fig. 3.
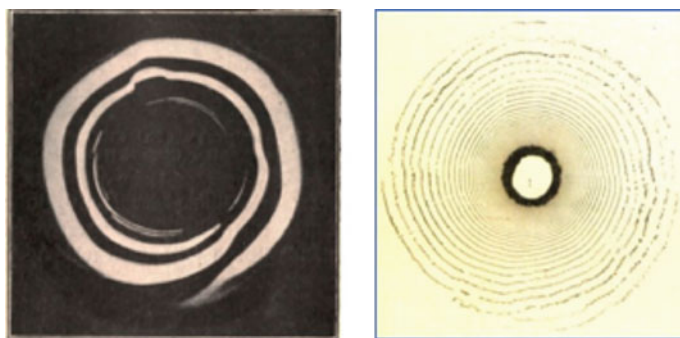
Fig. 1 Spirals on a plate dish. (Left) Single spiral of silver chromate in gelatine [18]. For other examples see [19, 20], (Right) Multi-armed spiral of silver chromate in gelatine [16]
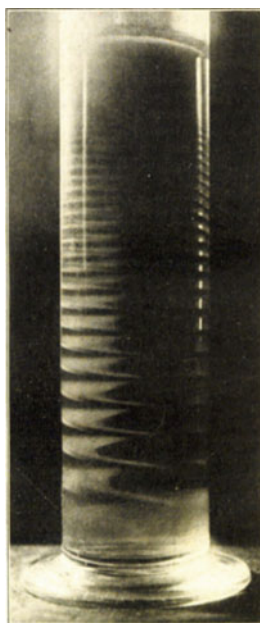
Fig. 2 Helix in a test tube prepared by K. Popp: cobalt hydroxide in gelatin, inner diameter 40 mm [5]. Other examples of helices: calcium hydrogen phosphate in gelatine [21], lead chromate in agar gel [22]
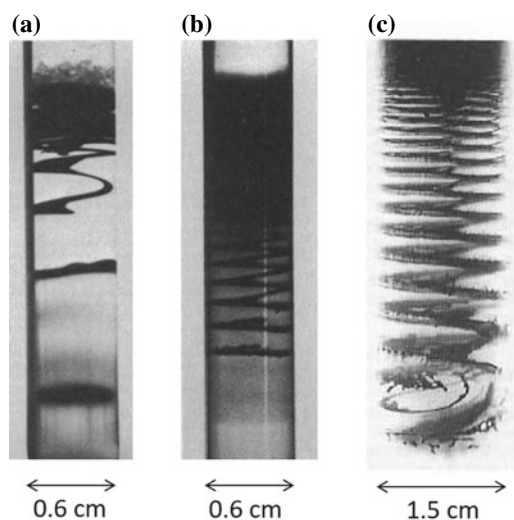
Fig. 3 Formation of helices in various chemical systems. **a**: Spiral band of $Mg(OH)_2$ in gelatine (8%) after 4 days, initial electrolytes NH_4OH and $MgSO_4$; middle: spiral band of $Ag_2Cr_2O_7$ in gelatine (5%) after 1 day. Initial electrolytes $AgNO_3$ and $K_2Cr_2O_7$ [11]. **c**: Extended helix of lead iodide in agar gel in a test tube, with electrolytes KI and $Pb(NO_3)_2$ [23]

3 Characteristics of Experimental Liesegang Systems

Liesegang and his contemporaries were fully aware of the broad significance of the rhythmic Liesegang structures and started establishing the basics for reproducible experimental arrangements [17, 21], as Liesegang structures do not always form in otherwise identical experimental setups, for example, when different gels, meaning different collagenic starting materials, are used. This quickly revealed that the gelatinous mass not only keeps the developing precipitates in their place of origin but also has other properties. In test series with several thousand (!) specimens, they discovered that the gelatinous medium must contain a small amount of acid, i.e. H^+ ions, in order to obtain a good banding.

However, an overly high concentration of both acid and diffusing cations (classically chromate) proved to be detrimental to good banding as it led to disperse homogeneous precipitation above a certain limit instead. Regarding the concentration ratios of the individual reagents to each other, Liesegang noticed that the compacting effect of the chromate is reversed when the acidity is changed at the same time. Such homogeneous rather than banded precipitations also occur when just the acidity is altered and thus the solubility of the silver chromate is increased by the H^+ ions. In summary, Liesegang states: 'By controlling the content of chromate, gel and especially acid, one can control the very different degrees of dispersity at which silver chromate develops in the gelatinous mass.' Cf. Figs. 4, 5, 6.
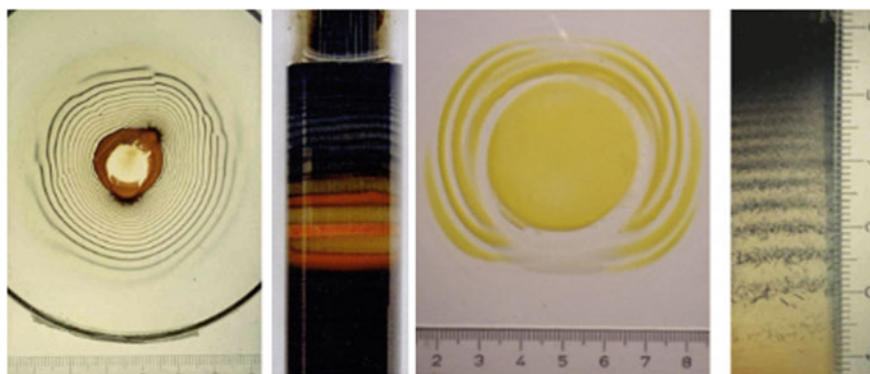
Fig. 4 Diverse shapes of Liesegang rings and bands. Classic Liesegang experiments in Petri dishes and test tubes: (Left) distinct rings in gelatine; (Center-left) disperse ruby-red bands in gelatine; (Center-right) disperse rings of lead iodide in gelatine; (Right) crystalloid alleys in silica gel [24, 25]
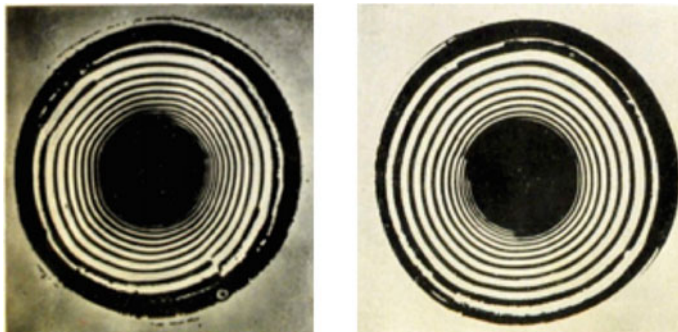
Fig. 5 Liesegang rings with different concentrations of the same reagents. Higher acid resp. chromate content, but still the same spiral or rings: (Left) 10 times higher $K_2Cr_2O_7$ content, (Right) 4 times higher H_2SO_4 content in the gelatin compared with classic Liesegang experiment [17]
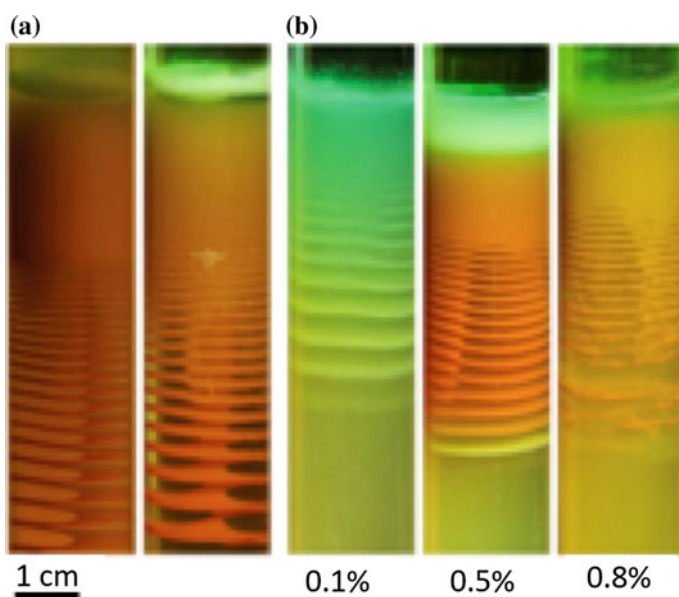
Fig. 6 Precipitation patterns in agarose, silica and mixed silica-agarose gels. **a** Helices in agarose gel (1%; left) and in silica gel (pH$=$7; right). **b** Patterns in mixed silica-agar gels (pH$=$7), numbers below the test tubes indicate the amount of agar in silica gels. Concentration of the outer ([$CuCl_2$]$=$0.5 M) and inner ([K_2CrO_4]$=$0.01 M) electrolytes [26]

More recently, these controllable properties of the Liesegang systems have gained attention from an application point of view because the processes enable, as an alternative to epitaxial processes, the deliberate growth of functional meso and microstructures and the potential production, for example, of electrocatalytic microreactors [27].

The occurrence of spirals or helices in Liesegang systems is a curiosity that is still not predictably controllable. A comprehensive analysis of the observed structures in Liesegang systems was attempted by Müller and Ross; in most cases, they did not detect any spiral structures [12]. Thomas et al. [28] illustrated that the probability of the formation of spirals and helices was dependent on the size of the experiment containers, cf. Fig. 7. Spirals or helices formed from a certain minimum container size. Their incidence increased with the increasing size of the container and then decreased again when the container reached a certain size.
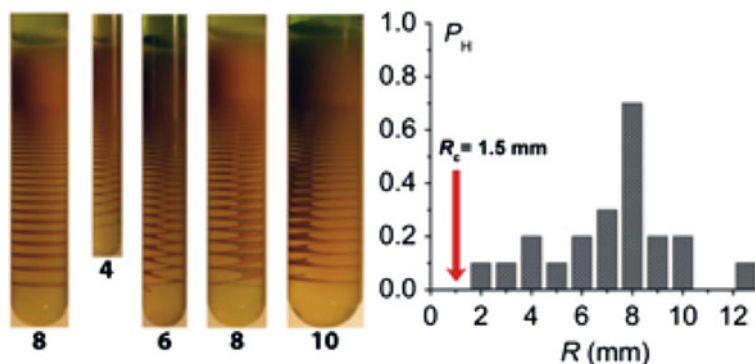
Fig. 7 Left: regular Liesegang (left tube) and helicoidal (all other tubes) patterns in agarose gel with the numbers corresponding to the tube radius R measured in mm. R is varied at fixed experimental conditions ($T = 22\,^\circ C$, $[Cu^{2+}]_0 = 0.5\,M$, and $[CrO_4^{2-}]_0 = 0.01\,M$); right: the probability of helicoid formation P_H. No helicoid appears for $R \leq R_c$ [28]

Even though spirals and helices are a special feature in Liesegang systems, they basically show the same properties as rings and bands. The distance and the shape of the individual lines in Liesegang rings and spirals are comparable. It is worth noting that bifurcations do not form any spiralling ends. The spirals and the bands develop in turbidity areas along the diffusion front into continuous lines or rows of crystals, cf. Figs. 3 and 4. Krug and Brandtstädter support these experimental observations with the results of numerical simulations of prenucleation and extended postnucleation models. They show that bifurcations develop from the unevenness of the initial point of diffusion or from differences in the concentration of the electrolyte that is diffused at the initial point of diffusion.

4   Endeavour to Model Liesegang Systems

This said, the models of Chernavskii et al. [13], Chopard et al. [29] and Krug and
Bandtstädter [14] are equally capable of displaying spiral or helical Liesegang struc-
tures.

   All models share the same boundary condition for the development of spirals
or helices, namely that irregularities must be present at the initial point of the dif-
fusing substance that are either a geometric nature of the boundary or are different
concentrations of the interdiffusing substance along the entrance boundary.

   For reasons of simplicity, the Liesegang process is displayed in the three models as
an irreversible non-ionic chemical reaction of two dissolved substances that react with
each other during the formation of a poorly soluble reaction product and in which the
poorly soluble reaction product deposits as precipitation. The three models examine
the processes of deposition closer, as the separate Liesegang rings are preceded by
an experimentally proven turbidity phase. The easily soluble reaction product is not
considered further. Here, an example for a system with silver monochromate is used:

Reaction

$2AgNO_3 + K_2CrO_4 \rightarrow Ag_2CrO_4 + 2KNO_3$
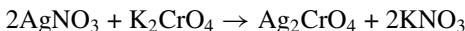
written with corresponding concentrations

$a + b \xrightarrow{k} c\downarrow$
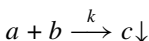
Reaction-diffusion equations

$$\frac{\partial a}{\partial t} = D_a \Delta a - kab \tag{1}$$

$$\frac{\partial b}{\partial t} = D_b \Delta b - kab \tag{2}$$

$$\frac{\partial c}{\partial t} = D_c \Delta c + kab - u(c,t) \tag{3}$$

$$\frac{\partial m}{\partial t} = u(c,t) \tag{4}$$

whereby a and b represent the concentrations of the two interdiffusing initial sub-
stances; c the concentration of the dissolved portion of the poorly soluble reaction
product; D the respective diffusion coefficients and k the reaction rate; and m the
mass density of the stationary precipitate of the reaction product. The difference in
the three models is in the nucleation and aggregation term 'u' for the precipitated
reaction product.

   Only the extended Competitive Particle Growth (CPG) Model of Krug and Brandt-
städter [14] explicitly considers the turbidity zone outside the outer precipitation ring
preceding the Liesegang rings for the nucleation process, i.e. the colloidal pre-phase,
cf., e.g. Fig. 3. The other two models work with dimensionless quantities and assume
a random or a given distribution of particles of different sizes for whose nucleation

rate a strong nonlinearity is given (as completely zero below a threshold or simply as a step function). In their cellular automata model, Chopard et al. [29] consider the colloidal precursor in a shortened form by postulating that, in the random presence of an already growing particle, freshly formed reaction product attaches to it. In their simplified model, Polezhaev and Müller [30] consider the colloidal precursor more explicitly by subdividing the stationary precipitate into small, dissolvable nuclei and large growing particles, each with a mean particle number density per volume unit.

To explicitly show the experimentally observed colloidal precursor, Krug and Brandtstädter used the actual material parameters of silver monochromate, size parameters measured by X-ray microscopy and, instead of the Gibbs–Thompson relation, introduced a polynomial equilibrium function for the supersaturation s^{eq}, cf. Fig. 8.
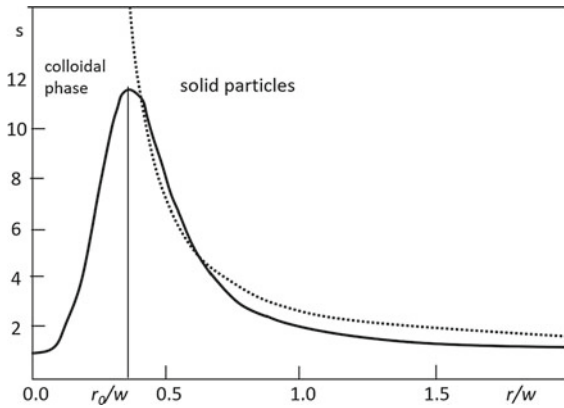
Fig. 8 Equilibrium curves of supersaturation $s^{eq}(r)$ of the CPG system. Solid curve: polynomial function $s^{eq}(r) = 1 + w^3 * r^3/(r^6 + r_c^6)$ with $r_c = 0.36w$. Dotted curve: Gibbs–Thompson relation $s^{eq}(r) = exp(w/r)$ [14], where r represents the particle radius of the poorly soluble reaction product; w the capillary length and r_c the critical value separating the colloid phase ($r < r_c$) of the poorly soluble reaction product from the phase of its solid particles ($r > r_c$)

This enabled them to consider that particles below a critical radius have no surface in the sense of the Gibbs–Thomson relation, i.e. are not subject to the Ostwald ripening processes. Then, the supersaturation function reaches its maximum as soon as a particle has grown to the critical radius r_c, from which it no longer reacts as a colloid process, i.e. dominated by its surface, but as a solid particle according to the Gibbs–Thompson relation, i.e. subject to its radius-dependent processes. For the Liesegang systems, this enabled them to successfully separate the contributions of the colloidal particles from those of the solid particles and depict the ring-forming development of generations of colloidal particles from which, in a subsequent step, coarse-grained bands or even crystals grow from competing nucleation.

Comparing the results shows that the fluffy bands modelled according to Dee's prenucleation model appropriately illustrate the Liesegang experiments in gels with protective colloid effect, meaning in gels that prevent the agglomeration of small

nuclei. The properties of the Liesegang experiments in gels without protective colloid effect illustrate the extended competitive particle growth model more fully because it takes both elements of the colloidal phase and elements of the growth phase into account. It must be noted that additional steps to improve the theoretical understanding of the Liesegang experiments under certain conditions also include quantum aspects, cf. Mares et al. [31].

From the theoretical viewpoint, conditions for the formation of helices were discussed in Refs. [13, 28, 30, 32]. Some experiments indicate that the helix starts to grow mainly on or near the inner surface of the test tube. Most likely the conditions for nucleation of the solid phase are more preferable there, i.e. the critical concentration for nucleation is lower at the container wall than in the bulk of the solution. This fact suggests to treat this case as taking place at the cylinder surface, e.g. in first approximation as a two-dimensional one. In fact, a numerical simulation within the framework of the model of Polezhaev and Müller [30] or Thomas et al. [32] in which the cylinder surface is unrolled on a plane and the evolution of a helical pattern is shown along one space coordinate has been performed, cf. Fig. 9.
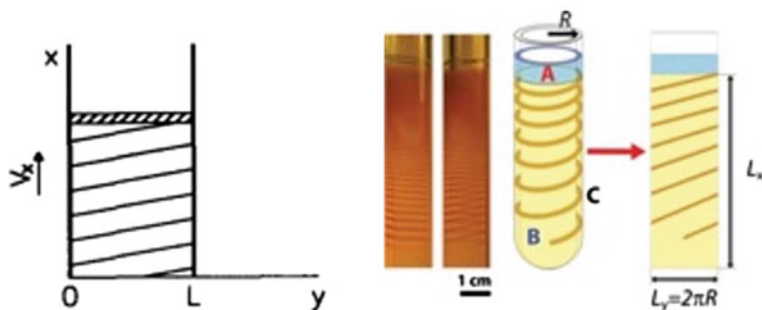
Fig. 9 (Left) A helical pattern on the evolvement of a cylinder. Full lines denote precipitation and shaded band denotes the reaction wave [13], (Right) Liesegang-type experiments with the precipitation patterns forming in the gel placed in-between two tubes of nearly equal radius (Liesegang rings in the leftmost tube and a helix in the next one). On the right, a schematic drawing is displayed showing the transformation of the thin layer of gel in the tube-in-tube experiment into a two-dimensional strip [28]

However, a model to simulate the full three-dimensional problem of helix growth is still lacking. In one respect, the qualitative treatment of the helix problem is in good agreement with experimental findings: the radius of the cylindrical container should be large enough to detect continuous helical patterns. Otherwise, even if successfully initiated, they will extend only over a few whorls. If the radius is too thin, this may not allow for initiation at all [22, 27]. As seen, for example, in Fig. 3a, b, the number of whorls is also correlated with the distance between subsequent whorls, which frequently increases with increasing distance from the initial electrolyte junction (a consequence of the spacing law often found in the Liesegang phenomenon [14, 32]).

Geometrical factors such as the relationship between helix pitch and tube diameter undoubtedly play an important role.

Because the occurrence of spirals or helices in Liesegang experiments is a curiosity that still cannot be controlled predictably, a further theoretical penetration and perfection of the models can help to create spirals and helices in Liesegang systems in reproducible experiments.

5 Concluding Remarks

Liesegang already recognized that 'diffusions and reactions in gelatinous masses are not exclusively a matter for the scientific laboratory, but also play an essential role in some areas of technology', as in tanning, photochemistry, geology and soil science, microsystem techniques and especially in living organisms [15, 16].

However, a continuous mathematical theory for the Liesegang structures has still not been developed. Attempts to extend the described structuring processes of precipitate reactions in gelatinous masses to other formation processes are still tentative. Recent systematic studies in connection with powerful computers and new mathematical foundations support interdisciplinary work and point to a more comprehensive application in the future. Were we to succeed in understanding the Liesegang systems well enough to grow self-organized structures, including spirals and helices, predictably and reproducibly, perspective opportunities for new and sophisticated applications would be opened.

References

1. F.F. Runge, (1855). Der Bildungstrieb der Stoffe: veranschaulicht in selbständig gewachsenen Bildern (Selbstverlag oranienburg)
2. W.M. Ord, *On the Influence of Colloids Upon Crystalline Form and Cohesion* (E. Stanford, London, 1879)
3. R.E. Liesegang, A-Linien, Liesegangs photographisches Archiv **800**, 305–309, 331–336, and 801, 321–326 (1896)
4. W. Ostwald, A-Linien von R.E. Liesegang (review). Z. Phys. Chem. **23**, 356 (1897)
5. W. Ostwald, Zur Theorie der Liesegang'schen Ringe, Kolloid Z. Suppl. to **36**, 380–390 (1925)
6. N.R. Dhar, A.C. Chatterji, Theorien der Liesegangringbildung. Kolloid Z. **37**, 2–9, 89–97 (1925)
7. C. Wagner, Mathematical analysis of the formation of periodic presipitations. J. Colloid Sci. **1**, 85–97 (1950)

8. B. Keller, S.I. Rubinow, Recurrent precipitation and Liesegang rings. J. Chem. Phys. **74**, 5000–5007 (1981)
9. J.T. Dee, Patterns produced by precipitation at a moving reaction front. Phys. Rev. Lett. **57**, 275–278 (1986)
10. P. Ortoleva, Solute reaction mediated precipitate patterns in cross gradient free systems. Z. Phys. B **49**, 149–156 (1982)
11. S.C. Müller, S. Kai, J. Ross, Curiosities in periodic precipitation patterns. Science **216**, 635–637 (1982)
12. S.C. Müller, J. Ross, Spatial structure formation in precipitation reactions. J. Phys. Chem. A **107**, 7997–8008 (2003)
13. D.S. Chernavskii, A.A. Polezhaev, S.C. Müller, A model of pattern formation by precipitation. Phys. D **54**, 160–170 (1991)
14. H.-J. Krug, H. Brandtstädter, Morphological characteristics of Liesegang rings and their simulations. J. Phys. Chem. A **103**, 7811–7820 (1999)
15. E.S. Hedges, *Liesegang Rings and Other Periodic Structures* (Chapman and Hall, London, 1932)
16. V. Rothmund, Löslichkeit und Löslichkeitsbeeinflussung, in *Handbuch der Angewandten Physikalischen Chemie in Einzeldarstellungen*, vol. 7, ed. by G. Bredig (Johann Ambrosius Barth, Leipzig, 1907), pp. 5–14
17. R.E. Liesegang, Silberchromatringe und -spiralen. Z. Phys. Chem. **88**, 1–12 (1914)
18. R.E. Liesegang, *Chemische Reaktionen in Gallerten* (Theodor Steinkopf, Dresden, 1924), p. 90
19. R.E. Liesegang, Spiralenbildung bei chemischen Niederschlägen. Naturwissenschaften **28**, 645–646 (1930)
20. R.E. Liesegang, Spiralenbildung bei Niederschlägen in Gallerten. Kolloid Z. **87**, 57–58 (1939)
21. E. Hatschek, A series of abnormal Liesegang stratifications. Biochem. J. **14**, 419–421 (1920)
22. E. Hatschek, Anomalous stratifications produced by the action of light. R. Soc. Proc. A **99**, 496–502 and plate 8 (1921)
23. S. Kai, S.C. Müller, Spatial and temporal macroscopic structures in chemical reaction systems - precipitation patterns and interfacial motion. Sci. Form **1**, 9–39 (1985)
24. H.-J. Krug, K.-H. Jacob, S. Dietrich, The formation and fragmentation of periodic bands through precipitation and Ostwald ripening, in *Fractals and Dynamic Systems in Geoscience*, ed. by H.-J. Kruhl (Springer, Berlin, 1994), pp. 269–282
25. S. Dietrich, K.-H. Jacob, Understanding earth: the self-organization concept and its geological significance; on the example of Liesegang-structures and electric fields, in *Complexity and Synergetics*, ed. by S.C. Müller, P.J. Plath, G. Radons, A. Fuchs (Springer, Cham, 2018), pp. 101–115
26. S. Thomas, G. Varhhese, D. Bárdfalvy, I. Lagazi, Z. Rácz, Helicoidal precipitation patterns in silica and agarose gels. Chem. Phys. Lett. **599**, 159–162 (2014)
27. R. Toth, R.M. Walliser, I. Lagzi, F. Bouoire, M. Düggelin, A. Braun, C.E. Housecroft, E.C. Constable, Probing the mystery of Liesegang band formation: revealing the origin of self-organized dual-frequency micro and nanoparticle arrays. Soft Matter **12**, 8367–8374 (2016)
28. S. Thomas, I. Lagzi, F. Molnár Jr., Z. Rácz, Probability of the emergence of helical precipitation patterns in the wake of reaction-diffusion fronts. Phys. Rev. Lett. **110**, 078303 (2013)
29. B. Chopard, P. Lüthi, M. Droz, Reaction-diffusion cellular automata model for the formation of Liesegang patterns. Phys. Rev. Lett. **72**, 1384–1387 (1994)
30. A.A. Polezhaev, S.C. Müller, Complexity of precipitation patterns: comparison of simulation with experiment. Chaos **4**, 634 (1994)
31. J. Mares, J. Stávek, J. Šesták, Quantum aspects of self-organized periodic chemical reactions. J. Chem. Phys. **21**, 1499–1503 (2004)
32. S. Thomas, F. Moinár, Z. Rácz, I. Lagzi, Matalon-Packter law for stretched helicoids formed in precipitation processes. Chem. Phys. Lett. **577**, 38–41 (2013)

Generation of Spirals in Excitable Media

Stefan C. Müller

Abstract The generation of dynamic spirals under conditions of excitability is presented. After a short description of some basic principles of nonlinear dynamics illustrated in the phase plane, we explain what excitable systems are, how excitation waves propagate, and why external forces influence rotating or moving spirals. Some images of such dynamic spirals are exhibited.

1 Introduction

There are two major categories of spirals we have learned about in chapter **Appearance in Nature**: those that have an immobile and static structure (horns of blackbucks or sheep, snails and seashells, pine cones or corals). Others rotate in time and space (galaxies, cyclones, air turbulence, the tail of a chameleon, a proboscis of butterfly, fish swarms or colonies of amoebae).

Artists will naturally create spiral pictures of a quiescent nature, as Gustav Klimt did in his frieze "Tree of life". His colleague Johannes Itten, on the other hand, painted a spiral which starts to move by the dynamic choice of colors within the structure. Motion becomes a central theme for Paul Klee who considers spirals that open and close towards the environment. Stormy spirals are captured in the works of Leonardo da Vinci (with his drawings of water turbulence), Vincent van Gogh (in the "excited" sky of his masterpiece "Starry Night") and Joseph Turner (living through a chaotic tempest in his painting "Snow storm"). See chapter **Arts and Beyond**.

In a preceding chapter **Spirals, Their Types and Peculiarities** mathematical presentations have provided some insight into the shape of various spirals that follow a spatially fixed path. In this chapter we will focus on rotating spirals. Dynamic spirals

S. C. Müller (✉)
Institute of Physics, Otto von Guericke University Magdeburg,
Universitätsplatz 2, 39106 Magdeburg, Germany
e-mail: tsuji-mueller@t-online.de

moving in space and forming vortices are frequently found in "excitable media" [1]. In fact, one finds that excitable media are dominating the scene: they occur in a large variety of systems of natural science, including chemistry, biology, neurobiophysics, biomedicine, and others.

Before dealing with excitable media coupled to physical transport processes, we will explain some of the general and basic principles about the phase plane and processes occuring in this plane. The brief introduction to the theory of dynamical systems may support readers to understand the following presentations, as well as articles in Part V.

In many experiments in excitable media rotating spirals can be generated by external forces. We will show schematically how an air blow breaks the excitable front, leading to curling of the open ends [2]. This way rotating spirals are created. The motion of their tips depend on chemical components and aging of the system. Further examples will illustrate how spiral motions are affected by electric fields [3] or laser light [4].

2 The Phase Plane

Let us write down a pair of ordinary differential equations (ODEs) of 1st degree for variables x and y, which are **linearly** coupled (by "+" or "−") in the form

$$\frac{dx}{dt} = ax + by$$

$$\frac{dy}{dt} = cx + dy$$

with a, b, c, d real and constant coefficients.
These ODEs are soluble.

Example: Harmonic oscillator

$x = space\ coordinate$

$y = \frac{dx}{dt} = velocity$
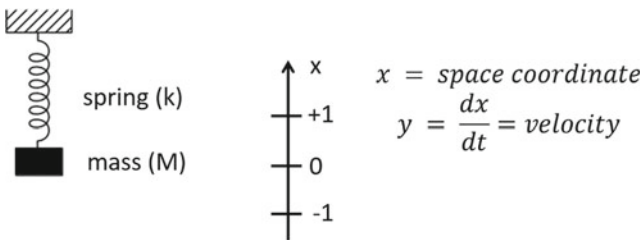
Equation of motion

$$M\frac{d^2x}{dt^2} + kx = 0$$

(ODE of 2nd degree).

With $M = 1, k = 1$ (dimensionless quantities):

$$\frac{d^2x}{dt^2} + x = 0.$$

By writing

$$\frac{dx}{dt} = y, \quad \frac{d^2x}{dt^2} = -x \quad \rightarrow \quad \frac{dy}{dt} = -x$$

we obtain the 2-variable first order system

$$\frac{dx}{dt} = y$$

$$\frac{dy}{dt} = -x.$$

Special solution:

$$x = \sin t$$

$$y = \cos t$$

$$(t: \text{dimensionless time}),$$

with initial conditions (for t = 0):

$$x_0 = 0$$

$$y_0 = 1$$

Representation in the **phase plane:**
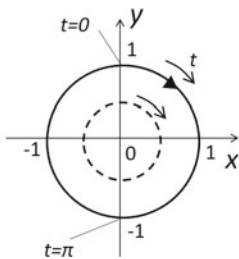
Cartesian coordinate system
with variables x, y:
Evolution along trajectory
(no explicit time)

Trajectory is a circle.
For different amplitudes of x and y
$\rightarrow$ ellipse

Isoclines:

These are curves with the same gradient (slope) of the phase plane trajectory: e.g., for the equation

$$\frac{dy}{dx} = f(x, y)$$

Set $f(x, y)$ equal to a constant m:

$$f(x, y) = m.$$

Especially useful are nullclines with $m = 0$.
Simple case: Harmonic oscillator

Nullclines:

$$f(x, y) = y = 0 \qquad\qquad\qquad\qquad y = 0$$

$$\rightarrow$$

$$g(x, y) = -x = 0 \qquad\qquad\qquad\qquad x = 0$$

Solution trajectories cross the
nullclines on the axes according to
the points marked in red.
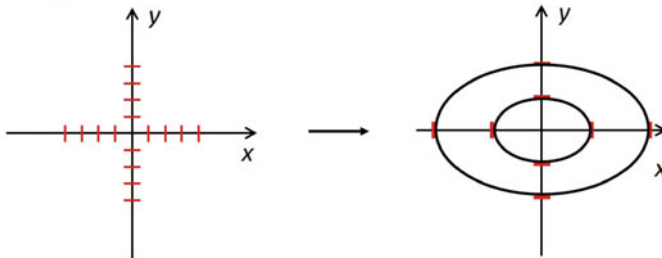
The nullcline picture fits
qualitatively for a circle or ellipse.

Nonlinear Case

A pair of nonlinear ODEs, (explicit and autonomous, i.e., no explicit dependence on t) can be written as

$$\frac{du}{dt} = f(u, v, \alpha, \beta, \ldots)$$

$$\frac{dv}{dt} = g(u, v, \alpha, \beta, \ldots)$$

with f, g some nonlinear functions of the variables u, v and α, β,... parameters.
(Certain mathematical conditions must be fulfilled to ensure existence and unique-
ness.)

The symbols u, v are used here for concentrations of chemical variables, e.g.,

$u = activator$
$v = inhibitor$

In general, these ODEs cannot be solved, but there are approximative techniques used according to the specific problem at hand.

3   Excitable Systems

Excitable systems are an important special case. In Fig. 1 the main properties are illustrated in the u, v-plane. u is supposed to vary quickly (the activator), v slowly in time (the inhibitor). According to appropriate kinetic models the nullcline of function
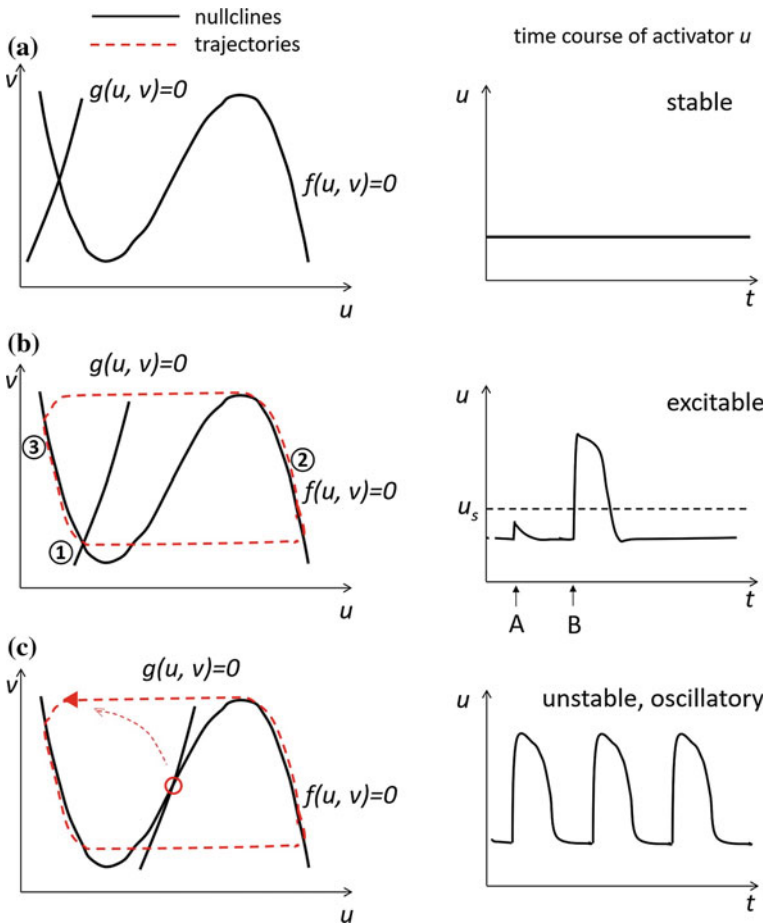
Fig. 1 Nullclines, see text

f [$f(u, v) = 0$], as a general supposition, has one minimum and one maximum. The parts with negative slope are stable, the rising part is unstable. The nullcline of function g [$g(u, v) = 0$] is monotonically increasing and stable. If these nullclines intersect, we obtain a fixed point, stable or unstable, without temporal evolution. There are the following scenarios (see Fig. 1):

(a) Both stable nullclines intersect → stable node, i.e., perturbations die out.
(b) Again there is at ① a stable intersection. The system is resting and excitable. But only perturbations smaller than the threshold value u_s decay (see A). If $u > u_s$ there follows a large but short excursion of u → excitable state ② (see B). After returning to $u \leq u_s$, the system recovers (relatively slowly) and moves to the original excitable state → refractory period ③. After reaching ① it waits for another superthreshold perturbation. Thus, in this case the system has mainly three states: excitable, excited (active), and refractory (resting).
(c) A stable nullcline intersects with the unstable (rising) part of $f(u, v) = 0$. The system will move away from the crossing point towards a stable trajectory, which in this case develops towards a limit cycle, i.e., to autonomous oscillations (without any rest state).

Excitation Pulse

Following the trajectory (dashed line) in Fig. 1b we derive for an excitable system the characteristic temporal profiles of variables u and v (Fig. 2). Activator u is produced

Fig. 2 Excitation pulse as a function of time
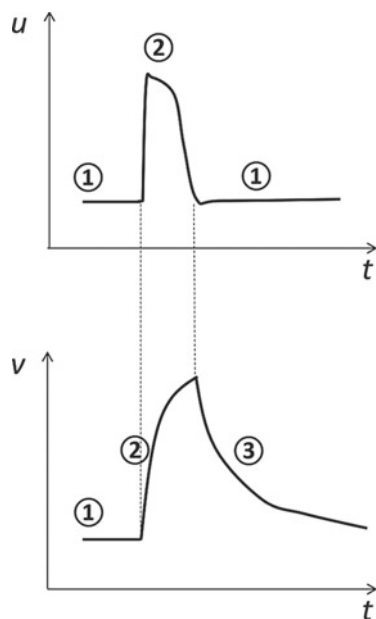
as a pulse at short time scale, inhibitor v responds on slower time scale with long refractory tail: separation of variables possible.

4 Excitation Waves

Propagation of waves is frequently observed in spatially extended oscillatory or excitable systems. They are described by solutions of reaction-diffusion equations.

For one spatial coordinate x these write:

$$\frac{\partial u}{\partial t} = D_u \frac{\partial^2 u}{\partial x^2} + f(u, v)$$

$$\frac{\partial v}{\partial t} = D_v \frac{\partial^2 v}{\partial x^2} + g(u, v)$$

with partial derivatives written as $\frac{\partial}{\partial t}$, $\frac{\partial}{\partial x}$, ... and D_u, D_v diffusion coefficients of species u and v, respectively. For three-dimensional space with coordinates x, y, and z, one uses the Laplace operator

$$\Delta = \frac{\partial^2}{\partial x^2} + \frac{\partial^2}{\partial y^2} + \frac{\partial^2}{\partial z^2}$$

The spatial profiles in a one-dimensional excitable system at a given time $t = t_0$ can be drawn as in Fig. 3.

Fig. 3 Spatial profiles of an excitation wave
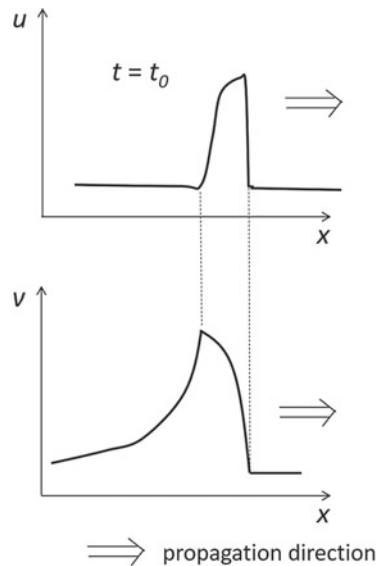
Introducing diffusion as a transport process opens the possibility of spatial contact between species leading to local coupling. The excitation pulse of activator u moving in x-direction will transfer the excited state to the molecules in front. This causes the propagation of excitation in that direction and leaves behind an unexcited refractory tail which will recover (slowly) to a newly excitable state. This way a backward propagation becomes impossible. (Often the spreading of a forest fire front is taken as an analogon: a small enough distance between trees will support the motion of the front, whereas the fire is extinguished behind the front due to lack of "fuel". The forest then recovers during a new growth phase.)

Such reaction-diffusion waves propagate with constant velocity, which depends on local concentrations and front curvature. They are frequently initiated in a thin excitable solution layer by a localized disturbance (immersion of a thin wire, gas bubble, dust particle, or laser spot). From there a circular wave would travel in outward direction. A periodically applied external disturbance would result in concentric rings - a so-called "target pattern". Then, the wave velocity will be a function of the distance between the waves governed by a dispersion relation.

5   Spiral Formation

Remarkable is the shape of spirals evolving and rotating in thin solution layers. Spirals can be created by disrupting a small section of a propagating wave front, for instance, with a gentle blast of air ejected from a pipette [2] or with a laser spot. Either well spontaneous breaks may occur due to a bubble or a dust particle.

The two open wave ends develop in time as shown in Fig. 4.
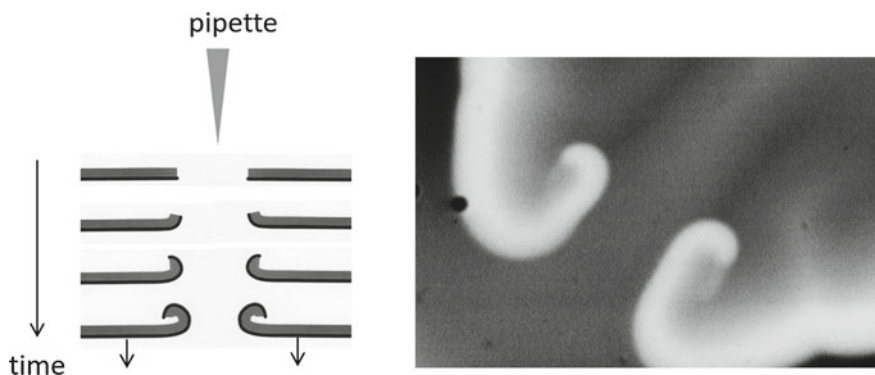
Fig. 4 Left: Evolution of open wave ends after disruption of the front. Black curve is excitable front, and grey part is refractory tail. The open ends curl around the refractory regions; right: image of the curling process

(a)

(b)

(c) rigid rotation

(d) compound motion*

determined by radius R,
period T , and center
coordinates

determined by 2 radii R_1 and R_2,
2 periods T_1 and T_2 ,
and center coordinates
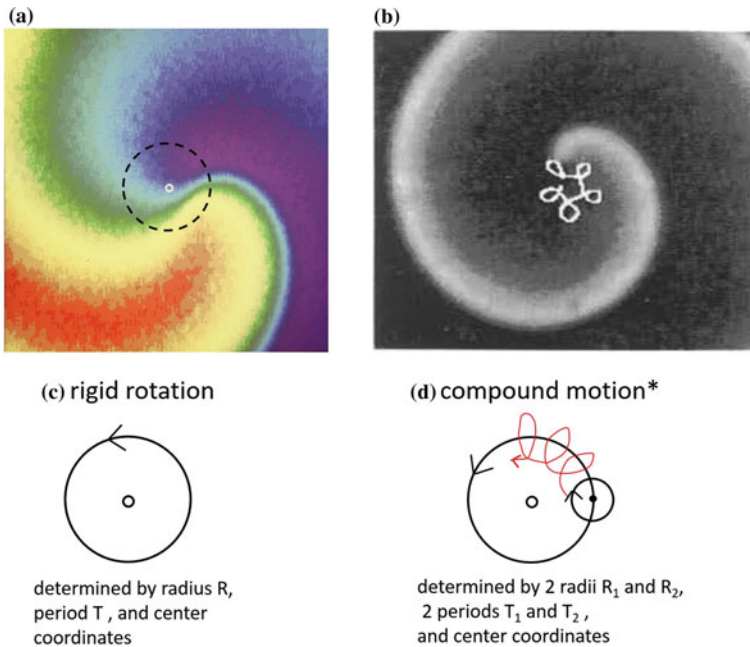
Fig. 5 **a** Enlargement of a spiral tip from Fig. 7 (see below). The black circle shows the rigid rotation of the tip around a central axis (white open circle). **b** When concentrations of the propagation medium are changed, the trajectory of the spiral tip may assume a compound (meandering) path [4]. Reprint permission from Nature. *This trace of a spiral tip is often erroneously called "hypocycloidal". **c** and **d** Simple drawings show these dynamic differences

After an initiation stage and under "standard" conditions the tip of the spiral rotates uniformly on a circle around a spatially fixed center (Fig. 5a). The spiral arm has an almost Archimedean shape.

Due to the rotation a new curled wave emanates from the central region after each turn. With this property the spiral is a true self-organized structure in that it keeps rotating and producing new curling waves without any external influence. This is different from the case of target patterns, where every additional circular wave needs an extra excitation pulse at the center for initiation. The spiral manages its independent dynamics through the action of diffusion. In fact, since its tip traces a small circle around the spiral center, it enters, after each turn, an area where the excitability has been again restored. Thus a "reentrant" activity flares up and the next spiral turn commences.

When conditions in the excitable medium are changed, the trajectory of a spiral may assume quite different paths. A first step is normally a transition to a "compound motion", when a second rotation period is superposed to the basic one (Fig. 5b).

A number of other, more complex traces of open wave ends have been observed: epicycles, loopy lines, irregular motion, straight or shrinking lines. We choose a
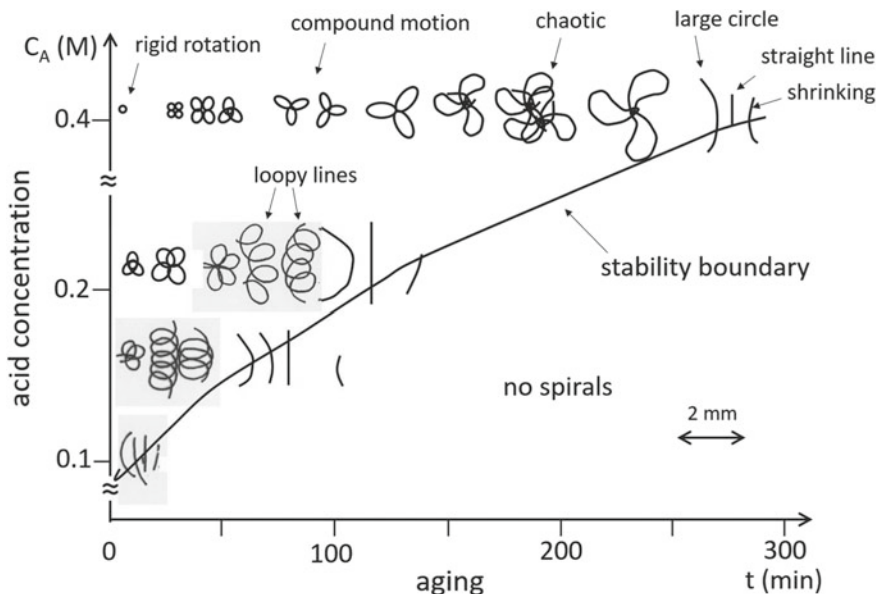
Fig. 6 Different trajectories of the spiral tip depending on acid concentration c_A and aging time of solution

graphic representation of trajectories measured during the aging of a chemical auto-catalytic reaction (the Belousov-Zabotinsky (BZ) reaction, see below), when the system passes though many of these trajectories during the course of time (Fig. 6).

6 Gallery of Dynamic Spirals

We proceed with a gallery of spiral images obtained from a special chemical system, the BZ-reaction which is, up to today, the most suitable medium to create spirals of various shapes and dynamics. This reaction will be introduced in the following chapter **Chemical Oscillations and Spiral Waves**.

Images were taken with sensitive monochrome cameras and partially converted to color images by means of appropriate software and pseudo-color techniques [5] For an example, see Fig. 7.

Among the techniques to influence the dynamics of an excitation wave by external means the application of an electrical current proves to be a most efficient tool. For the BZ reaction an electric field was applied via two parallel electrodes to the short edges of a rectangular dish containing a thin layer of solution. Numerous chemical species in this reaction are of an ionic nature, especially important the small negatively charged bromide ion (the inhibitor in the reaction). The microscopic driving force is electromigration of ionic species. Ions are pulled towards one of the electrode along

Fig. 7 Counter-rotating spirals in the BZ reaction, visualized in pseudo-color. Each of these spirals have an almost Archimedean shape and their tips rotate uniformly around a spatially fixed center. Note that wave fronts mutually annihilate each other upon collision. (Circular inclusions are CO_2 bubbles.) Reprint from [6], permission obtained from Springer Basel AG

Fig. 8 A pair of rigidly rotating spiral waves is perturbed by a constant electric field. Field lines are parallel and oriented vertically with the anode located at the bottom side of the figure. The electric field induces a spiral drift toward the anode and a strong deformation of the Archimedian spiral geometry. Loopy lines are directed along oblique angles determined by the chirality of spiral rotation
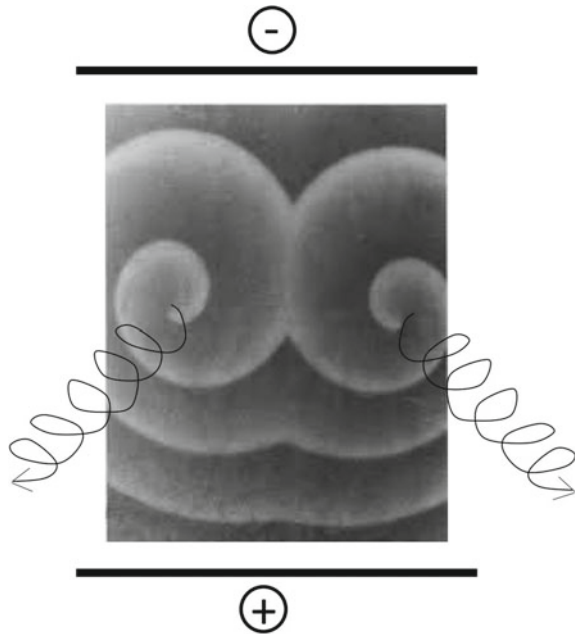
the electric field lines which can result in a local change of the concentration. In this case the major contribution is likely to stem from the small bromide ion migrating from the cathode towards the anode [7].

Fig. 9 By switching the
electrical field polarity with
respect to Fig. 8 the drift of
the spiral pair is reversed and
the loopy lines of the tips
approach each other in time.
Due to their symmetry and
opposite chirality they finally
collide, leading to mutual
annihilation. This is a
convenient method to get rid
of unwanted vortices.
Original picture from [3],
Nature
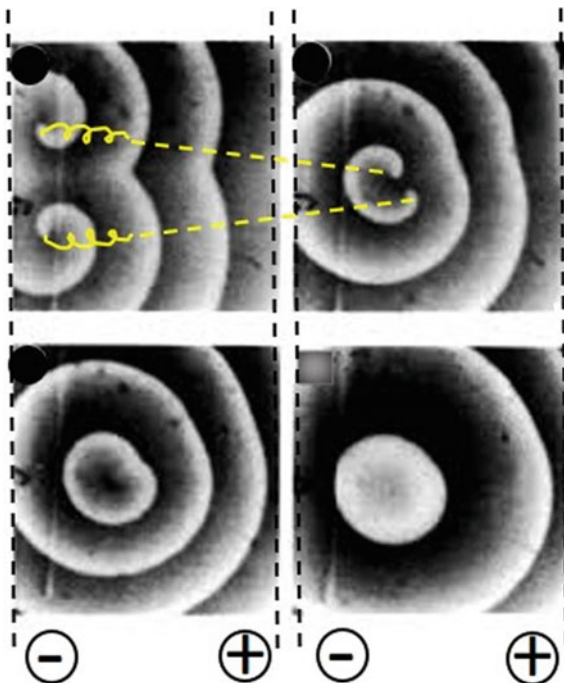
The direction of this field-induced drift depends on the chirality of the spirals, as
shown in Fig. 8. The left spiral, rotating clockwise, possesses an additional drift to
the left side. The other spiral, rotating couterclockwise, drifts towards the right side.
Switching off the current immediately stops the core drift. Changing the polarity of
the field causes a core drift towards the initial position [3] (Fig. 9).

Another powerful way for forcing the dynamics of a rotating spiral is offered by
laser light. When the excitability of the medium is modulated by a sinusoidal signal
over the entire solution layer, by an expanded laser beam, the effect of the external
frequency is reflected in the response of the trace of the spiral tip, which has been
investigated already in Fig. 6 during the aging of the system. Even more complex
behavior is now induced as a function of period and amplitude of the impinging light
[8]. A quite simple example is plotted in Fig. 10. The compound motion of a spiral
turns into a circular arrangement of multiple loops, due to phase-locking with the
external rhythm. The figure shows the case of twofold periodicity.

A different method to exploit the photosensitivity of the excitable solution lies
in the use of laser spots. If a laser spot of small diameter is directed into the
self-sustained core region of a rotating spiral, it may pin the spiral tip to this spot, if
the light has an inhibitory effect on the reaction (which can be produced by the choice
of a photosensitive catalyst). The increased size of the "quiescent" core region then
leads to a larger rotation period and consequently to a larger spiral pitch [9] (Fig. 11).

Fig. 10 Loopy line with twofold periodicity under the influence of an external periodic light field. Reprinted from [4], Nature
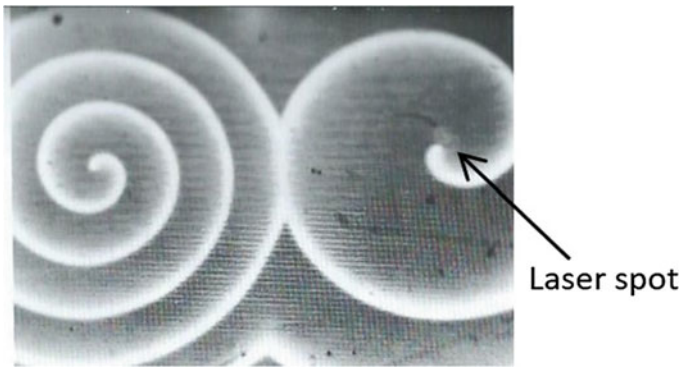
Fig. 11 In a photosensitive system, a laser spot can increase the the size of the autonomous spiral core (left) artificially (right) and thus cause the spiral to assume a much larger pitch. Reprint permission obtained from Elsevier

With help of such a spot open wave ends may be pinned and led along preselected paths. This way multiple spiral waves have been assembled [10]. In Fig. 12 (left) four open wave ends were created which, in the following, continue their dynamic paths and thus collide with each other. As a result a four-armed spiral is formed with an intricate mutual interaction.

A snapshot of this intricate interaction is shown in pseudo-color (Fig. 13).
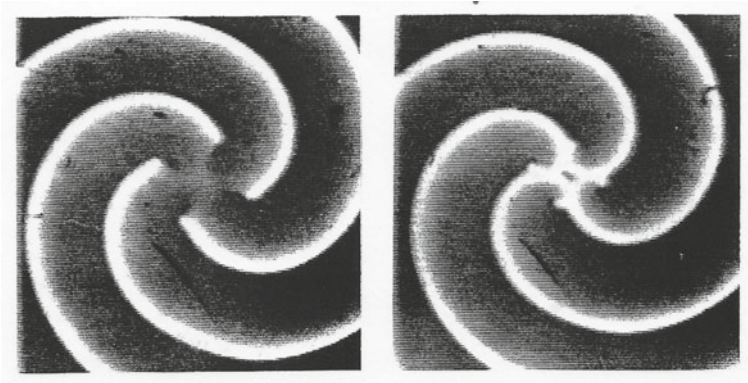
Fig. 12 Multiple spiral arms created by using a laser spot as a guiding obstacle. Left: four open wave ends assembled close to each other; right: their mutual collision

Fig. 13 Pseudo-color image of Fig. 12, right [11]. Reprint permission obtained from Springer Nature
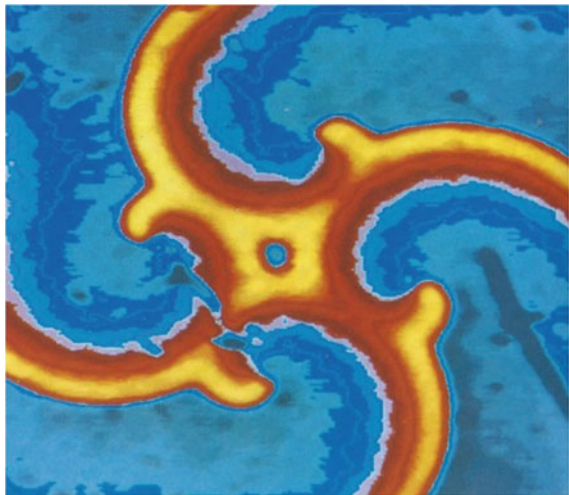
References

1. R. Kapral, K. Showalter (eds.), *Chemical Waves and Patterns* (Kluwer, Dordrecht, 1995)
2. S.C. Müller, T. Plesser, B. Hess, The structure of the core of the spiral wave in the Belousov-Zhabotinskii reaction. Science **230**, 661–663 (1985)
3. J. Schütze, O. Steinbock, S.C. Müller, Forced vortex interaction and annihilation in an active medium. Nature **356**, 45–47 (1992)
4. O. Steinbock, V.S. Zykov, S.C. Müller, Control of spiral waves in active media by periodic modulations of excitability. Nature **366**, 322–324 (1993)
5. S.C. Müller, T. Plesser, B. Hess, Two-dimensional spectrophotometry and pseudo-color representation of chemical reaction patterns. Naturwissenschaften **73**, 165–179 (1986)
6. H.-J. Hoffmann (ed.), *Verknüpfungen* (Birkhäuser, Basel, 1992), p. 58

7. O. Steinbock, J. Schütze, S.C. Müller, Electric field induced drift and deformation of spiral waves in an excitable medium. Phys. Rev. Lett. **68**, 248–251 (1992)
8. V. Zykov, O. Steinbock, S.C. Müller, External forcing of spiral waves. Chaos **4**, 509–518 (1994)
9. O. Steinbock, S.C. Müller, Chemical spiral rotation is controlled by light-induced artificial cores. Physica A **188**, 61–67 (1992)
10. O. Steinbock, S.C. Müller, Multi-armed spirals in a light-controlled excitable reaction. Int. J. Bifurcat. Chaos **3**, 437–443 (1993)
11. H.-J. Hoffmann (ed.), *Verknüpfungen* (Birkhäuser, Basel, 1992), p. 134

Chemical Oscillations and Spiral Waves

Patricia Pfeiffer

Abstract Pattern formation is one of nature's most fascinating phenomena. Starting with the evolution of life: cells and compartments start to differentiate such that they are able to undertake different tasks leading to life of complex organisms. Additionally, cells are able to release messenger substances, which may lead to an aggregation of cells as in the slime mold *Dictyostelium discoideum*. In this chapter, the formation of wave patterns, especially of spirals in non-equilibrium systems, is described. Starting with the revision of important aspects contributing to the historical development of synergetics, oscillating chemical reactions, such as the Belousov–Zhabotinsky reaction are described. Some theoretical aspects of reaction-diffusion systems and wave propagation in excitable media are outlined. The development and propagation of waves and thus, of spirals is described in such systems. At the end, the Belousov–Zhabotinsky reaction embedded in a compartmentalized system, namely an emulsion, is studied. Under the chosen conditions target patterns or spirals with segmented wave fronts evolve. These segmented waves (dashes) develop from a smooth one due to an instability. However, instead of forming a spiral turbulence, these dashes remain in an ordered configuration and form beautiful patterns.

1 Historical Remarks

Moving reaction waves occur in our everyday life even if we do not see them by eye. A remarkable example is our heart, in which waves trigger it to pump blood through our body (see chapter **Spiral Waves in the Heart**). The first person, who mentioned the existence of moving waves in a homogeneous medium was R. Luther in 1906 [1]. He already came to the conclusion that an autocatalytic reproduction of a chemical

P. Pfeiffer (✉)
Institute of Physics, Otto von Guericke University Magdeburg,
Universitätsplatz 2, 39106 Magdeburg, Germany
e-mail: patricia.pfeiffer@ovgu.de

species must be involved. Furthermore, Luther was able to give an equation for the calculation of the wave velocity v:

$$v = a\sqrt{kDC}, \tag{1}$$

where D represents the diffusion coefficient, k a rate constant of the chemical reaction, C a concentration and a a numerical constant. However, Luther gave no derivation for his equation.

Based on the work by Luther, B.P. Belousov started in 1951 to work on chemical oscillations in the catalyzed oscillatory bromate oxidation of citric acid. Since nobody believed in oscillating chemical reactions, Belousov was not able to publish his work before 1984 [2]. A.M. Zhabotinsky modified the reaction described by Belousov in 1961 in a fashion, which is still used today: the bromation of malonic acid, catalyzed by ferroin, which shows a color change from red to blue [3]. In 1974, Field and Noyes studied a semi-quantitative model of wave propagation in the reaction described by Belousov and Zhabotinsky. In their work, they were able to derive the equation given by Luther in 1906 [4]. Another remarkable aspect in the work of Luther was his comparison between chemical waves in a homogeneous medium and nerve impulses spreading over cell membranes, although he had no evidence for his suggestion [1]. In fact, there are structural analogies between both systems. The propagation velocity of a nerve pulse can be estimated using the Hodgkin–Huxley equation [5], which describes the propagation of stimuli throughout a nerve cell. They modeled the cell membrane as an electrical circuit, where the flow of ions can only be realized through ion selective channels and derived an equation which facilitate the calculation of the propagation of a nerve pulse over a membrane.

Oscillations in chemical systems were known much earlier than the propagating waves mentioned above. A brief summary of these historical experiments is given in the following: Already in 1829 F.F. Runge studied the contraction of a droplet of sulfuric acid on an area covered with mercury. He placed the acid on top of the mercury, where the droplet runs flat. Touching both with an iron wire, the acid contracts and forms a drop around the wire. Additionally, he observed that the mercury twitches slightly after touching. This system is nowadays known as the oscillating mercury heart [6]. At the end of the 19th century, R.E. Liesegang observed periodic precipitation patterns in gels (cf. **Liesegang Rings, Spirals and Helices**). In 1899 W. Ostwald observed the oscillating hydrogen production during the dissolution of chrome in acids. A theory of a hypothetical chemical reaction showing oscillations was given by A. Lotka in 1910. A more detailed description of his model is given in the next section. K.F. Bonhoeffer discovered in 1941 activity waves on passive iron wires. These wires were made passive by immersing them into sulfuric acid. Touching them with a piece of zinc, whereby it is locally cathodically polarized, an activity wave of local dissolution of the iron propagated along the wire [6].

2 Oscillations in Chemical Systems

The most prominent oscillating chemical reaction is the Belousov–Zhabotinsky (BZ) reaction. This reaction was first introduced by B.P. Belousov as a catalytic model for cancer cycles in which cerium ions are used instead of protein bounded metal ions, which are normally used by enzymes in living cells [6]. He described a periodic color change between colorless and yellow. In the default configuration, which is nowadays used, the color change in the BZ reaction is realized by the catalyst ferroin $(Fe(1,10\text{-phenanthrolin})_3^{2+})$, which changes its color from red to blue upon oxidation. In its reduced state, it has a positive charge of two and in its oxidized state it has a positive charge of three. In the reaction, an organic substrate (usually malonic acid) is oxidized by bromate in an acidified milieu via the metal ion catalyst (ferroin) [7]. The ion Br^- is playing the role of the inhibitor and $HBrO_2$ acts as the activator of the system since it is autocatalytically produced. The overall BZ reaction is governed by the oxidation of malonic acid due to bromination:

$$3\,H^+ + 3\,BrO_3^- + 5\,CH_2(COOH)_2 \rightarrow 3\,BrCH(COOH)_2 + 2\,HCOOH + 5\,H_2O + 4\,CO_2.$$

The entire reaction consists of a set of different chemical reactions that can be subdivided into three processes: First, the inhibitor Br^- is consumed until its concentration falls below a certain concentration, which triggers the second process. This process contains the autocatalytic production of the activator $HBrO_2$. Furthermore, the metal catalyst ferroin is oxidized in this process, which is responsible for the color change to blue. When the reduced version (red color) of the catalyst is depleted, the third process sets in. Here, malonic acid is brominated and the metal catalyst is reduced and gets back its red color. Additionally, Br^- is produced in the last process. Due to the increase of its concentration, the first process will be activated again [7]. If the above described system is stirred, it shows color oscillations in bulk. However, if it is performed in a Petri dish, it shows—depending on the initial concentrations of the reactants—spontaneously evolving patterns such as target patterns or spirals (see Sect. 4).

Another example of an oscillating reaction is the Briggs–Rauscher reaction, which is an oscillating iodine clock, cyclically changing its color from colorless to gold to blue. The reaction consist of the following ingredients: potassium iodate, hydrogen peroxide, perchloric acid, malonic acid, manganese(II)-sulfate and starch. This reaction works at room temperature, which makes it suitable for demonstrations (contrary to the Bray reaction, which is an early precursor of the Briggs–Rauscher reaction). The reaction shows visible concentration changes in iodine and the concentration of the iodine ion fluctuates. When the iodide concentration reaches a certain value, a starch complex is formed, which appears in blue color [8].

A theoretical analysis of a periodic reaction was given in 1910 by A. Lotka [6]. Nowadays it is referred to as Lotka–Volterra model. It represents a hypothetical chemical homogeneous system, which shows oscillations and is described by the following three reactions:

$$A + X_1 \xrightarrow{k_1} 2X_1,$$
$$X_1 + X_2 \xrightarrow{k_2} 2X_2, \tag{2}$$
$$X_2 \xrightarrow{k_3} F.$$
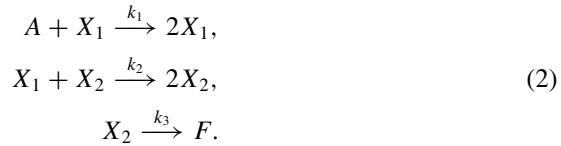
From the chemical point of view, the autocatalytic step (production of X_2) in the second equation does not make much sense, since the molecule X_1 must transform in presence of X_2 into X_2 as well. Thus, nowadays it is used to describe the relation between a predator and its prey. In this case, X_1 is referred to as rabbit, X_2 represents the predator (e.g., a lynx), A is the food of the rabbit and F quantity of the lynx having died of natural causes (with the death rate k_3).

The reactions from Eq. (2) result in a pair of nonlinear differential equations indicating the rates of change of the concentrations of the chemical species X_1 and X_2. The amount of food and the death rate (i.e., A and k_3) are assumed to be constant:

$$d[X_1]/dt = k_1[X_1][A] - k_2[X_1][X_2],$$
$$d[X_2]/dt = k_2[X_2][X_1] - k_3[X_2], \tag{3}$$

where k_i are constant reaction rates, and the values in brackets the concentrations of the corresponding species. Spoken in the predator-prey context, the oscillations occur in the amount of rabbits and lynx. If enough rabbits are present to feed on, the population of lynx will increase. However, this larger population will consume more rabbits, such that their population decreases and with this also the population of lynx.

3 Waves in Chemical Systems

3.1 Reaction-Diffusion Systems

Many patterns in nature arise in so-called *reaction-diffusion!systems* (cf. chapter **Reaction-Diffusion Patterns and Waves**). In these systems, a chemical reaction occurs locally and is transported in space by diffusion. A prominent reaction showing such patterns is the unstirred BZ reaction (Fig. 1). For a classical reaction-diffusion system, only one chemical component (here: u) is required:

$$\frac{\partial u}{\partial t} = D_u \frac{\partial^2 u}{\partial x^2} + f(u). \tag{4}$$

D_u denotes the diffusion of the component u, x the spatial dimension, t the time and f the reaction term. This is a partial differential equations with diffusion. If a second component is involved in this process, one typically speaks of an activator-inhibitor system. In this case, one of the species is produced autocatalytically, whereas the other one inhibits this production. Thus, Eq. (4) extends to:

$$\frac{\partial u}{\partial t} = D_u \frac{\partial^2 u}{\partial x^2} + f(u, w),$$

$$\frac{\partial w}{\partial t} = D_w \frac{\partial^2 w}{\partial x^2} + g(u, w).$$

$$(5)$$

D_u and D_w represent the diffusion of the corresponding species u and w, respectively.

Fig. 1 Target patterns and spiral waves in the BZ reaction. The dark spots are small bubbles, since gas is produced during the reaction (Image courtesy: S.C. Müller, personal communication)

In 1952 Alan Turing was the first, who described such systems mathematically. He showed that a chemical system will form stationary patterns, if some conditions for the diffusion constants are fulfilled, namely the diffusion of the activator must be much slower than that of the inhibitor [9]. The experimental observation of the patterns predicted by Turing took several decades, since the demanding conditions on the diffusion coefficients of activator and inhibitor in chemical solutions made it experimentally challenging. A "trick" was necessary to reduce the diffusion coefficient of the activator. In 1990 the first experimental observation of Turing patterns was realized by V. Castets et al. in the chlorine-dioxide-iodine-malonic acid reaction, as he trapped the activator in a gel matrix [10]. In nature, Turing patterns occur during morphogenesis, e.g., on animal skins.

In 1968 Prigogine and Lefever [11] formulated reaction-diffusion equations while they extended Turing's equations, such that their equations could explain the differentiation of biological cells with the aid of reactions and substance exchange of two different types of molecules. They declared the role of diffusion in a system having two tasks: First, diffusion increases the stability of a system, but second, it also increases the variety of perturbations, which are compatible with the macroscopic equations of change.

3.2 Excitable Media

Excitability is an important concept in biology and chemistry. Common examples in nature are the brain and the heart (cf. chapter **Spiral Waves in the Heart**). Through

these media electric pulses propagate forcing to change their state for a short time
[12]. An important example from the chemical field represents the BZ reaction [13].
In such systems a perturbation is overdamped, if it is smaller than a certain threshold.
A large perturbation, however, causes a response of the former. Due to the complete
recovery of the system after the passage of an excitation wave, many of those can
travel trough it. A single wave pulse is sketched in Fig. 2. The wave propagates
towards the left. In its front, the medium is excitable. A perturbation induces a wave
traveling through the system, where the wave front itself is in the excited regime.
Behind the pulse, the medium must recover and is in the refractory state. When the
system has fully recovered, a new perturbation can induce a new wave pulse. Within
a spatially distributed excitable medium the excitation propagates from one point to
the neighboring one by local coupling realized by diffusive transport [12]. Due to
the interplay of diffusion and chemical reactions, waves of excitation can propagate
through the medium, forming patterns like spiral waves in space or oscillations in
time [13] (see Sect. 4).

Fig. 2 Sketch of a propagating concentration wave [*u*] over time. Before the system is perturbed, it is in the excitable regime (low concentration of *u*). After it has passed the excited regime, it must recover, since the concentration of *u* is lower than in the excitable state, which makes it immune to a new perturbation
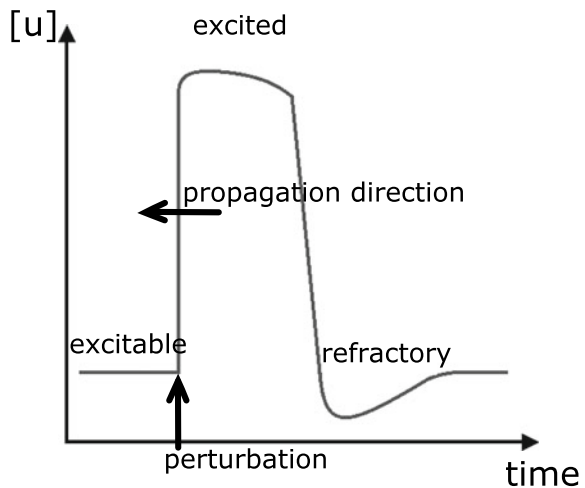
4 Creation and Propagation of Spiral Waves

The propagation of waves in excitable media depends mainly on diffusion. Its velocity
v can be calculated with the help of Eq. (1) with *D*, *k* and *C* being diffusion coefficient,
rate coefficient and concentration of the activator *u*, respectively. When several waves
emerge, such as concentric circles (see Fig. 1; also called *target pattern*)—induced
by a pacemaker in the system (e.g., an impurity)—wave propagation is governed by
the so-called *dispersion relation* of the system. It is defined as the velocity of a wave
v divided by the distance between single waves, i.e., the wavelength λ. In general,

this relation is positive in the BZ reaction, which means that the velocity of a wave decreases with decreasing distance between the waves [14]:

$$\frac{dv}{d\lambda} > 0. \tag{6}$$

Additionally, the velocity of a wave depends on its curvature K (which is equal the inverse radius r of a wave). Plain waves are faster than curved ones. This fact is described by the following equation, which is called eikonal equation:

$$v = v_0 - DK = v_0 - D\frac{1}{r}. \tag{7}$$

Here v describes the velocity of a curved wave in the normal direction, v_0 the velocity of a plain wave, and D is the diffusion coefficient. The eikonal equation describes, how the velocity of waves decrease with increasing curvature and it also places a stability condition on the wave front, since a uniform curvature of a wave is a stable solution of Eq. (7) [14]. This means that perturbations of the wave front, e.g., due to an obstacle balance out. Additionally, it is obvious that a critical curvature exists, where wave propagation fails:

$$K_{crit} = \frac{v_0}{D}. \tag{8}$$

This plays a crucial role in the formation of spiral waves. At the tip of a spiral, the highest curvature that is possible in the system is adopted, and with this, the velocity is lowest there.

In Fig. 3 the process of the formation of a pair of counter-rotating spiral waves is depicted. The propagating wave front (1) reaches an obstacle (e.g., a region of lower excitability), which causes the break up of the wave front (2). After leaving the obstacle, the wave front remains broken and at the open wave ends an additional velocity component is present, which is perpendicular to its initial one (3). The wave starts to curl yielding a slower propagation velocity at the tips (cf. Eq. (7)). Each open end forms a spiral, having an opposite sense of rotation (i.e., opposite chirality) (4). In the end, spirals of Archimedean shape have formed, rotating around a fixed center, called the spiral core, which is the organizing center of the spiral. In the direct vicinity of the core, however, the shape differs slightly from the Archimedean [15] (see involute in chapter **Spirals, Their Types and Peculiarities**).

The spiral tip is a singularity in the medium at which the spiral has the greatest curvature. This means that the normal velocity of a curved wave becomes zero ($\mathbf{v} = 0$, cf. Eq. (7)) and the tip moves tangentially along a circular trajectory, since the high curvature prohibits movement into the normal direction (Fig. 4) [16]. The area enclosed by the trajectory is called the spiral core and is not excitable. Spirals have the ability to organize an excitable medium, as they can take up the highest possible frequency in the medium. The value of this frequency is determined by the medium itself, as it depends, among other things, on its excitability. Higher frequencies do not exist, since otherwise, the excitation front would run into the refractory regime of its predecessor.

Fig. 3 Sketch of the formation of a pair of counter-rotating spiral waves. A plain wave (1) reaches an obstacle, which causes a breakup (2). At the open wave tips, the excitation can now propagate into the direction perpendicular to the direction of the plain excitation wave (3). Due to the slower propagation velocity of a curved wave, the wave tips can curl up to form a spiral (4)
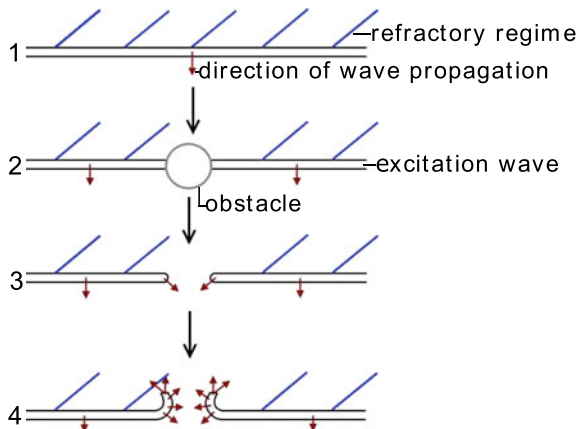
Fig. 4 Superposition of images of the spiral tip during one rotation around the core in pseudo-colors. The area never touched by the wave is colored in orange (copyright by Hess, Markus, Müller, Plesser, Dortmund 1987)

In the two-dimensional (2D) BZ reaction, spiral waves, target patterns or simple oscillations can occur and run through the entire system. Target patterns can be induced by touching the medium in a single spot with a silver wire for a few seconds. On the surface of the wire bromide ions (which act as the inhibitor) are bound, which locally reduces the concentration of these ions in the reaction. This induces the autocatalytic formation of the activator $HBrO_2$ (cf. Sect. 2). Spiral waves emerge, when an enclosed wave front is disturbed, such that it ruptures (Fig. 3). This can be forced, if a wave front is treated with an air jet. Even an obstacle can force the wave front to break, if it is large enough (otherwise the wave fronts will merge behind the

obstacle and no open wave end is created). With these methods, one gets always a pair of counter-rotating spirals as shown in the lower half of in Fig. 1. The initiation of a single spiral needs a little more experimental skills. Here a thin (quasi 2D) reaction container can be used, where a gel, in which the BZ reaction runs, is filled up to half. Then, a wave is initiated with a silver wire near one boundary. When one end of the wave reaches the boundary, the reaction container is filled up with the BZ gel and the wave can now propagate into the regime of the new gel. This method is described in detail in Ref. [17].

The wave propagation velocity v in the BZ reaction depends on the chemical composition of the reaction mixture, which determines the speed of the reaction and the transport processes. Especially, v is governed by the proton concentration $[H^+]$ and bromate concentration $[BrO_3^-]$ (cf. Eq. (1)) [18]:

$$v \sim \sqrt{k_u D_u [H^+][BrO_3^-]}, \tag{9}$$

where k_u is the reaction rate of the activator and D_u its diffusion coefficient. If the initial concentrations of malonic acid, sulfuric acid and sodium bromate are high compared to the concentration of ferroin, homogeneous oscillations occur in the system. A comparable ratio between ferroin and the other three reactants yields reduction waves in the BZ medium.

The BZ reaction can be inhibited by oxygen, which diffuses up to 2 mm depth into the liquid layer. The inhibition occurs due to oxidation of malonic acid by ferroin. When atmospheric oxygen diffuses into the reaction, malonic acid is no longer available for the reaction, since its radicals are caught by oxygen [19]. Thus, it is advisable to perform experiments in a closed container.

5 Patterns in Microemulsions

The BZ reaction can be embedded on the one hand into a gel, which does not affect any properties of the reaction, such as diffusion of chemical species. On the other hand, the reaction can be loaded into an emulsion, which is a mixture of oil and water. In the system discussed here, only water-in-oil emulsions are considered (i.e., a little amount of water in much oil). The small water droplets are stabilized with a surfactant and have a size of a few nanometers, leading to the name *micro*emulsion. They have certain physical properties, which are discussed in the following.

5.1 Physical Properties of Microemulsions

Almost everything in an emulsion is governed by the volume ratio between water and oil (cf. Fig. 5). Additionally the amount of surfactant is also important, since it is responsible for the stability of the system. Unless enough surfactant is available, the interface between water and oil cannot be fully covered with the surfactant and

no defined structure is formed. In Fig. 5 (right) possible configurations of the water phase in a microemulsion are depicted, together with a phase diagram which shows how the ratio between water, oil and surfactant affects the emerging configurations. Here, mainly the L_2 phase is considered, i.e., spherical water droplets, surrounded by a monolayer of the surfactant diffusing through the oil phase. The droplets collide and merge, forming droplet clusters, which can split again. As the solvent, a saturated hydrocarbon is used, like octane or hexane. The used surfactant is sodium-bis(2-ethylhexyl) sulfosuccinate (AOT, Fig. 5 (left)), which shows the L_2 phase over a wide range of concentrations. AOT is an anionic surfactant consisting of a polar head group (SO_3^-) and two hydrophobic tails [20].
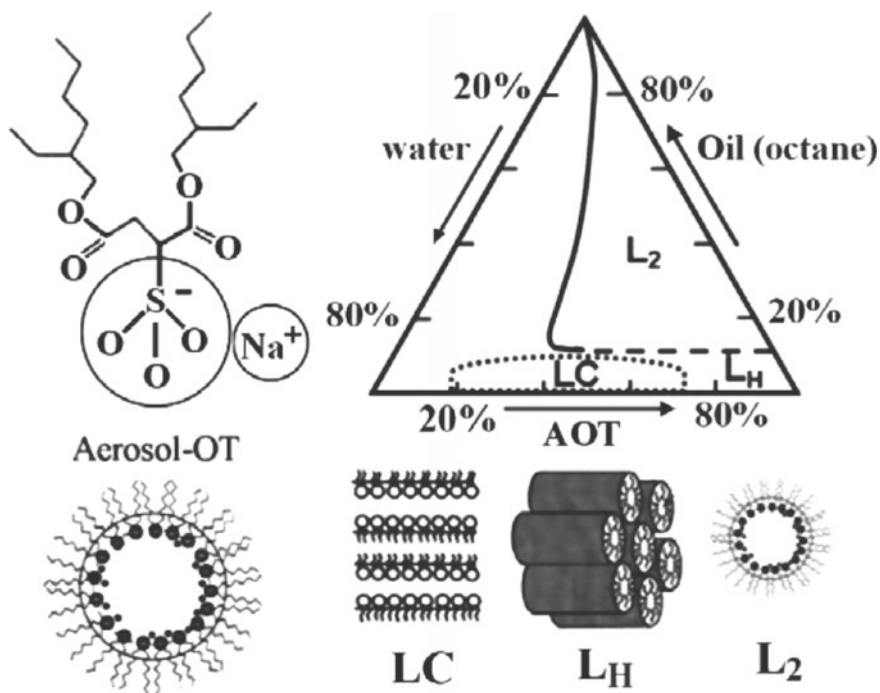
Fig. 5 Left: Sketch of the surfactant AOT with its polar head group SO_3^-. Right: Phase diagram of the water-AOT-oil system. The L_2 phase is a reverse microemulsion (water-in-oil microemulsion), in which most of the experiments in this work are performed. L_H – hexagonal phase; LC – lamellar phase (liquid crystal). Reprinted by permission from Springer: Patterns of Nanodroplets: The Belousov-Zhabotinsky-Aerosol OT-Microemulsion System, V. K. Vanag and I. R. Epstein [21], copyright 2008

The properties of an emulsion can be described with the help of two parameters: The molar ratio ω between water and AOT concentration [22]

$$\omega = \frac{[H_2O]}{[AOT]}, \tag{10}$$

and the volume droplet fraction of the dispersed phase φ_d, which is the ratio of the sum of the individual volumes of water (V_W) and AOT (V_{AOT}) and the entire volume of the emulsion:

$$\varphi_d = \frac{V_W + V_{AOT}}{V_W + V_{AOT} + V_{oil}}. \tag{11}$$

With the help of ω, the droplet radius R_ω of the water core (without the AOT-molecule [23]) can be estimated with the empirical equation

$$R_w[nm] = 0.17\omega. \tag{12}$$

To calculate the radius of the droplet including the surfactant, the length of the AOT-molecule must be added (≈ 1.1 nm) [24]. φ_d acts as an order parameter of the system, since it determines the configuration of water, oil and AOT (cf. Fig. 5).

5.2   Percolation

When changing the amount of water, the droplets of the L_2 phase merge and form water channels pervading the entire medium. This process is called *percolation*. In general it means that components of a system form connected clusters. If a cluster reaches all ends of a system, the latter is percolated. Some practical examples are water in a coffee filter or forest fires and their models.

In a mircoemulsion, the first infinite droplet cluster is formed around a droplet fraction of 0.5, which is referred to as critical droplet fraction φ_{cr} [24]. Due to this network of water channels, viscosity and electric conductivity increase as well. For $\varphi_d \ll \varphi_{cr}$, the droplets move nearly freely in the oil phase. The emulsion has a high viscosity due to the large amount of oil and its electric conductivity is close to that of pure oil. Above φ_{cr} the number of such clusters increases rapidly [25] and with them the electric conductivity. In fact, the latter can be used to measure the critical droplet fraction, above which the system is percolated. Thus, percolation causes a threshold-like behavior of physical quantities.

5.3   BZ Reaction in Microemulsions

Embedding the BZ reaction in a microemulsion (referred to as BZ-AOT system), which shows the L_2 phase, changes the emerging patterns significantly compared to the aqueous BZ reaction. The reaction only runs within the water droplets, such that the diffusion coefficient of the activator is reduced. It diffuses with the same velocity as the droplet itself. Some products of the BZ reaction, such as molecular bromine

Br_2 and the radical $BrO_2^{\bullet}$, which are inhibitors of the system, are soluble in the oil phase and can diffuse out of the droplets. Thus, their diffusion coefficient rises by 10–100 of the initial value. Hence, the conditions for Turing patterns are fulfilled (cf. Sect. 3) and the corresponding stationary patterns can occur in the BZ reaction [24]. Note that Turing patterns can only occur below the percolation threshold, due to the conditions on the diffusion coefficients of activator and inhibitor.
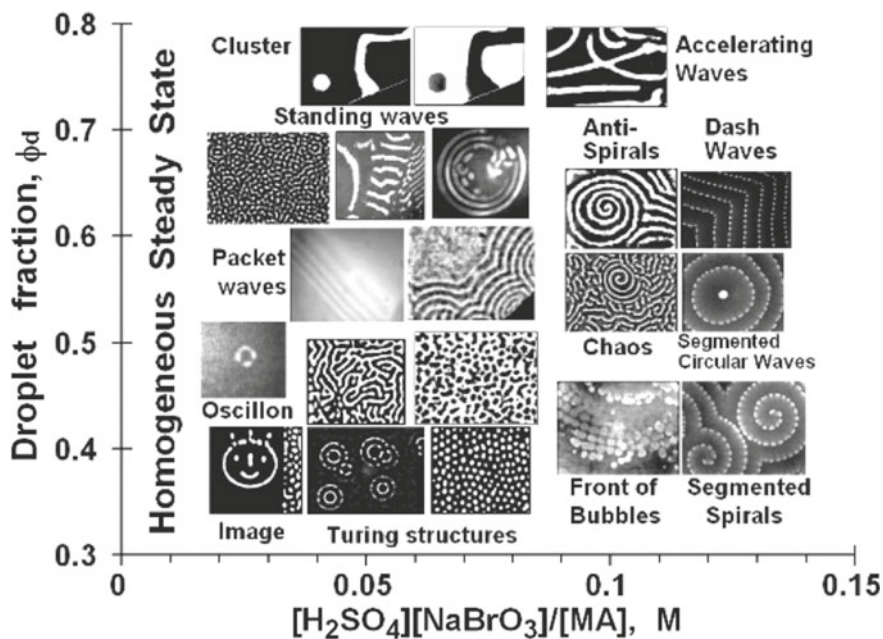
Fig. 6 Overview of patterns occurring in the BZ reaction embedded in a micro-emulsion. The patterns in the right column (above a chemical concentration relation of 0.1 M) are generated with another catalyst (bathoferroin). Reprinted by permission from Springer: Patterns of Nanodroplets: The Belousov-Zhabotinsky-Aerosol OT-Microemulsion System, V. K. Vanag and I. R. Epstein [21], copyright 2008

Figure 6 shows an overview of patterns, which can occur in a microemulsion, depending on the ratio between the chemicals (sulfuric acid, sodium bromate and malonic acid), and the droplet fraction. Above the percolation transition, a bimodal distribution of the droplet radius is found (below the transition, only one radius is found) [21], favoring the formation of discontinuously propagating waves (like jumping, rotating and bubble waves) and dash waves (see Fig. 6, above a chemical concentration relation $[H_2SO_4][NaBrO_3]/[MA]$ of 0.1 M). The latter develop from a smooth wave front, which splits up such that coherently moving wave segments separated by lateral gaps occur [21, 24]. These waves will be discussed briefly in the following section.

5.4 Segmented Waves

Segmented (or dash) waves occur mainly, when two pools of droplets exist, with radii of around 2 and 20 nm [21]. This is typical when using the catalyst bathoferroin, which is a derivate of the default catalyst ferroin. However, spirals cannot be induced in a controlled way as described in Sect. 4, but they have to form spontaneously (e.g., due to an impurity or small concentration differences). In the reaction with bathoferroin, dash waves or spirals, as well as discontinuously propagating waves, such as rotating and jumping waves evolve (Fig. 6).

Figure 7a shows dash waves in the upper left corner, with a negative (concave) curvature and (b) spiral waves with a positive (convex) curvature. Segmented waves evolve from ordinary (smooth) waves, which become unstable with time. They show so-called *ripples*, which means that some regions of the wave are propagating slower than their neighboring regions, and the curvature of these slow regimes becomes negative (box in Fig. 7b). In the course of time, the wave breaks in these regions, such that small segments of the original wave remain, which travel through the medium as if the wave front still exists. The instability occurs only, if the inhibitor diffuses fast (compared to the activator) and causes a wave break-up [26]. The former acts transverse to the wave front and it may occur through lateral inhibition or a kinetic interaction of the wave with a reactant in front of it [27, 28]. The segmentation of wave fronts always starts near the center of a spiral, since the curvature is highest there.

Dashes of one wave front propagate into the gaps of its precursor, which means that the dashes are displaced by the length of a dash relative to their precursor. In the dashes, the inhibitor is primarily generated, diffusing faster than the activator, and suppressing the autocatalytic reaction in the neighboring gaps. Additionally, this increases the time until the the medium has recovered when the subsequent wave front reaches it [21, 24]. The displacement of the dashes is visualized with the help of superposition of frames over time (Fig. 7c and d). The length of the dashes vary between 90 and $163 \pm 2\,\mu m$ and the length of the gaps from 40 to $104 \pm 2\,\mu m$. Convex wave fronts show a splitting of dashes, when reaching 1.7 to 1.9 ± 0.1 times their initial length. This is depicted in Fig. 7d (red box), since the dashes propagate away from each other. For a concave curvature (as in Fig. 7c, black box) a merging of dashes can be found. The gaps get smaller, such that the dashes move closer together until they merge. Splitting or merging of the dashes was not found for a curvature K between -0.10 and $0.21 \pm 0.1\,mm^{-1}$, i.e., for almost plain wave fronts—here, the dashes propagate straightforward without changing their length.
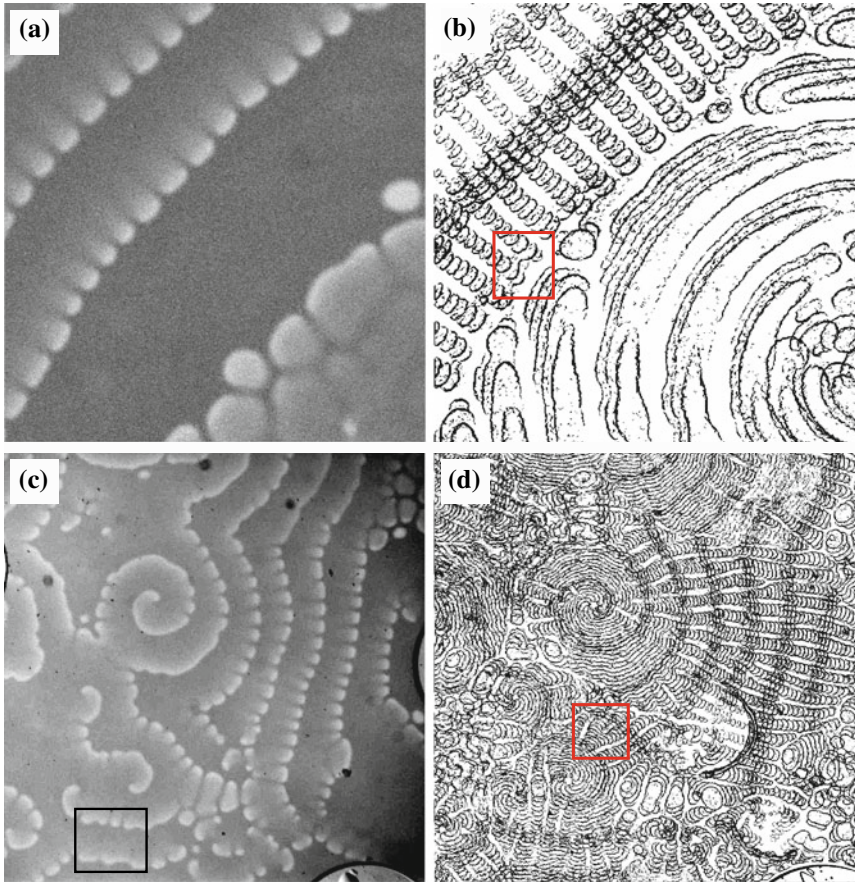
Fig. 7 Snapshots of patterns in the bathoferroin-catalyzed BZ-AOT system with $\omega = 12$ ($\varphi_d = 0.455$) at $t = 224.8$ min **a** in octane (size of images: $3 \times 3\,\text{mm}^2$) and **b** in hexane (size of images: $5.9 \times 6.1\,\text{mm}^2$). Superposition of binarized images **c** in octane between 180.0 and 189.2 min and **d** in hexane between 220.0 and 227.9 min with time interval of 40 s. Note that black lines in the superposition images represent the bright wave front. Reprinted with permission from P. Dähmlow, V. K. Vanag, and S. C. Müller, Phys. Rev. E 89, 010902 (2014) [29]. Copyright 2014 by the American Physical Society

The frequency distribution of the curvature, where splitting of dashes occurs, is shown in Fig. 8. For a mean curvature, the number of splitting dashes is much higher than that for small or large curvatures, since large curvatures occur only near the spiral core, where the number of dashes is much smaller than at the outer wave fronts.

The merging of wave fronts due to a decreasing distance between single segments is closely related to those studied in Ref. [30]. If the distance between the segments is smaller than the width of the wave front (i.e., the autocatalytic band),

Fig. 8 Histogram of the curvature K of a wave front for different experiments, in which a splitting of a dash occurs. The recipes are equal for all experiments: [MA] = 0.242 M, [NaBrO$_3$] = 0.174 M, [H$_2$SO$_4$] = 0.194 M, $\omega = 12$ and $\varphi_d = 0.455$. 1 - dashed spiral in Fig. 7b, 2 - dashed spiral wave, 3 - dashed target pattern
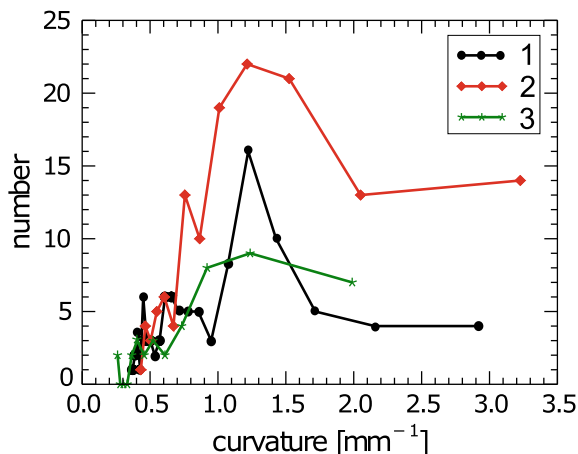
segments merge. An equal distance between both yields a constant length of single dashes. In our case, the distance between the dashes is also governed by the curvature of the initial wave. The segments are additionally forced to reduce their distance to each other at concave curvature of the initial wave front. A plain wave, where the distance between single dashes and the width of the wave front is equal shows a straight forward propagation of the segments, without any variations in length, as already described in Ref. [30].

6 Summary and Conclusion

Pattern formation in reaction-diffusion systems represents an important phenomenon in biological morphogenesis. In the early stages of the development of synergetics, people were fascinated by oscillatory chemical reactions, such as the mercury heart [6] or a periodic color change in the BZ reaction [2]. However, the scientific community doubted its existence, since self-organization of systems contradicted the increase in entropy and thus the second main theorem of thermodynamics. However, patterns can only form in systems, which are far away from thermodynamic equilibrium and have an energy- and/or mass transfer with their environment. This fact resolves the conflict.

In this chapter, the chronological sequence of important historical experiments contributing to the development of synergetics was given, especially in the context of pattern formation in reaction-diffusion systems. The most prominent example presents the BZ reaction, which shows both: periodic oscillations in a stirred solution and spatially expanding waves in an undisturbed system. The wave propagation in the spatially extended BZ reaction was studied in detail, and the influencing factors on the wave velocity (i.e., concentrations of reactants, reaction rate, diffusion, curvature

of the wave front and dispersion relation) and the mechanism of the formation of spiral waves were described.

Additionally, it is possible to load the BZ reaction into a water-in-oil emulsion, which afflicts the relation of the diffusion coefficients of activator and inhibitor significantly. This enables the system to form a wide range of possible patterns such as Turing patterns, discontinuously propagating waves (such as bubble and jumping waves) and segmented waves (cf. Fig. 6). Segmented waves evolve from an ordinary wave (target pattern or spiral wave), due to an instability. These dashes split or merge, depending on the curvature of the initial wave front, such that their length remains within a certain interval. However, the length of the gaps play an important role. Single segments are either able to curl and form new spirals or propagate ahead (as shown in Fig. 7). Larger gaps between the dashes would mean that not the entire area between the segments will be inhibited, wave propagation will become possible and the segments can start to curl and a spiral turbulence will develop.

We find that spiral waves represent an interesting and fascinating pattern, which can be found in many biological and chemical systems, as described throughout this book. They organize the medium in which they occur and oust many other pattern with time.

References

1. K. Showalter, J.J. Tyson, Luther's 1906 discovery and analysis of chemical waves. J. Chem. Educ. **64**, 742–744 (1987). https://doi.org/10.1021/ed064p742
2. B.P. Belousov, in *Oscillations and Traveling Waves in Chemical Systems*, ed. by R.J. Field, M. Burger (Wiley, New York, 1984), pp. 605–614. ISBN: 0-471-89384-6
3. A.M. Zhabotinsky, in *Oscillatory Processes in Biological and Chemical Systems*, ed. G.M. Frank (Science Publications, Moscow, 1967), p. 252
4. R.J. Field, R.M. Noyes, Oscillations in chemical systems. V. Quantitative explanation of band migration in the Belousov–Zhabotinskii reaction. J. Am. Chem. Soc. **96**, 2001–2006 (1974)
5. A.L. Hodgkin, A.F. Huxley, A quantitative description of membrane current and its application to conduction and excitation in nerve. J. Physiol. **117**, 500–544 (1952). https://doi.org/10.1113/jphysiol.1952.sp004764
6. H. Haken, P. Plath, W. Ebeling, Y. Romanovsky, *Beiträge zur Geschichte der Synergetik-Allgemeine Prinzipien der Selbstorganisation in Natur und Gesellschaft* (Springer Spektrum, Wiesbaden, 2016). https://doi.org/10.1007/978-3-658-12952-1
7. R.J. Field, E. Körös, R.M. Noyes, Oscillations in chemical systems. II. Thorough analysis of temporal oscillation in the bromate-cerium-malonic acid system. J. Am. Chem. Soc. **94**, 8649–8664 (1972). https://doi.org/10.1021/ja00780a001
8. T.S. Briggs, W.C. Rauscher, An oscillating iodine clock. J. Chem. Educ. **50**, 496 (1973). https://doi.org/10.1021/ed050p496
9. A.M. Turing, The chemical basis of morphogenesis. Philos. Trans. R. Soc. Lond. B **237**, 37–72 (1952). https://doi.org/10.1098/rstb.1952.0012
10. V. Castets, E. Dulos, J. Boissonade, P. De Kepper, Experimental evidence of a sustained standing turing-type nonequilibrium chemical pattern. Phys. Rev. Lett. **64**, 2953–2956 (1990). https://doi.org/10.1103/PhysRevLett.64.2953
11. I. Prigogine, R. Lefever, Symmetry breaking instabilities in dissipative systems. II. J. Chem. Phys. **48**, 1695–1700 (1968). https://doi.org/10.1063/1.1668896

12. A.T. Winfree, *The Geometry of Biological Time*, 2nd edn. (Springer, New York, 2001)
13. A.N. Zaikin, A.M. Zhabotinsky, Concentration wave propagation in two-dimensional liquid-phase self-oscillating system. Nature **225**, 535–537 (1970). https://doi.org/10.1038/225535b0
14. J.J. Tyson, J.P. Keener, Singular perturbation theory of traveling waves in excitable media (a review). Physica D **32**, 327–361 (1988). https://doi.org/10.1016/0167-2789(88)90062-0
15. S.C. Müller, T. Plesser, B. Hess, Two-dimensional spectrophotometry of spiral wave propagation in the Belousov–Zhabotinskii reaction: I. Experiments and digital data representation. Physica D **24**, 71–86 (1987). https://doi.org/10.1016/0167-2789(87)90067-4
16. A.M. Pertsov, M. Wellner, J. Jalife, Eikonal relation in highly dispersive excitable media. Phys. Rev. Lett. **78**, 2656–2659 (1997). https://doi.org/10.1103/PhysRevLett.78.2656
17. C. Luengviriya, U. Storb, M.J.B. Hauser, S.C. Müller, An elegant method to study an isolated spiral wave in a thin layer of a batch Belousov–Zhabotinsky reaction under oxygen-free conditions. Phys. Chem. Chem. Phys. **8**, 1425–1429 (2006). https://doi.org/10.1039/B517918A
18. R.J. Field, R.M. Noyes, Oscillations in chemical systems. IV. Limit cycle behavior in a model of a real chemical reaction. J. Chem. Phys. **60**, 1877–1884 (1974). https://doi.org/10.1063/1.1681288
19. A.F. Taylor, B.R. Johnson, S.K. Scott, Effect of oxygen on wave propagation in the ferroin-catalysed Belousov–Zhabotinsky reaction. J. Chem. Soc. Faraday Trans. **94**, 1029–1033 (1998). https://doi.org/10.1039/a708600h
20. H.-F. Eicke, J. Naudts, Non-linear field effects due to activation-energy controlled charge transport in microemulsions. Chem. Phys. Lett. **142**, 106–109 (1987). https://doi.org/10.1016/0009-2614(87)87260-3
21. V.K. Vanag, I.R. Epstein, Patterns of nanodroplets: the Belousov–Zhabotinsky–Aerosol OT-microemulsion system, in *Self-Organized Morphology in Nanostructured Materials*, ed. by K. Al-Shamery, J. Parisi. Springer Series in Materials Science, vol. 99 (Springer, Berlin, 2008), pp. 89–113. https://doi.org/10.1007/978-3-540-72675-3_5, ISBN: 978-3-540-72674-6
22. L.J. Schwartz, C.L. DeCiantis, S. Chapman, B.K. Kelley, J.P. Hornak, Motions of water, decane, and Bis(2-ethylhexyl)sulfosuccinate sodium salt in reverse micelle solutions. Langmuir **15**, 5461–5466 (1999). https://doi.org/10.1021/la9812119
23. V.K. Vanag, I.R. Epstein, Pattern formation in a tunable medium: the Belousov–Zhabotinsky reaction in an aerosol OT microemulsion. Phys. Rev. Lett. **87**, 228301 (2001). https://doi.org/10.1103/PhysRevLett.87.228301
24. V.K. Vanag, Waves and patterns in reaction-diffusion systems. Belousov–Zhabotinsky reaction in water-in-oil microemulsions. Phys.-Uspekhi **47**, 923–941 (2004). https://doi.org/10.1070/PU2004v047n09ABEH001742
25. Y. Feldman, N. Kozlovich, I. Nir, N. Garti, V. Archipov, Z. Idiyatullin, Y. Zuev, V. Fedotov, Mechanism of transport of charge carriers in the sodium Bis(2-ethylhexyl) sulfosuccinate-water-decane microemulsion near the percolation temperature threshold. J. Phys. Chem. **100**, 3745–3748 (1996). https://doi.org/10.1021/jp9525595
26. V.S. Zykov, A.S. Mikhailov, S.C. Müller, Wave instabilities in excitable media with fast inhibitor diffusion. Phys. Rev. Lett. **81**, 2811–2814 (1998). https://doi.org/10.1103/PhysRevLett.81.2811
27. D. Horváth, V. Petrov, S.K. Scott, K. Showalter, Instabilities in propagating reaction-diffusion fronts. J. Chem. Phys. **98**, 6332–6343 (1993). https://doi.org/10.1063/1.465062
28. M. Markus, G. Kloss, I. Kusch, Disordered waves in a homogeneous, motionless excitable medium. Nature **371**, 402–404 (1994). https://doi.org/10.1038/371402a0
29. P. Dähmlow, V.K. Vanag, S.C. Müller, Effect of solvents on the pattern formation in a Belousov–Zhabotinsky reaction embedded into a microemulsion. Phys. Rev. E **89**, 010902 (2014). https://doi.org/10.1103/PhysRevE.89.010902
30. Z. Nagy-Ungvarai, A.M. Pertsov, B. Hess, S.C. Müller, Lateral instabilities of a wave front in the Ce-catalyzed Belousov–Zhabotinsky reaction. Physica D **61**, 205–212 (1992). https://doi.org/10.1016/0167-2789(92)90163-H

Shedding Light on Chaos - Controlling Surface Reactions

Harm H. Rotermund

Abstract Although heterogeneous surface reactions have been studied for more than 200 years, only the introduction of several unique imaging techniques in the 1990s made it possible to visualize simple catalytic reactions occurring on the surface of platinum single crystals at a mesoscopic level. Specifically the CO-oxidation shows a phenomenal variety of patterns including spirals, target patterns, standing waves, spiral turbulence and chaos depending on several parameters. Control of these factors allows better understanding of the limits between chaos and order, which may have important implications ranging from cardiac fibrillation to corrosion phenomena. Two ways of controlling these surface reactions will be discussed, the first one being a time-dependent global feedback approach, where one of the reactant's partial pressure is controlled, the other one focusing on a local method where via a small laser spot the surface temperature is temporarily increased.

1 Introduction

About 200 years ago Johann Wolfgang Döbereiner's experiments focusing on the ignition of hydrogen in contact with powdered platinum led to the very first lighter, the so called Döbereiner's lamp, which was a great success [1]. These studies encouraged the Swedish chemist J. J. Berzelius to develop the concept of catalysis, although it was Wilhelm Ostwald in 1901 who gave the definition of a catalyst as a substance that will not appear within the final product of a chemical reaction, but has accelerated the reaction itself [2]. Heterogeneous catalysis narrows the field to catalysts that are in a different state of matter than the reactants themselves; for example, in Döbereiner's experiments hydrogen as well as oxygen are both in their gaseous state, while the catalyst platinum is in its solid state. Probably the most important

H. H. Rotermund (✉)

Department of Physics and Atmospheric Science, Dalhousie University, Halifax, Canada
e-mail: Harm.Rotermund@Dal.Ca

and man-made reaction is only possible due to heterogeneous catalysis; it is the Haber-Bosch process, which utilizes iron as catalyst with some promoters added to synthesize ammonia in a reaction of hydrogen with nitrogen. It is the "detonator" for the explosion of the world population [3]. Today roughly 450 million tons of ammonia are yearly produced and mainly used as fertilizer to grow crops.

Another important reaction is the oxidation of carbon monoxide (CO) over platinum (Pt), occurring in about a billion catalytic inverters in cars, trucks and power plants around the world. In addition of being tremendously environmentally important, this reaction exhibits, under certain reaction parameters such as temperature and partial pressures, an oscillatory behavior of the reaction rate, resulting in temporary changes of the product, namely carbon dioxide (CO_2). We will use this reaction to illustrate the amazing variety of patterns that occur in very simple oxidation reactions. Many reactions in heterogeneous catalysis can exhibit oscillatory behavior. The table on the next page, which was compiled by M. Slinko, shows a fraction of the reactions, which do so (Table 1).

2 Introduction to the CO-oxidation on Platinum

As is evident when looking at the table, CO-oxidation is one of the simplest reactions of all listed. It follows along the Langmuir-Hinshelwood mechanism, whereby both reactants have to be accommodated at the catalytic surface first before the reaction can happen. In the case of the CO-oxidation the oxygen has to dissociate into its atoms, which are only weakly bound to the catalytic Pt surface. If a CO molecule comes into contact with an oxygen atom they spontaneously react with each other to form CO_2. This product molecule leaves the surface and the "clean" Pt is recovered, an important aspect of a catalyst. The very first oscillations for this reaction were discovered in the early 1970 in E. Wicke's group at the university in Münster, Germany [4]. They investigated the oxidation of CO using a mixture of air and CO at atmospheric pressure over a heated Pt catalyst bed and very much to their astonishment found an oscillating behavior.

About a decade later G. Ertl and coworkers at the university in Munich verified these oscillations under well defined circumstances using single crystal Pt surfaces of various orientations and ultra high vacuum (UHV) conditions [5–7]. These investigations initiated the revival of nonlinear phenomena in heterogeneous catalysis, which had been forgotten for half a century. Already in 1926 a publication by E. S. Hedges and J. E. Myers with the title of "The Problem of Physico-Chemical Periodicity" had appeared, listing many observations in the field [8]. Even before the discoveries of Ertl's group B. P. Belousov, in 1951, had observed oscillating behavior in homogeneous catalysis. Two of his publication attempts failed; only when ten years later A. M. Zhabotinsky verified the earlier results during his graduate studies the reaction became more widely known. The now called Belousov-Zhabotinsky (BZ) reaction is the most studied reaction for nonlinear chemical systems by far [9, 10]. A detailed discussion can be found in this book in chapter **Chemical Oscillations and Spiral Waves** written by P. Pfeiffer.

Table 1 List of oscillating reactions in heterogeneous catalysis, courtesy of M. Slinko, Russian Academy of Sciences, Moscow, Russia

Reaction	Catalyst	Reaction	Catalyst
$CO + O_2$	Pt, Pd, Ir, Rh, Ru	$C_6H_{12} + O_2$	NaY, NaX, KY
$H_2 + O_2$	Ni, Pt, Pd, Rh	$C_6H_{14} + O_2$	Pd
$CO + NO$	Pt, Pd, Rh	C_7H_{16} (n-heptane) + O_2	Pt/Al$_2$O$_3$
$NO + H_2$	Pt, Rh, Ir	$C_8H_{18} + O_2$	Co$_2$O$_3$-Cr$_2$O$_3$
$NO + NH_3$	Pt, Rh	$(CH_3)C_6H_4$ (m-xylene) + O_2	Pd
$NH_3 + O_2$	PtRh, Pt	$(CH_3)C_6H_4$ (o-xylene) + O_2	Pt/HFAU zeolite
$CH_4 + O_2$	La$_2$-BaO-MgO, Pd, Ni, Co, Rh/H-ZSM-5, Ru	$CH_3OH + O_2$	Pd, Cu
$C_2H_6 + O_2$	Ni, Co, Pd	$C_2H_5OH + O_2$	Pd, V$_2$O$_3$
$C_2H_4 + O_2$	Pt, Ag, Rh	$HCOOH + O_2$	Pd
$C_2H_4 + O_2 + NO$	Pt-ZSM-5	$C_2H_4O + O_2$	Ag
$C_3H_8 + O_2$	Ni, Pt/YSZ, Co, Pd	$C_3H_6O + O_2$	Ag
$C_3H_8 + NO$	HZSM-5	$CO + H_2$	Fe-ZSM-5, Co-ZSM-5, Fe, Pd
$C_3H_6 + O_2$	Pt, Ag, CuO	$C_2H_4 + H_2$	Pt, Ni
$C_3H_6 + N_2O$	Pt	N_2O decomposition	Cu-ZSM-5, Rh/ZrO$_3$-Nd$_2$O$_3$, Fe/MFI, Co-ZSM-5
$C_4H_{10} + O_2$	Pd	$N_2O + H_2$	Ir
$C_6H_6 + O_2$	Pd	$N_2O + CO$	Pt
$C_6H_5CH_3 + O_2$	NaX	$NO_2 + H_2$	Pt
C_6H_1(2hexene-1) + O_2	Pd	CH_3NH_2 decomposition	Pt, Rh, Ir
		$PbNO_2 + H_2$	Cu, Ni

One important advantage in the research of nonlinear reactions occurring in heterogeneous catalysis is that for idealized surfaces, such as single crystals, the reactions are always strictly 2-dimensional. Furthermore the time scale is normally orders of magnitude faster, typically in the sub-second to minutes range, compared with minutes to hours for reactions in homogeneous catalysis, where the time scale is governed by the diffusion speed of molecules in liquids. As an example of a relatively slow oscillation, Fig. 1 presents the oscillation of the product rate during the CO-oxidation on Pt(110). The single crystal is kept at a constant temperature of 470 K, the partial pressure for CO is kept constant at 2.3×10^{-5} mbar, while the partial pressure for oxygen is increased from 1×10^{-4} to 1.5×10^{-4} mbar at t = 100 s in a single step. During the following couple of 100 s a steady increase of the
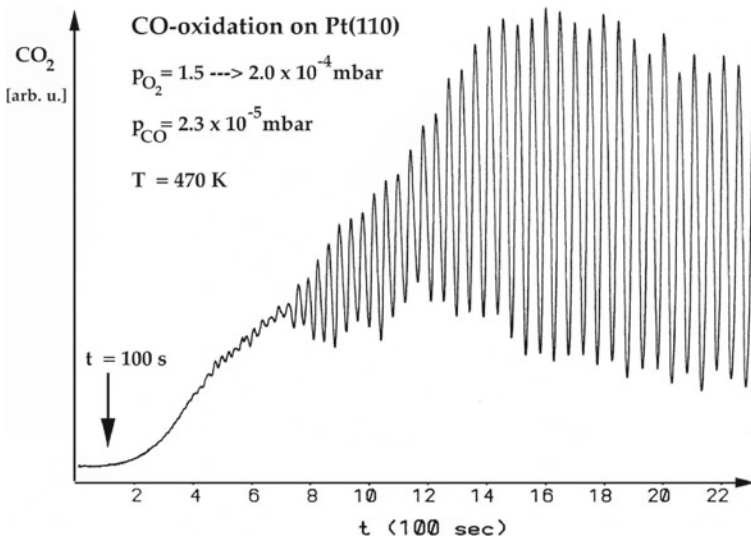
Fig. 1 CO_2 oscillations modified from the dissertation of Eiswirth [11]

reaction product CO_2 is observed, only to slowly start to oscillate around 400 s. These oscillations become quite dominant and regular, continuing for more than 1/2 h. At increased temperatures these oscillations become much faster, reaching up to several Hertz (Hz) at 550 K.

The underlying mechanism for the oscillations has been clarified in a publication of 1992, in which the authors, K. Krischer, M. Eiswirth and G. Ertl proposed a reconstruction model [5, 12], which is depicted in Fig. 2. Pt(110) reconstructs its surface, as many single crystal surfaces do, in a way to reduce its surface energy. Some adsorbents will lift this reconstruction, since for a system surface plus adsorbent a lower total energy may be achieved by lifting the reconstruction. The uncovered Pt(110) surface arranges itself into a missing row structure; adsorption of CO molecules will lift this reconstruction, happening already at microscopic scales when a coverage of 1/3 of a monolayer (ML) is locally reached, as was shown by Cox et al. [5].

The important difference between these two surface phases is the sticking probability for oxygen, s_{O_2}. It increases from 0.4 on the reconstructed surface to 0.6 on the unreconstructed surface. Obviously by choosing the right ratio between the partial pressures for oxygen versus CO a condition can be stabilized where CO will slowly build up in its coverage on the reconstructed surface while the adsorption of oxygen remains low. When a certain CO coverage is reached, typically between 0.3 and 0.5 ML of CO, the surface phase transits into the unreconstructed surface. It exhibits a 50% higher sticking probability for oxygen, thereby reacting away the CO molecules till the critical CO coverage is undercut; the reconstruction sets in again, one oscillation cycle has been completed. The moving around of metal atoms on a

Fig. 2 Reconstruction model for Pt (110), sometimes also called the KEE-model

Pt(110) - 1x2 (missing row)
$s_{O_2} \approx 0.4$

Lower O-adsorption increases CO-coverage, reconstruction is lifted

Higher O-adsorption decreases CO-coverage, reconstruction starts again

Pt(110) - 1x1
$s_{O_2} \approx 0.6$
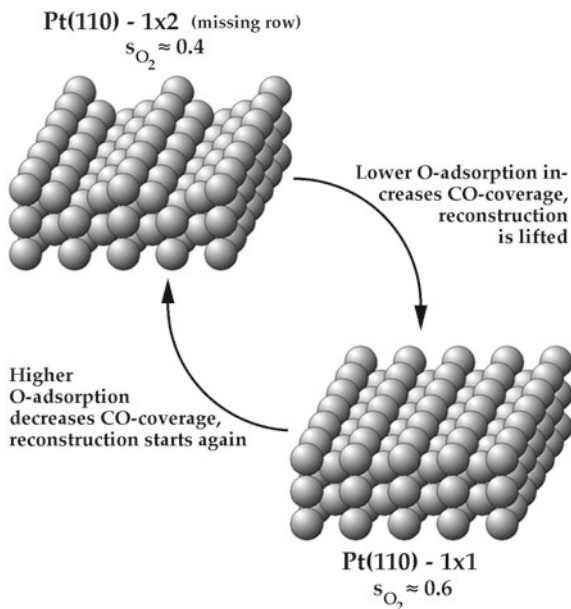
surface certainly needs activation energy; therefore strong temperature dependence can be expected. This can be corroborated by looking at the oscillation times in Fig. 1, being about 40 s (0.025 Hz) for a reaction temperature of T = 470 K, while when the temperature is 80 K higher the oscillation frequency is in the several Hz range.

Obviously the reconstruction model could be used quasi homogeneously for the whole surface without taking into account local modifications in time. The first attempt to find a hint of space-time patterns during the CO-oxidation on a Pt(100) was done by Cox et al. [5], who used low energy electron diffraction (LEED) scanning across the single crystal surface under reaction conditions. They found evidence of a wave like pattern on a time scale of 200 s and a lateral resolution in the mm range. To improve the spatial resolution a scanning photoemission microscope was designed and built, immediately showing the important aspect of the local conditions of a surface [13].

3 Experimental Set-up: the Photoemission Electron Microscope (PEEM)

Due to the mechanical nature of the scanning approach, the sample was moved back and forth, it became clear that an imaging photoemission electron microscope (PEEM) had to be constructed to improve the lateral and time resolution both by several orders of magnitude. This was accomplished with the help of Engel [14]. The
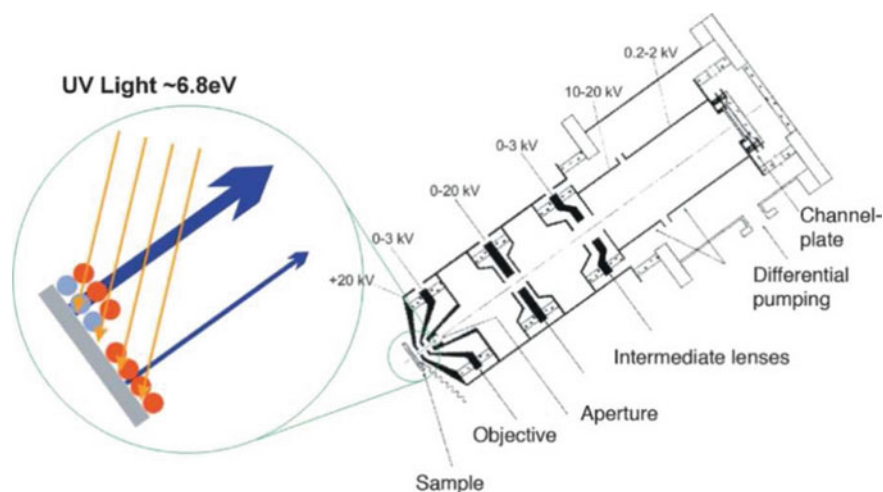
Fig. 3 PEEM sketch illustrating how different adsorbate layers on the surface result in contrast due to higher photoelectron emission

PEEM consisted of several purely electrostatic electron lenses at potentials between 0 and 20 kV with respect to the sample at ground potential.

The sample in front of the objective lens is illuminated homogeneously with UV-photons of up to 6.8 eV, the locally photon-emitted electrons are accelerated by the 20 kV electrode of the objective lens and imaged onto a channel plate and phosphorous screen at the end of the column. As illustrated by the sketch on the left side of Fig. 3, areas with CO coverage, envisioned by the blue/red circles, emit a large number of electrons while the oxygen atoms, red circles only, emit a smaller signal due to their higher work function. The work function is the energy barrier the electrons have to overcome to leave the surface. A clean platinum surface has a work function of 5.5 eV, areas covered with CO increase the work function a little (typically by + 0.1 eV), whereas oxygen atoms increase it by about 1 eV. This is the basic contrast mechanism, since it is quite substantial for the CO-oxidation and real time imaging can easily be done. To store the data a standard video recording system is utilized. Even the very first experiments with an unfinished PEEM (just the objective lens was installed) showed stunning patterns on the surface [14].

4   Observation of Pattern Formation

Soon after this first observation a large variety of pattern formations during the CO-oxidation specifically on the Pt(110) surface were discovered [15–17]. As an example, Fig. 4 presents snapshots of target patterns, evolving at T = 427 K reproduced at a time interval of 1 s.
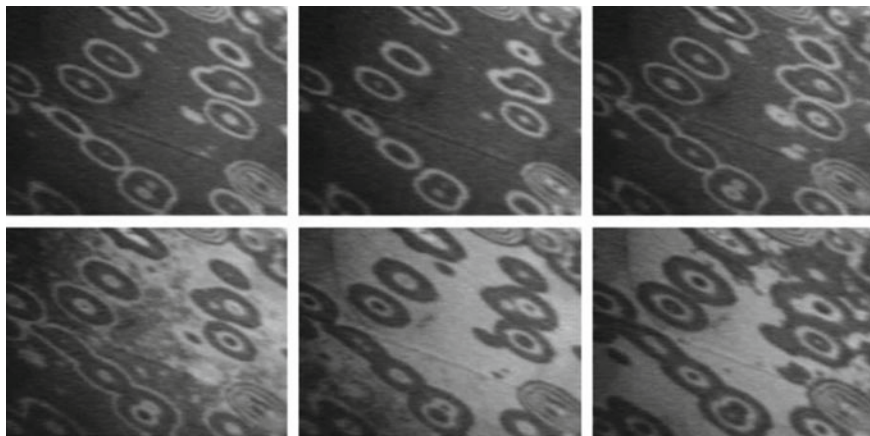
Fig. 4 Snapshots of Target patterns on Pt(110), $pO_2 = 3.2 \times 10^{-4}$ mbar, $pCO = 3 \times 10^{-5}$ mbar and T = 427 K, time interval 1 s, frame size $300 \times 227\,\mu$m

Two different phenomena can be seen in this figure: a fast oscillating background from a dark (oxygen covered) to a grey (CO covered) one within 5 s, while the target patterns themselves evolve at a much longer time scale. The background oscillations are ruled by a phenomenon known as "gas phase or global coupling", while the targets are diffusion coupled, governed by the diffusion speed of CO on the surface on the order of μm/s [18]. The former coupling mechanism is based on the changes of the CO partial pressure directly in front of the investigated surface and governed by the speed of molecules in the vacuum, which are many orders of magnitude higher.

Another example featuring evolving spirals, which are a highly dominant feature and easily reproduced under certain reaction conditions, is presented in Fig. 5. The figure is reproduced from Nettesheim et al. [19] and shows clockwise and anticlockwise rotating spirals which are all pinned to macroscopic defects, some of them becoming quite visible in the last frame of the figure.

For a different system, the NO + H_2 reaction on Rh(110), R. Imbihl and his group found spirals and target patterns with a nearly rectangular shape, which the authors explained via a state dependent anisotropy of the diffusion [20]. As mentioned earlier, one of the features of pattern formation on single crystal surfaces during heterogeneously catalyzed reactions is the 2-dimensionality, but for illustrative purposes it can be changed into an 3-dimensional image as reproduced in [21] In Fig. 6 the rendered spirals of the CO-oxidation from Fig. 5 are compared to a picture of spirals carved in stone found in a wall of a temple in Greece dating back to 1200 BC. Even over 3000 years ago spirals have been fascinating for the human kind; they appear on all length scales, from μm to meters to hundred thousands of light years in spiral galaxies, as illustrated in Fig. 7 (compare chapter **Appearance in Nature**).

In Fig. 7 a spectacular image of the large spiral galaxy NGC 1232 and its small neighbor NGC 1232a near the lower left side is reproduced. The distance to NGC
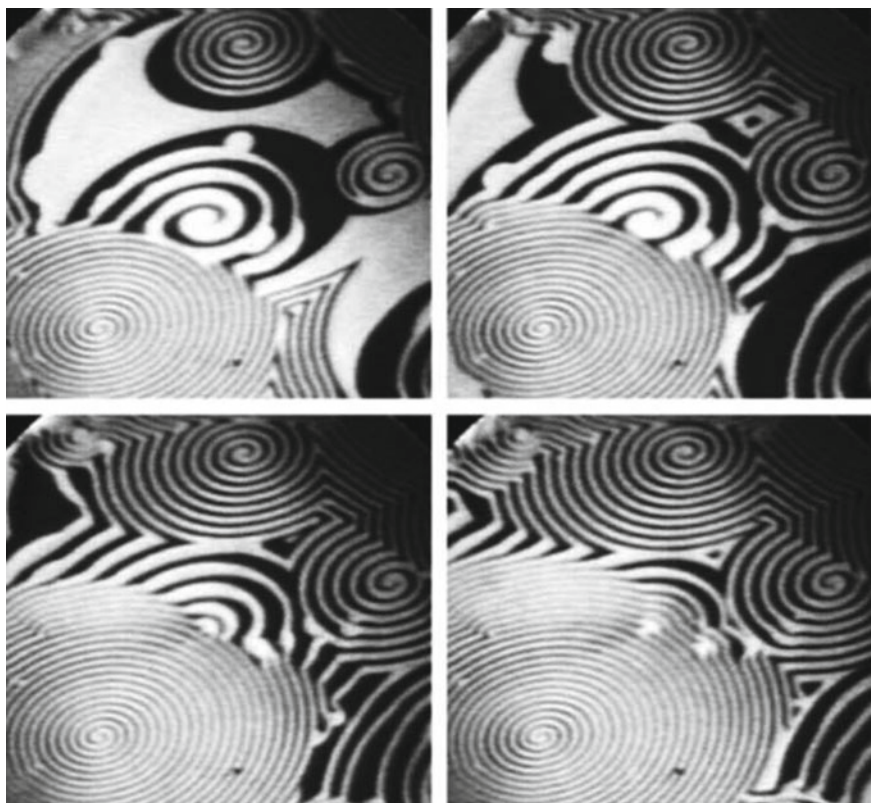
Fig. 5 Spiral waves on Pt(110). $pO_2 = 4 \times 10^{-4}$ mbar, $pCO = 4.3 \times 10^{-5}$ mbar, T = 448 K, time between frames 30 s, frame size 440×440 μm

Fig. 6 Three-dimensional illustration of spirals on a two-dimensional platinum surface compared to a wall ornament from a temple in Greece dating back to 1200 BC

Fig. 7 Image of the large spiral galaxy NGC 1232, obtained by the European Southern Observatory at its Paranal site in Chile with the Very Large Telescope array (VLT). It is composed by three exposures in ultra-violet, blue and red light, respectively. (See also Fig. 2 of chapter **Appearance in Nature**)

1232 is about 100 million light-years and its diameter is close to 200,000 light-years, about twice the size of our Milky Way galaxy. More images of galaxies can be found in chapter **Appearance in Nature**. Although spiral galaxies are the most abundant star pattern formation observed in the universe, probably with more than a billion in number, each containing billions of stars themselves, the spiral formation cannot be distinguishable with the naked eye. So it is safe to assume that early civilizations portrayed objects found on earth in their art, like spiral patterns on seashells.

Focusing again on the CO-oxidation on Pt(110), a zoo of pattern formation has been observed. When the reaction temperature is increased naturally, the reaction itself proceeds much faster and new patterns emerge. A well-studied phenomenon is the standing wave pattern. As is obvious when comparing the first four frames in Fig. 8, consecutive snapshots taken at a time interval of 150 ms, the reaction driven patterns change quite rapidly.

The drastic change from the highly regular form of standing waves into a turbulent or chaotic structure happens when one of the control parameters, in this case the partial pressure of CO, is slightly changed. In principle a cascade of period doublings should occur, similar to the Feigenbaum scenario in certain mathematical equations. In reality, the CO-oxidation noise cannot be avoided, so the step size for adjusting the partial pressure varies by the additional noise inherent in most natural systems. This results in nearly all cases with a sudden onset of turbulent behavior, as visible in the last two frames of Fig. 8. In nonlinear dynamics the control of turbulence is one of the holy grails.

5 Control of Surface Reactions

For simple systems occurring in 2D with an easy to describe reaction this can be achieved by a time dependent global feedback mechanism as illustrated in Fig. 9:
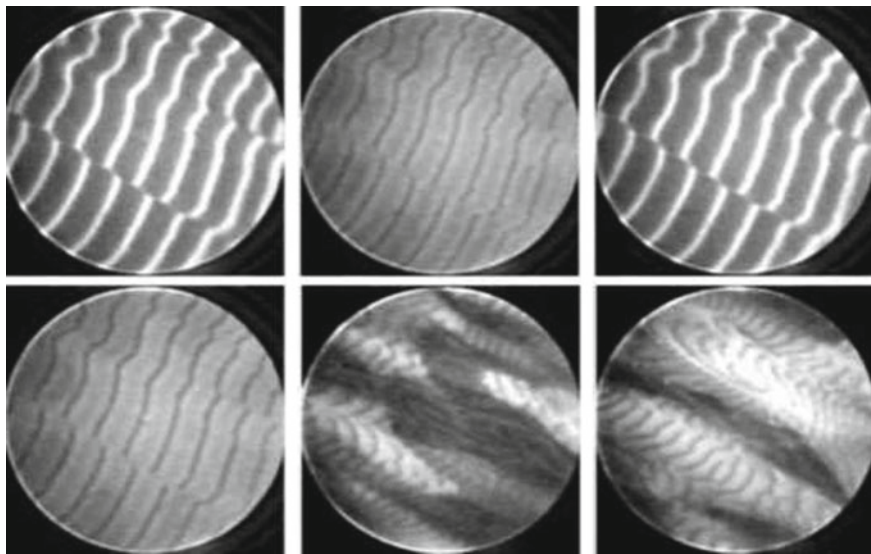
Fig. 8 Standing wave patterns; the original oscillation period is about 1.2 s, the first 4 snapshots are separated by just 250 ms, frame 5 was taken 30 s later, the last frame 8 s after #5, from [21]

Fig. 9 Schematic of a time-dependent global feedback loop, where the PEEM image is integrated, the background subtracted, and then after a time delay the signal is used to control one of the parameters such as the partial pressure of CO
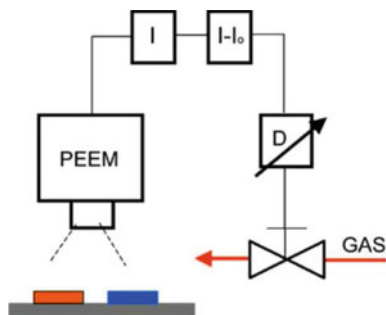
A variety of chaotic patterns have been investigated and via time dependent global feedback changed dramatically in their behavior. The main result is shown in Fig. 10, taken from Kim et al. [22]. In this experiment, chemical turbulence was first established as displayed in frame #1 of panel (a). These patterns are sometimes labeled spiral turbulence. As can be seen in the space-time plot below, no regular oscillations are present. The partial pressure of CO remains nearly constant in the beginning and only about 40 s into the experiments the feedback begins to show, soon leading to pressure oscillations with amplitudes of about 10% of the original set value for CO. The time delay of 0.6 s between the control signal I and its result on the partial pressure of CO is kept constant during these experiments. At about 65 s the space-time plot shows strong regular oscillations. Depending on the initial conditions the results
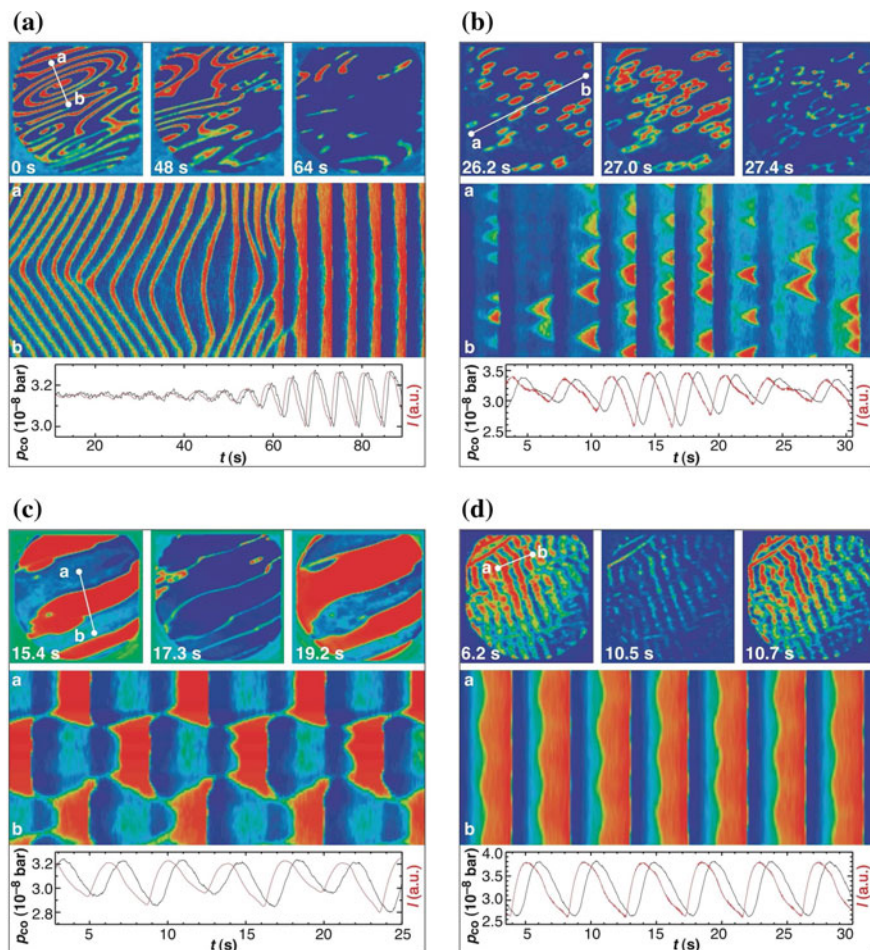
Fig. 10 Each subpanel shows in the upper row original PEEM images (diameter 500 μm) taken at the indicated times, followed below by space-time plots along the identified white lines drawn into the upper left panels: **a** suppression of spiral wave turbulence, **b** intermittent turbulence, **c** phase clusters, and **d** standing waves. The bottom graphs below each space-time diagram display the temporal variation of the CO partial pressure (black line) and the variation of the integral PEEM intensity (red line)

of the time delayed global feedback differs substantially. The subpanels (b) to (d) illustrate the three types of patterns that emerge when feedback is established.

The most striking result is presented in panel (c), where highly stable phase clusters have been observed. This type of pattern had not been seen in any previous experiments involving pattern formation in heterogeneous surface reactions.

Obviously the signal used in the feedback loop does not have to be the global response of the imaged area, but can be a frequency dependent smaller area of the

sample, which is analyzed via a fast Fourier transformation (FFT) and then utilized as the feedback signal [23].

A trivial approach to influence self-sustained pattern formation is direct forcing, in which the main oscillating frequency is analyzed and a higher harmonic is utilized to investigate the changes of patterns due to entrainment with $2\times, 3\times, 4\times$ frequency forcing [24].

Up to this point the results presented here were obtained with a PEEM, which is restricted to low-pressure investigations, since electrons are used to image the changes of the work function of the involved system. In heterogeneous catalysis the reaction of interest happens at atmospheric pressures (1bar) or at many bars of pressure, to achieve a reasonable product rate.

6 Imaging and Controlling Surface Reactions Using Light

A surface reaction imaging technique that can operate under any pressure was developed some time ago and utilizes the unique properties of linear polarized light. In principle at least two approaches have been successfully implemented and improved
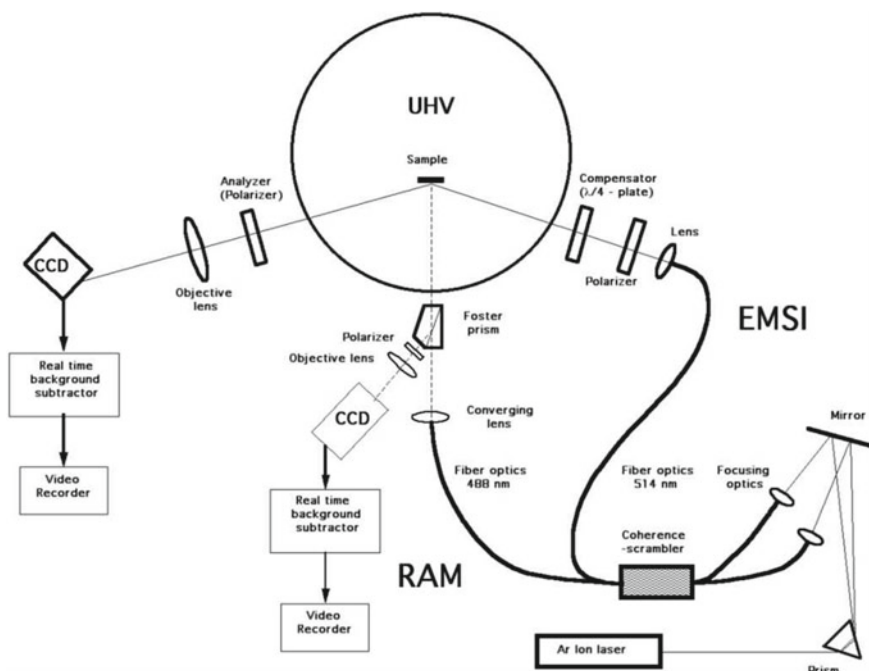
Fig. 11 Schematic of ellipso-microscopy for surface imaging (EMSI) and reflection anisotropy microscope (RAM)

over the years [25, 26]. The experimental setup is displayed in Fig. 11. The ellipso-microscopy for surface imaging (EMSI) uses monochromatic linear polarized light, which is reflected off the surface close to the Brewster angle and therefore becomes elliptically polarized light. It allows imaging of an adsorbent on a surface, as long as the covered areas are larger than 15–20 µm in size. The reflection anisotropy microscope (RAM) also utilizes linearly polarized light, however it can be white light and mainly takes its contrast from the rearranging surface atoms, for instance, the changes of the reconstruction due to CO adsorption in the case of Pt(110).
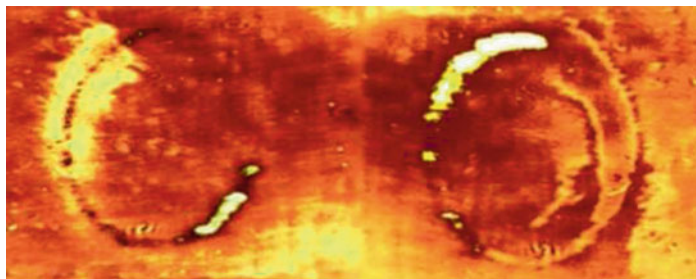
Fig. 12 A focused laser spot describing a circle on a Pt(110) surface during the CO-oxidation. Two snapshots are placed together to create the impression of "CO" written onto the surface; title page from [29]

In addition to being completely pressure independent - EMSI has been utilized even for corrosion studies of polished stainless steels in liquids [27] - the optical methods also allow a much easier access of the imaged surface: for instance, a focused laser spot could be directed onto the surface allowing local heating, thus influencing the emerging pattern formation. A playful illustration of the possibilities is presented in Fig. 12. Two snapshots of a circle heated by a focused laser are placed together to create the impression of "CO" written onto the surface. The temperature of the area underneath the laser spot is for some tenth of a second about 2–3 K higher, thus allowing more CO molecules to desorb and thereby having a microscopic effect change into an "artificial" macroscopic result. As it is obvious, having direct command of the local surface temperature allows for addressing the spatiotemporal pattern formation in real time. Some of these results, including references, have been compiled in [28].

7 Conclusion

The examples presented here show how well reaction-diffusion systems of hetero-geneously catalyzed reactions have been understood. The specific model system, the CO-oxidation on Pt(110), allows for the exploration of various control mechanisms in pattern forming reactions, opening new avenues for nonlinear systems. This is

one of the reasons why the CO-oxidation on Pt(110) has become the paradigm for nonlinear surface reactions.

References

1. J.W. Döbereiner, Vermischte Erfahrungen ueber Platina. Schweiggers Gährungschemie. J. für Chemie und Physik **54**, 412–426 (1828)
2. W. Ostwald, Periodische Erscheinungen bei der Auflösung des Chroms in Säuren. Z. Phys. Chem. **35**, 33–76 and 204–256 (1900)
3. V. Smil, Detonator of the population explosion. Nature **400**, 415 (1999)
4. M. Jakubith, Isotherme Oszillationen bei der CO-oxidation am Pt-Netz. Chem. Ing. Tech. **14**, 943–944 (1970)
5. M.P. Cox, G. Ertl, R. Imbihl, Spatial self-organization of surface structure during an oscillating catalytic reaction. Phys. Rev. Lett. **54**, 1725–1728 (1985)
6. G. Ertl, P.R. Norton, J. Rüstig, Kinetic oscillations in the platinum-catalysed oxidation of CO. Phys. Rev. Lett. **49**, 177–180 (1982)
7. R. Imbihl, M.P. Cox, G. Ertl, Kinetic oscillations in the catalytic oxidation on Pt(100): Experiments. J. Chem. Phys. **84**, 3519–3534 (1986)
8. E.S. Hedges, J.E. Myers, *The Problem of Physico-Chemical Periodicity* (Edward Arnold and Co., London, 1926)
9. A.T. Winfree, Spiral waves of chemical activity. Science **175**, 634–636 (1972)
10. A.M. Zhabotinsky, Eine oszillierende Oxydationsreaktion in flüssiger Phase. Proc. Acad. Sci. USSR **157**, 392–395 (1964)
11. R.M. Eiswirth, Phänomene der Selbstorganisation bei der Oxidation von CO an Pt(110). Dissertation, Technische Universität München (1987)
12. K. Krischer, M. Eiswirth, G. Ertl, Oscillatory CO oxidation on Pt(110): modeling of temporal self-organization. J. Chem. Phys. **96**, 9161–9172 (1992)
13. H.H. Rotermund, S. Jakubith, A.v. Oertzen, G. Ertl, Imaging of spatial pattern formation in an oscillatory surface reaction by scanning photoemission microscopy. J. Chem. Phys. **91**, 4942–4948 (1989)
14. H.H. Rotermund, W. Engel, M. Kordesch, G. Ertl, Imaging of spatio-temporal pattern evolution during carbon monoxide oxidation on platinum. Nature **343**, 355–357 (1990)
15. S. Jakubith, H.H. Rotermund, W. Engel, A.v. Oertzen, G. Ertl, Spatiotemporal concentration patterns in a surface reaction: Propagating and standing waves, rotating spirals, and turbulence. Phys. Rev. Lett. **65**, 3013–3016 (1990)
16. H.H. Rotermund, S. Jakubith, A.v. Oertzen, G. Ertl, Solitons in a surface reaction. Phys. Rev. Lett. **66**, 3083–3086 (1991)
17. M. Bär, M. Eiswirth, H.H. Rotermund, G. Ertl, Solitary-wave phenomena in an excitable surface reaction. Phys. Rev. Lett. **69**, 945–948 (1992)
18. H.H. Rotermund, Pattern formation in a surface reaction with global coupling. In *IMA Conference on Pattern Formation in Continuous and Coupled Systems, Minneapolis 1999*. The IMA Volumes in Mathematics and Its Application, ed. by M. Golubitsky, D. Luss, S.H. Strogatz (Springer, Berlin, 1999), pp. 231–249
19. S. Nettesheim, A.v. Oertzen, H.H. Rotermund, G. Ertl, Reaction diffusion patterns in the catalytic CO oxidation on Pt(110): front propagation and spiral waves. J. Chem. Phys. **98**, 9977–9985 (1993)
20. F. Mertens, R. Imbihl, Square chemical waves in the catalytic reaction NO + H_2 on Pt(110) surface. Nature **370**, 124–126 (1994)
21. H.H. Rotermund, Chaos und Ordnung auf Oberflächen. In *Materie in Raum und Zeit. Verhandlungen der Gesellschaft Deutscher Naturforscher und Ärzte 123. Versammlung, Passau, Germany 2004* (S. Hirzel Verlag, Stuttgart, 2005), pp. 69–88

22. M. Kim, M. Bertram, M. Pollmann, A. von Oertzen, A.S. Mikhailov, H.H. Rotermund, G. Ertl, Controlling chemical turbulence by global delayed feedback: Pattern formation in catalytic CO oxidation on Pt(110). Science **292**, 1357–1360 (2001)
23. C. Beta, G. Moula, A. Mikhailov, H.H. Rotermund, G. Ertl, Excitable CO oxidation on Pt(110) under nonuniform coupling. Phys. Rev. Lett. **93**, 188302 (2004)
24. P.S. Bodega, P. Kaira, C. Beta, D. Krefting, D. Bauer, B. Mirwald-Schulz, C. Punckt, H.H. Rotermund, High frequency periodic forcing of the oscillatory catalytic CO oxidation on Pt(110). New J. Phys. **9**, 61–79 (2007)
25. H.H. Rotermund, G. Haas, R.U. Franz, R.M. Tromp, G. Ertl, Imaging pattern formation in surface reactions from ultra-high vacuum to atmospheric pressures. Science **270**, 608–610 (1995)
26. C. Punckt, F.S. Merkt, H.H. Rotermund, Simple reflection anisotropy microscopy setup for CO oxidation studies. New J. Phys. **9**, 213–228 (2007)
27. C. Punckt, M. Bölscher, H.H. Rotermund, A.S. Mikhailov, L. Organ, N. Budiansky, J.R. Scully, J.L. Hudson, Sudden onset of pitting corrosion on stainless steel as a critical phenomenon. Science **305**, 1133–1136 (2004)
28. H.H. Rotermund, Real time imaging of catalytic reactions on surfaces: past, present and future. Surf. Sci. **603**, 1662–1670 (2009). https://doi.org/10.1016/j.susc.2008.11.048
29. J. Wolff, M. Stich, C. Beta, H.H. Rotermund, Laser-induced target patterns in the oscillatory CO oxidation on Pt(110). J. Phys. Chem. B **108**, 14282–14291 (2004)

Part IV
Spirals and Vortices in Biology, Physiology, and Medical Science

FOOL: Canst tell how an oyster makes his shell?
LEAR: No.
FOOL: Nor I neither; but I can tell why a snail has a house.

— William Shakespeare, King Lear

Spiral Waves of the Chemo-Attractant cAMP Organise Multicellular Development in the Social Amoebae *Dictyostelium discoideum*

Cornelis J. Weijer

Abstract Development of multicellular organisms requires precise spatial and temporal integration of key cellular behaviours such as cell division, cell differentiation and cell movement to form the complex tissues that make up the organism. These cell behaviours are controlled by highly dynamic cell-cell signalling while these cell behaviours in turn feedback on the cell-cell signalling to result in emergent behaviours at the tissue and organism level. *Dictyostelium discoideum* is a relatively simple eukaryotic organism that is a widely used to study these interactions between cell-cell signalling and cell behaviours both experimentally and theoretically. This chapter describes our current understanding of how excitable cell-cell signalling results in the formation and propagation of large scale spiral waves of a chemo-attractant. How these chemo-attractant waves control the aggregation of hundreds of thousands of cells into multicellular aggregates and how interactions between excitable cell-cell signalling and cell movement control the transformation of aggregates into mounds and migrating slugs, that then go on to form fruiting bodies.

1 Introduction

Many simple organisms including bacteria and eukaryotic cells live as single cells. They divide to multiply and most are able to move in order to find food. Many of these single celled organisms, such as primitive amoebae can undergo a transition to a dormant state and form cysts or spores to survive challenging environmental conditions. The evolution of multicellular organism has taken several independent routes, in some groups of organisms multicellularity arises via aggregation of large numbers of individual cells during part of their life cycle. The transition of hundreds of thousands of single cells into a multicellular organism via aggregation is well

C. J. Weijer (✉)

Division of Cell and Developmental Biology, School of Life Sciences, University of Dundee, Dundee DD1 5EH, UK

e-mail: c.j.weijer@dundee.ac.uk

documented by the development of the social amoebae or cellular slime moulds, the *Dictyostelids*. These are simple eukaryotic organisms that span a wide range of different shapes and forms. The ancestors of the simplest *Dictyostelium* species are single amoebae. These amoebae generally live in the soil and feed on bacteria and yeasts and divide. They have the ability to actively locate their food sources by detecting small molecules secreted by these bacteria and use this to locate sources of food and move towards these sources in a chemotactic process. When food becomes scarce they can either move to new locations where there is more food or encyst or sporulate to form dormant stages in which they can persist for long periods of time before germinating and releasing amoebae again [1].
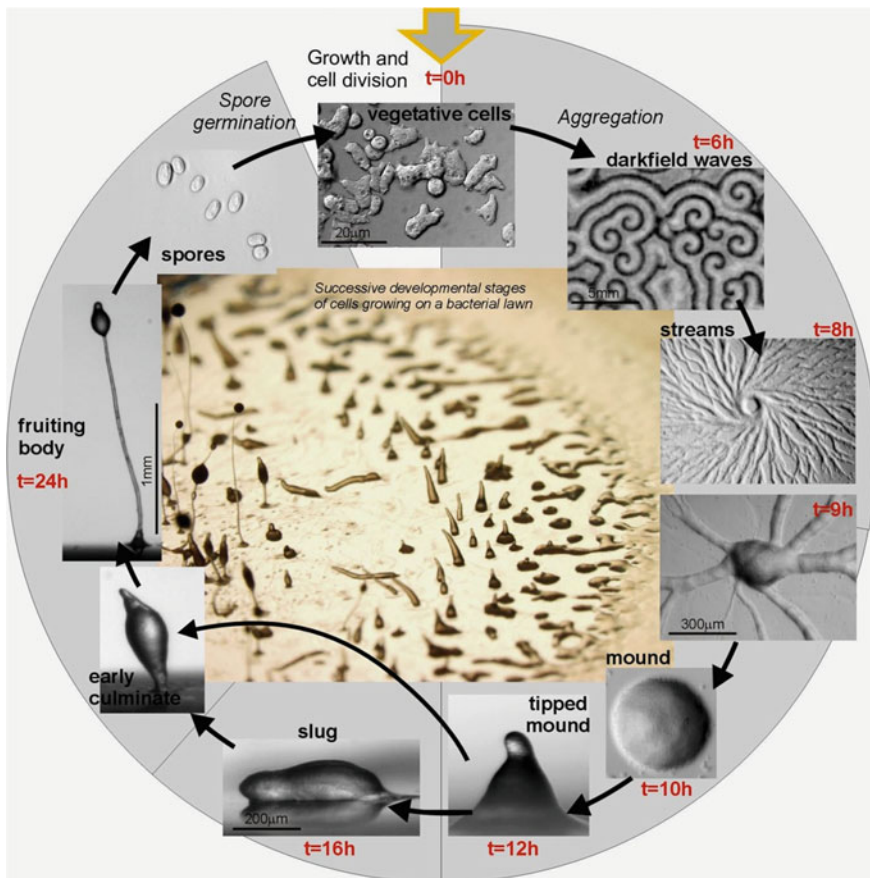
Fig. 1 *Dictyostelium discoideum* life cycle. Central image shows a *Dictyostelium* colony growing on a bacterial feeding plate. Feeding cells are located at the outer edge. When cells deplete the bacteria they start to aggregate, forming aggregation streams and mounds. These then make tipped mounds that transform into migratory slugs. Under conditions of low humidity and overhead light slugs will culminate and form fruiting bodies consisting of a stalk of dead vacuolated stalk cells that support a head of spores. The spores can disperse, germinate and start new colonies again closing the life cycle, which take around 24 h at 22 °C

Interestingly the *Dictyostelids* form a group of more complex species that are able to form multicellular aggregates via the aggregation of individual cells. These species use short range chemical cell-cell signalling of species specific chemo-attractants to aggregate. After aggregation they are able to form very small fruiting bodies consisting of a stalk of an extracellular matrix material and often dead vacuolated so called stalk cells that support a head of spores. The spores are raised from the substrate and therefore can most likely disperse more effectively than single spores.

However there exist more complex species within the *Dictyostelids* where up to hundreds of thousands of cells can aggregate to form larger fruiting bodies. By far the best investigated species is *Dictyostelium discoideum* (Dd). Its life cycle is illustrated in Fig. 1. Since *Dictyostelium* development takes place in the absence of food under starvation conditions only limited cell divisions occur during multicellular development. Morphogenesis therefore primarily results from the movement of individual differentiating cells into relatively simple multicellular structures, the mound and slug that will transform into fruiting bodies, consisting of roughly 75% spores and 25% stalk cells irrespective of its size, which can vary between hundreds and millions of cells. Key questions are, which signals guide the movement behaviour of thousands of cells during development. Which signals control the differentiation of the spore and stalk cells and how are cell-cell signalling, movement and differentiation integrated to form a fruiting body.

2   The Mechanism and Role of Chemotaxis

The aggregation of *Dictyostelium* cells has been extensively studied and shown to involve chemotaxis to 3'–5'cyclic AMP (cAMP), produced by the aggregating cells themselves. Chemotaxis is the process by which cells move either up or down gradients of diffusible signalling molecules. The mechanism of chemotaxis arose very early in evolution and was used by primitive single celled organisms including bacteria to translocate to sources of food. In multicellular organism chemotaxis is a key mechanism to generate complex cell migration patterns necessary to build complex structures during the embryonic development of most animals. In eukaryotic cells movement involves cycles of pseudopod or lamellipod extension at the front end of a migrating cell driven by localised actin filament formation, coupled with retraction of the actin-myosin network in the rear end of the cell (Fig. 3a). During chemotaxis cells measure gradients of the chemo-attractant along the length of the cell via attractant specific cell surface receptors that signal to the actin-myosin cytoskeleton to result in directional movement. High concentrations of the attractant promote and stabilise new protrusions in the direction of the increasing gradient and coordinate retraction of the cell at the low end of the gradient, resulting in net translocation up the gradient giving rise to directed cell movement [2].

It is currently thought that there exists a gradient sensing mechanism, the chemical compass, which is followed by an internal amplification mechanism that controls the polarisation of the cytoskeleton, which may well involve the cytoskeleton itself. Much

work is directed towards the investigation of the molecular mechanisms resulting in signal detection cell polarisation and its translation in directed movement. This has been extensively reviewed elsewhere recently and will not be covered here in detail [3]. Cells that are not exposed to directional signals tend to extend pseudopods in random locations around the cell, resulting in a very low persistence of directional migration resulting in what is known as a random walk [4].

3   Starving Cells Are Produced and Respond to Pulses of the Chemo-Attractant cAMP

Starvation triggers changes in gene expression that results in cells becoming able to detect cAMP via specific transmembrane cAMP receptors and they also acquire the ability to make and secrete cAMP using a specific starvation induced adenylyl cyclase (ACA) [5]. cAMP is degraded by a secreted cAMP specific phosphodiesterase [6]. Cells in an aggregation centre start to periodically produce and secrete cAMP. This cAMP diffuses to neighbouring cells, which detect and amplify the signal and pass it on to their neighbours, resulting in a periodic cAMP wave propagation process [7]. The cAMP waves propagate from the aggregation centre outwards and guide the chemotactic movement of the cells towards the aggregation centre resulting in the aggregation of up to hundreds of thousands of cells.

Although the underlying biochemistry of this excitable signalling system is rather complicated, we will briefly describe the main process and components here [8]. Binding of cAMP to the seven transmembrane cAMP receptors results in stimulation of a signal transduction cascade that leads to the activation of an ACA, that within tens of seconds produces cAMP part of which is secreted to the outside (Fig. 2a). The secreted cAMP binds to the cAMP receptor and thus is part of an autocatalytic feedback loop resulting in a rapid increase of cAMP production. However stimulation of the receptor also activates an adaptation process that, with a small time delay, results in inhibition of adenylyl cyclase activity and thus in a cessation of cAMP production. Since cAMP diffuses away into the extracellular medium and is also degraded by internal and secreted cAMP phosphodiesterases, this results in a drop in internal and external cAMP levels. This drop in extracellular cAMP in turn results in de-adaptation of the cells (Fig. 2b). This scheme has been the basis for many mathematical models for the cAMP oscillator that can describe key experimental results and the transition of excitable to oscillatory cAMP synthesis during development [9]. The details of the underlying biochemistry of the cAMP oscillator is rather complex and contains many components. Especially the biochemical basis for adaptation is not yet completely understood in molecular detail [10].
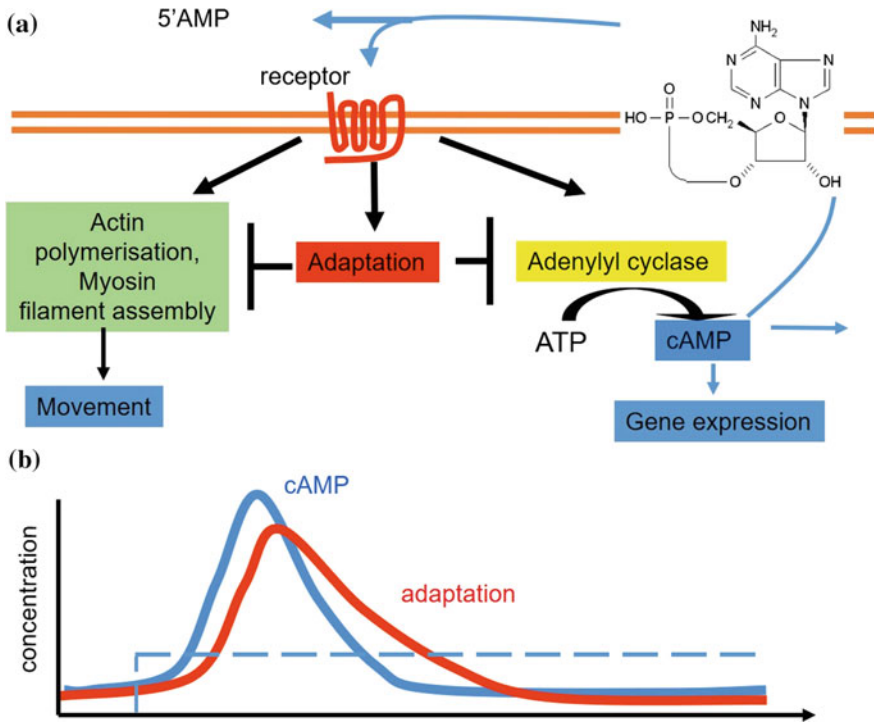
Fig. 2 Excitable cAMP signalling. **a**: Schematic of the extracellular space, above the double red line (plasma membrane) and the inside of a containing the main components to produce cAMP oscillations and cell movement. **b**: schematic of temporal changes in cAMP synthesis and adaptation in response to a constant stimulus of cAMP (stippled blue line)

4 Excitable Cell-Cell Signalling and Chemotaxis Result in Aggregation

During early development the cells undergo a transition from being unresponsive to cAMP to a state where they become excitable, i.e. they can produce cAMP when stimulated with an above threshold amount of cAMP, to a situation whether they become able to support sustained oscillations of cAMP. In the early phases of development most of the cAMP secreted is degraded by the secreted cAMP phosphodiesterase. However since gene expression is an essentially heterogeneous process, some cells will produce and secrete a little more cAMP than others. Due to this heterogeneity in gene expression and stochastic distribution of cells at the start of development, just by chance there will be an area where some cells can just produce enough cAMP to start the amplification of the signal through positive feedback [11]. This locally produced cAMP signal diffuses to neighbouring cells, which now detect an above threshold signal to which they respond by chemotaxis and also will start to amplify
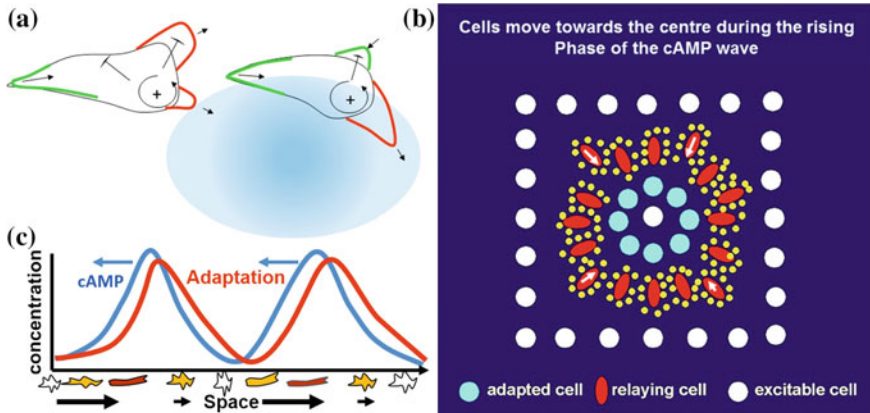
Fig. 3 a: Two successive images of a cell moving towards a local source of cAMP by the actin driven extending pseudopod (red) in the direction of the cAMP gradient and myosin (green) mediated retraction of pseudopods pointing away from the gradient. This results in a slow turning towards the source of cAMP (blue). **b**: schematic of a cAMP wave traveling outward through a population of cells. The red cells produces cAMP (yellow) dots). This diffuses away. Cells behind the wave front (blue circles) are refractory and cannot signal. Cells in front of the wave (white dots) are excitable and can signal. Simultaneously the relaying cells move up the cAMP gradient (the white arrows). **c**: cAMP waves traveling from right to left direct motion of cells during the rising phase of the wave. This results in cell shape changes that can be detected as light-scattering changes

the signal and pass it on to their neighbours. This process results in the formation of travelling waves of cAMP (Fig. 3b).

Desensitisation of the cAMP producing cells to cAMP results in the unidirectional propagation of waves of cAMP away from the aggregation centre. These waves guide the cells towards the aggregation centre. Effective aggregation requires that the cells move during the rising phase of the cAMP gradient in the direction of the signal, i.e. up the gradient, but do not turn around when the wave passes. If they did they would move backwards and forwards and not aggregate efficiently. This is known as the back of the wave problem. It has recently been shown that cells stay polarised and keep moving for wave periods of up to 10 min and that this involves adaptation in combination with a simple memory [12].

Due to the adaptation process colliding cAMP waves emitted from competing centres annihilate each other upon collision. This will result in the formation of aggregation territory boundaries. Since the cells move in the direction of the signal source this results in the cells moving away from the boundaries towards the aggregation centres resulting in contraction of the aggregation territories.

5 Visualising cAMP Wave Propagation

During the synchronised chemotactic movement phase the cells elongate slightly, while during the falling phase of the waves the cells stop moving and take on a less polarised shape (Fig. 3c). These locally synchronised cell behaviours can be visualised as changes in light scattering that reflect the propagating cAMP waves (Fig. 4) [13]. cAMP waves have also been measured directly using isotope dilution fluorography and these measurements showed that the optical density waves reflected the cAMP waves and that the concentrations varied between 10^{-9} and 10^{-6} M which is well within the K_d of the cAMP receptors [14]. Nowadays cAMP dependent cell-cell signalling can be measured directly by dynamic measurements of intracellular cAMP genetically engineered cAMP binding proteins using the principle of Fluorescence Resonance Energy Transfer (FRET) [11]. Furthermore it is possible to dynamically measure various components of the cAMP signal transduction machinery to cAMP relay and the actin-myosin cytoskeleton in single cells but also at the population level. These measurements can therefore not only be used to study the spatiotemporal dynamics of signal transduction but also to indirectly visualise the dynamics of cAMP wave propagation. Most recently it has been shown that a transcription factor gatC shuttles between the cytoplasm and the nucleus in response to cAMP stimulation and that this is a key part of the mechanism of pulsatile induced gene expression [15].

6 Competition Between Aggregation Centres

Observation of wave forms during aggregation reveals that there are essentially two types of waves that can be observed during aggregation. These are patterns of concentric waves that are periodically initiated by the aggregation centre and spiral waves (Fig. 4). In both cases the cAMP waves propagate over a large distance of up to several centimetres and pass over hundreds of thousands of cells. The period of the waves is initially quite long, in the order of 8 min but gradually goes to down to ∼3 min, while the wave propagation speed is initially high (∼1 mm/min) but then drops down as the cells come into closer contact. Centres arise at different times and oscillate with different frequencies [13].

Due to the fact that colliding waves annihilate each other faster oscillating centres can encroach on slower oscillating centres and can finally wipe them out. It has been described that spiral centres normally wipe out concentric centres [16]. Concentric centres can only exist when the cells in the centre are in an oscillatory mode, however spiral waves can exist both in excitable and oscillatory systems. In spiral waves the waves rotate around a central core, periodically re-stimulate themselves and are likely to run at the maximum frequency that the excitable or oscillatory medium can sustain and therefore are likely to dominate [7, 17]. Different strains show typically different types of waves during the aggregation stage. This is likely dependent on
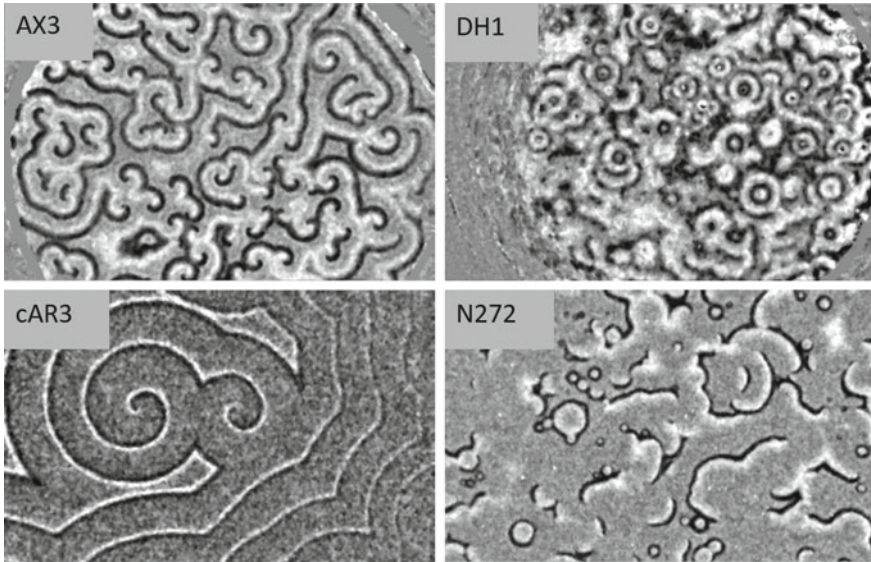
Fig. 4 Wave patterns observed during aggregation in wildtype and mutant strains. Strain Ax3 shows spiral waves, strain DH1 makes many concentric waves, the cAR3 strain is a mutant that expresses a lower affinity cAMP receptor and produces large spiral waves. The N272 strain expresses even lower affinity cAMP receptors, makes chaotic waves. They are not able to set up stable centres since the wave period is so slow that the cells disperse between waves, see [23] for further details

the exact composition of the molecular components making up the cAMP oscillatory machinery, which is not known in detail for all of the components in all of the strains.

7 Experimental Perturbation of cAMP Wave Propagation

Experiments have been performed with chemicals that interfere with components of the cAMP oscillatory system. These experiments have either used small molecule chemical inhibitors of critical components of the oscillatory molecular machinery or used mutants in essential components of the signalling process to perturb the oscillatory dynamics and study its effects on wave propagation dynamics and geometry. A widely used small molecule inhibitor is caffeine which has been shown to inhibit a critical step in the activation of the aggregation stage adenylyl cyclase, the enzyme responsible for the periodic generation of cAMP [18]. It has been shown that increasing concentrations of caffeine result in lower levels of activation of cyclase and lower levels of cAMP and that this in turn results in a slower period of the cAMP oscillations and in a larger wavelength of the waves [19]. Mutants lacking the aggregate stage adenylyl cyclase are deficient in aggregation, as are mutants in the cAMP receptor cAR1 and the extracellular cAMP phosphodiesterase. More subtle mutations have shown that the dynamics of the system can indeed be tuned. cAMP receptor

mutants with lower affinity for cAMP show altered patterns of wave propagation but also in extreme cases result in mutants that can still propagate waves. These wave fragments, however, do not set up aggregation centres. This is caused by the fact that the time it takes between two oscillations is too long and the cells will disperse again by random movement resulting in the generation of waves at other random locations (Fig. 4). A temperature sensitive mutant of adenylyl cyclase was shown to be effective in changing the wavelength in a temperature dependent manner [20]. More recently a high throughput analysis of several cAMP signalling mutants was performed [21]. Also other ways of interfering with the oscillatory system have become available: these are perturbations such as microinjection of cAMP in aggregation fields, the photo-activation of caged cAMP and the use of photo-genetics such as the use of light activated cyclase [22]. Experimental perturbation in combination with detailed mathematical modelling will provide a rich ground for further analysis of excitable biological systems.

8 Streaming Instability: Formation of Aggregation Streams

During development the cells initially move towards the aggregation centre as single cells, however, after 10–20 waves have passed the cells start to form bifurcating aggregation streams originating in the aggregation centre. Individual wave fronts initiated in the aggregation propagate along the aggregation streams outward and organise the periodic inward movement of the cells towards the aggregation centre (Fig. 5a, b, e). Experimentally stream formation has been shown to be dependent on the localisation of ACA in the rear of the aggregating cells, resulting in polarised cAMP secretion from the back of the cells [24]. During early development, when the cells are still single the waves propagate at speeds of more than 500 µm/min, but in the aggregation streams the wave propagation speed drops to around 50 µm/min [25]. This decrease in wave propagation speed leads to a large reduction of the chemical wavelength of the cAMP waves. In streams the cells make head to tail contacts via a calcium independent adhesion molecule, contact site A and side to side contacts via a calcium dependent contact molecule [26]. This coupling results in an increase in the persistence and overall speed of cell movement. The speed of cell moment in the streams increases to ∼20–30 µm/min which results in a considerable Doppler shift in the perception of the frequency of the cAMP signal, by the moving cells [25]. The biological implication of this is not yet completely clear but could put an upper limit on the speed of cell movement relative to the speed of signal propagation. Modelling has shown that stream formation does not require localised signalling, but is due to a streaming instability [27]. Recently it has been proposed that aggregation can be viewed as a self-induced criticality, resembling a phase transition in physical terms [28].

Mounds are characterised by rotating waves of cAMP that direct the counter-rotational periodic movement of the cells. These waves often take on the appearance of multi-armed spirals or pinwheels that organise the counter-rotational movement
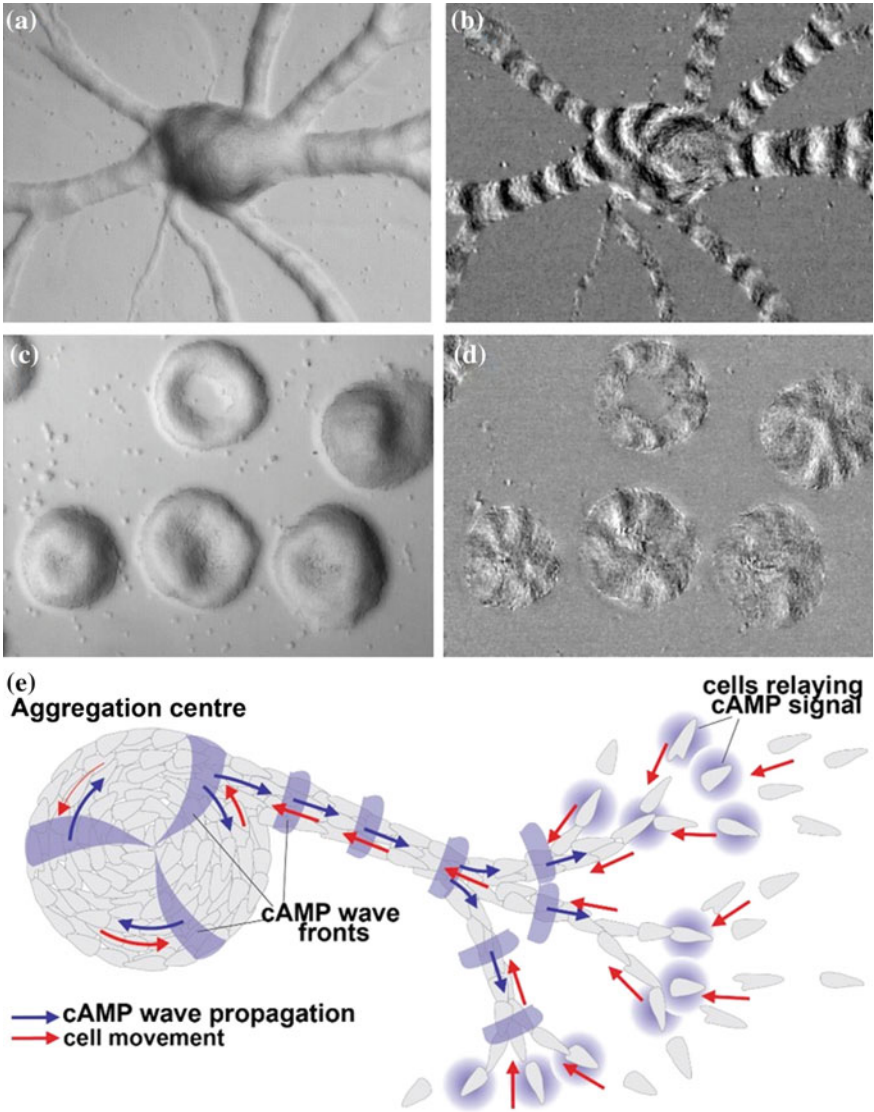
Fig. 5 During aggregation the initially randomly distributed cells start to form bifurcating aggregation streams (**a**). In these streams optical density waves are visible (**b**). The cAMP waves propagate from the aggregate outward into the streams, while the cells move inwards towards the aggregation centre. In the mound the waves take on a pinwheel like geometry. The cells move up the signal gradients in a direction opposite to that of wave rotation. In mutants with reduced cAMP excitability, the aggregation centres form rings that are still organised by large numbers of rotating waves (**c**, **d**). **e**: diagram of a streaming aggregate, blue arrows indicate direction of wave propagation, red arrows indicate direction of cell movement

of the cells (Fig. 5c, d). Depending on the strain, mounds can be short or longer lived and in many cases form intermediate ring-shaped structures. In these rings there can exist several wave fronts chasing each other and when they close again, they give rise to the pinwheel like structures in mounds (Fig. 5c, d) [29].

The differentiation of the prespore and prestalk cells starts during aggregation. There is even evidence that the initial differentiation is based on physiological biases like nutritional state and cell cycle position at the time of starvation already present in the population before aggregation [30]. As a result of this early differentiation there is little correlation between the time of arrival in the mound and differentiation fate. Initially the prestalk and prespore cell types display a salt and pepper distribution in the mound. During mound formation a subpopulation of prestalk cells sort out to form the tip, a nipple shaped structure on top of the mound. During tip formation the prestalk cells start to produce an extracellular matrix, the slime sheath, that surrounds the slug and encases the cells within the slug. The slug falls over and migrates away.

The tip has been shown to act as an organiser. It guides the movement of all the other cells in the aggregation during the transformation of the mound into a standing slug and during culmination to form a fruiting body [31].

Major questions are: what is the mechanism by which the tip controls the movement of all the other cells in the tipped mound, slug and culminate and what is the mechanism of cell sorting? Localised external cAMP has been shown to be able to direct cell sorting of prestalk cells at the mound stage [32]. Use of a temperature sensitive ACA mutant has shown that ACA activity is required *in vivo* for cells to be able to sort to the tip [33]. The action of the tip as an organiser can be mimicked by the periodic injection of cAMP pulses of the right frequency and duration [32, 34], suggesting that the tip might be a source of periodic cAMP waves, in agreement with the fact that prestalk cells express ACA and the extracellular cAMP phosphodiesterase pdeA [35].

The prestalk cells in the tip of a migrating slug typically rotate perpendicular to the direction of slug movement, especially when the tip is lifted from the substrate. In the back of the slug the cells move periodically forward and all cells move on the average with slug speed [29]. This has led to the suggestion that cell movement in the slug is organised by rotating scroll waves of cAMP in the tip and propagating planar waves in the back of the slug. The slug would therefore be essentially a composite of an aggregation centre organised by a rotation wave while the body of the slug mostly consisting mostly of prespore cells would resemble a 3D aggregation stream [38, 39]. Consistent with this notion, optical density waves can be seen to propagate from the middle of the prestalk zone to the back reflecting the periodic movement of the cells in forward direction (Fig. 6). These optical waves are strictly dependent on the presence of the tip, i.e. when the tip is removed no new waves are initiated and slug migration stops, while waves continue in the isolated tip that continues to migrate [34]. It has been reported that strains lacking ACA but overexpressing the catalytic subunit of protein kinase A, can still form migrating slugs [40]. This suggests that there either exists an ACA independent mechanism to produce periodic cAMP signals, that could involve cAMP generation by one of the two other adenylyl cyclases ACB or ACG that are expressed at the slug stage [5]. Alternatively it could
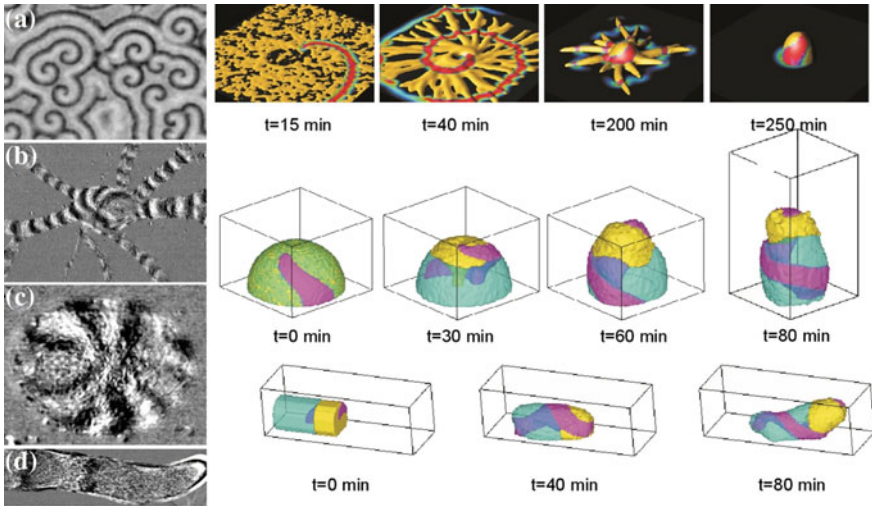
Fig. 6 a–d: optical density waves observed during early aggregation (**a**), streaming aggregate (**b**), in the mound stage (**c**) and in a migrating slug traveling from left to right (**d**). The right hand panels show results from a continuum three dimensional hydrodynamic simulation of aggregation, mound formation and slug migration showing spiral wave cAMP signal (red, purple) and cellular tissue. Aggregation stage cells are shown in yellow, in the mound the cells differentiate in prestalk cells (yellow) and prespore cells (blue) that are initially distributed in a salt and pepper patterns, but then the prestalk cells sort out for the tip and the prespore cells form the back of the slug. The cAMP waves form twisted scroll waves [36, 37]

be that there exist altogether different mechanisms that can control cell movement, such as cell contact induced cell-cell following [41]. This remains to be further characterised experimentally.

The interactions between cell-signalling and cell movement can be described by continuous mathematical models where the cell masses are described as a viscous fluid, incorporating excitable chemical kinetics in a robust way. It would appear that these processes are sufficient to explain *Dictyostelium* morphogenesis (Fig. 6) [37]. The life cycle has also been successfully modelled using assumptions of excitable cell-cell cAMP signalling, chemotaxis and differential adhesion with a variant of the cellular Potts model that enabled a description of the complete life cycle from aggregation via mound, slug formation and migration to and culmination and fruiting body formation [42]. This has been pioneering theoretical work and the experiments are still trying to catch up to confirm or disprove the details put forward by these models.

9 Outlook and Open Questions

As outlined above the oscillatory cAMP based cell-cell communication system controlling *Dictyostelium discoideum* aggregation is extensively studied and the basic mechanism of the excitable cAMP signalling during aggregation is understood, but many molecular details remain to be resolved. One of the key questions that needs to be answered experimentally is whether oscillatory cAMP signalling controls chemotactic movement of cells in the slug and during culmination or whether there exist other mechanisms that can take over. It has recently been argued on theoretical grounds that oscillations may disappear at the slug stages and could be replaced by continuous cAMP signalling [43]. Another interesting question is how the excitable cell-cell signalling evolved during evolution of the various *Dictyostelium* strains. The work on *Dictyostelium* aggregation has been a great inspiration for the generation of mathematical models describing the cAMP basic oscillator and to explore how excitable cell-cell signalling results in efficient long range cell-cell communication and importantly how it interacts with chemotactic cell movement. This is where the system differs considerably from chemical excitable systems such as the intensely studied Belousov-Zhabotinsky reaction discussed extensively in chapter **Chemical Oscillations and Spiral Waves**.

References

1. R. Kessin, *Dictyostelium* (Cambridge University, Cambridge, 2001)
2. A.J. Ridley, M.A. Schwartz, K. Burridge, R.A. Firtel, M.H. Ginsberg, G. Borisy, J.T. Parsons, A.R. Horwitz, Cell migration: integrating signals from front to back. Science **302**, 1704–1709 (2003)
3. P.N. Devreotes, S. Bhattacharya, M. Edwards, P.A. Iglesias, T. Lampert, Y. Miao, Excitable signal transduction networks in directed cell migration. Annu. Rev. Cell Dev. Biol. **33**, 103–125 (2017)
4. A.T. Sasaki, C. Janetopoulos, S. Lee, P.G. Charest, K. Takeda, L.W. Sundheimer, R. Meili, P.N. Devreotes, R.A. Firtel, G protein-independent Ras/PI3K/F-actin circuit regulates basic cell motility. J. Cell Biol. **178**, 185–191 (2007)
5. G.S. Pitt, N. Milona, J. Borleis, K.C. Lin, R.R. Reed, P.N. Devreotes, Structurally distinct and stage-specific adenylyl cyclase genes play different roles in *Dictyostelium* development. Cell **69**, 305–315 (1992)
6. S. Saran, M.E. Meima, E. Alvarez-Curto, K.E. Weening, D.E. Rozen, P. Schaap, cAMP signaling in *Dictyostelium*. Complexity of camp synthesis, degradation and detection. J. Muscle Res. Cell Motil. **23**, 793–802 (2002)
7. A.J. Durston, *Dictyostelium discoideum* aggregation fields as excitable media. J. Theor. Biol. **42**, 483–504 (1973)
8. G.L. Garcia, C.A. Parent, Signal relay during chemotaxis. J. Microsc. **231**, 529–534 (2008)
9. J. Lauzeral, J. Halloy, A. Goldbeter, Desynchronization of cells on the developmental path triggers the formation of spiral waves of cAMP during *Dictyostelium* aggregation. Proc. Natl. Acad. Sci. USA **94**, 9153–9158 (1997)
10. F.I. Comer, C.A. Parent, Phosphoinositide 3-kinase activity controls the chemoattractant-mediated activation and adaptation of adenylyl cyclase. Mol. Biol. Cell **17**, 357–366 (2006)

11. T. Gregor, K. Fujimoto, N. Masaki, S. Sawai, The onset of collective behavior in social amoebae. Science **328**, 1021–1025 (2010)

12. M. Skoge, H. Yue, M. Erickstad, A. Bae, H. Levine, A. Groisman, W.F. Loomis, W.J. Rappel, Cellular memory in eukaryotic chemotaxis. Proc. Natl. Acad. Sci. USA **111**, 14448–14453 (2014)

13. F. Alcantara, M. Monk, Signal propagation during aggregation in the slime mould *Dictyostelium discoideum*. J. Gen. Microbiol. **85**, 321–334 (1974)

14. K.J. Tomchik, P.N. Devreotes, Adenosine 3',5'-monophosphate waves in *Dictyostelium discoideum*: a demonstration by isotope dilution-fluorography technique. Science **212**, 443–446 (1982)

15. H. Cai, M. Katoh-Kurasawa, T. Muramoto, B. Santhanam, Y. Long, L. Li, M. Ueda, P.A. Iglesias, G. Shaulsky, P.N. Devreotes, Nucleocytoplasmic shuttling of a GATA transcription factor functions as a development timer. Science **343**, 1249531 (2014)

16. A.J. Durston, Pacemaker activity during aggregation in *Dictyostelium discoideum*. Dev. Biol. **37**, 225–235 (1974)

17. P. Foerster, S.C. Müller, B. Hess, Curvature and spiral geometry in aggregation patterns of *Dictyostelium discoideum*. Development **109**, 11–16 (1990)

18. A. Theibert, P. Devreotes, Adenosine and its derivatives inhibit the cAMP signaling response in *Dictyostelium discoideum*. Dev. Biol. **106**, 166–173 (1984)

19. F. Siegert, C. Weijer, Digital image processing of optical density wave propagation in *Dictyostelium discoideum* and analysis of the effects of caffeine and ammonia. J. Cell Sci. **93**, 325–335 (1989)

20. H. Patel, K. Guo, C. Parent, J. Gross, P.N. Devreotes, C.J. Weijer, A temperature-sensitive adenylyl cyclase mutant of *Dictyostelium*. EMBO J. **19**, 2247–2256 (2000)

21. S. Sawai, X.J. Guan, A. Kuspa, E.C. Cox, High-throughput analysis of spatio-temporal dynamics in *Dictyostelium*. Genome Biol. **8**, R144 (2007)

22. C. Beta, D. Wyatt, W.J. Rappel, E. Bodenschatz, Flow photolysis for spatiotemporal stimulation of single cells. Anal. Chem. **79**, 3940–3944 (2007)

23. D. Dormann, J.Y. Kim, P.N. Devreotes, C.J. Weijer, cAMP receptor affinity controls wave dynamics, geometry and morphogenesis in *Dictyostelium*. J. Cell Sci. **114**, 2513–2523 (2001)

24. P.W. Kriebel, V.A. Barr, C.A. Parent, Adenylyl cyclase localization regulates streaming during chemotaxis. Cell **112**, 549–560 (2003)

25. J. Rietdorf, F. Siegert, C.J. Weijer, Analysis of optical-density wave-propagation and cell-movement during mound formation in *Dictyostelium discoideum*. Dev. Biol. **177**, 427–438 (1996)

26. J.C. Coates, A.J. Harwood, Cell-cell adhesion and signal transduction during *Dictyostelium* development. J. Cell Sci. **114**, 4349–4358 (2001)

27. H. Levine, W. Reynolds, Streaming instability of aggregating slime mold amoebae. Phys. Rev. Lett. **66**, 2400–2403 (1991)

28. G. De Palo, D. Yi, R.G. Endres, A critical-like collective state leads to long-range cell communication in *Dictyostelium discoideum* aggregation. PLOS Biol. **15**, e1002602 (2017)

29. F. Siegert, C.J. Weijer, Spiral and concentric waves organize multicellular *Dictyostelium* mounds. Curr. Biol. **5**, 937–943 (1995)

30. G. Weeks, C.J. Weijer, The *Dictyostelium* cell cycle and its relationship to differentiation. FEMS Microbiol. Lett. **124**, 123–130 (1994)

31. C.J. Weijer, *Dictyostelium* morphogenesis. Curr. Opin. Genet. Dev. **14**, 392–398 (2004)

32. S. Matsukuma, A.J. Durston, Chemotactic cell sorting in *Dictyostelium discoideum*. J. Embryol. Exp. Morphol. **50**, 243–251 (1979)

33. H. Patel, K.D. Guo, C. Parent, J. Gross, P.N. Devreotes, C.J. Weijer, A temperature-sensitive adenylyl cyclase mutant of *Dictyostelium*. EMBO J. **19**, 2247–2256 (2000)

34. D. Dormann, C.J. Weijer, Propagating chemoattractant waves coordinate periodic cell movement in *Dictyostelium* slugs. Development **128**, 4535–4543 (2001)

35. I. Verkerke-van Wijk, M. Fukuzawa, P.N. Devreotes, P. Schaap, Adenylyl cyclase A expression is tip-specific in *Dictyostelium* slugs and directs StatA nuclear translocation and CudA gene expression. Dev. Biol. **234**, 151–160 (2001)

36. B. Vasiev, F. Siegert, C.J. Weijer, A hydrodynamic model for *Dictyostelium discoideum* mound formation. J. Theor. Biol. **184**, 441 (1997)
37. B. Vasiev, C.J. Weijer, Modelling of *Dictyostelium discoideum* slug migration. J. Theor. Biol. **223**, 347–359 (2003)
38. O. Steinbock, F. Siegert, S.C. Müller, C.J. Weijer, Three-dimensional waves of excitation during *Dictyostelium* morphogenesis. Proc. Natl. Acad. Sci. USA **90**, 7332–7335 (1993)
39. F. Siegert, C.J. Weijer, Three-dimensional scroll waves organize *Dictyostelium* slugs. Proc. Natl. Acad. Sci. USA **89**, 6433–6437 (1992)
40. B. Wang, A. Kuspa, *Dictyostelium* development in the absence of cAMP. Science **277**, 251–254 (1997)
41. T. Umeda, K. Inouye, Possible role of contact following in the generation of coherent motion of *Dictyostelium* cells. J. Theor. Biol. **219**, 301–308 (2002)
42. A.F.M. Maree, P. Hogeweg, How amoeboids self-organize into a fruiting body: multicellular coordination in *Dictyostelium discoideum*. Proc. Natl. Acad. Sci. USA **98**, 3879–3883 (2001)
43. A.J. Durston, Dislocation is a developmental mechanism in *Dictyostelium* and vertebrates. Proc. Natl. Acad. Sci. **110**, 19826 (2013)

Spiral Waves in the Heart

Alexander V. Panfilov

Abstract One of the most important applications of spiral waves is found in cardiology. Electrical waves in the heart which initiate cardiac contraction are similar to nonlinear waves in other excitable systems. In pathological situations they can form rotating spiral waves. Onset of spiral waves in the heart causes cardiac arrhythmias characterized by extremely fast and irregular heartbeat and can lead to cardiac arrest and sudden cardiac death. Although a general idea about the existence of spiral waves in the heart was proposed a long time ago, only recently it became possible to record them in experiment. In this chapter we provide the most known experimental examples of spiral wave activity in cardiac tissue. It includes experiments in slices of cardiac tissue, whole heart preparations and cultures of cardiac cells. We briefly describe properties of spiral waves in the heart and discuss how they differ from spiral waves in other excitable systems.

1   Introduction

The main physiological function of the heart is mechanical, the heart pumps the blood through the body. However, this process is controlled by electrical waves of excitation. The electrical wave propagates through the heart and initiates cardiac contraction. Under normal conditions the wave originates from a natural pacemaker of the heart called sinus node. Then it propagates through the upper chambers of the

A. V. Panfilov (✉)
Department of Physics and Astronomy, Gent University,
Krijgslaan 281, S9, 9000 Gent, Belgium

Laboratory of Experimental Cardiology, Department of Cardiology,
Heart Lung Center, Leiden University Medical Center,
2333, ZA Leiden, The Netherlands
e-mail: Alexander.Panfilov@UGent.be

heart atria, and initiates contraction of the atria. As a result blood from the atria is pumped into the lower chamber of the heart ventricles. Then, after a delay a wave propagates through the ventricles, initiates their contraction which provides the main pumping of blood into the circulatory system. The properties of this electrical wave in the heart are similar to the properties of other waves in excitable systems, and thus such waves can also form spiral waves. However, it is extremely difficult to observe nicely shaped spiral waves in the heart. This is due to several reasons. First of all, the cardiac tissue is anisotropic: the velocity of wave propagation in different directions can differ by 2–5 times [1].The structure of anisotropy by itself is quite complex [1]. Atria of the heart have thin walls so that they can be regarded as quasi 2D objects. Ventricles have thicker walls of 1.5–2 cm and here the 3D structure of the spiral wave becomes important [2]. Another complication is the presence of many non-local connections in the heart. In several regions of the atria there are so-called pectenate muscles which provide additional paths for excitation. There is also an own conduction system of the heart, the so-called Purkinje network, which either well provide a path for the excitation wave additional to the normal local propagation along cardiac tissue [2]. The presence of only these factors make observations of classical spirals in the heart extremely difficult. However, the spiral wave activity can still be observed in the whole heart and also in some simpler preparations made from cardiac cells. In this chapter we will briefly review experimental observations of spiral waves in various systems related to cardiac tissue.

2   First Observations of Spiral Waves in Cardiac Tissue

Rotational activity in cardiac tissue without obstacles was first recorded in the 1970s by Allessie et al. in small segments of rabbit atria [3]. They found that excitation waves can rotate in cardiac tissue without presence of any obstacles. Allessie et al. saw rotation of the excitation wave, however the wave front did not have a spiral shape (see e.g. Fig. 1 of [3]). This is because the size of the tissue is smaller than the characteristic wavelength of the spiral. Based on that observation Allessie et al. [3] formulated mechanism explaining the dynamics of this source as the leading circle hypothesis. In accordance with this hypothesis the excitation is driven by circulation along the smallest possible pathway in which the impulse can continue to circulate, which is called the "leading circle". It was also explicitly mentioned that the head of the circulating wave front is "continuously biting in its own tail of refractoriness" and thus the length of this pathway equals the "wavelength", which was defined as a product of the conduction velocity and the refractory period. Allessie et al. [3] also proposed that the tissue inside and outside of the leading circle is excited by waves coming from this rotational loop.

The modern concept of spiral waves in cardiac tissue was introduced in seminal papers of the Jalife group. In the paper by Davidenko et al. [4] a rotational activity in an isolated sheep ventricular muscle slice was studied. The authors used a novel methodology of voltage-sensitive dyes and they were able to record electrical activity
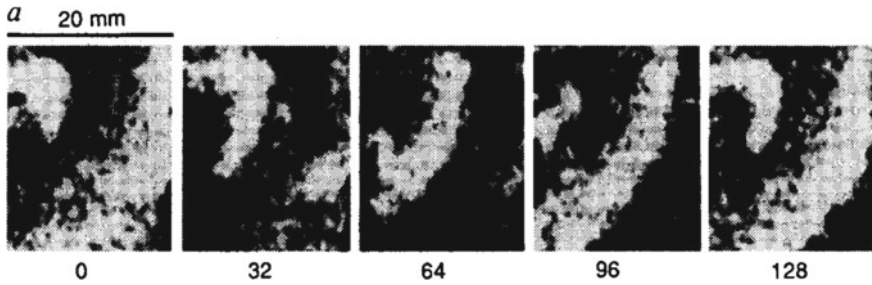
Fig. 1 Rotating spiral wave in a slice of canine heart. The white color denotes the excited region. We see a spiral wave rotating clockwise. Reproduced from [4] with permission

in large slices of the tissue with a high spatial accuracy. Figure 1 shows results of their experimental studies [4]. We see that the excitation wave here has a shape of a spiral wave rotating clockwise. Observation of this spiral shape became possible, because the preparations studied in Ref. [4] had much larger effective size (in terms of the wavelength) and recordings had also high spatial resolution. Davidenko et al. [4] were also able to study the dynamics of rotation of the spiral wave in their preparation. They found that in most of the cases spiral waves were non-stationary and drifted with a drift velocity about 10% of the velocity of the propagating waves. However, rotation of spiral waves can also stabilize around small anatomical obstacles and then they observed a stationary rotation. This phenomenon, which was called 'anchoring', turned out to be extremely important for spiral waves in the heart and for clinical applications.

3 Spiral Waves in the Whole Heart

Recording of a spiral wave in the whole heart is a very challenging problem. Because the upper chambers of the heart, the atria, are electrically isolated from the lower chambers ventricles [2], spiral waves can be observed either in atria or in ventricles. The excitation wave generated by spirals in the atria is very complex, due to the complex geometrical structure of the atria, the presence on non-local connections under the atrial surface and the presence of many veins and arteries intersecting the atrial surface. We can see it from simulations of spiral waves in an anatomical model of human atria. Studies of spiral waves in atria are extremely important. Clinical studies by Narayan et al. [5] identified stable spiral waves of rotational activity (rotors) during human atrial fibrillation. From the clinical perspective this was a very important finding. This is because atrial fibrillation (AF) is often referred to as the most common arrhythmia in clinical practice, it affects approximately 2% of the total population, but in age groups above 80 years old its occurrence is up to 17% and the total number of patients is expected to raise. Currently, the treatment of certain types of AF remains not effective and this is because we still do not understand
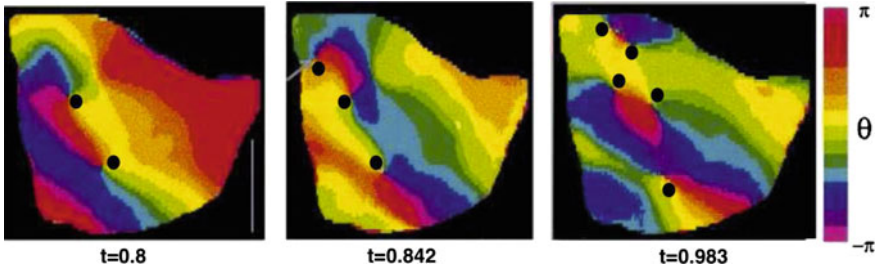
Fig. 2 Development of ventricular fibrillation in the rabbit heart. Excitation is represented using the phase mapping method. Time in seconds shown below of each frame. The centers of the rotating sources are marked by the black circles. Modified from [6] with permission

the organization of wave patterns during AF [5]. Clinical studies by Narayan et al. showed also that during AF there are stationary rotating spiral waves, and removal of these sources stops the overall fibrillating activity. Interestingly, these studies showed that in many cases just removing (ablation) of the center of a spiral is sufficient to stop the arrhythmia.

Ventricles of the heart have a simpler shape than the atria, and spiral waves there can be observed more easily. However, there is another problem here. If a spiral wave occurs in the ventricles of the heart it tends to deteriorate into a spatially chaotic pattern leading to ventricular fibrillation. Figure 2 illustrates typical dynamics in that case. At t = 0.8 we see two spiral waves rotating in opposite directions. At t = 0.842 a new clockwise rotating spiral wave appears. Then at t = 0.983 we observe further complication of the excitation pattern which now contains 5 rotating excitation sources.

Most of the recordings of spiral wave activity in the whole ventricles were performed in the heart of small animals, rabbits, mice etc. In hearts of large animals usually much more complex excitation patterns of spatiotemporal chaos corresponding to ventricular fibrillation are observed [7]. In Fig. 4 of [8] we can find a rear example of spiral waves in the heart of a large size observed during the initial phase of formation of ventricular fibrillation, by panoramic optical mapping of electrical excitation of the isolated pig hearts. It shows two counter-rotating spiral waves.

4 Spiral Waves in Cell Cultures

One of the most convenient systems where spiral waves can be studied experimentally are cardiac cell culture experiments. In this experimental approach a patch of cardiac tissue containing cardiac myocytes is created using methods of tissue engineering. Such cardiac tissue can conduct waves of excitation. Also, the velocity of these waves can be much slower than that in the normal heart, thus even small patches of such tissue (1–2 cm) can be sufficient to sustain rotating spiral waves [9]. Also, most types of cardiac cell cultures are isotropic, thus wave propagation there is close to what one
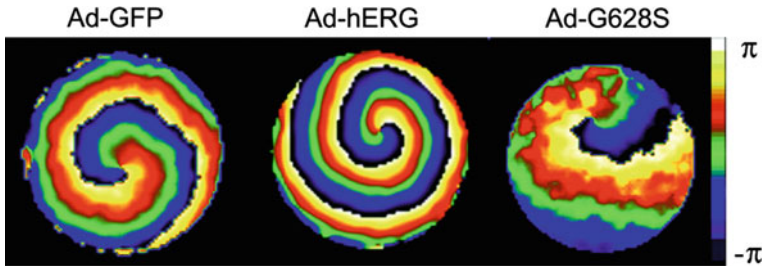
Fig. 3 Spiral waves in a culture of neonatal rat ventricular myocytes under different conditions. The cardiac cells have different expression of genes responsible for the duration of the action potential with shortest duration corresponding to Ad-hERG, medium to Ad-GFP and longest to Ad-G628S, achieved using adenoviral constructs. Reproduced from [10] with permission

observes in other types of excitable media, for example the Belousov-Zhabotinsky (BZ) reaction. Cardiac cell cultures are currently widely used in cardiac research. This is because when using them it is possible to manipulate properties of cardiac cells in a wide range, using drugs or methods of molecular biology. Figure 3 shows typical spiral waves in cell culture. We recognize a clear spiral shape. In study [10] the main focus was on so-called rapid rectifier potassium current which is extremely important for understanding the mechanisms of cardiac drugs and of cardio toxicity. This current was manipulated using methods of molecular biology and we see that it results in a substantial change in the wavelength of the spiral wave.

One interesting recent application in cell culture experiments is the ability to combine it with optogenetics. In such a methodology properties of cardiac cells can be controlled by light, similar to the photosensitive BZ reaction (see chapter **Generation of Spirals in Excitable Media**). Normally, in optogenetic cultures, light depolarizes cardiac cells, thus it tends to produce excitation. However, if the light is continuously applied after initial excitation, the tissue remains depolarized and can serve as a barrier for excitation waves. Such a property was used by Feolla et al. [11] to study the interaction of rotating spiral waves with unexcitable barriers. This mimics a procedure of ablation of cardiac arrhythmias widely used in clinics, in which a certain part of cardiac tissue is destroyed by local application of large electrical current or local feezing. However, in optogentic experiments such barriers are reversible and their shape and location can be easily manipulated. The rational of this work [11] was to study in experiment if creation of an unexcitable region at the core of a rotating spiral wave in the heart can stop spiral wave rotation, as was observed by Narayan et al. [5], mentioned above. Simple geometric theory predicts that in order to remove a spiral wave one needs to make a non-excitable region connecting the core of the spiral wave with the boundary of the tissue. From the results shown in Fig. 4 we see that when only the core of the spiral wave was targeted, it did not remove the spiral wave. However, if an unexcitable region connects the core of the spiral wave and unexcitable boundary, spiral wave activity was terminated. This way we see that as predicted by theory only ablation up to the boundary of the region should be successful. Thus the observations reported in [5] indeed require special analysis
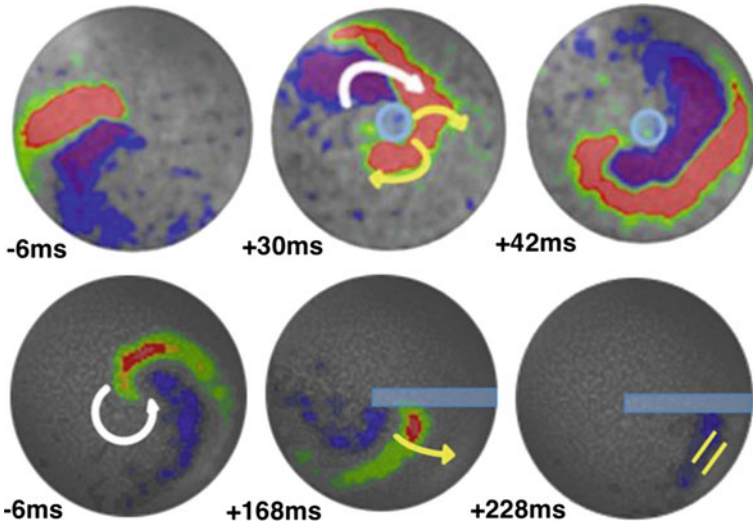
Fig. 4 Upper row: Effects of core region targeting with circular conduction blocks. Lower row: Effects of core region targeting with a linear conduction block reaching the boundary. Reproduced from Feola et al. [11] with permission
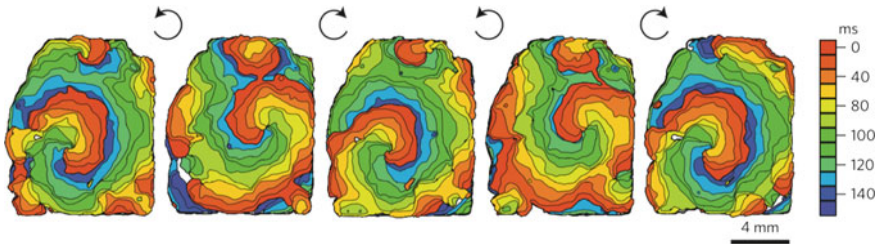
Fig. 5 The initial spiral wave (left) and the four spirals after each of the chirality reversals. Reproduced from Burton et al. [13] with permission

regarding the mechanisms of this effect. Several hypotheses were put forward to understand this fact [12]. Rappel et al. [12] proposed several mechanisms which can explain the disappearance of arrhythmia by modification of spiral wave dynamics after ablation of the center leading to their removal.

Another interesting observation of the manipulation of spiral wave dynamics using optogenetic effects is described by Burton et al. [13]. The authors were able to affect spiral wave dynamics via an optical-optogenetic setup. Figure 5 shows the following process. First a spiral wave was created (the left figure). Then an optical image was imposed showing a computer-generated counter-rotating spiral wave with a slightly higher frequency than that of the original spiral. It was found that the imposed optical pattern changes the direction of rotation of the original spiral. Figure 5 shows how such a change is performed four times. Although we see a small shift of the

spiral core, the procedure works robustly and requires application of the computer-generated image just during one or two rotations to change the spiral wave chirality.

Currently cardiac cell cultures provide one of the most advanced experimental technologies for studies of properties of spiral waves in cardiac tissue and for translation of research on spiral wave dynamics performed in other excitable systems to cardiology.

In this chapter we mention just a few examples of spiral wave dynamics in cardiac tissue. Additional information can be found in the review articles on this subject published in [7, 14, 15].

References

1. B.J. Caldwell, M.L. Trew, G.B. Sands, D.A. Hooks, I.J. LeGrice, B.H. Smaill, Three distinct directions of intramural activation reveal nonuniform side-to-side electrical coupling of ventricular myocytes. Circ. Arrhythm. Electrophysiol. **2**, 433–440 (2009)
2. J. Keener, J. Sneyd, *Mathematical Physiology* (Springer, New York, 1998)
3. M.A. Allessie, F.I.M. Bonke, F.J.G. Schopman, Circus movement in rabbit atrial muscle as a mechanism of tachycardia. III. The leading circle concept: a new model of circus movement in cardiac tissue without the involvement of an anatomical obstacle. Circ. Res. **41**, 9–18 (1977)
4. J.M. Davidenko, A.M. Pertsov, R. Salomonsz, W. Baxter, J. Jalife, Stationary and drifting spiral waves of excitation in isolated cardiac muscle. Nature **355**, 349–351 (1992)
5. S.M. Narayan, D.E. Krummen, K. Shivkumar, P. Clopton, W.-J. Rappel, J.M. Miller, Treatment of atrial fibrillation by the ablation of localized sources. J. Am. Coll. Cardiol. **60**, 628–636 (2012)
6. R.A. Gray, A.M. Pertsov, J. Jalife, Spatial and temporal organization during cardiac fibrillation. Nature **392**, 75–78 (1998)
7. S. Pandit, J. Jalife, Rotors and the dynamics of cardiac fibrillation. Circ. Res. **112**, 849–862 (2013)
8. E. Bourgeois, H. Reeves, J. Walcott, J. Rogers, Panoramic optical mapping shows wavebreak at a consistent anatomical site at the onset of ventricular fibrillation. Cardiovasc. Res. **93**, 272–279 (2012)
9. G. Bub, L. Glass, N. Publicover, A. Shrier, Bursting calcium rotors in cultured cardiac myocyte monolayers. Proc. Natl. Acad. Sci. USA **95**, 10283–10287 (1998)
10. L. Hou, M. Deo, P. Furspan, S. Pandit, S. Mironov, D. Auerbach, Q. Gong, Z. Zhou, O. Berenfeld, J. Jalife, A major role for hERG in determining frequency of reentry in neonatal rat ventricular myocyte monolayer. Circ. Res. **107**, 1503–1511 (2010)
11. I. Feola, L. Volkers, R. Majumder, A. Teplenin, M. Schalij, A. Panfilov, A. de Vries, D. Pijnappels, Localized optogenetic targeting of rotors in atrial cardiomyocyte monolayers. Circ. Arrhythm. Electrophysiol. **10**, e005591 (2017)
12. W.-J. Rappel, J. Zaman, S. Narayan, Mechanisms for the termination of atrial fibrillation by localized ablation: computational and clinical studies. Circ. Arrhythm. Electrophys. **8**, 1325–1333 (2015)
13. R. Burton, A. Klimas, C. Ambrosi, J. Tomek, A. Corbett, E. Entcheva, G. Bub, Optical control of excitation waves in cardiac tissue. Nat. Photonics **9**, 813–816 (2015)
14. A.V. Panfilov, Theory of reentry, in *Cardiac Electrophysiology: From Cell to Bedside*, ed. by D.P. Zipes, J. Jalife, 5th edn. (Saunders Philadelphia 2009), pp. 329–337
15. A.V. Panfilov, H. Dierckx, Theory of rotors and arrhythmias, in *Cardiac Electrophysiology: From Cell to Bedside*, ed. by D.P. Zipes, J. Jalife, W.Stevenson, 7th edn. (Elsevier Philadelphia 2018), pp. 325–334

Patterns and Humans

Niklas Manz and Flavio H. Fenton

Abstract The appearance of spiral structures on the human tongue (geographic tongue) and skin (pathological rashes) are described. Affected and often migrating areas on the tongue can be bistable, patch-like fronts or waves. Pathological rashes with an expanding region of redness is often a result of an autoimmune disease in which the human immune system becomes hyperactive and attacks healthy tissues. In addition, we show a rotating spiral created by humans, which has been described as a reaction-diffusion waves in an excitable medium.

1 Introduction

Nonlinear dynamical systems far from thermodynamic equilibrium reveal a fascinating wealth of spatial, temporal, and spatiotemporal structures on a macroscopic scale in various physical, chemical, and biological pattern-forming systems. And even within one field, for example biological systems, a wide variety of patterns can be observed. Here, we mention a few large scale organizations as, for example, population patterns (e.g., grey squirrels in Britain [1]), vegetation distributions (e.g., fairy circles [2]), the dynamics of living cells (e.g., cellular slime molds (see chapter **Spiral Waves of the Chemo-attractant cAMP Organise Multicellular Development in the Social Amoebae**) or bacterial colonies [3]), and epidemics (e.g., rabies in foxes [4], black death epidemic (1347–1351) in Europe [5], or the bubonic plague in China [6]).

N. Manz (✉)
Department of Physics, The College of Wooster, Wooster, OH, USA
e-mail: nmanz@wooster.edu

F. H. Fenton
School of Physics, Georgia Institute of Technology, Atlanta, GA, USA
e-mail: flavio.fenton@physics.gatech.edu

On a smaller scale and within the human body, we can observe electrical depolarization waves on the heart (see chapter **Spiral Waves in the Heart**), the brain (see **Yet More Spirals**), or excitation waves during labour in the uterus [7], and on the tongue [8].

In this chapter, we will focus on spatiotemporal spiral-like structures (see chapter **Chemical Oscillations and Spiral Waves**) on and with humans. The tongue and the skin can exhibit patterns of propagating fronts, a steady state change in a *bistable system* (two stable and one unstable fixed point between the two basins of attraction) or wave like structures as in an *excitable system* (one stable fixed point in the phase space: see **Generation of Spirals in Excitable Media**). The last section describes a spiral performed by humans.

2 Patterns on the Tongue

The tongue is primarily a muscle necessary for speaking and moving food for chewing and swallowing with a thin, upper layer, the *epithelium* which consists of a mucous membrane with small nodules of tissue. There are four types of these, *lingual papillae* called tiny, pinkish-white bumbs containing hair-like structures ($d \approx 35$ μm, $l \approx 250$ μm). One of these, the *filiform papillae* do not contain taste buds and are located in the front two-thirds of the tongue.

The mucous membrane of the human tongue, as of many animals, is susceptible to a wide variety of diseases, which is of interest for the field of nonlinear dynamics [9]. One example is the *inflammatory psoriasiform mucositis* of *filiform papillae* with smooth, red areas and often slightly raised, grayish white borders. Because of the sometimes map-like appearance of affected areas it is called *Geographic Tongue* (GT). Other medical terms for these patterns are, for example, *lingua geographica*, *benign migratory glossitis*, and *erythema migrans lingualis*. GT is painless but some patients report numbness and tingling of the affected areas. It can be found in (1–4)% of the population [10].

The first reports of GT were published by Rayer in 1831 [11], but the underlying mechanisms for the inflammatory reaction are still unknown. It appears at higher percentages in, for example, females than males [12] or children than adults [10]. Race/ethnicity affects its appearance, but numbers vary in publications. Genetic predisposition seems also to be responsible. Liang et al. report a significant correlation of GT with mutations in the Interleukin-36 receptor antagonist (*IL36RN*) gene [13], which has previously been shown to cause inflammatory skin diseases.

Several GT-associated health conditions have been reported, as, for example, allergies, diabetes, generalized pustular psoriasis (a chronic skin condition caused by an overactive immune system), fissured tongue (cracks, grooves, or clefts appear on the top and sides of the tongue), asthma, hormonal disturbances, juvenile diabetes, stress, and Down syndrome. External factors such as stress, vitamin deficiency, spicy and/or acidic food, and toothpaste with additives, whitening agents, or heavy flavoring have also been reported to increase the probability to have GT, whereas smoking has been reported to have an inverse association [14].

Because GT is not an infection, it cannot be transmitted (entirely benign), and there is no curative treatment. To minimize flare-ups, patients can use anti-inflammatory medication, mouth rinse with anesthetics, zinc supplements, topically applied steroids, and generally avoiding tobacco, nuts, and spicy/acidic food.

The affected, often migrating areas can be simply bistable, patch-like fronts (see upper left structure in Fig. 1) but can also appear as waves. Due to the anisotropic structure of the tongue, circular target pattern or real Archimedean spirals are unlikely. Therefore, elongated, elliptical 'target pattern' (small elliptical structure closer to the tip) or spirals (large structure on the side) can be found. More logarithmic appearing spirals have also been observed (see Fig. 2).

Patients with GT seem to display a tremendous variation in appearance and evolution of their tongue patterns. This includes (i) severity, the total number of lesions and their extent on the surface of the tongue; (ii) frequency of lesional formation, as some patients are never without lesions, while other have lesions very sporadically; and (iii) rapidity of the lesional evolution as some patients state that they can watch their tongues change and patterns enlarge from hour to hour, while other patients have lesions that do not change at all.

To date, only one publication has linked GT to a reaction-diffusion (RD) system [8]. Seiden and Curland simulated GT as an excitable medium using an anisotropic cellular automaton model (see chapter **A Lattice-Gas Cellular Automaton Model for Discrete Excitable Media**) and were able to reproduce the 'elongated' patches and predict the appearance of spirals. However, their generic model had no link to any physiological parameter and could not be used to gain any insights into GT.
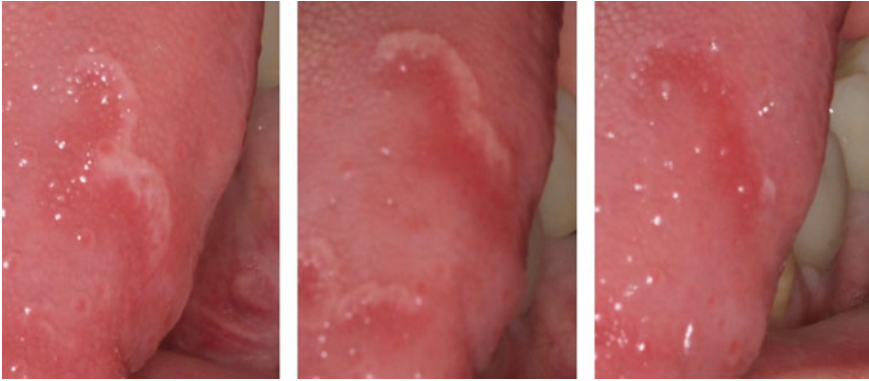
Fig. 3 Evolution of curved GT structures, revealing a RD wave behavior. Time between images: $\Delta t \approx 12$ h (copyright: Wooster Dental)

The only published propagation speed of GT has been given with 1 mm/day by Grosshans and Greber in 1983 [15]. Recent experimental research indicates possible higher propagation speeds (as reported by patients) and the observation of the 'kink eliminating effect' of two waves approaching each other in an angle. The angle between connected RD waves decreases until one straight front evolves. This effect is due to the higher speed of negatively curved front sections as shown in Fig. 3. Mathematically, this effect is given by the Eikonal equation $v = v_0 - DK$, with v, as the velocity of the curved front section, v_0 as the velocity of a straight front, D as a diffusion parameter, and K as the curvature of the front section [16].

3   Patterns on the Skin

The skin of the human body is susceptible to a wide variety of diseases and a resulting pathological redness (*erythema*) can have very different causes (injury, infection, or inflammation). Many abnormal skin conditions can manifest themselves in patterns similar to reaction-diffusion or precipitation waves.

There are numerous pathological and patho-physiological studies of various *erythema* in medical journals but none considers the intersection of reaction-diffusion waves/excitable system and dermatology. The only publication so far, is the report of propagating waves on the skin of a genetically modified mouse by Suzuki et al. in 2003 [17]. Another area of propagating pattern on the skin is in the field of avatars. In general, the skin tone/texture is defined and will not change but there are options to animate the textures of avatars.

The most common structure is an area of redness (*erythema*) in ring form (*annulare*), called a "bull's eye" rash. These patterns can be stationary or non-stationary (*erythema migrans*) spreading from the center (*erythema annulare centrifugum*), first described by Darier in 1916 [18].

Fig. 4 Lupus rash in the form of an early counter-rotating double spiral

Causes of these often expanding, target-like structures (*erythema chronicum migrans*) can be lyme disease (also called *Lyme borreliosis*), an infectious disease transferred primarily by a tick bite. The infection is caused by the spirochete *Borrelia burgdorferi* as identified in the 1980s as the etiological agent. It is the most often reported arthropod transmitted disease in humans in the United States, first reported by Afzelius in 1909 [19] and Lipschütz in 1913 [20]. Afzelius speculated in his 1921 publication that the rash came from the bite of an Ixodes tick [21].

The fungal infection called 'ringworm' (*Tinea corporis*) is a skin disease also appearing as front-like structures. The ringworm is characterized by a red ring of small blisters or scaly skin that grows outward as the infection spreads. This ring sometimes looks like a worm moving around the edges of the border. The center of the ring may clear up, while a new ring of infection develops at the edge of the old ring. Another, non-contagious skin condition is *granuloma annulare*, that usually causes a rash, manifesting in different ways.

Even spiral-like structures can be observed on the human skin. A structure similar to an early stage of a counter-rotating double spiral, as created by disturbing a planar RD wave front, can be seen in Fig. 4. The pattern is a result of *lupus erythematosus*, a name given to a collection of autoimmune diseases in which the human immune system becomes hyperactive and attacks healthy tissues.

A skin condition creating more often spiral-like structures, is *Erythema annulare centrifugum*, which refers to a number of chronic skin conditions which propagate up to 2−4 mm/day (Dutch website www.huidziekten.nl). Examples with spirals, very similar to chemical precipitation pattern as published by Haudin et al. in 2014 [22], are shown in Fig. 5.

Contrary to the Geographic Tongue structures in the previous section, patients with rashes are often treated by their dermatologists. Even if, for example, *Erythema Annulare Centrifugum* disappears on its own over an average of 11 month, patients are often treated with cortical creams. Possible underlying infections are treated with antibiotics and antimycotics as well as antibiotics with anti-inflammatory properties. Lupus and lyme disease are always treated due to their severe effect on the body.
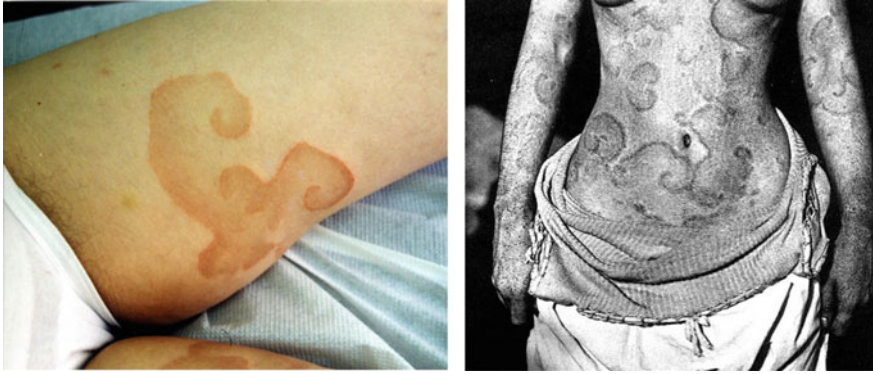
Fig. 5 Multiple spirals of *Erythema Annulare Centrifugum* on the inner thigh and upper body (copyright left: Efstathios Rallis)

4 Spiral with Humans

Besides patterns on humans as described in the previous two parts, there are a few other pattern forming systems *with* humans, which can be described as a reaction-diffusion wave in an excitable medium. In general, pedestrians and car traffic (caused by humans) show organized activities [23]. Other examples are the collective motion at moshpitts at heavy metal concerts [24], crowd disasters [25], but also the more organized wave observed in sports events, the well-known stadium, "La Ola", or Mexican wave [26]. For such a wave, rows of spectators stand up, raise their arms, and sit down again. The neighboring rows, which have not risen yet, will follow the same behavior and thus a wave moves through the spectator rows.

Fig. 6 Human spiral performed by about 550 people. The spiral is created by elevating yellow pages (enhanced for visualization). Image from video at https:// youtu.be/172yzGdEa6o

In contrast to a moving front, the largest spiral *with* humans so far has been performed by approximately 550 students, staff, and faculty at Georgia Institute of Technology in Atlanta, GA, USA (video on https://youtu.be/172yzGdEa6o) [27].

The spiral wave is formed with exactly the same rules as in the stadium wave, however for its initiation only a break is required in the symmetry of the propagating wave. Just as in the case of spiral waves in RD systems, a wave needs to be allowed to propagate in only one direction at the start to curl in [27] as shown in Fig. 6.

When a spiral wave is formed by the crowd, it will not stop and continue to rotate until the crowd gets tired. In some cases when some participants do not follow the rules in time, that is they are a bit too slow or a bit too fast, the spiral wave can break into multiple ones and lead to a chaotic dynamics with multiple waves in the system. This is equivalent to what happens in the heart when electrical waves break and there is a transition to fibrillation (see chapter **Spiral Waves in the Heart**).

References

1. M. Williamson, K.C. Brown, The analysis and modelling of British invasions. Phil. Trans. R. Soc. Lond. B **314**, 505–522 (1986)
2. D. Escaff, C. Fernandez-Oto, M.G. Clerc, M. Tlidi, Localized vegetation patterns, fairy circles, and localized patches in arid landscapes. Phys. Rev. E **91**, 022924 (2015)
3. Y. Yamazaki, T. Ikeda, H. Shimada, F. Hiramatsu, N. Kobayashi, J. Wakita, H. Itoh, S. Kurosu, Mi. Nakatsuchi, T. Matsuyama, M. Matsushitatitle, Periodic growth of bacterial colonies. Physica D **205**, 136–153 (2005)
4. A.B. Carey, R.H. Giles Jr., R.G. McLean, The landscape epidemiology of rabies in Virginia. Am. J. Trop. Med. Hyg. **27**, 573–580 (1978)
5. G. Christakos, R.A. Olea, New space-time perspectives on the propagation characteristics of the Black Death epidemic and its relation to bubonic plague. Stoch. Environ. Res. Risk Asses. **19**, 307–314 (2005)
6. A. Scott, *Biology of Plagues - Evidence from Historical Populations* (Cambridge University Press, Cambridge, 2001)
7. E. Pervolaraki, A.V. Holdentitle, Spatiotemporal patterning of uterine excitation patterns in human labour. Biosystems **112**, 63–72 (2013)
8. G. Seiden, S. Curland, The tongue as an excitable medium. New J. Phys. **17**, 033049 (2015)
9. L. Glass, Dynamical disease: challenges for nonlinear dynamics and medicine. Chaos **25**, 097603 (2015)
10. B. Picciani, S. Lavinas, T.A. Domingos, T. Teixeira-Souza, V.C.B. dos Santos, H.F.S. Gonzaga, J. Cardoso-Oliveira, A.C. Gripp, E.P. Dias, S. Carneiro, Geographic tongue and psoriasis: Clinical, histopathological, immunohistochemical and genetic correlation - a Literature review. Anais Brasileiros de Dermatologia **91**, 410–421 (2016)
11. H. Prinz, Wandering rash of the tongue. Dent. Cosmos **69**, 272–275 (1927)
12. J.D. Shulman, Prevalence of oral mucosal lesions in children and youths in the USA. Int. J. Paediatr. Dent. **15**, 89–97 (2005)
13. J. Liang, P. Huang, H. Li, J. Zhang, C. Ni, Y. Wang, J. Yirong, C. Shen, L. Li, J. Kang, H. Chen, Z. Zhang, Z. Wang, M.Li Zhang, Z. Yao, Mutations in IL36RN are associated with geographic tongue. Hum. Genet. **136**, 241–252 (2017)
14. J.D. Shulman, W.M. Carpenter, Prevalence and risk factors associated with geographic tongue among US adults. Oral Dis. **12**, 381–386 (2006)
15. E. Grosshans, F. Gerber, Cinétique des lésions de la langue géographique (Kinematics of lesions in geographic tongue). Ann. Dermatol. Venereol. **110**, 1037–1040 (1983)

16. V.S. Zykov, Analytical evaluation of the dependence of the speed of an excitation wave in a two-dimensional excitable medium on the curvature of its front. Biophys. **25**(5), 906–911 (1980)
17. N. Suzuki, M. Hirata, S. Kondo, Traveling stripes on the skin of a mutant mouse. Proc. Natl. Acad. Sci. USA **100**, 9680–9865 (2003)
18. F.-J. Darier, De l'érythème annulaire centrifuge (érythème papulo-circineé migrateuse et chronique) et de quelques éruptions analogues [Erythema annulare centrifugum (migratory and chronic papulo-circulatory erythema) and some similar eruptions]. Annales de dermatologie et de syphilographie **5**, 57–58 (1916)
19. A. Afzelius, Verhandlungen der Dermatologischen Gesellschaft zu Stockholm, Sitzung vom 28. Oktober 1909 [Proceedings of the Dermatological Society in Stockholm, Meeting 28 October 1909]. Archiv für Dermatologie und Syphilis **101**, 404 (1910)
20. B. Lipschütz, Über eine seltene Erythemform (Erythema chronicum migrans) [Concerning a rare form of erythema (erythema chronicum migrans)]. Archiv für Dermatologie und Syphilis **118**, 349–356 (1913)
21. A. Afzelius, Erythema chronicum migrans. Acta Dermato-Venereologica **2**, 120–125 (1921)
22. F. Haudin, J.H.E. Cartwright, F. Brau, A. De Wit, Spiral precipitation pattern in confined chemical gardens. Proc. Natl. Acad. Sci. USA **111**, 17363–17367 (2014)
23. D. Helbing, Traffic and related self-driven many-particle systems. Rev. Mod. Phys. **73**, 1067–1141 (2001)
24. J.L. Silverberg, M. Bierbaum, J.P. Sethna, I. Cohen, Collective motion of humans in mosh and circle pits at heavy metal concerts. Phys. Rev. Lett. **110**, 228701 (2013)
25. D. Helbing, A. Johansson, H. Al-Abideen, Dynamics of crowd disasters: an empirical study. Phys. Rev. E **75**, 046109 (2007)
26. I. Farkas, D. Helbing, T. Vicsek, Social behaviour: Mexican waves in an excitable medium. Nature **419**(4903), 131–132 (2002). https://doi.org/10.1038/419131a
27. A.J. Welsh, E.F. Greco, F.H. Fenton, Dynamics of a human spiral wave. Phys. Today **70**, 78–79 (2017)

Yet More Spirals

Thomas Mair, Markus A. Dahlem and Stefan C. Müller

Abstract Having presented several systems in which biologically and medically relevant processes induce rotating spiral waves, we add several more examples of comparable nature: glycolytic waves in yeast, calcium waves in egg cells, wave-like patterns during spreading depression, and spiral waves in the epileptic neocortex.

1 Glycolytic Oscillations

Rhythmicity is a common phenomenon of life, as we know from our daily experience. It occurs on all levels of biological organization and in a wide range of temporal and spatial scales. It is well known that cells and organs respond frequently to perturbations in their environment by rhythmic changes of cellular activity. Such a response requires the exchange of information between the cell and the environment and subsequent information processing within the cell. Obviously, oscillatory reactions can have important impact on biological information processing, the oscillations being a measure of time and/or signal strength.

Temporal oscillations in glycolysis were one of the first metabolic rhythms to be intensively studied since the early sixties [1]. The degradation of sugar (mostly glucose) to pyruvate via glycolysis represents the primary process for the genera-

T. Mair, Deceased author

M. A. Dahlem
Medical Affairs, Newsenselab GmbH, Blücherstraße, 10961 Berlin, Germany
e-mail: dahlem@newsenselab.com

S. C. Müller (✉)
Institute of Physics, Otto von Guericke University Magdeburg,
Universitätsplatz 2, 39106 Magdeburg, Germany
e-mail: tsuji-mueller@t-online.de

Fig. 1 Oscillating absorption signals in a cell-free extract from yeast cells under glucose input. The molecule NADH serves as an indicator absorption for 340 nm [2]
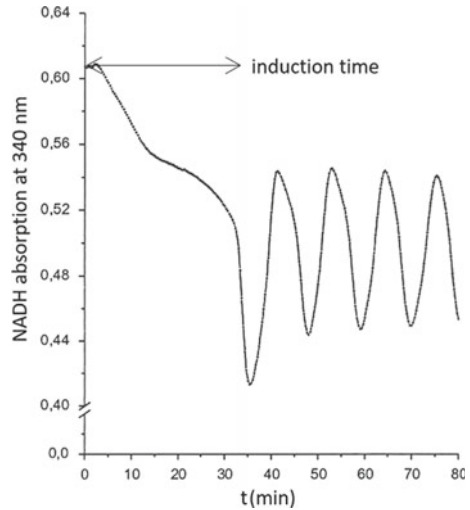
tion of energy in all living cells, except for a few bacteria. Glycolysis is intimately connected with many different pathways, thus representing a complex metabolic network. An important interconnected pathway is that of nicotinamide adenine dinucleotide (NAD), which in its reduced form NADH offers to measure the course of the reaction via absorption or fluorescence recordings. One observes, within concentration limits of appropriate effector molecules, autonomous glycolytic oscillations (Fig. 1). Thus, we have a classical example for self-organization in a biochemical system with intricate regulatory mechanisms.

Glycolysis as the enzymatic reaction chain for degragation of sugar to form alcohol (e.g. in yeast) or lactate (e.g. in muscle), gains during this process a high amount of energy in form of 2ATP = 64.6 kJ/mol (ATP: adenosine triphosphate). The main "actors" in the chain are: PFK = phosphofructokinase and PK = pyruvate kinase. Both enzymes are allosteric, i.e., their activity follows a sigmoidal characteristics and is cooperative. The activity of such enzymes depends in a nonlinear way on the substrate and product concentrations. They are apt to be influenced by the action of certain effector molecules and thus develop specific dynamical behavior.

An important step was taken, when propagating activity waves were demonstrated to occur in an extract from yeast embedded in an agarose gel (1.5%) containing a sufficient amount of trehalose as the substrate. (Trehalose is a disaccharide degraded at a much slower speed than glucose or other disaccharides like normal sugar.) The reaction does not take place uniformly in an extended layer, but the random initiation of waves under these conditions can be controlled by contacting the reaction gel with a small gel piece containing a high concentration of ADP (adenosine diphosphate). The subsequent propagation of a front can be seen in Fig. 2.

In a further step the occurrence of a rotating spiral wave could be shown. We notice in Fig. 3 the characteristic dynamics of two counter-rotating waves of excitation: they annihilate upon collision (image b), form a small segment of excited solution
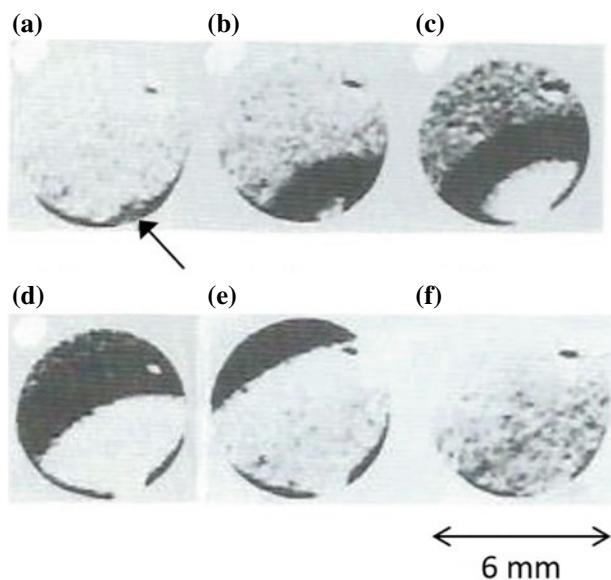
Fig. 2 Propagation of a chemical wave in a glycolytic gel. Time interval of pictures is 4 min. The wave started at the point stimulated with ADP, shown by an arrow in (**a**), lower right [3]. Reprint permission from Elsevier
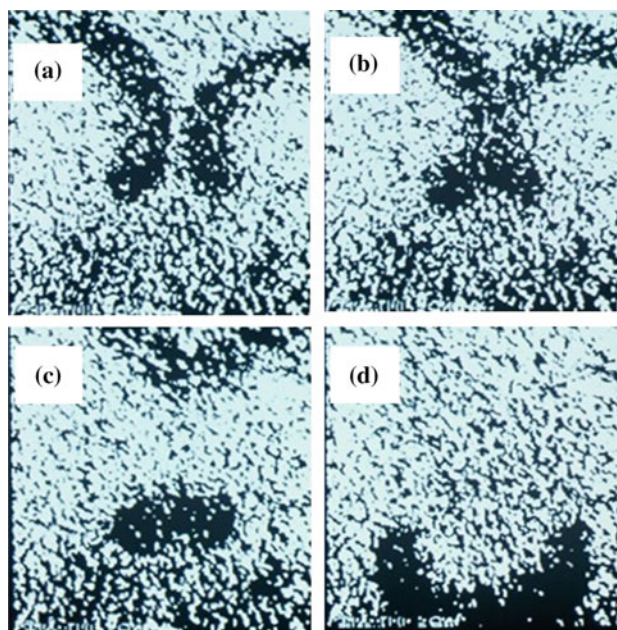
Fig. 3 Absorption image of the NADH distribution in a glycolytic spiral pair embedded in a thin layer of agarose gel. Reproduced from [4] with permission from the Royal Society of Chemistry

(image c) out of which a new spiral pair emanates (image d) [4]. In this experiment the initial breakup for the formation of a wave was undertaken by adding a small amount of activator fructose-2,6-bisphosphate for the enzyme PFK. This leads to the formation of a circular wave. The initial conditions for the spiral pair in Fig. 3 were due to a spontaneous breakup of a circular wave.

A possible function of glycolytic waves: they are not confined by cell boundaries, which is different from many other biological waves. Glycolytic waves provide energy instead of consuming it, and therefore, are possibly involved in the genesis of biological structures. Such properties might also have been of primary importance for the generation of a first primitive cell from an organic solution during the early days of evolution. Of course, the ancestor of the glycolytic pathway was surely constructed in a simpler way than the one we know from today's organisms. However, this does not exclude the fact that similar behavior and properties were active in a simple ancestor of glycolysis [5].

2 Calcium Waves

Oscillatory glycolysis has been taken as a suitable biochemical model to approach mechanisms for other periodic phenomena in biology, i.e. the peroxidase-oxidase reaction in horseradish, or in neuronal, cardiac and hormonal rhythms, as well as calcium oscillations [6]. Intracellular calcium is a ubiquitous second messenger. Its significance for maintaining control of cell functions and its role in signal transduction have been studied in detail [7]. In some cells the calcium activity is oscillatory, but also spatially distributed. A well known and intensively studied system are *Xenopus laevis* oocytes, egg cells of a frog, with a typical diameter of up to 1 mm, in which the intracellular milieu behaves as a regenerative excitable medium. Consequently,

Fig. 4 Spiral Ca^{2+}-wave pattern observed in *Xenopus laevis* oocytes (wavelength 60 μm, period 3 s). Ca^{2+}-release is mediated by IP_3 (inositol-trisphosphate) and detected by confocal laser scanning microscopy [8]. Reprint permission from Elsevier
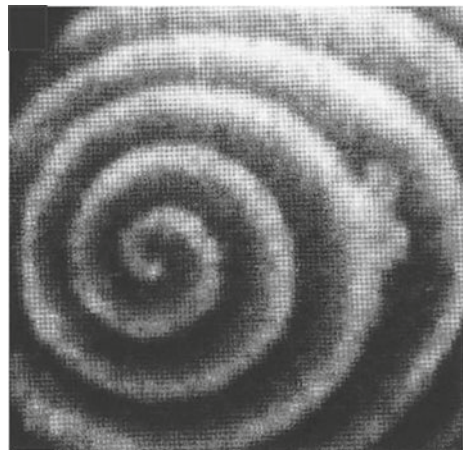
spiral waves of release of free Ca^{2+} were observed [8]. In Fig. 4 we present a confocal microscopic image of a calcium spiral as a proof for intracellular spatiotemporal dynamics of important biochemical variables.

3 Travelling Waves of Spreading Depression

We turn to the description of a spatiotemporal phenomenon with possible implications for dynamical diseases: spreading depression (SD) [9, 10]. This phenomenon occurs in all gray matter regions of the central nervous system (CNS) and has even been observed in the spinal cord. SD is named after early observations of a propagating transient depression of electric activity. Today, it is better characterized by a dramatic failure of ion homeostasis associated with the depression. In the cortex it has been often linked to the aura of classic migraine [11]. Moreover, it has common features with other patho-physiological disorders of brain tissue, as for example ischemia or anoxia. In addition, an interplay between SD and epilepsy has been reported [12]. From a biomedical point of view the intensive research of SD over the last half century is justified due to its pathological implications.

There is little doubt that SD belongs to the class of phenomena that are known as reaction-diffusion processes in excitable media. We know of standard wave propagation in these media, namely the propagation of circular or spiral-shaped waves. Since the discovery of retinal SD, many investigations have been performed with the isolated chicken retina. It is comparable to the cortex, at least with respect to its layer structure. This system combines several experimental advantages. Foremost, an intrinsic optical signal (IOS) with high amplitude is associated in the retina with SD. Changes in the optical properties of the retina during a SD attack can be seen with the naked eye as a milky wave front on a dark background [13]. The transition from transparent to milky tissue is likely to be caused by cell swelling. The chicken retina
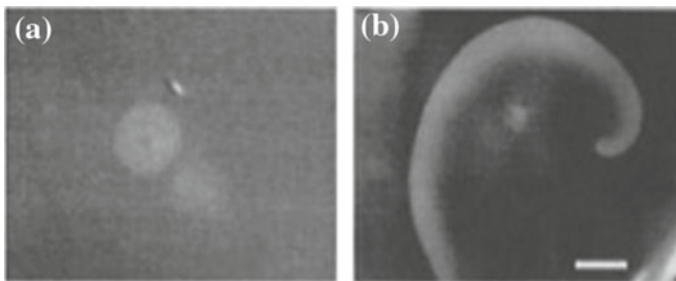
Fig. 5 Spreading depression waves in the chicken retina. **a**: Outward expanding circular wave; **b**: rotating spiral-shaped wave, induced by break-up of a circular wave front. Scale bar = 1 mm [10]. Reprint permission from Springer Nature

lacks a vascular system. Consequently, SD waves propagate through an essentially homogeneous system.

Spreading depression can be elicited by mechanical, electrical and chemical stimuli in all gray matter regions of the CNS. In the chicken retina, the susceptibility to SD is comparably high. Gently touching the retina with a sharp glass needle (diameter 50 μm) initiates an outward traveling SD wave. Tetanic electrical stimulation can also provoke SD, but it may trigger epileptiform seizures, too. The retina can be considered in good approximation as a naturally two-dimensional slice of nervous tissue. The possible topologies of wave patterns are restricted to rotating spirals and target patterns (concentric circles) known from well-investigated chemical model systems (see chapter **Chemical Oscillations and Spiral Waves**). Video image microscopy of excitation waves in the retina yields images as shown in Fig. 5, a circular (Fig. 5a) and a spiral-shaped (Fig. 5b) wave front of SD.

The refractory zone in the back of an excitation wave, where no new activation can occur, is characterized by the regeneration of the tissue. In the retina, the absolute refractory period is about 2.5 min corresponding to a wave distance of 10 mm, the wave velocity being 4 mm/min. The propagation dynamics of excitation waves, as for example the trajectory of spiral tips, is strongly affected by the size of the refractory zone.

For spiral waves it is important to analyze the properties of the spiral tip and its dynamical evolution. Common examples that one finds in excitable media are rigid rotation (circular trajectory) and meandering (compound trajectory). See **Generation of Spirals in Excitable Media**. A rotating spiral of retinal spreading depression has a more complex trajectory. Figure 6 shows an example obtained from a 10 min recording. We note from this trajectory that the motion of the spiral tip in this particular neuronal medium consists of a sequence of Z-type rotations, where four spiral rotations share almost the same pivot. The Z-shape points to some characteristic properties of the investigated system, which have to be elucidated by further investigations.

Fig. 6 Pattern of a spiral tip trajectory of the SD wave in chicken retina derived for four spiral rotations. Arrows indicate the direction of movement [10]. Reprint permission from Springer Nature
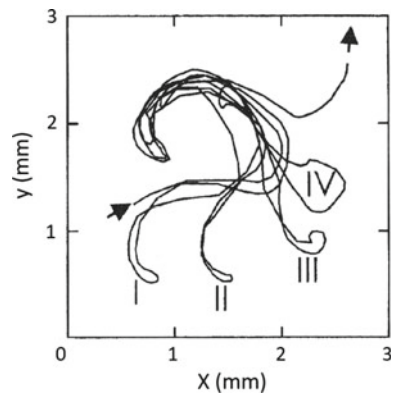
Fig. 7 Parameter space of an active medium, separated by bifurcation lines that mark sudden changes in the spatiotemporal patterns [14] (for details see text). Reprint permission from Elsevier
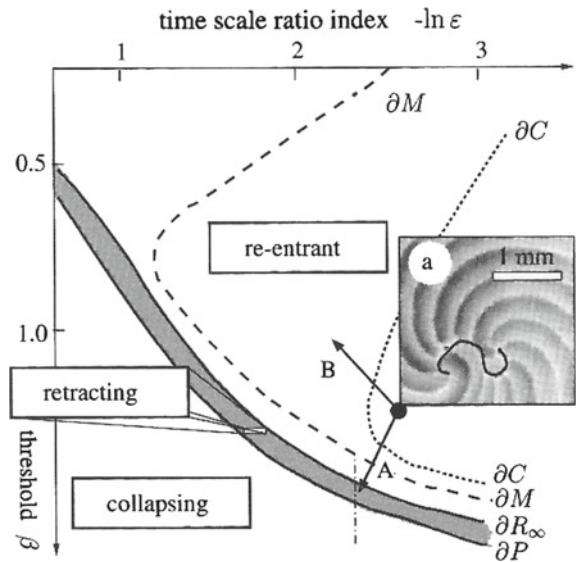
A generic reaction-diffusion model of the activator-inhibitor type, the Hodgkin-Grafstein model of SD [14], has been proposed, which can explain the emergence and transition between different spatiotemporal wave patterns in two spatial dimensions. In fact, one finds, depending on certain parameters of the model not to be specified here, that in the excitability plane of Fig. 7 certain bifurcations mark the emergence of specific spatiotemporal patterns. We note the existence of bifurcation lines ∂C, ∂M, ∂R_∞ and ∂P. They separate the different patterns in SD wave propagation from complex, meandering, and rigidly rotating spiral patterns, forming on the left of the corresponding bifurcation lines. When the propagation boundary ∂P is crossed, the medium becomes non-excitable, i.e., waves collapse. To the left of ∂P the system is non-excitable. The inset (a) shows the predicted location of a retinal spiral-shaped SD wave with the typical Z-shaped tip trajectory.

One finds in experiments that some of the emerging patterns can be seen in SD by observing the spiral tip dynamics and thus probing the tissue excitability and locate the occurrence of the patterns in the excitability plane of Fig. 7.

Implications for the Aura of Classical Migraine

Individuals suffering from classical migraine report an astonishing diversity of migraine aura [11]. A frequently reported symptom is a visual hallucination known as fortification illusion or zig-zag pattern (see Fig. 8a). Many migraine patients have illustrated such patterns appearing in the visual aura, some of them with an artistic touch [15]. The characteristic form and development of the fortification illusion suggests that the underlying phenomenon is a wave propagating through the primary visual cortex, possibly the cortical spreading depression (CSD). In fact, the first attempt to connect migraine with a cerebral propagation phenomenon was made

Fig. 8 a: Sketch of the fortification illusion drawn by Karl Lashley [16]. The kidney shaped visual disturbance exhibits a typical zig-zag pattern at its convex side, while the inner part corresponds to a scotoma (blind area). **b**: Simulation of the fortification illusion. Multiple bars with white margins were plotted in the order of their dominance. The pattern resembles a snapshot of a fraction of the moving zig-zag front [19]. Reprint permission from Springer Nature

by Lashley [16] 3 years before SD was discovered. While suffering from attacks of classical migraine, Lashley calculated, from knowledge of the retino-cortical projection, the speed of the traveling scotoma to be about 3 mm/min in the visual cortex. This result fits perfectly with the measured velocity of a SD wave, as noted by Milner [17]. The demonstration of unique changes of cerebral blood flow during attacks of migraine with aura have been replicated in animal experiments during CSD and thus constitute another important line of support for the SD theory. We have proposed that the perceived migraine hallucinations are generated by a planar excitation wave (CSD-like event) propagating across the primary visual cortex (V1), and that the peculiar zig-zag front of the fortification illusion reflects the cortical organization of orientation preference. Blind area would then be a consequence of refractoriness behind the front.

V1 is retinotopically organized such that stimulating neighboring points in the visual field leads to activation of neighboring neurons in the cortex. Another major functional property of visual cortical neurons is their orientation selectivity, i.e., the fact that the cells fire maximally, when a contour of a particular orientation appears within their receptive field. The layout of orientation preference in the visual cortex is characterized by iso-orientation domains that are arranged around centers in a pinwheel-like fashion [18].

Löwel and her colleagues have constructed an orientation preference map for neurons in the primary visual cortex from cats, using optical imaging of intrinsic signals. Based on this map, we have calculated the average orientation vector **v** for several fragments of this map [19]. These vectors were represented by a bar that was rotated such that its orientation was parallel to the direction of the vector. The magnitude of the vector is a measure of dominance among the fragments. The orientations were plotted as bars, each at its spatial location. Since the bars now possibly intersect, they were plotted in the order of their dominance on top of each

other as white-black-white steps, representing the basic structure of the receptive field of simple cells in V1. The resulting pattern is illustrated in Fig. 8b. It displays features of the fortification illusion: distinct domains of roughly parallel lines are present, each domain having a specific angle with respect to the adjacent domain. Our simulations led us to predict, that the zig-zag pattern perceived by individuals suffering from classical migraine reflect the organization of their visual cortical orientation map.

The simulation of the fortification illusion during a migraine attack is solely based on the idea of a reaction-diffusion wave traveling across the primary visual cortex, i.e., a nonlinear phenomenon, and the functional behavior of the underlying tissue. From a biomedical point of view it is of primary interest to control the propagation dynamics of the waves and/or to suppress their generation in order to prevent the migraine attacks. Such an external control should be possible by means of the well established methods from nonlinear dynamics, in particular, feed back control [20]. However, more knowledge about the basic mechanisms of spreading depression is required in order to apply such methods. The nature of the activating and of the inhibiting processes as well as the feed-back loops for the oscillatory reaction must be known. Deeper insights into the biochemical mechanisms of SD are necessary that determine the function and regulation of this complex phenomenon on a cellular level.

4 Spiral Waves in the Epileptic Neocortex

Epilepsy is a neurological condition characterized by sudden, recurrent episodes of synchronized neuronal activity. This pathological dynamic state in the neurocortex causes behavioral disturbances and abnormal movements. Typically, epileptic seizures show abnormal waveforms of electric potential in extended regions of the brain. Using electroencephalography (EEG), such seizures have been recorded for decades and their observations constitute a significant part of clinical diagnosis and treatment. Over the last years additional powerful methods have been applied to investigate such dynamics, including connectivity measures (correlation, causality, synchrony), spatiotemporal pattern recording and analyses, and modelling based on model neurons [21, 22].

In the context of this chapter we briefly demonstrate that spiral activity has been detected during epileptic seizures. This has been done in slices of neocortex within a certain area by applying voltage-sensitive dye imaging (see Fig. 9). In many cases experiments were performed *in vivo*, for instance, with epileptic Mongolian gerbils, but in other cases preparations were used in which a simplified state is evoked by using pharmacological agents for blocking certain receptors, a quite common method in "mesoscopic neurophysiology [23]". The inhibitor bicuculline and the cholinergic agonist carbachol create clear oscillatory or epileptiform states and are thus well suited to the analysis of spatial connectivity and propagation.

The weakly coupled oscillatory state induced by the mentioned inhibitors shows that spiral dynamics can serve as a stable organizing principle for mesoscopic activity
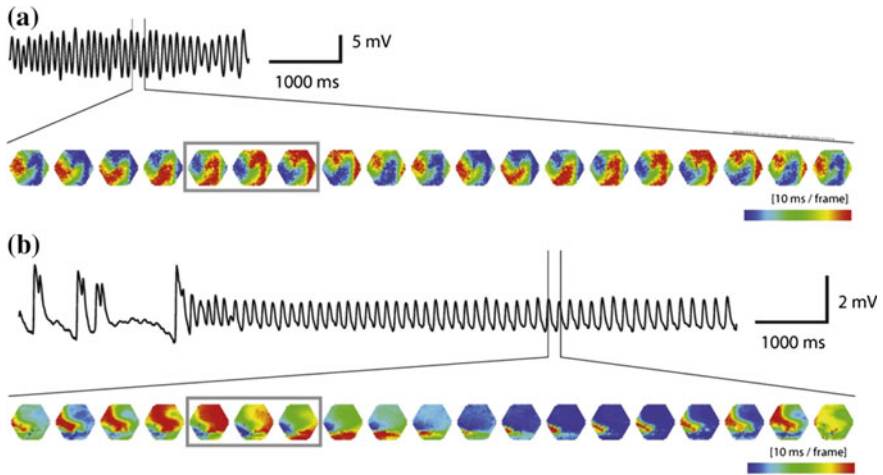
Fig. 9 Spiral rotation in the neocortex visualized by voltage-sensitive dye imaging. **a**: An example of stable spiral dynamics in a slice preparation treated with carbachol and bicuculline; **b**: in an epileptiform intact cortex from an epileptic Mongolian gerbil, recorded through a craniotomy [24]. Reprint permission from Elsevier

within the cortex (Fig. 9) [24]. On the other hand, the spiral patterns observed with the Mongolian gerbils suffering from epilepsy are much less stable *in vivo* than in drug-treated slice preparations. That may explain why *in vivo* the phenomenon had only little chance to be discovered at all.

Over the last decades, dynamical systems theory and computational modelling has largely progressed to characterize the nature of seizure-like activity [25]. Computational models have been employed to describe epileptic rhythms, especially in terms of nonlinear dynamics. For instance, starting from simplified models of population dynamics macroscale features of epileptic seizures can be described. Such simple models usually do not have a direct correlate in brain anatomy or physiology, but rather capture more abstract features of the brain. Then, the effects of individual parameters are easier to be interpreted [26, 27].

Nevertheless, the underlying pathophysiological mechanism and their relationship to the observed seizure phenomena are still not well understood.

References

1. B. Hess, A. Boiteux, Oscillatory phenomena in glycolysis. Annu. Rev. Biochem. **40**, 237–258 (1971)
2. T. Mair, Private communication
3. T. Shinjyo, Y. Nakagawa, T. Ueda, Hierarchic spatio-temporal dynamics in glycolysis. Physica D **84**, 212–219 (1995)
4. T. Mair, C. Warnke, S.C. Müller, Spatio-temporal dynamics in glycolysis. Faraday Discuss. **120**, 249–259 (2001)

5. E. Meléndez-Hevia, T.G. Waddell, R. Heinrich, F. Montero, Theoretical approaches to the evolutionary optimization of glycolysis: chemical analysis. Eur. J. Biochem. **244**, 527–543 (1997)
6. A. Goldbeter, *La Vie Oscillatoire au Coeur des Rythmes du Vivant* (Odile Jacob, Paris, 2010)
7. J. Lechleiter, S. Girard, D. Clapham, E. Peralta, Spiral calcium wave propagation and annihilation in *Xenopus laevis* oocytes. Science **252**, 123–126 (1991)
8. J.D. Lechleiter, D.E. Clapham, Molecular mechanisms of intracellular calcium excitability in *Xenopus laevis* oocytes. Cell **69**, 283–294 (1992)
9. A.A.P. Leão, Spreading depression of activity in the cerebral cortex. J. Neurophysiol. **7**, 359–390 (1944)
10. M.A. Dahlem, T. Mair, S.C. Müller, Spatio-temporal aspects of a dynamical disease: waves of spreading depression, in *Function and Regulation of Cellular Systems: Experiments and Models*, ed. by A. Deutsch, J. Howard, M. Falke, W. Zimmermann, (Birkhäuser, Basel, 2004)
11. M. Lauritzen, Pathophysiology of the migraine aura: the spreading depression therapy. Brain **117**, 199–210 (1994)
12. M. Avoli, C. Drapeau, J. Loevel, R. Pumain, A. Olivier, J.Q. Villemure, Epileptiform activity induced by low extracellular magnesium in the human cortex maintained in vitro. Ann. Neurol. **30**, 580–596 (1991)
13. H. Martins-Ferreira, G. Oliveira de Castro, Light-scattering changes accompanying spreading depression in isolated retina. J. Neurophysiol. **29**, 715–726 (1966)
14. M.A. Dahlem, R. Graf, A.J. Strong, J.P. Dreier, Y.A. Dahlem, M. Sieber, W. Hanke, K. Podoll, E. Schöll, Two-dimensional wave patterns of spreading depression. Physica D **239**, 889–903 (2010)
15. S.D. Silberstein, A. Stiles, W.B. Young (eds.), *Atlas of Migraine and Other Headaches* (Taylor and Francis, London, 2005)
16. K. Lashley, Patterns of cerebral integration indicated by the scotomas of migraine. Arch. Neurol. Psychiatry **46**, 331–341 (1941)
17. P.M. Milner, Note on a possible correspondence between the scotomas of migraine and the spreading depression of Leão Electroencephalography. Clin. Neurophysiol. **10**, 705–706 (1958)
18. T. Bonhoeffer, A. Grinvald, Iso-orientation domains in cat visual cortex are arranged in pinwheel-like patterns. Nature **353**, 420–431 (1991)
19. M.A. Dahlem, R. Engelmann, S. Löwel, S.C. Müller, Does the migraine aura reflect cortical organization? Eur. J. Neurosci. **12**, 767–770 (2000)
20. O. Steinbock, S.C. Müller, Control of spiral waves in excitable media by external perturbation, in *Handbook of Chaos Control*, ed. by H.G. Schuster (Wiley VCH, Weinheim, 1999), pp. 591–614
21. V.K. Jirsa, W.C. Stacey, P.P. Quilichini, A.I. Ivanov, On the nature of seizure dynamics. Brain **137**, 2210–2230 (2014)
22. W.J. Freeman, *Neurodynamics: An Exploration in Mesoscopic Brain Dynamics* (Springer, New York, 2000)
23. K. Takagaki, F.W. Ohl, Coarse-graining to investigate cerebral cortex dynamics, in *Complexity and Synergetics*, ed. by S.C. Müller, P.J. Plath, G. Radons, A. Fuchs (Springer, Cham, 2018), pp. 289–299
24. K. Takagaki, C. Zhang, J.-Y. Wu, F.W. Ohl, Flow detection of propagating waves with temporospatial correlation of activity. J. Neurosci. Methods **200**, 207–218 (2011)
25. W. Lytton, Computer modelling of epilepsy. Nat. Rev. Neurosci. **9**, 626–637 (2008)
26. Y. Wang, M. Goodfellow, P. Taylor, G. Baier, Phase space approach for modelling of epileptic dynamic activity. Epilepsis **44**, 72–83 (2003)
27. P.N. Taylor, M. Goodfellow, Y. Wang, G. Baier, Towards a large-scale model of patient-specific epileptic spike-wave discharges. Biol. Cybern. **107**, 83–94 (2013)

Part V
Concepts for Understanding the Creation of Spirals and Vortices

We are not going in circles, we are going upwards.
The path is a spiral; we have already climbed many steps.

— Hermann Hesse, Siddhartha

Reaction-Diffusion Patterns and Waves: From Chemical Reactions to Cardiac Arrhythmias

Markus Bär

Abstract Reaction-diffusion processes are behind many instances of pattern formation in chemical reactions and biological systems. Continuum reaction-diffusion equations have proved useful models for a wide variety of pattern dynamics starting with seminal work by Turing on the chemical basis of morphogenesis and by Hodgkin and Huxley on the propagation of electrical impulses along neurons in 1952. This article reviews basic concepts for and applications of reaction-diffusion models with an emphasis on spiral and vortex dynamics, related instabilities like spiral and scroll wave breakup and their potential role in cardiac arrhythmias.

1 Patterns in Reaction-Diffusion Systems

Spontaneous pattern formation under natural and laboratory conditions is a trademark of systems far from thermodynamic equilibrium. These systems are typically subject to a constant through flow of matter and energy and can be classified as open and dissipative systems. In closed systems patterns that may emerge initially typically decay in the long run and the systems often approach a featureless, spatially homogeneous state - thermodynamic equilibrium. This is in line with the demands of the second law of thermodynamics: the entropy in a closed system increases until equilibrium is reached. Open systems, however, are not subject to the constraint of the second law - they can export entropy to their surroundings.

Theoretical research has initially focused on the question under which nonequilibrium conditions a system switches from a homogeneous state to a pattern. These transitions are known as instabilities or bifurcations and can be classified [1]. For example, one can distinguish between continuous (supercritical) and discontinuous

M. Bär (✉)
Physikalisch-Technische Bundesanstalt, Abbestr. 2-12, 10587 Berlin, Germany
e-mail: markus.baer@ptb.de

239
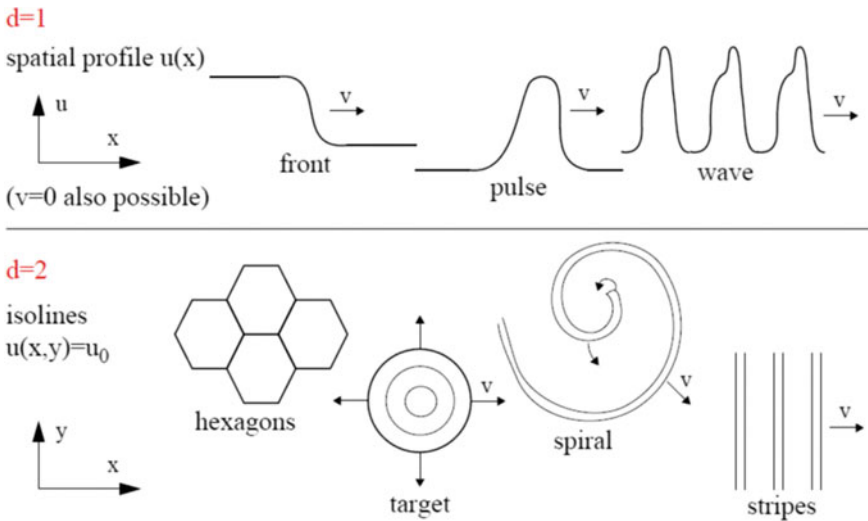
Fig. 1 Examples for simple reaction-diffusion patterns in one, two and three dimensions

(subcritical) instabilities. The emerging pattern may be stationary (Turing instability) or dynamic (Hopf instability) as well as of either periodic or localized nature. In one spatial dimension, periodic stationary patterns are typically stripes, while the range of dynamic patterns comprises traveling and standing periodic waves. In higher dimensions, periodic patterns display various symmetries, e.g. in two dimensions parallel stripes, hexagons and square patterns are known. Localized patterns include traveling and stationary fronts and pulses in one dimension. Some examples are given in Fig. 1.

A rotating spiral represents an interesting combination between a localized and a periodic pattern since it has a well defined pointlike center of rotation (core), from which periodic waves are emitted in all radial directions. In three dimensions, spiral cores in the plane are transformed into lines that are called filaments. If the filament forms a straight line, one speaks of a scroll wave.

2 A Short History of Reaction-Diffusion Systems

The most remarkable property of reaction-diffusion systems is doubtless the spontaneous formation of a great variety of patterns. These structures do not offer only aesthetical pleasure, but can also provide efficient means of communication and signal transmission. For the latter purpose, a reaction-diffusion medium has to be sensitive to small stimuli from the environment and must be able to propagate them in a reliable and fast fashion. Excitable media are particularly well suited for that purpose. They have a stable rest state and a threshold. Perturbations larger than the

threshold may cause a large response, while small perturbations and noise decay immediately. Superthreshold perturbations lead via diffusion to propagation of fast reaction-diffusion waves that transmit information in a reliable fashion. A second important application of reaction-diffusion systems is their ability to form stationary periodic patterns (Turing structures). Such structures a play an important role in morphogenesis and the development of structures in living organism.

The field of reaction-diffusion systems can to a large extent be traced back to two quite different landmark papers published in 1952. British mathematician Turing considered the "Chemical Basis of Morphogenesis" [2] and showed that the interplay of nonlinear reaction and diffusion transport may lead to sustained stationary concentration patterns, henceforth often called "Turing structures". The first example of an excitable medium derived from underlying physico-chemical processes has been provided in 1952 by British physiologists Hodgkin and Huxley. They derived a set of ordinary differential equations neglecting spatial variations from extensive measurements of ionic currents at the membrane of the squid giant axon [3]. Their nobelprizewinning effort is still considered the most successful model in physiology and the basis for many more detailed models of electrical excitation propagation in neurons or in cardiac tissue [4].

The resulting Hodkin–Huxley model accounts for the dynamics of action potentials in neurons. The equations describe the dynamics of the fast membrane potential dynamics and its dependency on the dynamics of slow gating variables for sodium channel activation and deactivation and for potassium channel activation, respectively. The concept of an excitable medium described by continuous variables has found many applications in pattern forming chemical and biological systems [5]. Since the Hodgkin–Huxley equations are coupled nonlinear ordinary differential equations, they have largely resisted analytical treatment and have been mostly studied numerically. A simplified version has been derived by FitzHugh and Nagumo in the early 60s. It is known as the FitzHugh–Nagumo model [6]. One version of it reads

$$\frac{du}{dt} = u^3 + u - v = f(u, v),$$
$$\frac{dv}{dt} = \varepsilon(u - rv + \beta) = \varepsilon g(u, v). \tag{1}$$

Originally, the activator u is derived from the membrane voltage of the Hodgkin–Huxley equations, while the inhibitor v represents a slow gating variable. If one allows for a spatial variation of the variables one can simply add transport by diffusion and obtains a coupled set of nonlinear partial differential equations

$$\partial_t u = f(u, v) + D_u \Delta u,$$
$$\partial_t v = \varepsilon g(u, v) + D_v \Delta v. \tag{2}$$

If one intends to use the FitzHugh–Nagumo model as a description for propagating action potentials, inhibitor diffusion has to be neglected, i. e. $D_v = 0$. The spatiotem-

poral dynamics of these equations is governed by control parameters including ε and the diffusion constants D_u and D_v. The variables are often specified as fast activator (u) and slow inhibitor (v) after Gierer and Meinhardt [7]. A nice feature of the FitzHugh–Nagumo model is that it contains both the Turing patterns and the excitable medium as special cases depending on the choice of the parameters. Requirements for excitation waves are fast activator dynamics ($\varepsilon \ll 1$) and diffusion ($D_u/D_v > 1$) and a suitable form of the functions f and g, whereas Turing pattern require long-range inhibitor diffusion ($D_u/D_v \ll 1$).

A computationally more efficient version of the FitzHugh–Nagumo model for the study of excitable media ($D_v = 0$) has been provided by Barkley [8] and modified by Bär and Eiswirth to study spatiotemporal chaos [9]. Its general form reads:

$$\begin{aligned}
\partial_t u &= \tfrac{1}{\varepsilon} u(1-u)\left(u - \tfrac{b+v}{a}\right), \\
\partial_t v &= h(u) - v.
\end{aligned} \tag{3}$$

Barkley's original version uses a linear inhibitor production $h(u) = u$. For excitable conditions, the medium then has a single homogeneous fixed point $(u, v) = (0, 0)$ like the original FitzHugh–Nagumo model (cf. **Generation of Spirals in Excitable Media**). The modification of Bär and Eiswirth introduces a nonlinear function $h(u)$ for the inhibitor production, that leads to additional unstable homogeneous fixed points. The simple change leads to interesting new nonlinear wave physics including appearance of spatiotemporal chaos via pulse backfiring in one and spiral breakup in two dimension.

Excitable media usually appear near oscillatory regimes. Bistable systems should exhibit fronts between the two stable states that typically travel with constant speed and shape. For excitable conditions, Eq. 3 typically possess one stable fixed point (the rest state) and, depending on the shape of the function $h(u)$ in Eq. 3, zero or two more additional unstable fixed points. For oscillatory conditions, the system of Eq. 3 typically contains only one unstable spatially homogeneous fixed point. Note, that spirals and vortices can occur for excitable as well as for oscillatory and bistable conditions. In the course of the 1960s, the interest for "dissipative structures" in chemical systems started to grow. As a simplification of Turing's model, Lefever, Nicolis and Prigogine suggested the following reaction scheme

$$\begin{aligned}
A &\to U; \qquad\quad B + U \to V + D; \\
2U + V &\to 3U; \quad\; U \to E.
\end{aligned}$$
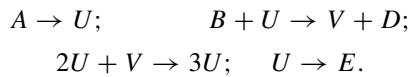
where the concentrations of A and B are used as control parameters and have constant values a and b, respectively. The chemical species U and V play similar roles as activator and inhibitor, respectively, in the FitzHugh–Nagumo and Barkley models. The corresponding reaction-diffusion model is widely known as the "Brusselator" and reads

$$\partial_t u = a - (b+1)u + u^2 v + D_u \Delta u,$$
$$\partial_t v = bu - u^2 v + D_v \Delta v, \tag{4}$$

where $u(x,t)$ and $v(x,t)$ denote the concentrations of U and V. All rate constants have been set to unity. The Brusselator allows for oscillations, if $a > a_C = b^2 + 1$ and $D_u > D_v$, and for a Turing instability, if $D_u \ll D_v$. It has been often used as a prototype model for pattern formation and may serve here as a simple example for a strategy widely used in the modeling of chemical and biological reaction-diffusion systems. First, identify the kinetic scheme for a particular system, second write down the corresponding set of differential equations, third add the relevant transport processes (diffusion) and last but not least look out for bistability as well as dynamic, oscillatory respectively. pattern forming instabilities. Since the arrival of the Brusselator, this strategy has been applied to many systems in homogeneously and heterogeneously catalyzed chemical reaction [10] as well as in biochemical and biological systems [11].

In parallel to the first studies of the Brusselator model, first experimental observations of reaction-diffusion waves in the form of target patterns [12] and spiral waves [13] have been reported in the Belousov–Zhabotinsky (BZ) reaction. The BZ reaction is the oxidation of malonic acid and involves more than 100 chemical species. Nevertheless, Field, Köros and Noyes extracted a core mechanism of the reaction that has become known as the Oregonator model [14]; it explicitly includes only three species and is often even reduced further to a typical two-variable activator-inhibitor form. Until the early 1990s, more and more details of spiral dynamics in the BZ reaction have been investigated [15]. However, many results until then have been limited due to the use of "closed" reaction vessels (see chapter **Chemical Oscillations and Spiral Waves**).

A major breakthrough has been the design and use of open reactors both in homogeneously and heterogeneously catalyzed reactions (see Fig. 2). They allow for steady supply of educts and removal of products, thus maintaining constant concentrations of key species and keeping the system far away from chemical equilibrium. Turing structures have been discovered in 1D and 2D set-ups of the Chlorid-Iodid-Malonic-Acid (CIMA) reaction [16, 17]. The second half of the 1990s has then seen the discovery of further structures under bistable conditions, namely labyrinthine patterns [18] and replicating spots [19]. A second exciting line of research in pattern-forming chemical systems originated from the study of reaction on catalytic surfaces [20–22] after 1990 (see chapter **Shedding Light on Chaos - Controlling Surface Reactions**). Catalytic reactions can be operated under a wide range of external conditions regarding pressure and temperature and they are truly two-dimensional (Fig. 2, right).

The use of open reactors also enabled a systematic study of transitions between stable spirals and spatiotemporal chaos in experiments [23–25], in the next section we will adress the theoretical understanding of these phenomena.

Another important field where reaction-diffusion processes play a prominent role are nonlinear waves and pattern formation in biological systems. Pioneering experiments in aggregating slime mold colonies revealed spiral waves of chemoattractant
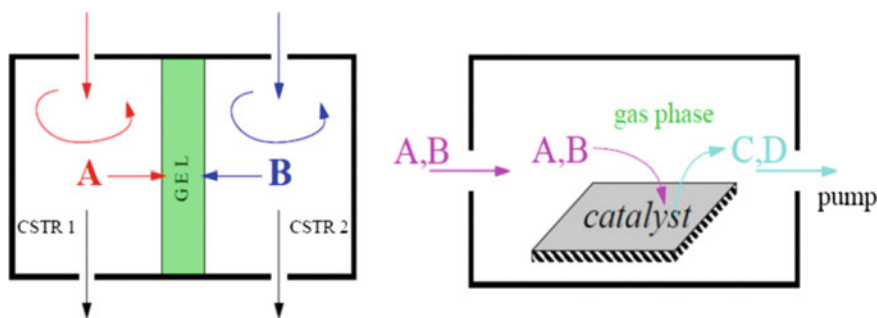
Fig. 2 Sketch of open reactor types used in homogeneous catalysis. Left: continuously fed unstirred reactor (CFUR) with two continuously stirred tank reactors (CSTR), right: in heterogeneous catalysis

in the early aggregation stage [26]. By now the whole cycle of aggregation and the spatial patterns associated with its stages have been thoroughly studied [27, 28] (see chapter **Spiral Waves of the Chemo-Attractant cAMP Organise Multicellular Development in the Social Amoebae**). Another frequently studied example of reaction-diffusion behavior in biology are intracellular calcium waves [29, 30] (see **Yet More Spirals**). Somewhat surprisingly, the simple activator-inhibitor picture as well as the concept of an excitable medium could be applied to many of these examples.

Since 2000, a dominating theme in biological reaction-diffusion systems have been the discovery and investigation of intracellular protein patterns, most prominently standing and traveling waves of the so-called Min proteins found in *in-vivo* experiments of *Escherichia Coli* bacteria [31] and *in-vitro* experiments of a reactive solutions of Min proteins at lipid monolayers [32]. Since the Min patterns are crucial in the regulation of cell division, many theorists have worked to obtain quantitative models for this system; for reviews see e.g. [33, 34]. In general, it seems that protein patterns can often be explained by models that assume a total conservation of one or more protein species [34] which clearly distinguishes these system from chemical reactions in open reactors subject to a constant throughflow of reactants and products. In chemical pattern formation a prominent direction after the year 2000 was control of patterns e.g. by tuning of diffusion coeffients in microemulsions [35] or by feedback strategies [36, 37]. Finally, the decade after 2000 also lead to detailed studies of scroll waves [38, 39] and Turing patterns in 3D [40] in BZ systems.

3 Instabilities of Spiral and Scroll Waves: From Chemical Reactions to Arrhythmias in the Heart

An important motivation for the study of excitable media has been the quest for the cause of irregular high-frequency electrical activity in cardiac muscle typically observed during ventricular and atrial fibrillation [41]. The reason for the onset

of ventricular fibrillation as well as possible treatments remain subjects of intense experimental and theoretical research. Rotors (or spirals) of electrical excitation are still in the focus of researchers addressing cardiac arrhythmias and dynamical diseases such as atrial and ventricular fibrillation, see [42] and the chapter **Spiral Waves in the Heart** in this book. Over the years many different aspects of cardiac dynamics have been linked with theory of reaction-diffusion systems and nonlinear dynamics; for recent reviews see e.g. [43–45].

Early experiments in thin sheets of heart tissue displayed only stable spirals in contrast with the irregular activity seen in experiments with whole hearts. In addition, hearts with small mass and, in particular, small wall thicknesses were found not to support irregular spiral turbulence-like electrical dynamics. Consequently, Winfree suggested that irregular activity in the heart might be a genuinely 3D phenomenon [46]. In parallel, the phenomenon of spiral breakup has emerged as a candidate mechanism for ventricular and atrial fibrillation and shall be briefly reviewed in this section. For a comprehensive discussion of spiral breakup in simple models and chemical reactions, compare [47].

3.1 Breakup of 2D Spirals

In excitable reaction-diffusion media, the mechanism of spiral breakup has been linked to radial instabilities that are observed frequently in cardiac models [43–45, 48], typically unstable modes in the radial direction cause spiral instability and possibly breakup. In what follows, we shall concentrate mostly on destabilization against modes in the radial direction, since these are the most relevant ones for cardiac dynamics exhibiting spiral breakup. Simple equations like Eq. 4 have been found to contain transitions directly from stable rotation to spatiotemporal chaos via spiral breakup. These examples have been also at the focus of a number of papers employing numerical stability analysis (see [9, 49]). As a result it is now firmly established that spiral breakup results from a linear instability of the stable rotating spiral.

It is crucial to note that in all examples of radial spiral breakup in reaction-diffusion models and related experiments two different scenarios are observed: spirals may break first close to their core or alternatively far away from the core, see Fig. 3. The core breakup in Fig. 3a is accompanied by a meander instability, which introduces a Doppler effect into the waves emitted from the spiral core. Breakup near the core is found in simulations in excitable media [9, 47] and in experiments with a chemical reaction [24], whereas breakup far away from the core as in Fig. 3b is typically seen under oscillatory conditions both in chemical experiments [23, 25] and in simulations of the complex Ginzburg-Landau equation (CGLE) [50] and of oscillatory reaction-diffusion systems [47].

(a)

(b)
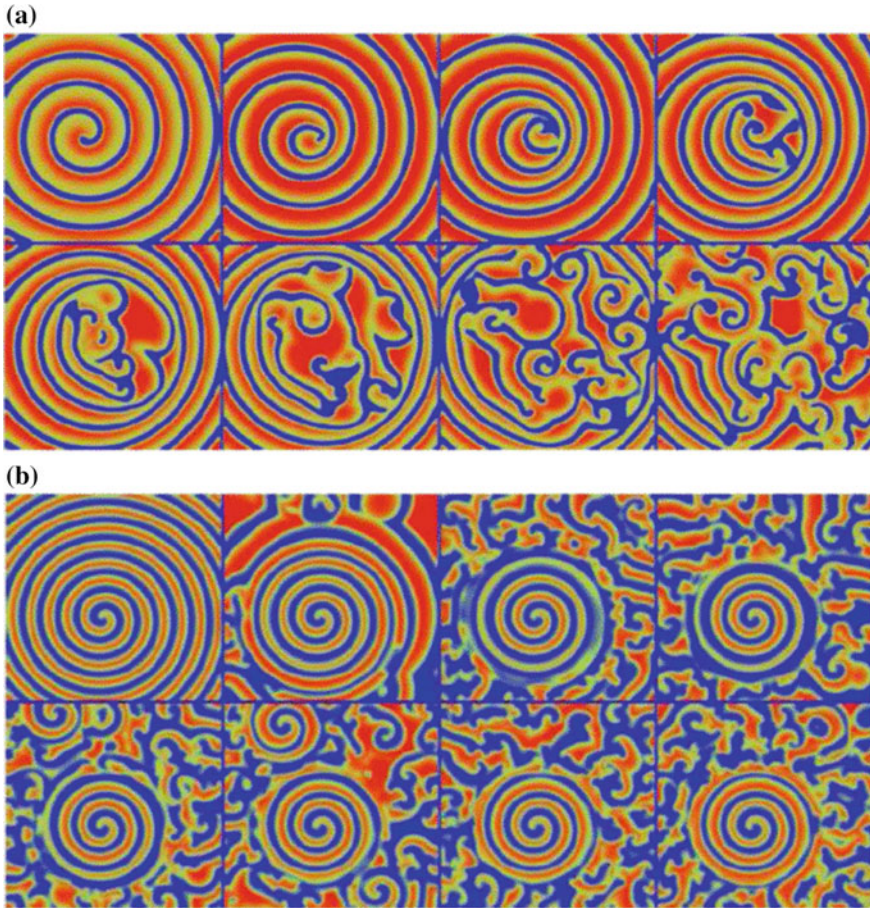
Fig. 3 Two different scenarios of spiral breakup shown at different stages in time. Both scenarios lead to irregular dynamics. **a** The breakup appears first close to the center and spreads then outward. **b** The breakup appears first far away from the center. At the end, a stable spiral fragment with finite radius is left, surrounded by a "turbulent" bath. The figures show simulations of the model, Eq. 4. (Taken from [47])

3.2 Breakup of 3D Scroll Waves

The natural extension of spiral waves in two dimensions are scroll waves in three dimensions. Straight scroll waves rotate with constant frequency. However, under certain conditions the filament of the scroll is not straight but takes a helical shape under meandering or when an external twist is imposed. Complex unstable dynamics may occur if the tension of the filament is negative. Three-dimensional waves rotate around the center filament.
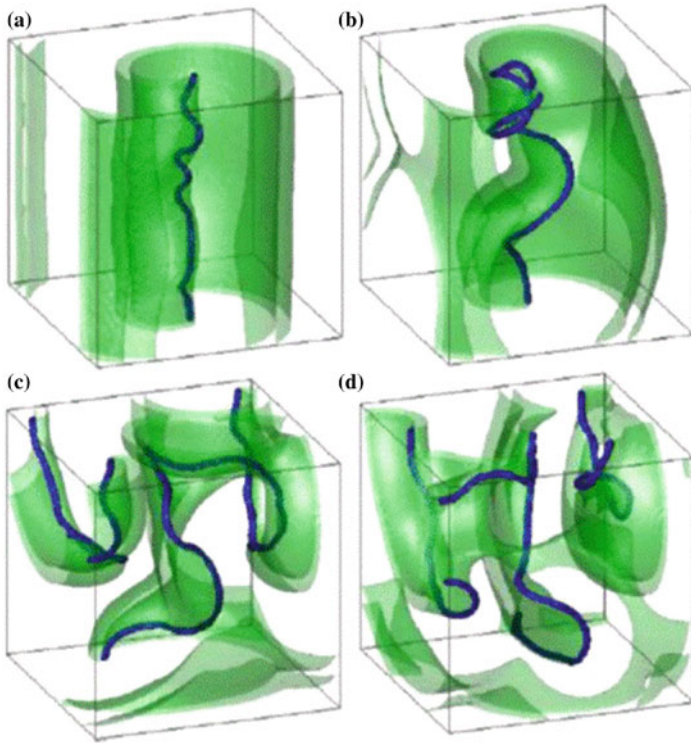
Fig. 4 Numerical simulations of a scroll wave with negative filament tension: **a** initial deformed filament, **b** bending of the filament, **c** breakup of the filament at the boundaries, **d** stationary chaotic dynamics. Simulations done with the Luo-Rudy model for excitation propagation in cardiac tissue (taken from [45])

Even if the scroll filaments are just convenient mathematical entities, their dynamics permits to assign them physical magnitudes like tension. An illustration how negative line tension of filament leads to scroll wave breakup and subsequent turbulent dynamics is given in Fig. 4. An initial almost straight filament develops a wiggly structure whose amplitude grows in time. Once, the filament hits the boundaries of the container the scroll waves break and irregular dynamics ensues (cf. Fig. 4); for a more extensive discussion see e.g. [45].

3.3 Breakup in Heterogeneous Excitable Media

Small-scale heterogeneities are inevitable and omnipresent in cardiac tissues. This is due to the variability of individual cells, the presence of different cell types as well as the potential inclusion of non-functional fibrotic cells inside otherwise

healthy tissue. Another factor is the discrete nature of the tissue that is composed of myocytes separated by extracellular space filled with interstitial fluids. If the fraction of non-conducting cells reaches fractions close to the percolation threshold where the conducting parts of the tissue become disconnected. An example how reentry appears in a discrete heterogeneous model for cardiac tissue near the percolation threshold is shown in Fig. 5 [51].

The wave has already quite an irregular shape with a rough interface and many holes. For the realization of a random medium shown in Fig. 5, a large non-conducting cluster appears (see Fig. 5a). In its vicinity the excitation wave is broken and reentry appears, which leads to an overall persistent irregular dynamics.
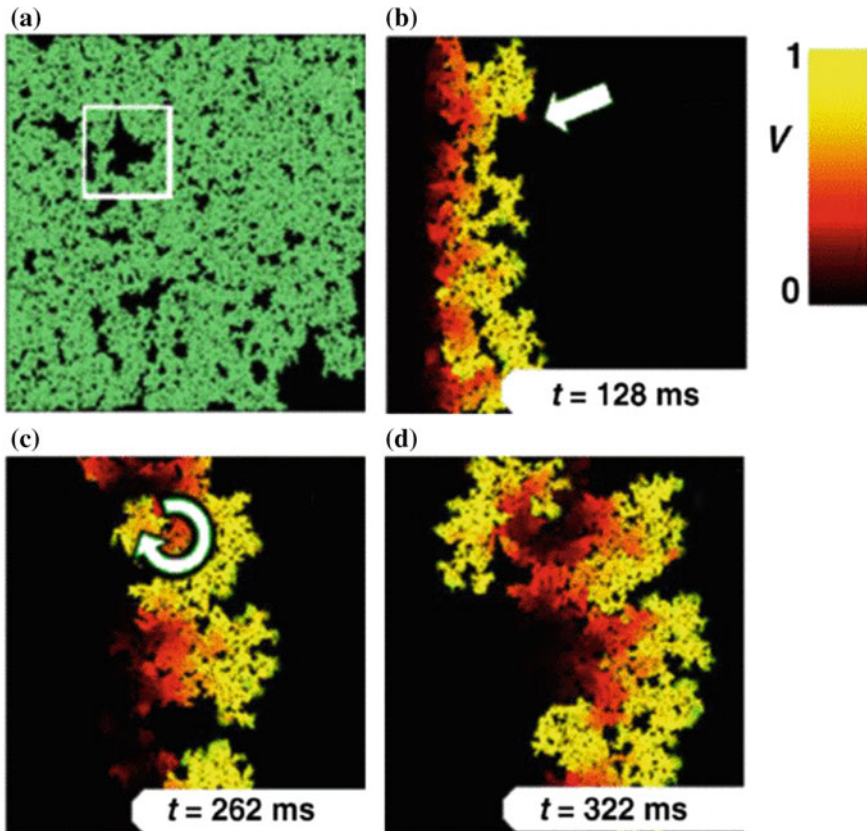
Fig. 5 Heterogeneities induce breakup of an initially planar wave in a two-dimensional simulation of a variant Fenton-Karma-model for cardiac tissue (taken from [51]). Panel **a** shows non-conducting areas (black) embedded into the conducting area (green). White square marks a large cluster responsible for the reentry and the wave breakup in the heterogeneous medium seen in simulations in panels **b**–**d**. Straight arrow in **b** marks the place of reentry and circular arrow in **c** follows the reentry direction

In this section, we have discussed three different mechanisms for transition from regular spiral or scrolls to irregular, chaotic dynamics. While in chemical systems these mechanism could be explored separately, the challenge in biological systems like the heart is that all three aspects may contribute simultaneously or even cooperatively.

4 Conclusion

Reaction-diffusion systems enter the stage in 1952 with the publication of the two seminal papers by Turing, that suggested a potential role for reaction-diffusion processes in morphogenesis, and by Hodgkin and Huxley, who based on experimental data developed a first model for impulse propagation in neurons that became a cornerstone of mathematical physiology. During the 1960s and 1970s Prigogine, Nicolis and co-workers extended the early concept of Turing by introducing the notion of "dissipative" structures. In parallel, experimental studies of the Belousov–Zhabotinsky reaction revealed rotating spiral waves as a particular beautiful example of such structures. In the 1990s, the field of chemical pattern formation reached maturity by introducing open reactors and experimental systems that showed a large variety of patterns both in homogeneous and heterogeneous catalysis including the realization of chemical Turing patterns. A concise summary of the history of chemical complexity was recently provided by Ertl and Mikhailov [52]. Improved imaging techniques in cell biology have subsequently led to the discovery of protein patterns in the late 1990s. A number of important unsolved questions concern the role that vortices namely rotating spiral and scroll waves play in the emergence of cardiac arrhythmias and potential strategies to control and suppress such dangerous physiological states. Here, recent progress in imaging of electrical and mechanical waves in cardiac muscle fuels hope for future discoveries [53].

References

1. M.C. Cross, P.C. Hohenberg, Pattern formation outside of equilibrium. Rev. Mod. Phys. **65**, 851 (1993)
2. A.M. Turing, The chemical basis of morphogenesis. Phil. Trans. Roy. Soc. Lond. B **237**, 37 (1952)
3. A.L. Hodgkin, A.F. Huxley, A quantitative description of membrane current and its application to conduction and excitation in nerve. J. Physiol. Lond. **117**, 500 (1952)
4. J. Keener, J. Sneyd, *Mathematical Physiology* (Springer, New York, 1998)
5. E. Meron, Pattern formation in excitable media. Phys. Rep. **218**, 1 (1992)
6. R. FitzHugh, Impulses and physiological states in theoretical models of nerve membrane. Biophys. J. **1**, 445 (1961)
7. A. Gierer, H. Meinhardt, Theory for biological pattern formation. Kybernetik **12**, 30 (1972)
8. D. Barkley, A model for fast computer simulation of waves in excitable media. Physica D **49**, 61 (1991)

9. M. Bär, M. Eiswirth, Turbulence due to spiral breakup in a continuous excitable medium. Phys. Rev. E **48**, 1635 (1993)

10. R. Kapral, K. Showalter (eds.), *Chemical Waves and Patterns* (Kluwer, Dordrecht, 1994)

11. A. Goldbeter, *Biochemical Oscillations and Cellular Rhythms: The Molecular Bases of Periodic and Chaotic Behavior* (Cambridge University, Cambridge, 1996)

12. A.N. Zaikin, A.M. Zhabotinsky, Concentration wave propagation in 2-dimensional liquid phase self-oscillating system. Nature **225**, 535 (1970)

13. A.T. Winfree, Spiral waves of chemical activity. Science **175**, 634 (1972)

14. R.J. Field, R.M. Noyes, E. Körös, Oscillations in chemical systems 2: Thorough analysis of temporal oscillations in Bromate-Cerium-Malonic acid system. J. Am. Chem. Soc. **94**, 8649 (1972)

15. S.C. Müller, Th. Plesser, B. Hess, The structure of the core of the spiral wave in the Belousov-Zhabotinsky reaction. Science **230**, 661 (1985)

16. V. Castets, E. Dulos, J. Boissonade, P. de Kepper, Experimental evidence of a sustained standing turing-type nonequilibrium chemical pattern. Phys. Rev. Lett. **64**, 2953 (1990)

17. Q. Ouyang, H.L. Swinney, Transition from a uniform state to hexagonal and striped turing patterns. Nature **352**, 610 (1991)

18. K.J. Lee, W.D. McCormick, Q. Ouyang, H.L. Swinney, Pattern formation by interacting chemical fronts. Science **261**, 183 (1993)

19. K.J. Lee, W.D. McCormick, J. Pearson, H.L. Swinney, Experimental observation of self-replicating spots in a reaction-diffusion system. Nature **369**, 215 (1994)

20. A. Hagberg, E. Meron, Complex patterns in reaction-diffusion systems: a tale of two front instabilities. Chaos **4**, 477 (1994)

21. S. Jakubith, A. von Oertzen, W. Engel, H.H. Rotermund, G. Ertl, Spatiotemporal concentration patterns in a surface reaction - propagating and standing waves, rotating spirals, and turbulence. Phys. Rev. Lett. **65**, 3013 (1990)

22. R. Imbihl, G. Ertl, Oscillatory kinetics in heterogeneous catalysis. Chem. Rev. **95**, 697 (1995)

23. Q. Ouyang, J.M. Flesselles, Transition from spirals to defect turbulence driven by a convective instability. Nature **379**, 143 (1996)

24. Q. Ouyang, H.L. Swinney, G. Li, Transition from spirals to defect-mediated turbulence driven by a Doppler instability. Phys. Rev. Lett. **84**, 1047 (2000)

25. L.Q. Zhou, Q. Ouyang, Experimental studies on long-wavelength instability and spiral breakup in a reaction-diffusion system. Phys. Rev. Lett. **85**, 1650 (2000)

26. G. Gerisch, Periodic signals control pattern formation in cell aggregations. Naturwissenschaften **58**, 430 (1971)

27. F. Siegert, C. Weijer, Three dimensional scroll waves organize *dictyostelium* slugs. Proc. Natl. Acad. Sci. USA **89**, 6433 (1992)

28. E. Ben-Jacob, I. Cohen, H. Levine, Cooperative self-organization of microorganism. Adv. Phys. **49**, 395 (2000)

29. J. Lechleiter, S. Girard, E. Peralta, D. Clapham, Spiral calcium wave propagation and annihilation in *Xenopus laevis* oocytes. Science **252**, 123 (1992)

30. M. Falcke, Reading the patterns in living cells: the physics of Ca^{2+} signaling. Adv. Phys. **53**, 255 (2004)

31. D.M. Raskin, P.A. De Boer, Rapid pole-to-pole oscillation of a protein required for directing division to the middle of *Escherichia Coli*. Proc. Natl. Acad. Sci. USA **96**, 4971 (1999)

32. M. Loose, E. Fischer-Friedrich, J. Ries, K. Kruse, P. Schwille, Spatial regulators for bacterial cell division self-organize into surface waves in vitro. Science **320**, 789–792 (2008)

33. C. Beta, K. Kruse, Intracellular oscillations and waves. Ann. Rev. Cond. Math. Phys. **8**, 239–264 (2017)

34. J. Halatek, F. Brauns, E. Frey, Self-organization principles of intracellular pattern formation. Phil. Trans. R. Soc. B **373**, 20170107 (2018)

35. V.K. Vanag, I.R. Epstein, Pattern formation in a tunable medium: the Belousov-Zhabotinsky reaction in an aerosol OT microemulsion. Phys. Rev. Lett. **87**, 228301 (2001)

36. S. Alonso, F. Sagués, A.S. Mikhailov, Taming winfree turbulence of scroll waves in excitable media. Science **299**, 1722 (2003)
37. A.S. Mikhailov, K. Showalter, Control of waves, patterns and turbulence in chemical systems. Phys. Rep. **425**, 79–194 (2006)
38. T. Bánsági Jr., O. Steinbock, Nucleation and collapse of scroll rings in excitable media. Phys. Rev. Lett. **97**, 198301 (2006)
39. C. Luengviriya, U. Storb, G. Lindner, S.C. Müller, M. Bär, M.J.B. Hauser, Scroll wave instabilities in an excitable chemical medium. Phys. Rev. Lett. **100**, 148302 (2008)
40. T. Bánsági, V.K. Vanag, I.R. Epstein, Tomography of reaction-diffusion microemulsions reveals three-dimensional turing patterns. Science **331**, 1309–1312 (2011)
41. A.T. Winfree, *When Time Breaks Down: The Three-Dimensional Dynamics of Electrochemical Waves and Cardiac Arrhythmias* (Princeton University, Princeton, 1987)
42. S.V. Pandit, J. Jalife, Rotors and the dynamics of cardiac fibrillation. Circ. Res. **112**, 849 (2013)
43. A. Karma, Physics of cardiac arrhythmogenesis. Ann. Rev. Cond. Math. Phys. **4**, 313 (2013)
44. Z. Qu, G. Hu, A. Garfinkel, J.N. Weiss, Nonlinear and stochastic dynamics in the heart. Phys. Rep. **543**, 61 (2014)
45. S. Alonso, M. Bär, B. Echebarria, Nonlinear physics of electrical wave propagation in the heart: a review. Rep. Prog. Phys. **79**, 096601 (2016)
46. A.T. Winfree, Electrical turbulence in three-dimensional heart muscle. Science **266**, 1003 (1994)
47. M. Bär, L. Brusch, Breakup of spiral waves caused by radial dynamics: Eckhaus and finite wavenumber instabilities. New J. Phys. **6**, 5 (2004)
48. F.H. Fenton, E.M. Cherry, H.M. Hastings, S.J. Evans, Multiple mechanisms of spiral wave breakup in a model of cardiac electrical activity. Chaos **12**, 852 (2002)
49. P. Wheeler, D. Barkley, Computation of spiral spectra. SIAM J. Appl. Dyn. Syst. **5**, 15777 (2006)
50. I.S. Aranson, L. Kramer, The world of the complex Ginzburg-Landau equation. Rev. Mod. Phys. **74**, 92 (2002)
51. S. Alonso, M. Bär, Reentry near the percolation threshold in a heterogeneous discrete model for cardiac tissue. Phys. Rev. Lett. **110**, 158101 (2013)
52. A.S. Mikhailov, G. Ertl, *Chemical Complexity - Self-Organization Processes in Molecular Systems* (Springer International Publishing Company, Cham, 2017)
53. J. Christoph, M. Chebbok, C. Richter, J. Schröder-Schetelig, P. Bittihn, S. Stein, I. Uzelac, F.H. Fenton, G. Hasenfuß, R.F. Gilmour Jr., S. Luther, Electro-mechanical vortex filaments during cardiac fibrillation. Nature **555**, 667 (2018)

A Lattice-Gas Cellular Automaton Model for Discrete Excitable Media

Simon Syga, Josué M. Nava-Sedeño, Lutz Brusch and Andreas Deutsch

Abstract How do ordered structures like spirals cope with stochastic events? Several phenomena in chemistry and biology provide examples of excitable media and spiral pattern formation and are intrinsically stochastic. Here, we present a novel lattice-gas cellular automaton model for discrete excitable media. In this stochastic model, two discrete interacting biological species determine each other's birth and death probabilities. We show that this birth-death process, coupled to a random walk, is equivalent to a classical partial differential equation (PDE) model of excitable media in the macroscopic limit, and able to form spiral density waves. Importantly, our cellular automaton model includes a parameter which defines the maximum local number of individuals and influences the onset of spiral waves. We find that small values of this parameter allow spiral pattern formation even in situations where the corresponding deterministic PDE model predicts that no spirals are formed, reminiscent of stochastic resonance effects.

1 Introduction

An excitable medium is a spatially extended system in which a wave (or "excited" state) can propagate without attenuation once it is initiated, but is unable to propagate in regions where a wave has recently passed ("refractory" state) [1]. Biological systems comprising cells or organisms are inherently discrete and several of them behave as excitable media with the ability of spiral pattern formation in appropriate parameter ranges [2]. Examples include *Dictyostelium discoideum* aggregation [3] (see chapter **Spiral Waves of the Chemo-Attractant cAMP Organise Multicellular Development in the Social Amoebae**) and epidemiological spreading [4].

S. Syga (✉) · J. M. Nava-Sedeño · L. Brusch · A. Deutsch
Centre for Information Services and High Performance Computing, Technische Universität Dresden, Nöthnitzer Straße 46, 01062 Dresden, Germany
e-mail: simon.syga@tu-dresden.de

To study continuous excitable media, several models have been constructed. These models are typically formulated as continuous and deterministic partial differential equations (PDEs) [5–9]. Their continuous nature allows fitting to continuous media properties such as chemical concentrations. However, PDE models are not appropriate to study discrete excitable media.

To explicitly account for discrete entities, one can use cellular automaton (CA) models [10]. The term "cellular automaton" originates from work by John von Neumann and Stanislaw Ulam, who were interested in the question of self-reproduction of discrete entities, which required non-continuum concepts [11]. A CA is a discrete dynamical system, where space, time and state space are discrete. In particular, a CA is characterized by a regular lattice, where every lattice node (or "cell") is assigned a discrete state. The dynamics is defined by a transition rule that depends on the state and the states in the local interaction neighborhood. Various CA models for discrete excitable media have been introduced [12–20]. Typically, these models are motivated by a top-down perspective and attempt to capture aspects of continuous excitable media in a discrete model. In contrast, here we apply a bottom-up approach by assuming discrete individuals and birth/death rules mimicking excitable dynamics.

We adopt a lattice-gas cellular automaton (LGCA) model. This CA model can describe discrete individuals interacting stochastically and moving in space. LGCA models were introduced to simulate aspects of fluid dynamics [21], but have also been used successfully to investigate collective cell migration, biological pattern formation and the growth and invasion of tumors [22–35]. LGCA models are cell-based, computationally efficient, and allow to integrate statistical and biophysical models for different levels of biological knowledge [36–40]. Here, we define an LGCA model for two interacting biological or chemical species with simple birth-death dynamics. Our LGCA model does not only incorporate stochastic effects not included in classic PDE models, but also allows to bridge the gap between microscopic, single-individual dynamics, and macroscopic PDE models. In particular, we are able to derive a classic Barkley PDE approximation in the macroscopic diffusive limit [5]. By comparing spiral wave patterns in the stochastic LGCA and spiral solutions of the corresponding deterministic PDE model, we show that stochastic fluctuations allow spiral pattern formation in a larger parameter regime compared to the deterministic PDE model. Our stochastic model can be especially useful for studying macroscopic pattern formation in systems with a small number of interacting individuals, such as biological systems, which are more sensitive to fluctuations. The LGCA model framework can likewise be applied to oscillatory media to study stochastic effects of spiral wave formation therein.

2 Model Definition

2.1 Lattice-Gas Cellular Automata

We briefly introduce the general LGCA model formalism, and present our specific LGCA model of excitable media. From the LGCA microdynamical equations, we derive a system of PDEs describing the ensemble-averaged spatiotemporal dynamics. We employ a hexagonal lattice, which attenuates spatial anisotropies compared to a square lattice [21]. Compared to classic CA, LGCA have a node substructure. Every node has $K = a + b$ channels, $\vec{c}_i$, $1 < i \leq K$, where b channels are called velocity channels, which point into the direction of next neighbor nodes. Therefore, the number b of velocity channels is determined by the lattice geometry. In the case of a hexagonal lattice, $b = 6$. The remaining $a := K - b$ channels are called rest channels, and have $\vec{c}_i = (0, 0)$, $b < i \leq K$. The precise number a of rest channels can be considered a parameter of the model. Each of these channels may be occupied by at most one particle at any time step, the channel state space is $\mathcal{E} = \{0, 1\}$. The node state at a position $\vec{r} \in \mathcal{L}$ at a time step $k \in \mathbb{N}$ is called the node configuration, $\vec{\eta}(\vec{r}, k) \in \mathcal{E}^K$, whose ith component represents the presence or absence of a particle in the ith velocity channel. The number of particles at node $\vec{r}$ at time k is given by

$$n(\vec{\eta}(\vec{r}, k)) = \sum_{i=1}^{K} \eta_i(\vec{r}, k). \tag{1}$$

It is evident that a node can hold a maximum number of K particles at any given time.

The configuration of the lattice evolves by the simultaneous application of a local rule to all nodes at every time step. The rule consists of two separate steps: a stochastic interaction step followed by a deterministic transport step, see Fig. 1. During the interaction step, every node configuration $\vec{\eta}(\vec{r}, k)$ is replaced by a post-interaction configuration $\vec{\eta}^{\mathcal{I}}(\vec{r}, k)$. The post-interaction configurationn is selected according to a probability distribution which may depend on the node configuration $\vec{\eta}(\vec{r}, k)$, as well as the configurations of neighboring nodes. During the transport step, particles in velocity channels are deterministically translocated to corresponding nearest neighbors, while particles in rest channels remain in their original node. More formally,

$$\eta_i(\vec{r}, k + 1) = \eta_i^{\mathcal{I}}(\vec{r} - \vec{c}_i, k). \tag{2}$$

The separation of the local, stochastic interaction from the deterministic transport endows the LGCA model class with two benefits: efficient numerical simulation and, more importantly, analytic tractability, enabling us to derive a PDE approximation in the macroscopic limit.
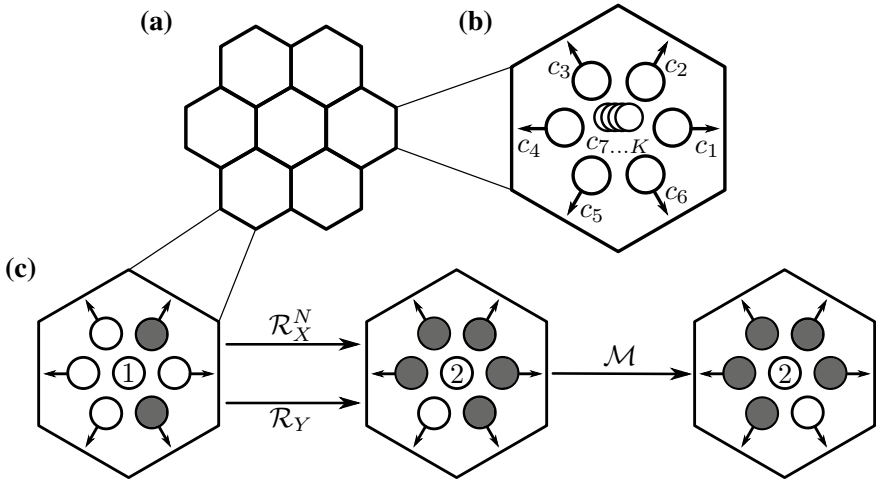
Fig. 1 Interaction dynamics of the LGCA excitable medium model. Within a node (**b**) in the lattice (**a**), the number of particles in rest channels (species Y, number in center) is increased and/or decreased by 1 (maximum a, minimum 0), according to the operator $\mathcal{R}_Y$ (**c**). The operator $\mathcal{R}_X$ is applied N consecutive times to particles in velocity channels so that several particles can be created or destroyed in a single time step (species X, occupied = black, empty = white, circles with velocity vectors). After particles have been created/destroyed, particles of species X are randomly redistributed among the velocity channels according to the mixing operator $\mathcal{M}$. See text for the parametrization of the update probabilities

2.2 The LGCA Excitable Media Model

We consider the spatial distributions of two species X and Y. One species, termed X, is motile and can reproduce and/or die swiftly, representing the excited state. The second species, termed Y, is immobile and reproduces and/or dies slowly, representing the refractory state. Species X is modeled as particles residing in velocity channels, while species Y is modeled as particles residing in rest channels. Following Eq. (1), the numbers of particles of species X and Y are given by

$$n_X\left(\vec{\eta}\left(\vec{r}, k\right)\right) = \sum_{i=1}^{b} \eta_i\left(\vec{r}, k\right), \text{ and} \tag{3a}$$

$$n_Y\left(\vec{\eta}\left(\vec{r}, k\right)\right) = \sum_{i=b+1}^{K} \eta_i\left(\vec{r}, k\right). \tag{3b}$$

Likewise, the normalized fraction of particles of each species residing in a given node is defined as

$$\rho_X(\vec{r}, k) = \frac{1}{b} n_X(\vec{\eta}(\vec{r}, k)), \text{ and} \tag{4a}$$

$$\rho_Y(\vec{r}, k) = \frac{1}{a} n_Y(\vec{\eta}(\vec{r}, k)). \tag{4b}$$

The general idea of the model is to amplify and modulate excitations, depending on the local state of the medium. We translate this idea into a LGCA rule and define the following operators. The *stochastic birth* operator of species $Z \in \{X, Y\}$, $\mathcal{B}_Z : \mathcal{E}^K \mapsto \mathcal{E}^K$ adds one particle of species Z to the configuration with probability $P_Z^+ := P_Z^+(\vec{\eta}(\vec{r}, k))$, which depends on the fraction of particles of both species in the node, as long as there is a free channel at the node that can be occupied by species Z. Analogously, the *stochastic death* operator of species Z, $\mathcal{D}_Z : \mathcal{E}^K \mapsto \mathcal{E}^K$ removes one particle of species Z from the configuration with a probability $P_Z^- := P_Z^-(\vec{\eta}(\vec{r}, k))$, which depends on the fraction of particles of both species in the node, as long as there is at least one particle of species Z to remove. We define the *reaction* operator of species Z, $\mathcal{R}_Z : \mathcal{E}^K \mapsto \mathcal{E}^K$ as the subsequent application of birth and death operators. Defining the mean change of particles of species Z after reaction as $\Delta n_Z := \langle n_Z(\mathcal{R}_Z[\vec{\eta}(\vec{r}, k)]) - n_Z(\vec{\eta}(\vec{r}, k)) \rangle$, it can be shown that

$$\Delta n_Z = P_Z^+ - P_Z^-. \tag{5}$$

Due to the direct dependencies of the probabilities P_Z^+ and P_Z^- on the particle fractions $\rho_X(\vec{r}, k)$ and $\rho_Y(\vec{r}, k)$, Δn_Z also depends on these fractions. For ease of notation, we define the particle change functions $f(\rho_X, \rho_Y) := \Delta n_X$, and $g(\rho_X, \rho_Y) := \Delta n_Y$. For a particular choice of probabilities and functions, see Eqs. (9) and (10). Importantly, the particular choice of the particle change functions $f(\rho_X, \rho_Y)$, $g(\rho_X, \rho_Y)$ leads to a typical phase space of an excitable medium, with a single stable steady state, a quickly changing variable ρ_X and a slowly changing variable ρ_Y, so that sufficiently large deviations from the steady state cause a large excitation followed by a refractory period leading back to the steady state, see Fig. 2c,d and chapter **Generation of Spirals in Excitable Media**.

Finally, we define the *stochastic mixing* operator $\mathcal{M} : \mathcal{E}^K \mapsto \mathcal{E}^K$. This operator acts on a configuration $\vec{\eta}(\vec{r}, k)$ and randomly reshuffles particles within velocity channels, while leaving particles in rest channels unchanged.

Using these operators, the *interaction step* is defined as follows. At the beginning of the interaction step, $\mathcal{R}_Y$ is applied once to the configuration of every node. To simulate the swift change in species X compared to the slow change of species Y, $\mathcal{R}_X$ is applied N times, where the value of N is a free parameter. Note that the maximum absolute change of the density of the slowly changing species Y in each time step is given by the inverse number of rest channels $|\Delta\rho_{Y,\max}| = \frac{1}{a}$. Therefore, the number of rest channels is inversely proportional to the amplitude of the stochastic fluctuations of species Y and controls the sensitivity of the model towards stochastic fluctuations. On the other hand, N successive applications of $\mathcal{R}_X$ may increase the excitation dramatically, or conversely, inhibit it greatly, depending on the value of the particle change function $f(\rho_X, \rho_Y)$. Strong amplification and inhibition of excitations above certain thresholds are the defining characteristics of an excitable medium [41], and

constitute the essence of this LGCA model. Finally, the mixing operator is applied to the resulting configuration. The post-interaction configuration is given by

$$\vec{\eta}^{\mathcal{I}}(\vec{r}, k) = \mathcal{R}_Y \circ \mathcal{R}_X^N \circ \mathcal{M}\left[\vec{\eta}(\vec{r}, k)\right], \qquad (6)$$

where the symbol $\circ$ denotes the ordered application of the operators. See Fig. 1 for a visualization. After the interaction step, the *deterministic transport* step follows according to Eq. (2). Simulations of spirals in this LGCA model (Fig. 2a) will be presented in detail after the following theoretical analysis.
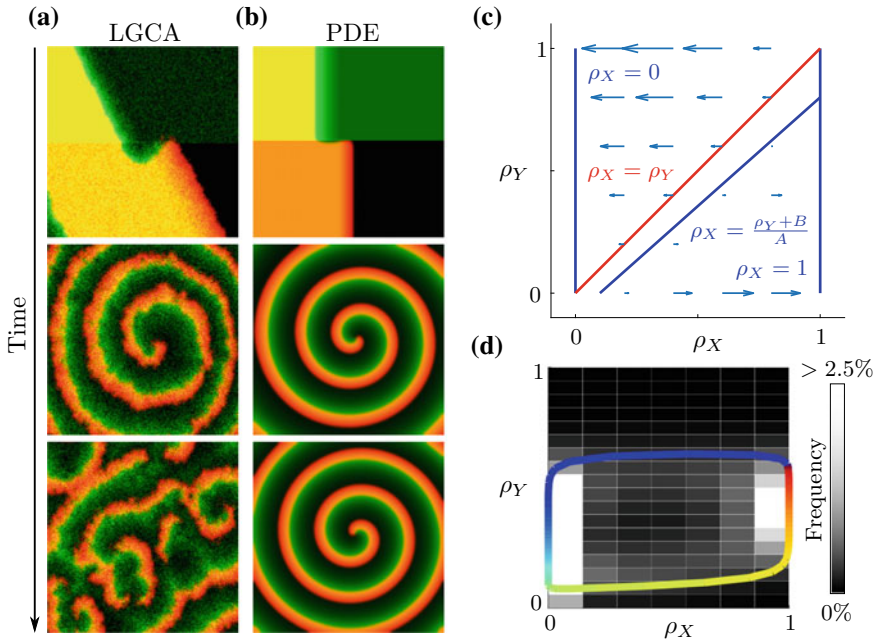
Fig. 2 Comparison of spiral wave dynamics in the stochastic LGCA excitable medium model and the mean-field PDE model. Panels **a** and **b** show snapshots of computer simulations. To encode two local variable values in one color, the red color intensity is proportional to ρ_X and green is proportional to ρ_Y and high values of both appear yellow. A hexagonal lattice and absorbing boundary conditions were used. **c** Nullclines of the reaction rate $f = \rho_X (1 - \rho_X)\left(\rho_X - \frac{\rho_Y + B}{A}\right)$ are shown in blue, the nullcline of $g = \rho_X - \rho_Y$ in red. Arrows represent the evolution of ρ_X. **d** Shows the phase space trajectory of the mean-field PDE model (8) (solid line), where the color of the trajectory changes with time from blue ($t = 0$) to red ($t = t_{max}$); and a histogram of the LGCA node states across many realizations (grayscale boxes). The intensity of the underlying heat map is proportional to the probability of finding a node in the LGCA model with a certain value of ρ_X and ρ_Y. The density map was obtained with information of 8×10^5 nodes, after a transient period of 2000 time steps. The values of ρ_X and ρ_Y at a fixed position and different points in time are plotted for the PDE model. Parameters are $A = 0.75$, $B = 0.02$, $N = 50$, and $K = 23$. PDE data was obtained using an open source program by Barkley and Dowle [42]

3   Mean-Field Theory

We next derive a PDE system which describes the evolution of the expected value of the density patterns of both species in the continuous limit. The following theory is based on the mean-field approximation, which means that we approximate all stochastic variables by their mean values. Under this approximation, and using Eqs. (2), (5) and (6), the finite difference equations (FDEs) for the mean densities on the node $\vec{r}$ at time step $k + 1$ are

$$\langle \rho_X (\vec{r}, k+1) \rangle = \frac{1}{b} \sum_{i=1}^{b} \Bigg[\langle \rho_X (\vec{r} - \vec{c}_i, k) \rangle +$$

$$\sum_{m=1}^{N} f \left(\langle \rho_X (\vec{r} - \vec{c}_i, k + m\kappa) \rangle, \langle \rho_Y (\vec{r} - \vec{c}_i, k + m\kappa) \rangle \right) \Bigg], \quad (7a)$$

$$\langle \rho_Y (\vec{r}, k+1) \rangle = \langle \rho_Y (\vec{r}, k) \rangle + g \left(\langle \rho_X (\vec{r}, k) \rangle, \langle \rho_Y (\vec{r}, k) \rangle \right), \quad (7b)$$

where $\kappa = \frac{1}{N}$ connects the fast time scale of the reaction dynamics of X with the slower time scale of the diffusion and reaction dynamics of Y. To transform the discrete FDEs into continuous PDEs, we identify the mean fractions $\langle \rho_X (\vec{r}, k) \rangle$, $\langle \rho_Y (\vec{r}, k) \rangle$ with their continuous counterparts $\langle \rho_X (\vec{x}, t) \rangle, \langle \rho_Y (\vec{x}, t) \rangle$, where $\vec{x} = \vec{r}\varepsilon \in \mathbb{R}^2$ and $t = k\tau \in \mathbb{R}^+$ with small $\varepsilon, \tau \in \mathbb{R}^+$, and the discrete particle changes f, g with the continuous particle changes $\tau f, \tau g$. The precise values of ε and τ are chosen such that the rescaled LGCA model matches the PDE's spatial and temporal scales. Furthermore, we take the diffusive limit $\tau, \varepsilon \to 0$ with $\lim_{\tau, \varepsilon \to 0} \frac{\varepsilon^2}{4\tau} =: D$, expand the expected densities in Taylor series up to terms of order τ and ε^2, and approximate the reaction rates by the zeroth-order term $\mathcal{O}$ of their Taylor expansion

$$f \left(\left\langle \rho_X \left(\vec{x} - \varepsilon\vec{c}_i, t + \frac{n\tau}{N} \right) \right\rangle, \left\langle \rho_Y \left(\vec{x} - \varepsilon\vec{c}_i, t + \frac{n\tau}{N} \right) \right\rangle \right)$$
$$\approx f \left(\langle \rho_X (\vec{x}, t) \rangle, \langle \rho_Y (\vec{x}, t) \rangle \right) + \mathcal{O}(\varepsilon, \tau),$$

to obtain the PDE system

$$\frac{\partial}{\partial t} \langle \rho_X \rangle = D \nabla^2 \langle \rho_X \rangle + N f \left(\langle \rho_X \rangle, \langle \rho_Y \rangle \right), \quad (8a)$$

$$\frac{\partial}{\partial t} \langle \rho_Y \rangle = g \left(\langle \rho_X \rangle, \langle \rho_Y \rangle \right). \quad (8b)$$

Defining simple linear birth and death probabilities for species Y, and nonlinear birth and death probabilities for species X, corresponding to an excitable medium (see above), as

$$P_X^+ = \rho_X^2 \left(1 + \frac{\rho_Y + B}{A} \right), \tag{9a}$$

$$P_X^- = \rho_X \frac{\rho_Y + B}{A} + \rho_X^3, \tag{9b}$$

$$P_Y^+ = \rho_X, \tag{9c}$$

$$P_Y^- = \rho_Y, \tag{9d}$$

where A and B are free parameters, translate into the reaction rates

$$f(\rho_X, \rho_Y) = \rho_X (1 - \rho_X) \left(\rho_X - \frac{\rho_Y + B}{A} \right), \tag{10a}$$

$$g(\rho_X, \rho_Y) = \rho_X - \rho_Y. \tag{10b}$$

The PDE system (8) with the reaction rates (10) is the well-known Barkley model [5], a prototype for excitable media with spiral wave solutions as numerically shown in Fig. 2b. The phase space of the Barkley model is depicted in Fig. 2c. The nullclines of the reaction rates coincide with the fixed points of the reaction operators of the LGCA. Due to the rapid dynamics of species X compared to species Y, species X tends to either saturate or die off (see arrows in Fig. 2c). A third steady state of species X (diagonal line) is unstable. There is a linearly stable single fixed point of the system ($\rho_X = \rho_Y = 0$); however if the parameters A and B are such that the unstable steady state of species X is close to this fixed point, sufficiently large perturbations can shift the system above this excitability threshold and, due to neighbor coupling, into a stable, periodic orbit.

4   Simulation of Spiral Waves

To qualitatively compare the LGCA model with the mean-field PDE model, computer simulations of both models were performed, see Fig. 2a, b. The values of the parameters A, B, and N were identical in both models, see Table 1. The number of channels K was varied between 12 and 100. Simulations with $K < 12$ underwent spiral breakup almost immediately, whereas $K > 100$ leads to very large wave lengths of the spiral pattern. In the LGCA model, $12 \leq K \leq 30$ always resulted in spirals independently of the initial conditions (not shown). In the PDE model, spiral formation requires non-symmetric initial conditions. Therefore, to produce a single spiral wave, both models were initialized in the following way. At $t = 0$ ($k = 0$) the space was partitioned into four quadrants, one with $\rho_X = \rho_Y = 0$, another with $\rho_X = 1, \rho_Y = 0$, a third with $\rho_X = 0, \rho_Y = 1$, and the last with $\rho_X = \rho_Y = 1$. As can be seen in Fig. 2a, b, at short times both models show qualitatively similar behavior. At long times, however, stochastic fluctuations in the LGCA model start to appear, which ultimately break the starting spiral into several smaller spirals. Spiral breakup

Table 1 Parameters in the LGCA and corresponding PDE models in Fig. 2

Parameter	LGCA	PDE
A	0.75	0.75
B	0.02	0.02
N	50	50
K	23	—

has been observed widely in various stochastic models of excitable media [41]. As a histogram of the states of the nodes in the LGCA model reveals, both the initial big spirals and the late smaller spirals describe approximately the same phase space orbits as spirals in the PDE model (Fig. 2d).

Next, we investigated the effect of stochasticity on the spiral phase diagram. The parameter space of the Barkley model has been studied extensively [43]. Below certain values of parameters A and B, excitation pulses die out without formation of any spirals. Above these values, stable spirals are formed for certain initial conditions, with complicated behavior like spiral center meandering in certain regions above the spiral threshold, see Fig. 3c. To check if spirals are formed in the stochastic LGCA model, we used the mean return time as an observable. The mean return time measures the mean number of time steps needed for any given node to contain the same amount of particles of species X and Y it contained at some predefined past time step. If no spirals are formed, the whole lattice will be near the stable state $\rho_X = \rho_Y = 0$, at every time step after the disappearance of the initial pulse, so the mean return time will be close to 1. If spirals form, then each node performs an orbit (see Fig. 2d) before returning to its original state, which would increase the mean return time.

We performed simulations varying the value of A and fixing the values of the remaining parameters at $B = 0.05$, $N = 50$, and $K = 12$ for maximum stochasticity. We allow transients to relax for 500 time steps. Afterwards, a node was picked at random and its state recorded. The number of time steps for the same node to reach the same state was averaged over 100 realizations, to estimate the value of the mean return time. The mean return time as a function of the parameter A is shown in Fig. 3a. We find a typical spiral rotation period of 53.3 time steps. When comparing this plot with the parameter space of Barkley's PDE model (Fig. 3c), we find good correspondence between both models. In the LGCA model, however, short period spirals appear already at lower values of the parameter A. After a short transition region, spirals with longer periods appear. The region of the parameter space allowing spirals is therefore larger and the transition smoother in the LGCA model than in its PDE counterpart, compare Fig. 3b, c. This observation reinforces that stochasticity may act as a facilitator of spiral formation, as known from stochastic resonance [41, 44, 45], and from the analysis of an LGCA model for Turing pattern formation [32].
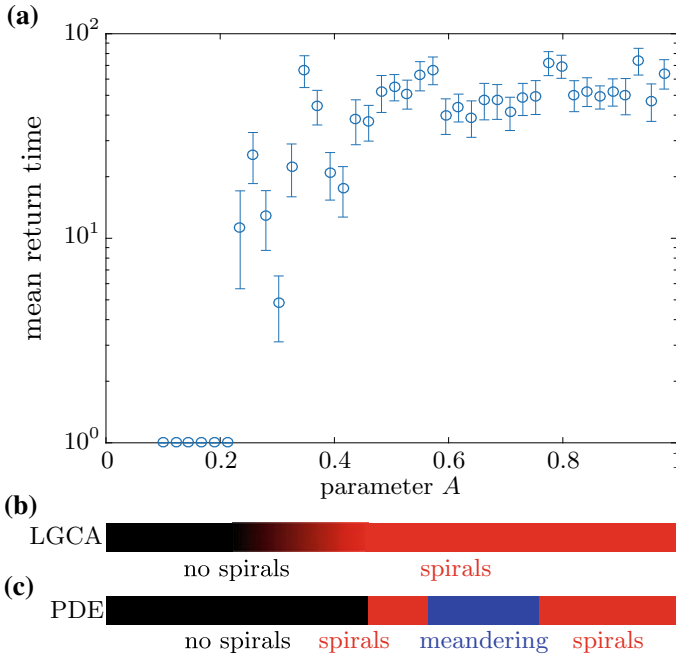
Fig. 3 Comparison of spiral formation in the LGCA and the mean-field PDE model. **a** Mean time for a node in the LGCA model to return to a previously visited state when parameter A is varied and B, N, K are fixed. For the node capacity we choose $K = a + b = 12$ so that stochastic fluctuations are relatively big and deviations from the mean-field PDE appear (see text for explanations). The mean return time estimates the rotation period in case a spiral wave solution is found. The parameter-averaged mean return time in the spiral-forming region is 53.3 time steps. The return time was averaged over 100 realizations. Symbols denote the average and its standard deviation. **b, c** Axis of parameter A is color-coded according to the spirals that are observed in simulations of the LGCA model (for $B = 0.05$, $N = 50$, $K = 12$) and in the corresponding mean-field PDE model. The black color corresponds to no spiral formation, red to stable spiral formation, blue to "meandering" spirals with moving centers. In the LGCA model the transition from the non-spiral forming to the spiral-forming regime is smooth due to transient spirals, in contrast to the PDE system. Moreover, the quantification of spiral meandering for the LGCA requires better statistics and is omitted here. Solution types in the PDE model were obtained with information from [43]

5   Conclusions

Following the methodology of the Lattice-Gas Cellular Automaton, we constructed an excitable birth-death model with tunable stochasticity. We chose the time scale of the birth and death process of the motile "excited" species to be much faster compared to that of the immobile "refractory" species. Stochasticity is tunable through parameter a, which represents the level of spatial coarsening. We showed that the mean collective behavior of the LGCA model can be described by Barkley's PDE model. Using computer simulations, we showed how our LGCA model at finite particle number differs from Barkley's model, revealing stochastic behavior such as spiral breakup and a wider parameter range for the appearance of spiral patterns.

Several interesting theoretical research questions remain, including a nonlinear stability analysis. This analysis would allow to predict a critical parameter set for spiral formation, the spiral wavelength, and dispersion relations. Furthermore, the study of secondary instabilities of the spiral wave pattern would allow to characterize the meandering of the spiral center.

References

1. M.C. Cross, P.C. Hohenberg, Pattern formation outside of equilibrium. Rev. Mod. Phys. **65**, 851–1112 (1993). https://doi.org/10.1103/RevModPhys.65.851
2. E. Meron, Pattern formation in excitable media. Phys. Rep. **218**, 1–66 (1992)
3. J.C. Dallon et al., in *Dynamics of Cell and Tissue Motion*, ed. by W. Alt, A. Deutsch, G.A. Dunn (Birkhäuser, Basel, 1997), pp. 193–202. https://doi.org/10.1007/978-3-0348-8916-2_23
4. J.D. Murray, E.A. Stanley, D.L. Brown, On the spatial spread of rabies among foxes. Proc. R. Soc. Lond. B **229**, 111–150 (1986)
5. D. Barkley, A model for fast computer simulation of waves in excitable media. Phys. D **49**, 61–70 (1991)
6. E.M. Cherry, F.H. Fenton, Visualization of spiral and scroll waves in simulated and experimental cardiac tissue. New J. Phys. **10**, 125016 (2008)
7. H. Zhang, A.V. Holden, Chaotic meander of spiral waves in the FitzHugh-Nagumo system. Chaos Solitons Fractals **5**, 661–670 (1995)
8. W. Jahnke, W.E. Skaggs, A.T. Winfree, Chemical vortex dynamics in the Belousov-Zhabotinskii reaction and in the two-variable Oregonator model. J. Phys. Chem. **93**, 740–749 (1989)
9. J.P. Keener, A geometrical theory for spiral waves in excitable media. SIAM J. Appl. Math. **46**, 1039–1056 (1986)
10. S.A. Wolfram, *A New Kind of Science* (Wolfram Media, Inc., 2002)
11. J. Von Neumann, A.W. Burks, *Theory of Self-reproducing Automata* (University of Illinois Press, Urbana, 1996)
12. J.M. Greenberg, S.P. Hastings, Spatial patterns for discrete models of diffusion in excitable media. SIAM J. Appl. Math. **34**, 515–523 (1978)
13. L.V. Reshodko, J. Bureš, Computer simulation of reverberating spreading depression in a network of cell automata. Biol. Cybern. **18**, 181–189 (1975)
14. B.F. Madore, W.L. Freedman, Computer simulations of the Belousov-Zhabotinsky reaction. Science **222**, 615–616 (1983)
15. A.T. Winfree, E.M. Winfree, H. Seifert, Organizing centers in a cellular excitable medium. Phys. D **17**, 109–115 (1985)
16. V.S. Zykov, A.S. Mikhailov, Rotating spiral waves in a simple model of an excitable medium. Sov. Phys. Dokl. **31**, 51–52 (1986)
17. A.S. Mikhailov, *Foundations of Synergetics I: Distributed Active Systems* (Springer, Berlin, 1990), pp. 32–80. https://doi.org/10.1007/978-3-642-97269-0_3
18. M. Gerhardt, H. Schuster, J.J. Tyson, A cellular automation model of excitable media including curvature and dispersion. Science **247**, 1563–1566 (1990)
19. M. Markus, B. Hess, Isotropic cellular automaton for modelling excitable media. Nature **347**, 56–58 (1990)
20. J.R. Weimar, J.J. Tyson, L.T. Watson, Third generation cellular automaton for modeling excitable media. Phys. D **55**, 328–339 (1992)
21. U. Frisch, B. Hasslacher, Y. Pomeau, Lattice-gas automata for the Navier-Stokes equation. Phys. Rev. Lett. **56**, 1505–1508 (1986)

22. A. Deutsch, S. Dormann, *Cellular Automaton Modeling of Biological Pattern Formation: Characterization, Applications, and Analysis*, 2nd edn. (Birkhäuser, Boston, 2018)
23. K. Böttger, H. Hatzikirou, A. Voss-Böhme, E.A. Cavalcanti-Adam, M.A. Herrero, A. Deutsch, An emerging Allee effect is critical for tumor initiation and persistence. PLOS Comput. Biol. **11**, 1–14 (2015). https://doi.org/10.1371/journal.pcbi.1004366
24. H. Hatzikirou, K. Böttger, A. Deutsch, Model-based comparison of cell density-dependent cell migration strategies. Math. Model. Nat. Phenom. **10**, 94–107 (2015)
25. K. Böttger, H. Hatzikirou, A. Chauviere, A. Deutsch, Investigation of the migration/proliferation dichotomy and its impact on avascular glioma invasion. Math. Model. Nat. Phenom. **7**, 105–135 (2012)
26. C. Mente, I. Prade, L. Brusch, G. Breier, A. Deutsch, A lattice-gas cellular automaton model for in vitro sprouting angiogenesis. Acta Phys. Pol. B **5**, 99–115 (2012)
27. S. De Franciscis, H. Hatzikirou, A. Deutsch, Analysis of lattice-gas cellular automaton models for tumor growth by means of fractal scaling. Acta Phys. Pol. B Proc. Suppl. **4**, 167 (2011)
28. M. Tektonidis et al., Identification of intrinsic in vitro cellular mechanisms for glioma invasion. J. Theor. Biol. **287**, 131–147 (2011)
29. B. Chopard, R. Ouared, A. Deutsch, H. Hatzikirou, D. Wolf-Gladrow, Lattice-gas cellular automaton models for biology: from fluids to cells. Acta Biotheor. **58**, 329–340 (2010)
30. H. Hatzikirou, A. Deutsch, Cellular automata as microscopic models of cell migration in heterogeneous environments. Curr. Top. Dev. Biol. **81**, 401–434 (2008)
31. S. Dormann, A. Deutsch, Modeling of self-organized avascular tumor growth with a hybrid cellular automaton. Silico Biol. **2**, 393–406 (2002)
32. S. Dormann, A. Deutsch, A.T. Lawniczak, Fourier analysis of Turing-like pattern formation in cellular automaton models. Futur. Gener. Comput. Syst. **17**, 901–909 (2001). https://doi.org/10.1016/S0167-739X(00)00068-6
33. A. Deutsch, A new mechanism of aggregation in a lattice-gas cellular automaton model. Math. Comput. Model. **31**, 35–40 (2000)
34. H.J. Bussemaker, A. Deutsch, E. Geigant, Mean-field analysis of a dynamical phase transition in a cellular automaton model for collective motion. Phys. Rev. Lett. **78**, 5018–5021 (1997). https://doi.org/10.1103/PhysRevLett.78.5018
35. A. Deutsch, Towards analyzing complex swarming patterns in biological systems with the help of lattice-gas cellular automata. J. Biol. Syst. **3**, 947–955 (1995)
36. J.M. Nava-Sedeño, H. Hatzikirou, R. Klages, A. Deutsch, Cellular automaton models for time-correlated random walks: derivation and analysis. Sci. Rep. **7**, 16952 (2017)
37. J.M. Nava-Sedeño, H. Hatzikirou, F. Peruani, A. Deutsch, Extracting cellular automaton rules from physical Langevin equation models for single and collective cell migration. J. Math. Biol. **75**, 1075–1100 (2017)
38. H. Hatzikirou, L. Brusch, A. Deutsch, From cellular automaton rules to a macroscopic mean-field description. Acta Phys. Pol. B Proc. Suppl. **3**, 399–416 (2010)
39. C. Mente, I. Prade, L. Brusch, G. Breier, A. Deutsch, Parameter estimation with a novel gradient-based optimization method for biological lattice-gas cellular automaton models. J. Math. Biol. **63**, 173–200 (2010)
40. A. Deutsch, A.T. Lawniczak, Probabilistic lattice models of collective motion and aggregation: from individual to collective dynamics. Math. Biosci. **156**, 255–269 (1999)
41. B. Lindner, J. García-Ojalvo, A. Neiman, L. Schimansky-Geier, Effects of noise in excitable systems. Phys. Rep. **392**, 321–424 (2004)
42. D. Barkley, EZ-spiral: a code for simulating spiral waves Version 3.2 (2007), http://homepages.warwick.ac.uk/staff/D.Barkley/Software/ez_software.html
43. D. Barkley, Euclidean symmetry and the dynamics of rotating spiral waves. Phys. Rev. Lett. **72**, 164–167 (1994). https://doi.org/10.1103/PhysRevLett.72.164
44. S. Kadar, J.C. Wang, K. Showalter, Noise-supported travelling waves in sub-excitable media. Nature **391**, 770–772 (1998)
45. M. Perc, Spatial coherence resonance in excitable media. Phys. Rev. E **72**, 016207 (2005). https://doi.org/10.1103/PhysRevE.72.016207

Kinematics of Spiral Waves in Excitable Media

Vladimir S. Zykov

Abstract Spiral waves rigidly rotating in excitable media sometimes play a constructive role in self-organization, while in many cases they cause an undesirable and dangerous activity. An understanding of spiral wave kinematics can help to control or to prevent this self-sustained activity. A description of the spiral wave kinematics performed by use of a free-boundary approach, reveals the selection principle which determines the shape and the rotation frequency of spiral waves in an unbounded medium with a given excitability. It is shown that a rigidly rotating spiral in a medium with strongly reduced refractoriness is supported within an excitability range restricted by two universal limits. At the low excitability limit, the spiral core radius diverges, while it vanishes at the high excitability limit and the spiral wave resembles the Yin-Yang pattern.

1 Introduction

An excitable medium can be considered as a population of active elements coupled locally through diffusion-like transport processes. Each individual active element is stable with respect to small external perturbations. However, it can be excited by the application of a super-threshold stimulus. Therefore, an excitation induced locally is able to propagate through the population of diffusively coupled elements as a self-sustained wave. After a recovery process, the medium returns to the resting state.

Rotating self-sustained spiral waves are among the most prominent examples of self-organized patterns in excitable media. They have been observed in systems of quite different nature like the social amoebae colonies [1] (see also chapter **Spiral Waves of the Chemo-Attractant cAMP Organise Multicellular Development**

V. S. Zykov (✉)
Max Planck Institute for Dynamics and Self-Organization, 37077 Göttingen, Germany
e-mail: vladzykov@googlemail.com

in the Social Amoebae), the chemical Belousov–Zhabotinsky (BZ) reaction [2] (chapter **Chemical Oscillation and Spiral Waves**), heart muscle [3] (chapter **Spiral Waves in the Heart**), the retina of the eye [4] (chapter **Yet More Spirals**), the oxidation of CO to CO_2 on platinum single crystal surfaces [5] (chapter **Shedding Light on Chaos**), yeast extracts during glycolysis [6] (chapter **Yet More Spirals**), and so on.

In the simplest case, the spiral rotates rigidly and its tip describes a circular orbit around the core [7, 8]. Varying the parameters of the midium one can effectively control the motion of spiral waves which can be used to destroy undesirable wave activity [9–12]. From this point of view the selection principles that determine the shape and the rotating frequency of spiral waves have to be understood.

From a mathematical point of view the main dynamical features of a broad class of excitable media can be simulated by a two-component reaction-diffusion system.

$$\frac{\partial u}{\partial t} = D\Delta u + F(u, v), \tag{1}$$

$$\frac{\partial v}{\partial t} = D_v \Delta v + \varepsilon G(u, v). \tag{2}$$

Here the local kinetics of an activator u and an inhibitor v is specified by the nonlinear functions $F(u, v)$ and $G(u, v)$. The diffusion coefficients D, D_v and the small multiplier ε are important control parameters. They are universal and applicable to a broad variety of models (see chapter **Reaction-Diffusion Patterns and Waves.**

From the experimental point of view, there is also some universality because there are many common kinematical features of spiral waves observed in quite different chemical and biological excitable media.

In this chapter we concentrate on an approximation of the reaction-diffusion model, as indicated in Eqs. 1 and 2, that allows us to reach a deeper understanding of the kinematical features of spiral waves. In the framework of this approach we are interested mostly in the motion of the boundary restricting an excited region. We will show that this so-called free-boundary approach essentially simplifies and generalizes the theoretical consideration of the spiral wave dynamics. Simultaneously, this approach helps us to reveal such important medium parameters, which can be measured experimentally.

2 Two First Steps Towards Spiral Wave Kinematics

In their seminal theoretical work, Wiener and Rosenblueth [13] showed in 1946 that the self-sustained activity in the cardiac muscle can be associated with an excitation wave rotating around an obstacle. In particular, they considered a motion of a wave rotating around a round obstacle as shown in Fig. 1a. In this very simplified kinematical model, they assumed that an excited part of the propagating wave is restricted by a very thin boundary consisting of a wave front (thick solid) and a wave back (thin

solid). It was also assumed that all points of the boundary are moving in the normal direction at the same velocity $c_n = const$. If the radius of the circular obstacle is given as R, the rotational frequency of the spiral wave should be $\omega = 2\pi R/c_n$. The shape of the wave front is also well determined in this case and represents the involute of the obstacle boundary. It means that the length of the interval AB of a tangent is equal to the arc length AC (see chapter **Spirals, Their Types and Peculiarities**). The wave back following the wave front has the same shape if turned around the rotational center by the angle ωd_u, where d_u is the duration of the excited state.
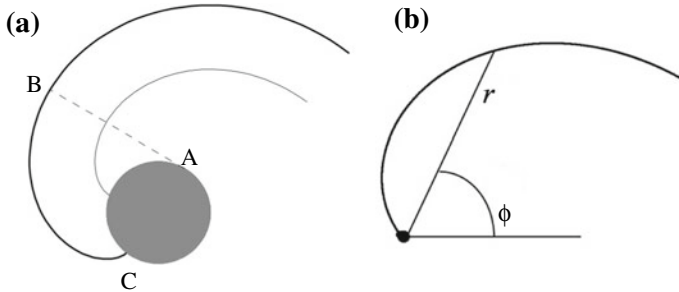
Fig. 1 Two examples of spiral wave kinematics. **a** Spiral wave rotating around a round unexcitable obstacle (dark region). **b** Top view on a screw dislocation growing on a crystal surface

A second important example shown in Fig. 1b represents the shape of a screw dislocation growing on a crystal surface [14]. In contrast to the first example, the authors assumed that the normal velocity of the wave front is not a constant, but strongly depends on the front curvature, namely

$$c_n = c_p - Dk, \qquad (3)$$

where c_p is the velocity of a planar front and k is its curvature. In the modern literature this relationship has obtained the name eikonal equation (see chapter **Chemical Oscillations and Spiral Waves**). Note, that in this case the wave front is rotating around a central point. In the vicinity of this point the front velocity c_n vanishes, and the front curvature reaches the value c_p/D in accordance with Eq. 3. The shape of the wave front is suitably expressed in the polar coordinates (r, ϕ) with the origin at the rotational center

$$x = r \cos[\phi(r) - \omega r], \quad y = r \sin[\phi(r) - \omega r], \qquad (4)$$

where ω is the rotational frequency of the wave front.

A detailed numerical analysis has shown that an acceptable solution $\phi(r)$ of Eqs. 3 and 4 does exist only for a single value of the rotational frequency

$$\omega = 0.331 c_p^2/D. \qquad (5)$$

It is important that both shapes of the spiral wave fronts shown in Fig. 1 are approaching the Archimedean spiral far away from the rotational center.

3   Free Boundary Approach

The next relevant step in the understanding of the spiral wave kinematics has been done by Pelcé and Sun [15]. They recognized that in both cases mentioned in Sect. 2 the wave front kinematics is completely independent of the wave back motion. In contrast to this the wave front and the wave back are usually interacting with each other. It can be clearly seen in Fig. 2, where a snapshot of a counterclockwise rotating spiral is shown. This picture resembles a typical pattern of spiral wave rotating within a homogeneous chemical or biological medium around a core of finite size (see chapter **Reaction-Diffusion Patterns and Waves**).

At one part of the excited state boundary the activator u is growing ($du/dt > 0$) that corresponds to the wave front. At another part of the boundary $du/dt < 0$ that corresponds to the wave back. These two parts meet each other at a so-called phase change point [16]. This point q describes a circular pathway around the circulation center, which represents the spiral wave core.

Another interesting point Q is located at the place, where the radial direction is a tangent to the excited state boundary. Here the normal front velocity is orthogonal to the radial direction and, hence, the point Q also describes a circular pathway around the circulation center.

The kinematics of the wave front and the wave back are closely connected and should be considered in parallel. To this aim it is very useful to describe the boundary of the excited state by the so-called natural equation which determines the boundary curvature k as a function of the arc length s counted from the phase change point q [17, 18].

Then the Cartesian coordinates $x(s)$, $y(s)$ of the boundary and the angle $\Theta(s)$ which determines the normal direction obey the obvious equations:

$$\Theta(s) = \Theta(0) - \int_0^s k(s')ds', \tag{6}$$

$$x(s) = x(0) + \int_0^s \cos(\Theta(s'))ds', \tag{7}$$

$$y(s) = y(0) + \int_0^s \sin(\Theta(s'))ds'. \tag{8}$$

During the boundary rotation, each of its point is moving at the velocity ωr around the rotational center. This velocity can be represented as a sum of a normal velocity $c_n(s)$ (orthogonal to the boundary) and the tangential velocity $c_\tau(s)$ (along the boundary), as drawn in Fig. 3. It was shown that for a rigidly rotating spiral these two velocities and $k(s)$ obey the following system of differential equations [17]

$$\frac{dc_n}{ds} = \omega + kc_\tau, \tag{9}$$

$$\frac{dc_\tau}{ds} = -kc_n. \tag{10}$$
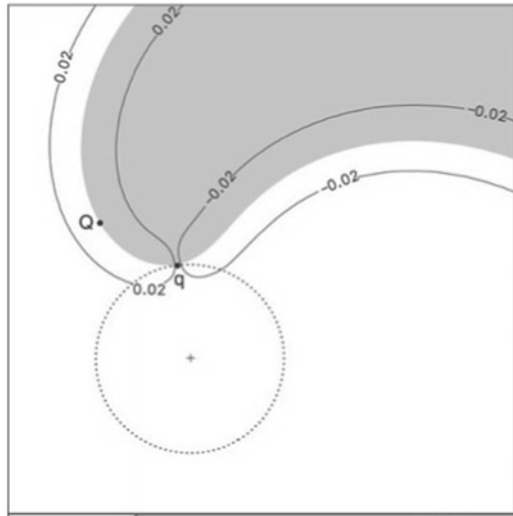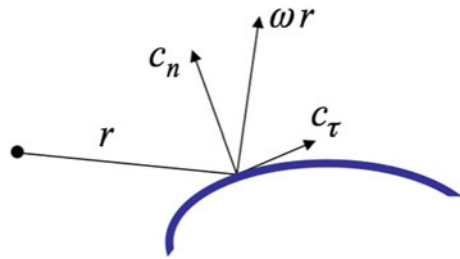
After rescaling $(S = sc_p/D, R = rc_p/D, C = c/c_p, K = Dk/c_p, \Omega = \omega D/c_p^2)$,
Eqs. 9 and 10 transform into the dimensionless form

$$\frac{dC_n}{dS} = \Omega + KC_\tau, \tag{11}$$

$$\frac{dC_\tau}{dS} = -KC_n. \tag{12}$$

Equations 11 and 12 are the result of a pure kinematical consideration. To describe
the boundary shape of a spiral wave rotating in an excitable medium, this system
should be supplemented by the eikonal equation describing the velocity-curvature
relationship written in dimensionless form in accordance with Eq. 3 as

$$C_n^+ = 1 - K^+. \tag{13}$$

The phase portrait of Eqs. 11–13 computed for $\Omega = 0.1333$ is shown in Fig. 4.
A trajectory describing the wave front starts at the line, where $C_n^+(0) = 0$ and
$0 \leq C_\tau(0) \leq 1$. In Fig. 4 three trajectories of the system computed for different
$C_t \equiv C_\tau(0)$ are shown. At the beginning of all trajectories C_n^+ increases and

C_τ^+ decreases. However, the normal velocity C_n^+ reaches a maximum and starts to decrease along the trajectory computed for $C_t = 0.3$. Moreover, this trajectory includes a part, where $C_n^+ < 0$, which contradicts the definition of a wave front. The trajectory crosses the line $C_n = 0$ again at $C_\tau \approx 0.61$. This point can be considered as the starting point of a separate, fourth trajectory, which firstly crosses the line $C_n = 1$ and then approaches the nullcline $C_n = 1 + \Omega/C_\tau$ for $C_\tau \to \infty$.

The trajectory computed for $C_t = 0.5$ crosses the line $C_\tau = 0$ twice and also approaches the nullcline $C_n = 1 + \Omega/C_\tau$ for $C_\tau \to \infty$.

Fig. 4 The phase portrait of the free-boundary equations (Eqs. 11–13) corresponding to $\Omega = 0.1333$. Dashed lines show nullclines of the system ($dC_n/dS = 0$ and $dC_\tau/dS = 0$). Black dots mark starting points of the trajectories computed for different values of $C_t \equiv C_\tau(0)$. Dash-dotted line corresponds to $C_t = 0.3$, thick solid is obtained for $C_t = 0.42055$. The first part of the trajectory computed for $C_t = 0.5$ is depicted by a thin solid line and the following part is shown by dotted line. Taken from [18]
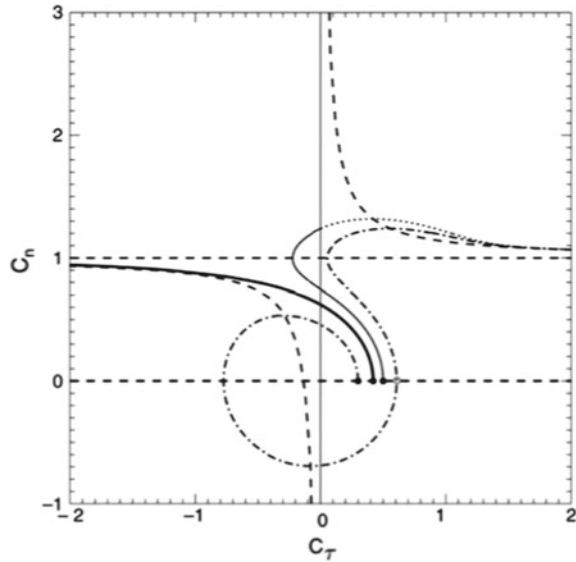
The front shapes corresponding to these two trajectories ($C_t = 0.3$ and $C_t = 0.5$) are shown in Fig. 5a. They are obtained by substitution of the computed function $K(s)$ into Eqs. 6–8 with $\Theta(0) = \pi/2$, $X(0) = 0$, and $Y(0) = C_t/\Omega$. It can be seen that the trajectory starting at $C_t = 0.3$ (dash-dotted line) has no physical sense. Another trajectory, corresponding to $C_t = 0.5$, contains a part depicted by thin solid, which can be considered as a front of a wave rotating within a disk of radius R_D with a no-flux boundary. The first intersection of this trajectory with the line $C_\tau = 0$ corresponds to the point Q. The second intersection occurs at the disk boundary, where $C_n^+ = \Omega R_D$. The part of the trajectory outside the disk of radius R_D does not match any rotating waves in excitable media. It resembles antispirals [19] or twisted spirals [20] observed in oscillatory media.

By starting at $C_t = 0.5$ and continuously decreasing C_t one can compute trajectories corresponding to an increasing disk radius R_D. The limiting case $R_D \to \infty$ is obtained for $C_t = 0.42055$ and is shown in Fig. 5b by the thick solid line. The corresponding trajectory is presented in Fig. 4 by the thick solid. Obviously, this solution of Eqs. 11–13 represents a spiral wave front in an unbounded medium rotating at the

given angular velocity Ω. Asymptotics of this solution for $S \to \infty$ can be specified as in [17]

$$C_n^+(\infty) = 1, \quad C_\tau^+(S) = \sqrt{2\Omega S}, \quad K(S) = \sqrt{\frac{\Omega}{2S}}. \tag{14}$$

Fig. 5 Wave front shapes corresponding to the trajectories shown in Fig. 4. **a** Front shapes computed for $C_t = 0.3$ (dash-dotted line) and $C_t = 0.5$ (thin solid and dotted lines). **b** Front shape obtained for $C_t = 0.42055$. Taken from [18]
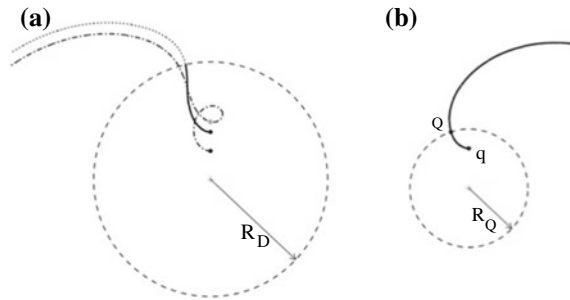
A repetition of similar computations for different values of Ω reveals a unique relationship $\Omega = \Omega(C_t)$ depicted in Fig. 6. Here C_t varies within the whole physically available range $0 \le C_t \le 1$. The angular velocity Ω vanishes at $C_\tau = 1$. This limiting case corresponds to the low excitability limit studied in [21], where an analytical expression $\Omega = 0.198(1 - C_t)^{3/2}$ has been derived. This expression shown by the dotted line in Fig. 6 approximates very well the relation found numerically for $C_t \approx 1$. However, it strongly deviates from numerical data obtained for small C_t.

Fig. 6 Angular velocity Ω of a wave front as a function of the tangential velocity C_t of the spiral tip. The dashed line depicts the approximation given by Eq. 15. The dotted line corresponds to the asymptotic found in [21] specified by the first term in Eq. 15. Taken from [18]
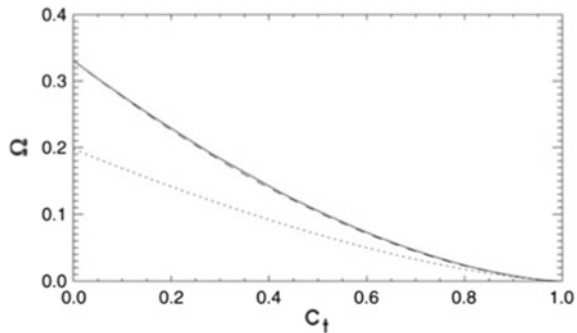
In another limiting case, the value $\Omega = 0.331$ computed for $C_t = 0$ coincides with the result obtained firstly by Burton, Cabrera and Frank [14] for screw dislocations growing on crystal surface (see chapter **Appearance in Nature**) and reproduced later many times [17, 21, 22].

The suitable approximation of the relationship $\Omega(C_t)$ obtained numerically for the whole range $0 \le C_t \le 1$ reads

$$\Omega = 0.198(1 - C_t)^{3/2} + 0.133(1 - C_t)^2. \tag{15}$$

It supplies a nice accuracy within the whole range $0 \leq C_t \leq 1$, as can be seen in Fig. 6.

Thus, the front shape of a rigidly rotating spiral wave and its angular velocity Ω are uniquely determined by the tangential velocity C_t of the spiral tip.

The results obtained for the wave front have to be used to integrate Eqs. 11 and 12 for the spiral wave back taking into account that during the excited state, the inhibitor value is increasing from $v = v^+$ at the wave front till $v = v^-$ at the wave back. The value v^- of the inhibitor at the wave back can be found from Eq. 2 under the assumption that the value $G(u_e(v), v)$ remains practically constant and equal to G^* during the excited state. Note that for many systems under consideration, e.g. cardiac tissue, the inhibitor diffusion $D_v = 0$, which simplifies the analysis.

Since the pattern is rotating at a constant angular velocity ω, the value of the inhibitor near the wave back is expressed in accordance with Eq. 2 as

$$v^-(R) = v^+ + \frac{G^* \varepsilon}{\omega} [\gamma^+(R) - \gamma^-(R)], \tag{16}$$

where γ^+ and γ^- specify the location of the front and the back, respectively, as shown in Fig. 7. The thick solid line in Fig. 7 represents the front of the rotating wave computed for a given value of $\Omega = 0.1333$. The front curvature $K(s)$ obtained during these computations has to be substituted into Eqs. 6–8 in order to determine the front shape in the Cartesian and polar coordinates.

The inhibitor v^- strongly affects the normal propagation velocity. In order to reflect this fact, the eikonal equation (Eq. 3) should be modified to

$$c_n^- = c_p(v^-) - Dk. \tag{17}$$

Substituting the value v^- expressed by Eq. 16 into Eq. 17 we get after rescaling

$$C_n^- = 1 - K^- - \frac{B}{\Omega} [\gamma^+(R) - \gamma^-(R)]. \tag{18}$$

The multiplier B appearing in this dimensionless expression is a very important control parameter and reads as

$$B = \frac{2D}{c_0^2 d_u}. \tag{19}$$

In order to obtain the shape of the wave back Eqs. 11–12 and 18 have to be integrated in the reverse arclength direction starting at $S = 0$ with initial conditions $C_n^-(0) = 0$ and $C_\tau^-(0) = C_t$. The obtained values of $K^-(S)$ have to be substituted into Eqs. 6–8 with $\Theta(0) = \pi/2$, $X(0) = 0$, and $Y(0) = C_t/\Omega$ in order to determine the dependence $\gamma^-(R)$.

It is important to emphasize that the shape of the wave back is strongly depended on the parameter B as shown in Fig. 7. It is expected for a physically correct solution that the derivatives $d\gamma^-/dS$ and dR^-/dS are positive. If B is relatively small, the derivative $d\gamma^-/dS$ vanishes at some S and becomes negative (see dotted line). If B

Fig. 7 Spiral wave shape obtained for $\Omega = 0.1333$. The front shape corresponds to Fig. 5b. The back shape is computed from Eqs. 11, 12, and 18 for different values of the dimensionless parameter B. Dotted and dashed lines correspond to $B = 0.2971$ and $B = 0.3008$, respectively. Thin solid line corresponds to $B = 0.2979$ found by a trial and error method. Taken from [18]
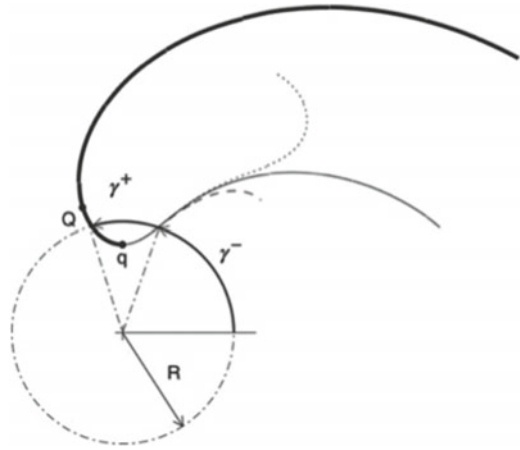
is relatively large, the derivative dR^-/dS vanishes (see dashed line). Using a trial and error method, one must vary the value of B trying to obtain the solution with the asymptotic $C_n^-(-\infty) = -1$.

Fig. 8 The dimensionless angular velocity of a rigidly rotating spiral $\Omega = \Omega_{FB}(B)$ selected as a solution of the free-boundary problem based on Eqs. 11–13, and 18 versus the dimensionless parameter B characterizing the excitability of the medium. Taken from [18]
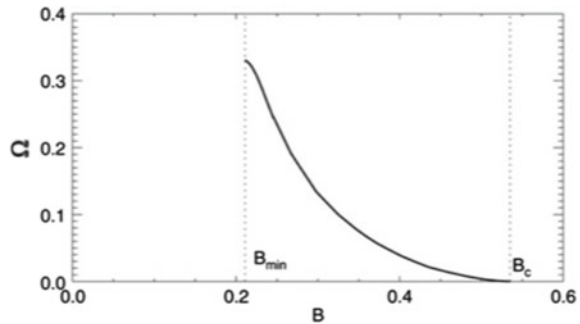
Thus, the obtained solution of the free-boundary problem for a spiral wave in an unbounded medium is uniquely determined by the value of the dimensionless parameter B for a given value of the angular velocity Ω. Repetition of these computations for different values of Ω from the interval $0 < \Omega < 1$ yields the universal relationship $\Omega = \Omega(B)$ shown in Fig. 8.

4 Two Limiting Cases

There are two limiting cases which characterize the relationship shown in Fig. 8. Firstly, our computations show that the highest angular velocity $\Omega = 0.331$ is reached at $B = B_{min} \approx 0.211$. Secondly, it is known that an undamped excitation wave in

a two-dimensional medium is supported only if $B < B_c \approx 0.535$ [23–25]. Hence, in a medium with a strongly reduced refractoriness a rigidly rotating spiral can be obtained only within the interval $B_{min} < B < B_c$.
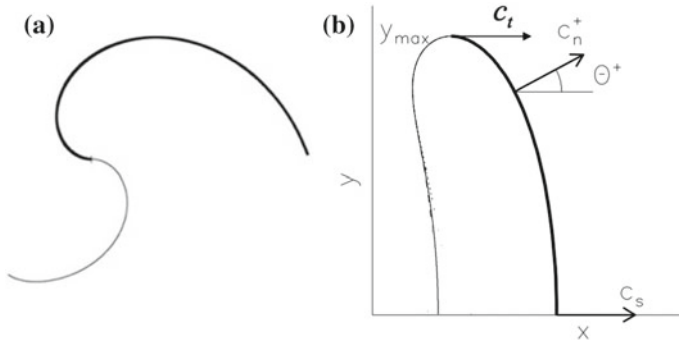
Fig. 9 The solution of the free-boundary problem Eqs. 11–13 and 18 corresponding to the limiting cases **a** $B = B_{min}$ and **b** $B = B_c$

The solution of the free-boundary problem obtained for $B = B_{min}$ is illustrated in Fig. 9a. Comparing Figs. 9a and 7 one can conclude that in this limiting case the point Q coincides with the spiral tip q, and they both are located at the rotation center. The radius of the spiral tip trajectory, $R_q = C_t / \Omega$, vanishes in the limit $B = B_{min}$. The curvature K_Q reaches the maximum $K_Q = 1$. The shape of the wave front is identical to that obtained by Burton, Cabrera and Frank [14]. The shape of the wave back reproduces the front shape, except for the immediate vicinity of the spiral tip. The wave back is turned by angle π with respect to the front, and the Cartesian coordinates of the wave boundary and their first derivatives are smooth functions of the arc length. In fact, in this limit the spiral wave form approaches the Yin-Yang pattern.

In the second limiting case, $B = B_c$, the angular velocity vanishes and the radius of the spiral wave core diverges. The shape of the spiral wave approaches the critical finger first studied in [23] and illustrated in Fig. 9b. The boundary of the excited region shown here undergoes a translational motion along the X axis at a constant velocity. Obviously, this velocity should be equal to the velocity c_p of a planar wave.

Thus, in a medium with a strongly reduced refractoriness the dimensionless angular velocity Ω is a unique monotonously decreasing function of the dimensionless parameter B. This function $\Omega = \Omega(B)$ changes between 0.331 and zero within the interval $B_{min} < B < B_c$. The radius of the spiral tip trajectory vanishes at $B = B_{min}$ and diverges at $B = B_c$.

5 Concluding Remarks

In this chapter we have demonstrated that the free-boundary approach allows us to clarify the basic principles of spiral wave selection in excitable media. It is shown that the rotational frequency and the spiral core radius in a medium with a short refractoriness are completely determined by a single dimensionless parameter B determined by Eq. 19. The value of this parameter can be estimated numerically or even analytically for quite different mathematical models. Moreover, it can be obtained as a result of direct experimental measurements.

However, the kinematical description of the rigidly rotating spiral waves represented in this work is, in fact, only an important limiting case of a much more complicated problem. As an example, three very important tasks, which should be solved in the near future are listed below.

First of all, note that the propagation velocity of a stationary propagating wave front is a nonlinear function of the front curvature [17]. A linear eikonal equation (Eq. 3) can be obtained only for $\varepsilon = 0$. For any $\varepsilon > 0$ there is a critical value of the front curvature K_{cr}, which restricts the region, where undamped wave propagation is supported. Point Q (see Fig. 7) is in stationary movement along a circular trajectory. The wave front at this point is curved and its curvature cannot exceed K_{cr}. This also restricts the angular velocity of a spiral wave [17]. This circumstance should be taken into account, when a medium with $B \approx B_{min}$ is considered [18].

Another very important issue is, of course, the role of the refractoriness of the medium. This problem is currently not solved. An important step in this direction is a recently developed kinematical description of a periodic sequence of the wave segments [26].

Finally, the described kinematical theory is applicable to so-called trigger-trigger waves [22]. However, under corresponding parameter variations, these waves can be transformed to so-called trigger-phase waves [27–29]. Moreover, there is a continuous transition between these two types of spiral kinematics [30], which should be studied in detail.

Thus, the kinematical theory of spiral waves represents a very interesting and intensively growing field for future investigations aimed, e.g., to find out efficient ways to prevent or to suppress an undesirable and dangerous self-sustained wave activity in excitable media.

References

1. G. Gerisch, Periodische Signale steuern die Musterbildung in Zellverbänden. Naturwissenschaften **58**, 430–438 (1971)
2. A.T. Winfree, Spiral waves of chemical activity. Science **175**, 634–636 (1972)
3. M.A. Allessie, F.I.M. Bonke, F.J.G. Schopman, Circus movement in rabbit atrial muscle as a mechanism of tachycardia. Circ. Res. **33**, 54–62 (1973)
4. N.A. Gorelova, J. Bures, Spiral waves of spreading depression in the isolated chicken retina. J. Neurobiol. **14**, 353–363 (1983)

5. S. Jakubith, H.H. Rotermund, W. Engel, A. von Oertzen, G. Ertl, Spatiotemporal concentration patterns in a surface reaction: propagating and standing waves, rotating spirals, and turbulence. Phys. Rev. Lett. **65**, 3013–3016 (1990)
6. T. Mair, S.C. Müller, Traveling NADH and proton waves during oscillatory glycolysis in vitro. J. Biol. Chem. **271**, 627–630 (1996)
7. S.C. Müller, T. Plesser, B. Hess, The structure of the core of the spiral wave in the Belousov-Zhabotinskii reaction. Science **230**, 661–663 (1985)
8. G.S. Skinner, H.L. Swinney, Periodic to quasiperiodic transition of chemical spiral rotation. Physica D **48**, 1–16 (1991)
9. K.I. Agladze, V.A. Davydov, A.S. Mikhailov, An observation of resonance of spiral waves in distributed excitable medium. JETP Lett. **45**, 601–603 (1987)
10. O. Steinbock, V.S. Zykov, S.C. Müller, Control of spiral-wave dynamics in active media by periodic modulation of excitability. Nature **366**, 322–324 (1993)
11. V.N. Biktashev, A. Holden, Design principles of a low voltage cardiac defibrillator based on the effect of feedback resonant drift. J. Theor. Biol. **169**, 101–112 (1994)
12. A.V. Panfilov, S.C. Müller, V.S. Zykov, J.P. Keener, Elimination of spiral waves in cardiac tissue by multiple electrical shocks. Phys. Rev. E **61**, 4644–4647 (2000)
13. N. Wiener, A. Rosenblueth, The mathematical formulation of the problem of conduction of impulses in a network of connected excitable elements, specifically in cardiac muscle. Arch. Inst. Cardiol. de Mex. **16**, 205–265 (1946)
14. W.K. Burton, N. Cabrera, F.C. Frank, The growth of crystals and the equilibrium structure of their surfaces. Philos. Trans. R. Soc. Lond. Ser. A **243**, 299–358 (1951)
15. P. Pelcé, J. Sun, Wave front interaction in steadily rotating spirals. Physica D **48**, 353–366 (1991)
16. F.B. Gul'ko, A.A. Petrov, Mechanism of formation of closed propagation pathways in excitable media. Biofizika **17**, 261–270 (1972)
17. V.S. Zykov, *Simulation of Wave Processes in Excitable Media* (Manchester University Press, Manchester, 1987)
18. V.S. Zykov, Kinematics of rigidly rotating spiral waves. Physica D **238**, 931–940 (2009)
19. I. Aranson, L. Kramer, The world of the complex Ginzburg-Landau equation. Rev. Mod. Phys. **74**, 99–143 (2002)
20. O. Rudzik, A.S. Mikhailov, Front reversals, wave traps, and twisted spirals in periodically forced oscillatory media. Phys. Rev. Lett. **96**, 018302 (2006)
21. V. Hakim, A. Karma, Theory of spiral wave dynamics in weakly excitable media: asymptotic reduction to a kinematic model and applications. Phys. Rev. E **60**, 5073–5105 (1999)
22. J.J. Tyson, J. Keener, Singular perturbation theory of traveling waves in excitable media (a review). Physica D **32**, 327–361 (1988)
23. A. Karma, Universal limit of spiral wave propagation in excitable media. Phys. Rev. Lett. **66**, 2274–2277 (1991)
24. V.S. Zykov, K. Showalter, Wave front interaction model of stabilized propagating wave segments. Phys. Rev. Lett. **94**, 068302 (2005)
25. A. Kothe, V.S. Zykov, H. Engel, Second universal limit of wave segment propagation in excitable media. Phys. Rev. Lett. **103**, 154102 (2009)
26. V.S. Zykov, E. Bodenschatz, Periodic sequence of stabilized wave segments in an excitable medium. Phys. Rev. E **97**(3), 030201(R) (2018)
27. V.S. Zykov, N. Oikawa, E. Bodenschatz, Selection of spiral waves in excitable media with a phase wave at the wave back. Phys. Rev. Lett. **107**, 254101 (2011)
28. V.S. Zykov, E. Bodenschatz, Stabilized wave segments in an excitable medium with a phase wave at the wave back. New J. Phys. **16**, 043030 (2014)
29. N. Oikawa, E. Bodenschatz, V. Zykov, Unusual spiral wave dynamics in the Kessler-Levine model of an excitable medium. Chaos **25**, 053115 (2015)
30. V.S. Zykov, E. Bodenschatz, Continuous transition between two limits of spiral wave dynamics in an excitable medium. Phys. Rev. Lett. **112**, 054101 (2014)

Correction to: Acoustic Spirals: Analysis of Bach's Prelude in C Major

Kinko Tsuji

Correction to:
Chapter "Acoustic Spirals: Analysis of Bach's Prelude in C Major" in: K. Tsuji and S. C. Müller (eds.), *Spirals and Vortices*, The Frontiers Collection,
https://doi.org/10.1007/978-3-030-05798-5_5

The original version of the book was inadvertently published with an incorrect equation (2) on page 116 in chapter 5. The chapter and book have been updated with the following change:

from
$$y_p = y \sin \alpha + z \cos \alpha$$
to
$$y_p = y \cos \alpha + z \sin \alpha$$

The updated version of this chapter can be found at
https://doi.org/10.1007/978-3-030-05798-5_5

Epilogue

We are the days and the nights
And the stars,
That illuminate the darkness.
We are holy beings,
Recalling this truth,
We feel the Sun and the Moon
In our body
Like Dancing Spirals

The secrets of existence unfold within us.

— American Indian Wisdom

List of References for General Information

1. C.W. Ceram, *Götter, Gräber und Gelehrte*, 1st edn. 1949 (Rowohlt, Reinbek bei Hamburg, 2008)
2. S. Chandrasekhar, *Hydrodynamic and Hydromagnetic Stability* (Dover, London, 1961)
3. M.C. Cross, P.C. Hohenberg, Pattern formation outside of equilibrium. Rev. Mod. Phys. **65**, 851 (1993)
4. A. Deutsch (ed.), *Muster des Lebendigen* (Vieweg, Braunschweig, 1994)
5. J. Diamond, *Guns, Germs, and Steel* (W.W. Norton and Company, New York, 1999)
6. I.R. Epstein, J. Pojman, *An Introduction to Nonlinear Chemical Dynamics* (Oxford University Press, Oxford, 1998)
7. R. Ettinghausen, O. Grabar, M. Jenkins-Madina, *Islamic Art and Architecture 650-1250* (2nd ed.) (Yale University Press, Yale, 2003)
8. A. Feininger, *Das Antlitz der Natur* (Knauer, München, 1957)
9. G. Gerisch, Periodische Signale steuern die Musterbildung in Zellverbänden. Naturwissenschaften **58**, 430–438 (1971)
10. A. Goldbeter, *La Vie Oscillatoire* (Odile Jacob, Paris, 2010)
11. H. Haberland, *Amerikanische Archäologie - Geschichte, Theorie, Kulturentwicklung* (Wissenschaftliche Buchgesellschaft, Darmstadt 1992)
12. H. Haken, *Synergetics - Introduction and Advanced Topics* (Springer, Berlin, 2004)
13. H. Haken, P.J. Plath, W.E. Ebeling, Y.M. Romanosky (eds.), *Beitäge zur Geschichte der Synergetik* (Springer-Spektrum, Heidelberg, 2016)
14. I. Hargittai, C.A. Pickover (eds.), *Spiral Symmetry* (World Scientific, Hong Kong, 1992)
15. M. Hauser, O. Steinbock (eds.), Emergent phenomena in spatially distributed systems - in Honor of Stefan C. Müller. Physica D **239** (2010)
16. E.S. Hedges, J.E. Myers, *The Problem of Physicochemical Periodicity* (Edward Arnold and Co., London, 1926)
17. A.L. Hodgkin, A.F. Huxley, A quantitative description of membrane current and its application to conduction and excitation in nerve. J. Physiol. Lond. **117**, 500 (1952)
18. H.-J. Hoffmann (ed.), *Verknüpfungen* (Birkhäuser, Boston, 1992)
19. G. Jules, *Die Alhambra zu Granada* (new edition) (Wernersche Verlagsgesellschaft, Worms, 2008)
20. R. Kapral, K. Showalter (eds.), *Chemical Waves and Patterns* (Kluwer, Dordrecht, 1995)
21. M. Kemp, *Leonardo* (C.H. Beck, München, 2004)
22. R. Kessin, *Dictyostelium* (Cambridge University Press, Cambridge, 2001)
23. Y. Kuramoto, *Chemical Oscillations, Waves and Turbulence* (Springer, Heidelberg, 1984)
24. H. Meinhardt, *The Algorithmic Beauty of Sea Shells* (Springer, Heidelberg)

25. A.S. Mikhailov, G. Ertl, *Chemical Complexity* (Springer, Switzerland, 2017)
26. S.C. Müller, P.J. Plath, G. Radons, A. Fuchs (eds.), *Complexity and Synergetics* (Springer, Switzerland, 2018)
27. J.D. Murray, *Mathematical Biology I. An Introduction*, 2 edn. (Springer, Heidelberg, 1993)
28. G. Nicolis, I. Prigogine, *Exploring Complexity* (R. Piper, München, 1989)
29. R.T. Paine, A. Soper, *The Art and Architecture of Japan* (3rd ed.), (Yale University Press Pelican History of Art, Yale, 1981)
30. J. Parisi, S.C. Müller, W. Zimmermann, *A Perspective Look at Nonlinear Media - From Physics to Biology and Social Sciences* (Springer, Berlin, Heidelberg, 1998)
31. H.O. Peitgen, P.H. Richter *The Beauty of Fractals* (Springer, Tokyo, 1986)
32. J. Ross *Thermodynamics and Fluctuations Far from Equilibrium* (Springer, Heidelberg, 2008)
33. F.W. Schneider, A.F. Münster, *Nichtlineare Dynamik in der Chemie* (Spektrum Akademischer Verlag, Oxford, 1996)
34. K. Seike, M. Kudo, W. Schmidt, *Japanische Gärten und Gartenteile* (Ulmer, Stuttgart, 1980)
35. S.H. Strogatz, *Nonlinear Dynamics and Chaos with Applications to Physics, Biology, Chemistry, and Engineering*, 2 edn. (CRC Press, Boca Reton, 2014)
36. D.W. Thompson, *On Growth and Form* (Cambridge University Press, Cambridge, 1966)
37. A.M. Turing, The chemical basis of morphogenesis. Philos. Trans. R. Soc. Lond. B **237**, 37 (1952)
38. D.S. Whitley, *Introduction to Rock Art Research* (Left Coast Press, Walnut Creek, 2009)
39. N. Wiener, A. Rosenblueth, The mathematical formulation of the problem of conduction of impulses in a network of connected excitable elements, specifically in cardiac muscle. Arch. Inst. Cardiologia de México **16**, 205–265 (1946)
40. A.T. Winfree, *The Geometry of Biological Time* (Springer, Berlin, 1980)

Glossary

Activator a substance which accelerates or stimulates a reaction.

ADP, AMP see **ATP**.

Allosteric The term allostery comes from the Greek allos "other", and stereos "solid (object)". This is in reference to the fact that the regulatory site of a protein (called allosteric site) is different from its active site.

Anoxia an absence or deficiency of oxygen reaching the tissues.

ATP (adenosine triphosphate) a complex organic chemical which is used for intracellular energy transfer. When consumed in metabolic processes, it converts to either **ADP (adenosine diphospate)** or **AMP (adenosine monophosphate)**.

Attractor points, loops (limit cycles), surfaces (tori), and other geometrical subsets (chaotic and fractal), where a dynamical system reaches (or approximates) stable configuration or its "death". For example, the center bottom position of a damped pendulum is a point attractor: the pendulum is losing energy (energy dissipation) due to friction time by time and finally it stops at the bottom.

Autocatalysis a catalysis of a reaction by one of its own products.

Avatar a word in Hinduism, means incarnation.

Belousov–Zhabotinsky (BZ) Reaction one of chemical reactions occurring along the laws of non-equilibrium thermodynamics, showing chemical oscillations. The oscillatory behavior is observed temporally and/or spatially. The essential elements in this oscillator are the autocatalytic species $HBrO_2$ as activator, bromide as inhibitor, and a catalyst/color indicator. Under excitable conditions it forms propagating concentration waves.

Brewster Angle an incident angle at which a particular polarized light is transmitted without reflection.

Carolingian script combining characteristics of cursive and half uncial, developed in France in the 8th century (when the Carolingian dynasty governed).

Cellular Automaton a discrete model studied typically in complexity science and theoretical biology. It consists of a regular grid of cells, each in one of a finite number of states, such as "on" and "off''. For each cell, a set of cells called its neighborhood is defined relative to the specified cell in discrete time steps.

Chemotaxis movement of cells or organisms due to gradient of chemical agents (see also **phototaxis**).

Conservative System incompressible flux in phase space, phase space volume is conserved. For example, trajectories of harmonic oscillator or planet movement around the Sun. (↔ **dissipative system**).

Convection thermally or chemically produced upward or downward movement of fluids (liquids or gases).

CNS (central nervous system) the part of the nervous system consisting of the brain and spinal cord.

Craniotomy the surgical removal of part of the bone from the skull to expose the brain.

Deterministic a deterministic system is a system in which no randomness is involved in the development of future states of the system. A deterministic model will always produce the same output from a given initial state.

Dissipative System phase space volume contracts in time. For example, damped oscillator. (↔ **conservative system**).

Dolmen a prehistoric monument consisting of two or more stones supporting a horizontal stone slab.

Exoskeleton an external skeleton or supportive covering an animal (↔ **endoskeleton**).

Feigenbaum Scenario a mathematical scenario to cause deterministic chaos from order by period doubling.

Fractal infinitely repeating similar pattern (self-similar pattern) at increasing smaller scales, usually due to its non-integer dimension.

Gabel (Wimperg in German) the vertical triangular portion of a wall between the edges of intersecting roof pitches, often used in the architecture of churches.

Geoglyph a large mark or motif produced on the ground, formed by stones, stone fragments, live trees, gravel, or earth.

Heaviside Function a step function, whose value is zero for negative argument and one for positive argument.

Inhibitor a substance that interferes with a chemical process or reaction, e.g., by suppressing growth.

Ischemia an inadequate blood supply to an organ or part of the body, especially the heart muscles.

Laminar Flow streamline flow in which a fluid flows in parallel layers, with no disruption between the layers ($\leftrightarrow$ **turbulence**).

Luciferase an oxidative enzyme which acts on luciforin. Resulting excited state intermediate emits light upon decaying to its ground state which produces bioluminescence.

Mean Field Theory Mean field theory studies the behavior of large and complex stochastic models by studying a simpler model. Such models consider a large number of small individual components which interact with each other. The effect of all the other individuals on any given individual is approximated by a single averaged effect, thus reducing a many-body problem to a one-body problem.

Metamorphosis change into a different physical or biological form.

Morphogenesis the biological process that causes an organism to develop its shape, for example, control of cell growth and cellular differentiation.

Nacre iridescent inner layer of some shellfish, known as "mother of pearl".

NAD (nicotinamide adenine dinucleotide) a coenzyme existing in all living cells in two forms: an oxidized and reduced form NAD+ and NADH, respectively, functioning for electron transfer in cells.

NGC (New General Catalogue) a catalogue of 7840 deep-sky objects, including galaxies, star clusters, emission nebulae and absorption nebulae.

Non-equilibrium In thermodynamic equilibrium there are no net macroscopic flows of matter or of energy, either within a system or between systems. In non-equilibrium systems, by contrast, there are net flows of matter or energy. The role of entropy has to be considered.

Nonlinear Dynamics a field of physics that studies systems governed by equations more complex than the linear $aX + b$ form. Nonlinear systems, such as the weather or neurons, often appear unpredictable, but still they are not random.

Normal Velocity In mathematics, given a velocity vector at a point on a curve, that vector can be decomposed uniquely as a sum of two vectors, one tangent to the curve, called the tangential component of the vector, and another one perpendicular to the curve, called the normal component of the vector.

Phototaxis movements of cells or organisms due to light gradient (see also **chemotaxis**).

Proboscis a sucking organ of insects or some other invertebrates, or a flexible conspicuously long snout of some mammals.

Refractory unresponsive to stimuli, a resting state.

Self-Organization a process where some form of overall order arises from local interactions between parts of an initially disordered system. The process is often spontaneous structuration out of a homogeneous initial state, triggered by random

fluctuations and amplified by positive feedback. Examples are: crystallization, thermal convection of fluids, chemical oscillation, animal swarming, neural networks, and others.

Self-Similarity for objects being exactly or approximately similar to a part of itself.

Stochastic a system that is randomly determined; variables proceed by probabilities, or guesswork.

Swarm Intelligence the collective behavior of decentralized, self-organized systems such as insect, bird or fish colonies.

Tetanic Stimulation a way of stimulation of a neuron with a high frequency repetition (like tetanus suffering).

Thermodynamic Equilibrium a state of a physical system in which it is in mechanical, chemical and thermal equilibrium and in which there is no tendency for spontaneous change.

Trade Wind a wind blowing almost continuously from the northeast in the Northern Hemisphere and from the southeast in the Southern Hemisphere, acting as the steering flow for tropical storms. They have been used for sailing ships to cross the world's oceans for centuries.

Trajectory indicates in phase space the progression or line of development of the evolving system.

Tropopause the boundary region between the troposphere (the lowest layer of the atmosphere) and stratosphere (the layer above the troposphere).

Turbulence any pattern of fluid motion characterized by chaotic changes in pressure and flow velocity ($\leftrightarrow$ **laminar flow**). Turbulence is commonly observed in everyday phenomena such as surf, fast flowing rivers, billowing storm clouds, or smoke from a chimney. Most fluid flows occurring in nature and created in engineering applications are turbulent.

Turing Patterns patterns appearing in nature (biological organisms as well as other natural systems, like sand patterns formed by wind). Stripes and spots arising naturally out of a homogeneous, uniform state, introduced by Alan Turing in 1952, due to reaction-diffusion coupling of a fast activator and slow inhibitor.

Visual Cortex a part of the cerebral cortex that processes visual information.

:= a mathematical symbol meaning "is defined to be equal to"

Index

Titles in This Series

Quantum Mechanics and Gravity
By Mendel Sachs

Quantum-Classical Correspondence
Dynamical Quantization and the Classical Limit
By A.O. Bolivar

Knowledge and the World: Challenges Beyond the Science Wars
Ed. by M. Carrier, J. Roggenhofer, G. Küppers and P. Blanchard

Quantum-Classical Analogies
By Daniela Dragoman and Mircea Dragoman

Quo Vadis Quantum Mechanics?
Ed. by Avshalom C. Elitzur, Shahar Dolev and Nancy Kolenda

Information and Its Role in Nature
By Juan G. Roederer

Extreme Events in Nature and Society
Ed. by Sergio Albeverio, Volker Jentsch and Holger Kantz

The Thermodynamic Machinery of Life
By Michal Kurzynski

Weak Links
The Universal Key to the Stability of Networks and Complex Systems
By Csermely Peter

The Emerging Physics of Consciousness
Ed. by Jack A. Tuszynski

Quantum Mechanics at the Crossroads
New Perspectives from History, Philosophy and Physics
Ed. by James Evans and Alan S. Thorndike

Searching for Extraterrestrial Intelligence
SETI Past, Present, and Future
Ed. by H. Paul Shuch

Essential Building Blocks of Human Nature
Ed. by Ulrich J. Frey, Charlotte Störmer and Kai P. Willführ

Mindful Universe
Quantum Mechanics and the Participating Observer
By Henry P. Stapp

Principles of Evolution
From the Planck Epoch to Complex Multicellular Life
Ed. by Hildegard Meyer-Ortmanns and Stefan Thurner

The Second Law of Economics
Energy, Entropy, and the Origins of Wealth
By Reiner Kümmel

States of Consciousness
Experimental Insights into Meditation, Waking, Sleep and Dreams
Ed. by Dean Cvetkovic and Irena Cosic

Elegance and Enigma
The Quantum Interviews
Ed. by Maximilian Schlosshauer

Humans on Earth
From Origins to Possible Futures
By Filipe Duarte Santos

Evolution 2.0
Implications of Darwinism in Philosophy and the Social and Natural Sciences
Ed. by Martin Brinkworth and Friedel Weinert

Probability in Physics
Ed. by Yemima Ben-Menahem and Meir Hemmo

Chips 2020
A Guide to the Future of Nanoelectronics
Ed. by Bernd Hoefflinger

From the Web to the Grid and Beyond
Computing Paradigms Driven by High-Energy Physics
Ed. by René Brun, Frederico Carminati and Giuliana Galli-Carminati

The Language Phenomenon
Human Communication from Milliseconds to Millennia
Ed. by P.-M. Binder and K. Smith

The Dual Nature of Life
Interplay of the Individual and the Genome
By Gennadiy Zhegunov

Natural Fabrications
Science, Emergence and Consciousness
By William Seager

Ultimate Horizons
Probing the Limits of the Universe
By Helmut Satz

Physics, Nature and Society
A Guide to Order and Complexity in Our World
By Joaquín Marro

Extraterrestrial Altruism
Evolution and Ethics in the Cosmos
Ed. by Douglas A. Vakoch

The Beginning and the End
The Meaning of Life in a Cosmological Perspective
By Clément Vidal

A Brief History of String Theory
From Dual Models to M-Theory
By Dean Rickles

Singularity Hypotheses
A Scientific and Philosophical Assessment
Ed. by Amnon H. Eden, James H. Moor, Johnny H. Søraker and Eric Steinhart

Why More Is Different
Philosophical Issues in Condensed Matter Physics and Complex Systems
Ed. by Brigitte Falkenburg and Margaret Morrison

Questioning the Foundations of Physics
Which of Our Fundamental Assumptions Are Wrong?
Ed. by Anthony Aguirre, Brendan Foster and Zeeya Merali

It from Bit or Bit from It?
On Physics and Information
Ed. by Anthony Aguirre, Brendan Foster and Zeeya Merali

How Should Humanity Steer the Future?
Ed. by Anthony Aguirre, Brendan Foster and Zeeya Merali

Trick or Truth?
The Mysterious Connection Between Physics and Mathematics
Ed. by Anthony Aguirre, Brendan Foster and Zeeya Merali

The Challenge of Chance
A Multidisciplinary Approach from Science and the Humanities
Ed. by Klaas Landsman, Ellen van Wolde

Quantum [Un]Speakables II
Half a Century of Bell's Theorem
Ed. by Reinhold Bertlmann, Anton Zeilinger

Energy, Complexity and Wealth Maximization
Ed. by Robert Ayres

Ancestors, Territoriality and Gods
A Natural History of Religion
By Ina Wunn, Davina Grojnowski

Space, Time and the Limits of Human Understanding
Ed. by Shyam Wuppuluri, Giancarlo Ghirardi

Information and Interaction
Eddington, Wheeler, and the Limits of Knowledge
Ed. by Ian T. Durham, Dean Rickles

The Technological Singularity
Managing the Journey
Ed. by V. Callaghan, J. Miller, R. Yampolskiy, S. Armstrong

How Can Physics Underlie the Mind?
Top-Down Causation in the Human Context
By George Ellis

The Unknown as an Engine for Science
An Essay on the Definite and the Indefinite
Hans J. Pirner

CHIPS 2020 Vol. 2
New Vistas in Nanoelectronics
Ed. by Bernd Hoefflinger

Life - As a Matter of Fat
Lipids in a Membrane Biophysics Perspective
Ole G. Mouritsen, Luis A. Bagatolli

The Quantum World
Philosophical Debates on Quantum Physics
Ed. by Bernard D'Espagnat, Hervé Zwirn

The Seneca Effect
Why Growth is Slow but Collapse is Rapid
By Ugo Bardi

Chemical Complexity
Self-Organization Processes in Molecular Systems
By Alexander S. Mikhailov, Gerhard Ertl

The Essential Tension
Competition, Cooperation and Multilevel Selection in Evolution
By Sonya Bahar

The Computability of the World
How Far Can Science Take Us?
By Bernd-Olaf Küppers

The Map and the Territory
Exploring the Foundations of Science, Thought and Reality
By Shyam Wuppuluri, Francisco A. Doria

Wandering Towards a Goal
How Can Mindless Mathematical Laws Give Rise to Aims and Intention?
Ed. by Anthony Aguirre, Brendan Foster and Zeeya Merali

Computer Simulations in Science and Engineering
Concepts - Practices - Perspectives
By Juan M. Durán

Stepping Stones to Synthetic Biology
By Sergio Carrà

Information–Consciousness–Reality
How a New Understanding of the Universe Can Help Answer Age-Old Questions
of Existence
By James B. Glattfelder

Spirals and Vortices
In Culture, Nature, and Science
Ed. by Kinko Tsuji, Stefan C. Müller

What is Fundamental?
Ed. by Anthony Aguirre, Brendan Foster, Zeeya Merali

Particles, Fields and Forces
A Conceptual Guide to Quantum Field Theory and the Standard Model
By Wouter Schmitz

The Reality of Time Flow
Local Becoming in Modern Physics
By Richard T. W. Arthur

NANO-CHIPS 2030
AI On-Chip and Autonomous Chip Systems
Ed. by Boris Murmann, Yiannos Monoli, Bernd Hoefflinger